

GEOLOGICAL SURVEY OF CANADA

OPEN FILE 1707

This document was produced
by scanning the original publication.

Ce document a été produit par
numérisation de la publication originale.

**GEOTECHNICAL INVESTIGATIONS OFF
NORTHERN RICHARDS ISLAND, N.W.T. - 1987**

Compiled and edited by

P.J. Kurfurst¹

Contributors:

**J.G. Bisson¹, R.A. Burns¹, S.R. Dallimore¹, R.M. Gagné¹,
R.L. Good¹, J.A. Hunter¹, A.S. Judge¹, P. Lafleche¹,
S.E. Pullan¹, C.R. Burn², W.D. Harrison³, J.L. Morack³,
K.G. Neave⁴ and H.A. MacAulay⁴**

¹ Geological Survey of Canada, Terrain Sciences Division, Ottawa

² University of British Columbia, Department of Geography, Vancouver, B.C.

³ University of Alaska, Physics Department and Geophysical Institute, Fairbanks, Alaska, U.S.A.

⁴ Northern Seismic Analysis Ltd., Echo Bay, Ontario

CONTENTS

List of Tables	iii
List of Figures	iv
1. Introduction (P.J. Kurfurst)	1
2. Geology (S.R. Dallimore)	3
3. Geotechnical drilling and testing (J.G. Bisson, S.R. Dallimore, P.J. Kurfurst)	6
3.1 Drilling and Sampling	6
3.2 Cone Penetration Tests	9
4. Borehole geophysical tests (J.A. Hunter, S.E. Pullan, R.A. Burns, R.L. Good, R.M. Gagné)	12
4.1 Temperature measurements	12
4.2 Borehole logging	14
4.3 Uphole seismic measurements	20
5. Borehole heating experiment (J.L. Morack, W.D. Harrison)	23
6. Ground probing radar (P. Lafleche, A.S. Judge)	26
7. Seismic refraction measurements (K.G. Neave, H.A. MacAulay)	29
8. Frost heave tests (C.R. Burn)	31
Acknowledgments	38
References	39

List of Tables

3-1 Borehole information	7
3-2 Jet-drilled hole information	8
3-3 CPT information	10
8-1 Detailed borehole stratigraphy	33

List of Figures

1-1	General location map	40
2-1	Generalized geology map	41
2-2	Coastal retreat map	42
3-1	Location of boreholes and CPTs	43
3-2	Cross-section of geological conditions	44
3-3	Cross-section of ground ice conditions	45
3-4	Borehole log legend	46
3-5	Detailed borehole logs - BH 87-1	47
3-6	Detailed borehole logs - BH 87-2	48
3-7	Detailed borehole logs - BH 87-3	49
3-8	Detailed borehole logs - BH 87-4	50
3-9	Detailed borehole logs - BH 87-5	51
3-10	Detailed borehole logs - BH 87-6	52
3-11	Detailed borehole logs - BH 87-7	53
3-12	Detailed borehole logs - BH 87-8	54
3-13	Detailed borehole logs - BH 87-10	55
3-14	Detailed borehole logs - BH 87-11	56
3-15	Detailed borehole logs - BH 87-12	57
3-16	Detailed borehole logs - BH 87-13	58
3-17	Cone penetration test data - C 87-01	59
3-18	Cone penetration test data - C 87-02	60
3-19	Cone penetration test data - C 87-03	61
3-20	Cone penetration test data - C 87-04	62
3-21	Cone penetration test data - C 87-05	63
3-22	Cone penetration test data - C 87-06	64

3-23	Cone penetration test data - C 87-07	65
3-24	Cone penetration test data - C 87-08	66
3-25a	CPT temperature dissipation vs. time plot	67
3-25b	Comparison of CPT and thermistor cable temperature data	67
4-1	Equilibrium temperature profile - BH 87-1	68
4-2	Equilibrium temperature profile - BH 87-2	69
4-3	Equilibrium temperature profile - BH 87-3	70
4-4	Equilibrium temperature profile - BH 87-4	71
4-5	Equilibrium temperature profile - BH 87-5	72
4-6	Equilibrium temperature profile - BH 87-6	73
4-7	Equilibrium temperature profile - BH 87-	74
4-8	Equilibrium temperature profile - BH 87-8	75
4-9	Equilibrium temperature profile - BH 87-9	76
4-10	Equilibrium temperature profile - BH 87-10	77
4-11	Equilibrium temperature profile - BH 87-11	78
4-12	Equilibrium temperature profile - BH 87-12	79
4-13	Equilibrium temperature profile - BH 87-13	80
4-14	Equilibrium temperature profile - JD-1	81
4-15	Equilibrium temperature profile - JD-2	82
4-16	Equilibrium temperature profile - JD-3	83
4-17	Equilibrium temperature profile - JD-4	84
4-18	Temperature profile along drill transect (300 to 1500 m) - winter 1987	85a
4-19	Temperature profile along drill transect (-80 to 150 m) - winter 1987	86a
4-20	Temperature profile along drill transect - summer 1987	87a
4-21	Geophysical borehole logs - BH 87-1	88
4-22	Geophysical borehole logs - BH 87-2	89

4-23	Geophysical borehole logs - BH 87-3	90
4-24	Geophysical borehole logs - BH 87-4	91
4-25	Geophysical borehole logs - BH 87-5	92
4-26	Geophysical borehole logs - BH 87-6	93
4-27	Geophysical borehole logs - BH 87-	94
4-28	Geophysical borehole logs - BH 87-9	95
4-29	Geophysical borehole logs - BH 87-10	96
4-30	Geophysical borehole logs - BH 87-11	97
4-31	Geophysical borehole logs - BH 87-12	98
4-32	Geophysical borehole logs - BH 87-13	99
4-33a	Travel time vs. distance - BH 87-1	100
4-33b	Reduced travel time vs. distance - BH 87-1	101
4-33c	Interval velocity vs. depth - BH 87-1	102
4-34a	Travel time vs. distance - BH 87-3	103
4-34b	Reduced travel time vs. distance - BH 87-3	104
4-34c	Interval velocity vs. depth - BH 87-3	105
4-35a	Travel time vs. distance - BH 87-4	106
4-35b	Reduced travel time vs. distance - BH 87-4	107
4-35c	Interval velocity vs. depth - BH 87-4	108
4-36a	Travel time vs. distance - BH 87-5	109
4-36b	Reduced travel time vs. distance - BH 87-5	110
4-36c	Interval velocity vs. depth - BH 87-5	111
4-37a	Travel time vs. distance - BH 87-6	112
4-37b	Reduced travel time vs. distance - BH 87-6	113
4-37c	Interval velocity vs. depth - BH 87-6	114
4-38a	Travel time vs. distance - BH 87-7	115

4-38b	Reduced travel time vs. distance - BH 87-7	116
4-38c	Interval velocity vs. depth - BH 87-7	117
4-39a	Travel time vs. distance - BH 87-8	118
4-39b	Reduced travel time vs. distance - BH 87-8	119
4-39c	Interval velocity vs. depth - BH 87-8	120
4-40a	Travel time vs. distance - BH 87-9	121
4-40b	Reduced travel time vs. distance - BH 87-9	122
4-40c	Interval velocity vs. depth - BH 87-9	123
4-41a	Travel time vs. distance - BH 87-10	124
4-41b	Reduced travel time vs. distance - BH 87-10	125
4-41c	Interval velocity vs. depth - BH 87-10	126
4-42a	Travel time vs. distance - BH 87-11	127
4-42b	Reduced travel time vs. distance - BH 87-11	128
4-42c	Interval velocity vs. depth - BH 87-11	129
5-1a	Time vs. temperature data - BH 87-10	130
5-1b	Time vs. temperature data - BH 87-10	131
5-2	Summary of geophysical data - BH 87-10	132
6-1a	Radar profile (offshore section) - April 1987, raw data	133
6-1b	Radar profile (offshore section) - April 1987, interpretation	134
6-2a	Radar profile (onshore section) - April 1987, raw data	135
6-2b	Radar profile (onshore section) - April 1987, interpretation	136
6-3a	Radar profile (onshore section) - September 1987, raw data	137
6-3b	Radar profile (onshore section) - September 1987, interpretation	138

7-1	Travel time vs. distance plot	139
7-2	Cross-section - top of permafrost	140
8-1	Laboratory results - BH 87-1	141
8-2	Laboratory results - CB 1	142
8-3	Laboratory results - BH 87-3	143
8-4	Laboratory results - CB 2	144
8-5	Laboratory results - BH 87-4	145
8-6	Laboratory results - BH 86-4	146
8-7	Laboratory results - BH 86-6	147

1. INTRODUCTION

P.J. Kurfurst

A multi-discipline program of detailed geotechnical investigations of the near-shore zone sediments was carried out off North Head, northern Richards Island near Tuktoyaktuk, N.W.T. in the spring of 1987. This program, undertaken in a zone of rapid coastal retreat in an area near proposed pipeline routes, was a continuation of investigations of the near-shore sediments carried out by the Geological Survey of Canada in this general area in previous years (Kurfurst, 1984, 1986). The majority of fieldwork, supported by a mobile camp, started March 28 and was completed April 9, 1987; specialized geological surveys continued until the end of April. Supplementary radar survey and thermistor cable installation were done during two weeks in August 1987. The general location of the investigated area is shown in Figure 1-1.

The objective of the program was to obtain detailed information required for evaluation of physical and engineering properties of the seabottom sediments in the near-shore zone and to compare them with their geophysical properties. These data will be used as the basis for a comparison between geophysical, geotechnical and thermal parameters of various soils at various ice contents.

The major part of the field program consisted of geotechnical drilling, sampling, instrumenting and testing of eleven offshore and two onshore-located boreholes and of various geophysical surveys.

The multi-disciplinary approach used throughout the program required participation of scientists and technical personnel from several scientific fields. The field participants, included J.G. Bisson, R.A. Burns, S.R. Dallimore, R.M. Gagné, R.L. Good, J.A. Hunter, A.S. Judge, P.J. Kurfurst, P. Lafleche and S.E. Pullan from the Terrain Sciences Division of GSC, C.R. Burn from University of British Columbia and L. Dyke from Queen's University. J.L. Morack and W.D.

Harrison from the University of Alaska in Fairbanks, U.S.A., evaluated and interpreted data collected during the field borehole heating experiment.

The program components included:

Geology and geological engineering: drilling, sampling, core logging, core temperature measurements, cone penetrometer tests, cone penetrometer temperature measurements, surficial mapping and frost heave tests.

Geophysics: uphole seismic measurements, temperature measurements, standard borehole logging (resistivity, natural gamma and SP), borehole heating test, seismic refraction measurements and ground probing radar surveys.

The details of the program field data are described and preliminary results are discussed in the following chapters.

2. GEOLOGY

S.R. Dallimore

Onshore conditions

A summary of the surficial geology of northern Richards Island is shown on Figure 2-1. The area is low lying with numerous small and large lakes, some of which have been either inundated by the sea or partially drained leaving flat-lying lacustrine basins. Upland areas are typically covered by a thin and discontinuous veneer of glacial till thought to be deposited during the early Wisconsin, Toker Point glaciation (Rampton, in press). The till is underlain by a sequence of older sands referred to by Rampton (in press) as the Kittigazuit and the Kidluit sands.

The differentiation of the Kittigazuit and Kidluit sands is sometimes difficult when examining outcrops in the area. The Kittigazuit sand is more common in the eastern part of the island where sections up to 15 m high expose fine-grained brown sand with large scale cross-stratification often over 5 m thick. The Kittigazuit sand is largely absent in exposures on the western part of the island where a fine- to medium-grained sand with occasional clay interbeds and shells is found. This sequence may represent the Kidluit sand or the Kendall sediments which are thought to occur beneath the Kidluit (Rampton, in press). Differentiation of the sand units is further complicated on the west side of the island by extensive faulting and folding caused by glaciotectionic deformation assumed to have occurred during the Toker Point glaciation.

Near-shore conditions

The near-shore zone is characterized by a transgressive sequence typified by a seaward thickening wedge of marine sediments unconformably overlying older sediments which were once subaerially exposed. Sediment supplied to the near-shore

zone is derived primarily from erosion of terrestrial material from the coast and by material entering the near-shore system from the Mackenzie River which debouches into the Beaufort Sea approximately 40 km to the west. The presence of the plume of sediment-laden Mackenzie River water can be easily detected during the summer from the air or by satellite photography.

The thermal regime of the near-shore area is complex with seabottom temperatures being affected by water depth, sea ice thickness, and the source of water. Sea water temperatures at the seabottom were collected during a 34-day period from July 29 to September 1, 1987. Seabottom temperatures, measured approximately 500 m offshore at the 1987 and the 1986 sites, show similar trends with periods of warm water temperatures (up to 10.7°C) and several short periods of colder water temperatures (about 4°C). The colder periods have been tentatively related to upwelling due to major storm events.

Ground ice

Ground ice is an important component of onshore materials occurring as pore ice, wedge ice, thin segregated ice lenses and massive bodies of nearly pure ice which may be over 10 m thick. Pingos, although common on Richards Island, are rare in the vicinity of the study area.

In the vicinity of the drill transect, ice wedges up to 0.5 m thick truncate surficial sediments and extend to 3-6 m depth. A zone of ice-rich sediments also occurs close to the surface, most likely representing recent aggradational ice. The most prominent ground ice occurrences are found in the lower sands. This ice has been substantially deformed by glacial activity, in a similar manner to the surrounding sediments, resulting in a complex ground ice pattern. A zone of brecciated ice, with individual clasts up to 1 m² in size, extends over a 50 m long vertical face approximately 200 m south of the drill

sites. In other areas isolated bodies of foliated ground ice are present in the sands. These ice bodies are often folded and have irregular shapes.

Coastal Retreat

Much of the present coastline of Richards Island is undergoing substantial coastal erosion. In areas where lakes occur close to the coast, this erosion may cause inundation of basin areas. The area of the 1987 drilling transect was part of Richards Island in 1935 when oblique air photographs were taken. The 1947 air photographs show that a low-lying lake basin had been breached and this area was actually separated from the main island.

A summary of the rates of coastal change, calculated by comparing the position of the coastline measured from vertical air photographs taken in 1947 and 1985, is shown on Figure 2-2. The average change of 1.8 m/a at the drilling transect results from a retreat rate of about 1.2 m/a from 1947 and 1973 and a retreat rate of 3.0 m/a between 1973 and 1985.

Observations of coastal retreat at the drill site have been made since 1986 and a detailed grid of survey markers was laid out during the summer of 1987. These studies suggest that a major part of coastal retreat at the site results from accelerated erosion during major storm events. During a two-week period at the end of August, when a major storm occurred, extensive undercutting and erosional niching was observed at the beach level along the entire upland area (horizontal distance of 420 m). The average undercut during this single event was estimated to be between 6 and 10 m deep and over 50 cm high. Head wall retreat averaged 1.7 m and rates as high as 2.8 m were measured. An estimate, made by considering uniform retreat of the cliff face at a rate equal to the head wall retreat, indicated that more than 10 000 m³ of material was removed during this period. This estimate is likely conservative, since removal of the debris cones and slough material which mantled the lower parts of the cliff, was not considered in calculations.

3. GEOTECHNICAL DRILLING AND TESTING

J.G. Bisson, S.R. Dallimore, P.J. Kurfurst

3.1 Drilling and Sampling

Thirteen boreholes, ranging from 15 to 33 m in depth, were drilled along a transect extending from 258 m onshore to 1500 m offshore. Two additional boreholes were drilled to depths of 3 m. Locations of all boreholes are shown in Figure 3-1. The borehole numbers, locations/chainage, depths, ice and water depths and type of sampling are summarized in Table 3-1.

Boreholes were drilled using a mobile CME 750 drill on rubber tires with top drive head. The seven offshore boreholes were drilled using fluid while the remaining boreholes were dry-cored using a CRREL barrel.

An HW-casing drill string was used in wet boreholes with mud return at sea bottom. Bentonite and KCl were used as drilling mud. Shelby tube samplers or split spoon samplers (7.6 cm diameter) were deployed through the casing to collect up to 90 cm long cores at 1.5 m intervals. Near-shore and onshore boreholes that were entirely frozen were cored with a CRREL barrel backed with 12 cm diameter flight augers which produced a continuous 10 cm diameter core.

All cores retrieved by the drillers were passed to the GSC staff for further handling. The temperature probe was immediately inserted in the bottom of all unfrozen and marginally frozen cores to record their temperatures. The core was then extruded into a split PVC casing, its length was measured and the core was photographed. A brief soil type description, and the presence of ground ice and its type, when observed, were then recorded. Samples for future standard physical tests were then selected and transferred into containers and the remaining samples were sealed and transported to the Ottawa laboratories to be stored for future detailed logging and specialized tests.

Table 3-1
Borehole Information

Borehole	Location/Chainage (m)	Depth (m)	Ice depth (m)	Water depth (m)	Samples
BH87-1	0+006	30.30	1.00	---	CRREL
BH87-2	0+025	30.50	1.04	---	CRREL
BH87-3	0+050	28.45	1.60	---	CRREL
BH87-4	0+082	21.00	1.27	---	CRREL
BH87-5	0-075	30.80	--	---	CRREL
BH87-6	0-258	30.18	--	---	CRREL
BH87-7	0+300	32.25	1.80	1.60	Shelby
BH87-8	0+150	34.40	1.70	1.35	Shelby
BH87-9	0+227	15.15	1.85	1.20	Shelby
BH87-10	0+600	32.45	1.85	1.70	Shelby
BH87-11	1+000	33.86	1.80	1.88	Shelby
BH87-12	1+500	31.88	1.85	1.95	Shelby
BH87-13	0+525	30.45	1.85	1.80	Shelby
CB-1	0+035	3.15	1.10	---	CRREL
CB-2	0+064	3.02	1.60	---	CRREL

The sediments encountered ranged from clays and silts to sands; ice type documented in the cores varied from visible ice bonding to massive ice lenses. The geological and ground ice conditions are summarized in simplified cross-sections presented in Figures 3-2 and 3-3 respectively. The detailed information for each borehole is given in Figures 3-4 to 3-16.

Four holes were drilled during the spring 1987 field program, using hydraulic jetting, for installation of thermistor cables. The depth of these holes ranged from 10.9 to 16.0 m. Six additional holes were jet-drilled during August 1987, to depths varying between 13.5 and 33.0 m (Northern Seismic Analysis Ltd., 1987) and were instrumented with thermistor cables. The detailed information about the jet-drilled holes is presented in Table 3-2.

Table 3-2
Jet-drilled Hole Information

Hole	Location/Chainage (m)	Depth (m)	Ice depth (m)	Water depth (m)
JD-1	0+100	12.1	1.80	0.30
JD-2	0+200	10.9	1.80	1.60
JD-3	0+400	13.7	2.00	1.80
JD-4	0+500	16.0	1.80	2.00
NSA-82	0+082	33.0	--	1.30
NSA-100	0+100	32.5	--	2.10
NSA-200	0+200	14.0	--	2.90
NSA-400	0+400	13.5	--	3.50
NSA-500	0+500	17.2	--	3.60
NSA-600	0+600	14.8	--	3.60

3.2 Cone Penetration Tests (CPT)

The cone penetration tests were carried out between April 6 and 9, 1987 as part of the drilling program (ConeTec Investigations Ltd., 1987). A 10 ton Hogentogler subtraction-type cone was used for all soundings. The cone recorded the following parameters at 5 m intervals during each test: tip resistance, sleeve friction, dynamic pore pressure, temperature, cone inclination, and shear and compressional wave velocities. These parameters, excluding the acoustic wave velocities, were simultaneously printed and stored on a cassette cartridge for future analysis and reference. A complete set of baseline readings was taken prior to and after the completion of each sounding to determine temperature shifts and zero load offsets.

Cone penetration tests were located from 3 to 5 m from the existing boreholes to avoid any disturbance which may have been caused by drilling, or at locations requiring additional CPT or thermal data (Figure 3-1). Prior to each test, a hole was augered through the ice and steel casing was set to the mudline to prevent buckling of the cone rods during penetration. The cone was pushed using the CME 750 drill rig used for borehole coring. A total of eight cone penetration tests were carried out to depths ranging from 12.5 to 19.7 m below seabottom. Table 3-3 presents a summary of CPT locations and penetration depths.

The CPT data in graphical form are given in Figures 3-17 to 3-24.

Interpretation of the CPT data shows that the soils in the study area consist of soft silt with some clay from the mudline to depths which varied between 0.7 and 2.0 m. This deposit is underlain by a layer of stiff, overconsolidated

Table 3-3
Cone Penetration Test Information

CPT	Location/Chainage (m)	Penetration below seabottom (m)
CP10/C87-04	0+600	13.75
CP11/C87-01	0+300	13.60
CP12/C87-02	0+450	16.70
CP13/C87-06	1+000	12.50
CP14/C87-08	1+500	15.85
CP15/C87-07	1+250	19.70
CP16/C87-05	0+800	15.75
CP17/C87-03	0+525	13.55

Note: CP11 test was stopped on frozen ground, remaining CPT were stopped on dense sand.

clayey silt with fine sand seams. Beneath the silt, a layer of dense sand extends to depths of 20 m below mudline. The cone penetration tests were stopped on dense sand layers or at the contact with permanently frozen ground. Ice bonded materials can be identified on the cone records by pore pressure and temperature response. Contact with ice results in the generation of high positive pore pressures and recording of negative (below 0°C) temperatures.

Soil temperature measurements were taken during six CPT soundings. The temperatures fluctuated significantly during actual penetration, depending on the nature of the material being penetrated. Penetration through cohesionless soils with high sleeve friction values generated substantial amount of heat, causing temperatures to rise several degrees Celsius above the ambient temperature. In order to establish the equilibrium soil or water temperature at specific depth, the change in temperature with time was recorded for intervals ranging between 500 and 1000 seconds. After reviewing the records and comparing these data with thermistor cable data, it was concluded that a dissipation time of about 600 to 900 seconds was sufficient to obtain accurate ambient equilibrium temperatures. Figure 3-25a, showing typical temperature dissipation records for sand and clayey silt, clearly illustrates the longer dissipation time required for sands.

Temperature records obtained at varied depth intervals during six cone penetration tests show that ground temperatures are generally lower closer to the shore and increase with increased distance from the shore. These profiles also show that ground temperatures increase with depth (from -0.2° to 1.3°C) and then gradually decrease as the cone penetrates closer to the permanently frozen ground. The ambient temperature of the sea water at the mudline was found, to be relatively constant at -0.2°C .

When the CPT temperature data are compared to the thermistor cable data, there is an excellent agreement with variations of less than $\pm 0.2^{\circ}\text{C}$. Figure 3-25b shows a comparison of temperature data measured by at a thermistor cable (BH87-7) and by the cone penetrometer in the adjacent CPT hole (CP11) at Station 1+500.

4. BOREHOLE GEOPHYSICAL TESTS

J.A. Hunter, S.E. Pullan, R.A. Burns. R.M. Gagné and R.L. Good

4.1 Temperature measurements

Thermistor cables were installed in boreholes drilled in April and August 1987 in order to provide detailed information on winter and summer thermal regime along the drilling transect.

April 1987

Each of the thirteen geotechnical boreholes drilled during April 1987 was cased with 5 cm diameter plastic pipe (PVC), and filled with a mixture of antifreeze and water. Thermistor cables were then installed in the cased holes. Each cable consisted of 12 YSI 44033 thermistors (accurate to within 0.1°C), with the upper three thermistors 1.5 m apart and the lower nine thermistors 3 m apart. The total active length of the cable was 30 m. In cases where the borehole was drilled to less than 30 m (BH-87-9), or slumping prevented the installation of the plastic pipe to the full borehole depth (BH-87-4), the thermistor cable was doubled back to provide 1.5 m spacing over a total active length of 16.5 m.

In addition to the thirteen geotechnical boreholes, thermistor cables were installed in four holes that were drilled using hydraulic jetting techniques at Stations 0+105, 0+200, 0+400 and 0+500 m offshore. In these holes the cables were installed in the 2.5 cm diameter steel pipe that was used for jetting, again in a mixture of antifreeze and water. These four holes were all shallow, reaching a maximum depth of only 16 m below ice surface due to the difficulty of jet-drilling in unfrozen sand.

All thermistor cables were monitored daily from the time of installation immediately after drilling until equilibrium temperatures were re-established.

Midway during the survey, temperature measurements indicated that the extreme temperature gradients in the upper portion of the boreholes on land (BH-87-6 and BH-87-5) and those offshore where the ice was frozen to seabottom (BH-87-1 to BH-87-4) were causing thermal instabilities in the antifreeze mixture inside the plastic pipe. The first attempt to prevent this by adding neoprene baffles to the cable between each thermistor was only partially successful. The problem was finally solved by re-installing the thermistor cables inside 2.5 cm diameter steel pipe, which was placed inside the original plastic casing.

Final equilibrium temperature profiles for each of the thirteen boreholes and four jet-drilled holes are shown in Figures 4-1 to 4-17. They clearly illustrate the general warming trend from onshore to offshore, as well as the strong cold wave in the upper part of the profiles of the onshore and near-shore boreholes.

The data are presented in section form in Figures 4-18 and 4-19. Figure 4-18 shows the entire temperature section from 300 m onshore to 1500 m offshore with a vertical exaggeration of X10. Figure 4-19 is a blow-up of the shoreline section with no vertical exaggeration. These sections show the warming trend from an onshore equilibrium temperature at 10 m below surface of -8°C , to offshore (>500 m offshore) temperatures at 10 m below seabottom above 0°C . In the near-shore region, a warm bulb is present where the winter cold wave is superimposed on the general warming caused by the inundation of the Beaufort Sea. An obvious break is observed between 85 and 105 m offshore where the water is too deep to be frozen to bottom. At this point the winter cold wave is no longer transmitted into the sediments and freezeback does not occur at the seabottom.

August 1987

A further set of temperature measurements was obtained in August 1987 (Northern Seismic Analysis, Ltd., 1987). One cable onshore (BH-87- 6) and those within 50 m off the shoreline (BH-87-1 to BH-87-3) had survived break-up and could be read again. The hydraulic jet-drilling technique was used to drill 7 additional holes to install temperature cables. However, difficulties encountered with rough seas while drilling and attempting to obtain temperature measurements resulted in only a limited amount of equilibrium temperature data from August/September 1987.

Summer temperature profiles for boreholes BH-87-6, BH-87-1 to BH-87-3 and the jet-drilled hole at BH-87-4 respectively are shown in Figures 4-5, 4-1 to 4-3 and 4- 14 alongside the winter measurements. The summer time warming at the surface can be seen propagating downwards in boreholes BH-87-6, BH-87-1 and BH-87-2. The residual of the cold wave from the previous winter can be seen at a depth of approximately 10 m. Further offshore (BH-87-3 and BH-87-4), both the warm and cold pulses are reduced in amplitude because of the insulating effect of the water.

A summer time section of the temperature data at the shoreline is shown in Figure 4-20. It clearly shows the reversal of the temperature gradient in the upper 6 to 8 m below ground surface in comparison to the winter time section (Figure 4-18). The point at which the water is frozen to bottom in the winter (approximately 95 m offshore) again marks a substantial change in the thermal regime. Beyond this point warming and melting of the permafrost proceed at a faster rate because no cold wave reaches the sediments.

4.2 Borehole Logging

Resistivity, spontaneous potential (SP), and natural gamma logs were measured with a portable analog logging system (OYO Geologger 3000). For various reasons, which will be discussed below, it was not possible to run all three logs in each of the thirteen boreholes. However, the logs that were obtained show

remarkably good correlation with the geological logs, and are an excellent illustration of the usefulness and importance of borehole logging.

The resistivity and SP logs had to be run in a fluid-filled uncased hole, and so were obtained immediately after completion of drilling before the plastic casing was lowered into the borehole. For the onshore and near-shore boreholes which were dry, it was necessary to fill them with water before the logs could be run. For the offshore boreholes, the drill rig had to be held on site while the logs were run.

The resistivity logging required two current electrodes to be planted at the surface close to the borehole, and two potential electrodes lowered down the hole. The Geologger normal resistivity probe has three switch-selectable potential electrode spacings ($a = 0.25, 0.50$ and 1.00 m). The larger spacings average the response over a greater volume of material surrounding the borehole.

The SP logging required one current electrode on surface and one electrode in the borehole. The results can be affected by temperature variations in the probe and by any salinity in the fluid in the borehole. It was found very difficult to obtain reproducible results in this survey. Only two SP logs that respond to geological signals (BH87-1 and BH87-11) are included in the figures.

The natural gamma logs could be run in the antifreeze/water-filled plastic casing, and so were not subject to the time constraints imposed on the electrical logs. As a result, there are natural gamma logs for all boreholes except those in which a bend or constriction in the plastic pipe prevented lowering of the gamma probe.

BH-87-1 (0+006 m, Figure 4-21)

All three logs were obtained for this borehole, though the electrical logs could not be run in the upper half of the borehole due to the water draining

away through fractures or unfrozen zones. The resistivity logs indicate a highly resistive layer from 13.5 to 16 m below surface, perhaps indicating high ice content. From 17 to 21 m below surface is a zone of lower resistivity with a positive SP response which corresponds to a siltier layer on the geological logs. The organic-rich sand at the bottom of the borehole produces a strong resistivity response. The natural gamma log is an excellent indicator (0 cps) of the massive ice found at the surface (0-1 m) and in the upper portion of the borehole (3.5-8 m).

BH-87-2 (0+025 m, Figure 4-22)

The resistivity logs for this borehole are very similar to those for BH-87-1 with zones of high resistivity from 13.5 m to 16.5 m below surface (excess ice?), and below 26.5 m (organic-rich sand). The layer of massive ice from 2.5 to 6 m below surface is also indicated by a zone of high resistivity. Although the natural gamma log could only be run to 4 m below surface because of an ice-block in the plastic casing, it is an excellent indicator of massive ice lenses.

BH-87-3 (0+050 m, Figure 4-23)

No resistivity or SP logs were recorded for this borehole because of difficulties in coupling the current electrodes to the ground through 1.5 m of sea ice. The natural gamma log clearly delineates the layer of sea ice at the surface, and gives an indication of the ice-rich zone from 25.5 to 26.8 m below surface. The average counts/second (cps) also appear to be slightly lower (<10 cps) at 15 m and 16 m below surface which may indicate other ice-rich zones not documented in core samples.

BH-87-4 (0+082 m, Figure 4-24)

No resistivity or SP log were obtained for this borehole because of slumping. Only 12 m of plastic pipe could be pushed into the hole though 22 m were drilled. A natural gamma log obtained for the upper 12 m clearly shows massive ice at the surface.

BH-87-5 (0-075 m, Figure 4-25)

Both the resistivity and natural gamma logs for this borehole are striking indicators of the massive ice body from 17 to 27 m below surface; both logs also respond well to the thin sand layer within the ice at 25 m. The natural gamma log shows a slightly higher count rate (18 cps) in the clay unit from 15 to 17 m below surface, and a low count rate (<10 cps) in the ice-rich zones from 2.5 to 4 m below surface and from seabottom to 1 m below surface.

BH-87-6 (0-258 m, Figure 4-26)

The ice lenses encountered in this borehole from 5.5 to 6 m and from 23.6 to 24.3 m below surface can be seen as high resistivity anomalies on the resistivity logs and as zones of near-zero counts on the natural gamma log (the depths do not agree with the geological log, as the starting point on this log was determined incorrectly). A small resistivity high at 9 m depth corresponds to a low count zone on the natural gamma log and may indicate an ice vein or lense. A small resistivity low between 12 and 13 m below surface may indicate a thin layer of silt or clay.

BH-87-7 (0+300 m)

This borehole was cased with plastic pipe immediately after completion of drilling to avoid losing the hole completely due to slumping, thus preventing recording of either resistivity or SP logs. The plastic pipe bent at the bottom of the ice when it froze in, and it was impossible to get the gamma probe down the hole. No geophysical logs are available for this borehole.

BH-87-8 (0+150 m, Figure 4-27)

The drill casing was pulled up to 9 m below ice surface and left there while the resistivity logs were run to prevent any slumping of the unfrozen materials at the seabottom. The resistivity logs show four distinct zones below this depth. A zone of low resistivity from 11 to 15 m below surface corresponds to a marginally frozen sand layer with low ice content. The high ice-content layer from 15 to 19 m below surface is indicated by high resistivities. The small resistivity anomaly at 23 m suggests that a zone of interbedded sands and silts contains a thin ice-rich layer. Finally, the organic-rich sand which was seen at the bottom of boreholes BH-87-1 and BH-87-2, is again indicated by very high resistivities below 28 m. No natural gamma log is available for this borehole because a bend in the plastic casing in the sea ice prevented insertion of the probe.

Borehole-87-9 (0+226 m, Figure 4-28)

No resistivity or SP logs are available for this borehole, which was cut short at 14.5 m below the surface. The natural gamma log shows a near-zero count rate through the sea ice and water column. The only anomaly on the log is a low count rate between 13 and 13.5 m below surface which could indicate an ice-rich layer at this depth.

Borehole-87-10 (0+600 m, Figure 4-29)

No resistivity or SP logs are available for this borehole because it was slumping in, and was cased with plastic pipe before pulling the drill casing. The clay layer from seabottom to 12 m below ice surface is indicated by the slightly higher count rate in this zone (20 cps) than in the sand layer below (15 cps). The

clay layer at the bottom of the borehole may also be indicated by the high count rates recorded at the very end of the log.

Borehole-87-11 (1+000 m, Figure 4-30)

All three logs were obtained for this borehole. The low resistivity values (note the change of scale on the figure in comparison to previous boreholes) indicate unfrozen materials. All three logs show an anomaly between 17 and 18 m below surface which cannot be explained by the geological log. This anomaly could be caused by a higher silt or clay content than in layers above or below it. The natural gamma log clearly indicates the clay layer from seabottom to 11.5 m below ice surface (20 cps). The bottom of this layer may also be indicated on the resistivity logs, though the drill casing prevented electrical logging through most of the clay. The clay at the bottom of the borehole appears to be indicated by the high count rates below 32 m.

Borehole-87-12 (1+500 m, Figure 4-31)

No resistivity logs were obtained for this borehole because of a break in the connection to the probe. Only 15 m of plastic casing could be put down the hole, so the natural gamma log only goes to that depth. The log again clearly indicates the clay/sand contact at 9 m below surface.

Borehole-87-13 (0+525 m, Figure 4-32)

Only two resistivity logs were obtained for this borehole because of a break in the probe, but they show several interesting features. The change from higher to lower resistivity at 14 m below surface marks the clay/sand interface which can also be seen clearly on the natural gamma log. The clay layer from 21 to 23 m is indicated by a high natural gamma count. Three zones of high resistivity

are found between 22 and 31 m below surface. It is possible that these correspond to icy zones in the massive sand layer in this depth range. The clay at the bottom of the borehole is clearly indicated by the high count rate on the natural gamma log below 32 m.

4.3 Uphole Seismic Measurements

Uphole seismic measurements were made in ten boreholes (BH-87-1, BH-87-3 to BH-87-11) in order to determine the compressional wave velocity as a function of depth.

A single seismocap was used as a source of acoustic energy. For the onshore and near-shore boreholes, the seismocap was detonated in the bottom of a small drillhole (0.6 - 1 m deep) 1 m away from the borehole. The shot hole was filled with water or antifreeze/water to improve the coupling to the ground. For the offshore boreholes, a hole was drilled through the ice, and the seismocap was detonated in the water just beneath the ice.

The receiver was a hydrophone hanging freely in the fluid-filled plastic-cased borehole. The receiver was moved up the hole in 1 m increments and the signals were recorded using either a Nimbus 1210F or ES-1225 engineering seismograph and a digital tape recorder.

The data were transferred to floppy disk storage and the arrival times of the acoustic energy were picked using interactive routines on a microcomputer. The distances travelled were determined from the depth of the receiver with corrections for the shot offset and shot depth.

Data quality was excellent, and errors in picking the times of arrival are estimated to be in the order of ± 0.05 ms for most boreholes. The exceptions are BH- 87-10 and BH-87-11 where interference from a casing wave caused a deterioration in the quality of the data. Hydrophone position errors are estimated

to be ± 5 cm. One other potential source of error with the single receiver system is the accurate determination of zero time. Tests with a reference phone located close to the shot in two of the offshore boreholes suggest that this uncertainty is also within 0.05 ms.

A conservative approach has been used to interpret interval velocities as a function of depth. The travel-time/distance (t - x) data were plotted (Figures 4-33a to 4-42a), but because of the difficulty in accurately differentiating subtle changes in slopes on these plots, "reduced" travel-times were plotted to enhance the breakovers. The reduced travel-time (t_R) is defined as:

$$t_R = t - \frac{x}{V_R}$$

where

- t = measured travel time
- x = distance travelled
- V_R = reducing velocity

The reduced travel times (t_R) are plotted against distance travelled (x) in Figures 4-33b to 4-42b. It is obvious that changes in slope are greatly enhanced in this presentation of the data. Error bars of ± 0.10 ms are shown on these plots, and individual line segments were then fitted to these data. The velocity structure is defined in terms of layers several metres in thickness, since no line segment was considered unless it could be defined by more than two points.

The t - x data corresponding to each line segment were then used to determine an interval velocity by least-squares analysis. The line segments and interval velocities are shown on the t - x plots in Figures 4-33a to 4-42a, and are plotted against depth below ice surface in Figures 4-33c to 4-42c so that they can be compared directly to the geological logs.

Ice-bonded materials in the onshore and nearshore boreholes are characterized by compressional wave velocities that are of the order of 3000-3500 m/s. Excellent correlation between the geological log and the interval velocities was found in borehole BH-87-5 (Figure 4-36). The icy material at the top of the hole has a very high velocity of 4220 m/s, while the brown sand from 4.5 to 15 m below surface has a well-determined velocity of 3310 m/s. The 2 m clay layer 15 m below surface is characterized by a slightly lower velocity of 2850 m/s and this layer can be clearly seen on the reduced travel-time plot (Figure 4-36b). The massive ice below 17 m has a higher velocity of 3760 m/s.

Borehole BH-87-3 illustrates the ability of uphole seismic measurements to pinpoint the top of ice-bonded material. It is clear from Figures 4-34, that a substantial increase in velocity occurs at a depth of approximately 12 m. This marks the interface between material which may be marginally frozen but is not ice-bonded, and ice-bonded material below.

Moving farther offshore (150 to 300 m, boreholes BH-87-7 and BH-87-8, Figures 4-38 and 4-39), these measurements indicate that the marginally frozen sand (-1° to -3°C) is characterized by a compressional wave velocity of approximately 1900 m/s. Where temperatures have reached 0°C , 1 km offshore, typical sand velocities of 1650 m/s are found (BH-87-11, Figures 4-42).

5. BOREHOLE HEATING EXPERIMENT

J.L. Morack and W.D. Harrison

Scientists from the University of Alaska were invited to participate in the 1987 Geological Survey of Canada spring drilling program in the Beaufort Sea. One of the boreholes drilled (BH87-10) during this program was electrically heated and its temperature response was measured. The field results were then evaluated and interpreted at the University.

The drill log of the borehole shows clay extending from the seabottom to a depth of 8.8 m, underlain by sand to the bottom of the borehole. The log shows no frozen sediments above 23.5 m depth. The bottom of the heater was therefore placed at 25.2 m depth to ensure its location within the ice bearing sediments. The uphole seismic survey of this borehole measured compressional velocities of 1625 m/s from the seabottom to about 16 m depth and 1765 m/s from 16 m to the bottom of the borehole.

The borehole was heated with 37.8 W/m for 5.8 hours, which in most cases was sufficient to raise the temperature several degrees Celsius. The temperature was then monitored at several depths for seven days until all sediments returned to thermal equilibrium. Where no ice is present, the approach to equilibrium after heating can usually be interpreted to give the thermal conductivity. For the cylindrical geometry used (Harrison and Morack, 1985), the temperature response, T , is given by the expression.

$$\Delta T = (P/4\pi k) \ln(t/t-s),$$

where P is the power per unit length, s is the time of heating, k is the thermal conductivity, and t is the time elapsed since the start of the heating. Analysis of the borehole data at several depths is shown in Figures 5.1a and 5-1b. The time scales shown in these figures indicate the relationship between the \ln function and

the time elapsed after the heating was stopped. Because of the finite size of the iron pipe containing the heating cable, the thermistor string, and ethylene glycol, the data from the early phase of the heating experiment do not fit the theory. However, after a short elapsed time the data follow a straight line. The data from a depth of 17.7 m and below do not follow the theory. The cooling curves (Figure 5-1b) level off indicating that refreezing of the material had started. Further drop of the cooling curves toward the equilibrium temperature indicates that the material has completely refrozen. The measured slopes of the curves at the depths of 2.7, 5.7, and 8.7 m equate to the thermal conductivity values of 1.24, 1.28 and 1.28 W/mC respectively. The curves at 11.7 and 14.7 m depths equate to the thermal conductivity of 1.59 and 1.61 W/mC indicating a more conductive material than those above. The limited data from the depths below 14.7 m, although indicating presence of the ice-bearing sediments, preclude calculations of the thermal conductivity for these materials.

A summary of the geophysical data is given in Figure 5-2. The drill log indicates frozen materials below 23.5 m. The heating data indicate presence of ice-bearing materials from 16 m depth. This discrepancy is due to use of warm drilling fluid which often melts partially frozen soils before they can be visually detected. The seismic data clearly indicate the boundary between the ice-free and ice-bearing materials, but do not detect the material change at 8.8 m depth as recorded in the drill log. The heating experiment thus allows a significantly better correlation of the geophysical and drill log data as well as determination of the thermal conductivity of the ice-free materials.

The heating experiment can also contribute to better determination of the equilibrium temperatures of the ice-bearing materials. Figure 5-1b shows presence of the ice-bearing materials and the cooling curves show when the material has completely refrozen. This effect can be easily missed if only temperature versus

time curves are plotted. The slope of the curve after this point can then be used to accurately determine the correct equilibrium temperature of the sediments.

6. GROUND PROBING RADAR

P. Lafleche and A.S. Judge

Ground probing radar (GPR) surveys were conducted along approximately 1 km of the drilling transect during April and September of 1987. The April survey included five offshore and two onshore common depth point (CDP) soundings and cross-lines, perpendicular to the main transect, surveyed at offshore Stations 0+025, 0+056, 0+075, 0+200 and 0+300 m and at onshore stations 0-075 and 0-258 m. The September survey included only the onshore portion of the transect. The equipment used was an A-cubed Inc. Pulse EKKO III Digital GPR system. The operational frequency was 50 MHz and transmitter-receiver antenna separation used was 2 m. Station spacing was 2 m and 1 m for the April and September surveys respectively. The onshore section extended from Station 0-010 m to Station 0-450 m, while the offshore survey covered two areas between Stations 0+004 and 0+500 m and between Stations 0+750 and 0+850 m (Fig. 3-1).

Offshore Transect

Figure 6-1a and 6-1b respectively show the raw data and their interpretation of the offshore portion of the main transect radar profile. CDP soundings indicate that the radar propagation velocity in the sea ice is 0.14 m/ns which is consistent with other known ice velocity measurements. The velocity of the thin sea water layer (up to 1.5 m) has been calculated at 0.03 m/ns using published (A-Cubed Inc., 1983) values for the permittivity and conductivity of sea water measured at 100 MHz frequency. The velocity of the unfrozen seabottom sands has been similarly calculated at 0.06 m/ns. The ice grounding line is visible in the radar profile at Station 0+100 m. A two-layer model (ice, unfrozen sand) and a three-layer model (ice, sea water, unfrozen sand) respectively have been used for interpretation of data from the onshore and offshore section from the grounding

line on the transect. Numerous fractures in the ice, readily observable on the surface as cracks up to 6 cm wide, are visible on the profile at Stations 0+90, 0+110, 0+365 and 0+480 m.

Layering within the soil is visible on the profile between stations 0+010 and 0+025 m and is attributed to banding within the fine- to medium-grained sands. Signal reflections from the cliff face obscure the deep ground reflectors within the sediments for the first 30 m of the profile. Massive ground ice, intersected in boreholes BH87-1 and BH87-2, is visible on the radar profile between Stations 0+060 and 0+025 m. A broad reflector directly under borehole BH87-7 most likely represents the 1 m thick clayey silt horizon identified by drilling.

The shaded areas around boreholes BH87-3 and BH87-4 show the effects of the boreholes as multiple reflections are caused by pulses propagating up and down the boreholes. Stratification within the soil is also visible on the radar profile between Stations 0+120 and 0+140 m and Stations 0+155 and 0+215 m.

Onshore Transect

Figures 6-2a, 6-2b, 6-3a and 6-3b show the raw data and their interpretation of the onshore portion of the main transect radar profile, as surveyed in April and September 1987. The penetration of the radar pulse is much more limited than in the offshore survey. The September survey, carried out late in the thaw season, shows extremely limited penetration of the radar signal.

The onshore portion of the transect is characterized by a peat layer underlain by a diamicton and thick sand horizon, as much as 15 m thick. A strong reflector, corresponding with the boundary between the diamicton and underlying sands, is marked on the profile (Figures 6-2 and 6-3). A 2 m thick clay unit was detected between 3 and 5 m depth in borehole BH87-6. Although its presence is not clearly visible in the radar profile, stratification in the soil is evident at this

location. Several linear reflectors have been recognized between stations 0-250 m and the end of the profile. These are interpreted as variations in grain size within the sand horizon. The radar survey cannot penetrate through to the base of the sands using the 50 MHz operational frequency.

7. SEISMIC REFRACTION MEASUREMENTS

K.G. Neave and H.A. MacAulay

An additional set of temperature measurements and a seismic refraction survey along the drilling transect to approximately 600 m offshore were carried out in August 1987 (Northern Seismic Analysis Ltd., 1987). The objective of the refraction survey was to determine the depth to the top of ice-bonded material (characterized by high seismic velocities) as a function of distance from the present-day shoreline.

The refraction seismic survey was carried out between 50 m and 600 m offshore. A hydrophone cable with 15-m spacing and a digital 12-channel recording system were provided by the GSC. The cable was spread along the line and moved three times to give continuous coverage between 100 and 600 m. Additional off-end shots were recorded to cover the zone between 50 and 100 m. Intermediate shot points near 300 and 400 m provided redundant coverage of parts of the line and allowed confirmation of the refraction velocity.

The interpretation was carried out using a time-term analysis. The time-distance plot in Figure 7-1 shows a high velocity refractor on both the forward and reversed data. There is some scatter in the arrival times, which is taken as an indication of some variation in the depth of the refractor. The offshore shot-point at 500 m also has a low-velocity component at 1.56 km/s.

When the forward arrival times are subtracted from the reverse times, the differences indicate the refractor velocity. The redundant readings confirm that the high velocity is 3.2 km/s.

The delay times for each detector provide a cross-section (Figure 7-2). This depicts a sloping hummocky upper surface for the high-velocity permafrost. Its depth increases from 1 to 2 m at 75 m offshore to 75 m at the 600-m station. The depths are minimum values since the velocity of the upper layer may be greater than

the 1.5 km/s assumed in this interpretation (see discussion of Uphole Seismic Measurements in Chapter 4.3).

The temperature data can be compared to the seismic data 100 m offshore where the depth of the high velocity refractor is 22 m. On the temperature profile (Figure 4-4), the temperature at this depth is approximately -3.2°C . One must assume low ice content in the sediments above 22 m to explain the low velocity in those sediments.

8. FROST HEAVE TESTS

C.R. Burn

Although the presence of frozen materials in submarine environments is well-documented, little attention has been paid to ice segregation and thaw settlement, processes commonly associated with the development and decay of ground ice, in offshore sediments. This chapter describes briefly an investigation of winter frost heave in the uppermost two metres of five boreholes drilled along the 1987 drilling transect, and two boreholes drilled along the 1986 drilling transect (Kurfurst, 1986).

During the summer, when warm Mackenzie River water covers the coastal sediments, an active layer similar to that on land develops in the sea bed sediments. After sea ice has frozen to the seabottom in winter, cold temperatures penetrate the underlying sediments. Such frost penetration may result in seafloor heave, however the salinity of pore water and the coarse texture of the sediments should restrict ice segregation.

Sampling and Laboratory Analysis

Core samples from five boreholes drilled along the 1987 transect (BH87-1 at 0+006 m, CB1 at 0+038 m, BH87-3 at 0+050 m, CB2 at 0+064 m and BH87-4 at 0+082 m) and from two boreholes cored at Stations 0+100 (BH 86-4) and 0+300 m (BH86-6) along the 1986 transect were used for frost heave analysis and tests.

Frozen core was cut into 10 cm long samples, when possible, weighed and the bulk density was determined. The core was then thawed in closed, tight-fitting containers, and the amount of water released was measured. This data provided an estimate of the excess water content of each 10 cm interval and, hence, of frost heave. A sample from the remainder of the core was oven-dried to determine gravimetric water content.

The total water content of each sample, calculated as a gravimetric quantity, was determined by adding the mass of water released on thawing to the water content of the remainder. The volumetric ice content was calculated by multiplying the total water content by factor 1.09 and dividing by the volume of the sample. The electrical conductivity of pore water from the samples was also determined. The following parameters, formulas and units were used for calculations:

$$\begin{aligned} \text{Bulk Density:} & \quad \frac{\text{Mass of frozen core } M_t}{\text{Volume of core } V_t} \quad (\text{gcm}^{-3}) \\ \text{Gravimetric water content:} & \quad \frac{\text{Mass of water } M_w}{\text{Mass of solids } M_s} \quad (\%) \\ \text{Volumetric ice content:} & \quad \frac{\text{Volume of water } V_i \times 1.09}{\text{Volume of core } V_t} \quad (\%) \\ \text{Excess ice content:} & \quad \frac{\text{Volume of excess water } V_i - V_i \text{ sat} \times 1.09}{\text{Volume of core } V_t} \quad (\%) \\ \text{Conductivity of pore fluid:} & \quad (\text{mmhos cm}^{-1}) \end{aligned}$$

Core description

A summary description of core recovered is presented in Table 8-1. Although sea ice had frozen to the seabottom at all sites, and subsequent measurements indicated that the temperature of the ice-sediment interface was about -3°C , sea water flowed into the boreholes at sites BH87-3, CB-2, and BH87-4.

Table 8-1

Detailed Borehole Stratigraphy

BH 87-1 (0+006 m)

100-125 cm	Sand, brown, with thin bands of clay (diamicton), pebbles >1 cm, Nbn
125-131 cm	Sand, brown, massive
131-135 cm	Diamicton
135-190 cm	Sand, brown, massive, ice lenses 1-2 mm thick, Nbn
From 190 cm	Sand, silty, few ice lenses

CB 1 (0+035 m)

120-145 cm	Clay, silty
145-200 cm	Clay with sand bands, thin ice lenses
200-220 cm	Sand, ice lenses 1 mm thick, Nbn
From 220 cm	Massive ice

BH 87-3 (0+050 m)

245-255 cm	Sand, fine, thin ice lenses, Nbn to V _r
255-300 cm	Silt, clayey with sand, Nbn to V _r
310-420 cm	Sand, brown, massive

CB 2 (0+064.5 m)

160-185 cm	Sand, brown with pebbles and silt
185-198 cm	Sand, brown with ice lenses
198-200 cm	Sand with opaque, spherical ice bubbles
From 200 cm	Sand, unfrozen, slurried

BH 87-4 (0+082 m)

128-139 cm	Sand, brown, Nbe
139-141 cm	Ice lenses
141-144 cm	Sand, brown
144-161 cm	Ice with sand inclusions
161-170 cm	Sand with ice inclusions
170-220 cm	No recovery
220-255 cm	Sand, occas. pebbles and clay bands
From 255 cm	Sand, massive

BH 86-4

36-39 cm	Sand, slurried
39-78 cm	Sand, massive
78-105 cm	Sand, massive, ice lenses and ice spheres
105-158 cm	Sand with organics, occas. ice laminations
158-172 cm	Sand

BH 86-6

105-108 cm	Clay, organic, 2 mm thick ice lenses
108-120 cm	Sand, brown
120-160 cm	Sand, brown to grey with laminations. Evidence of cryoturbation from 134 to 138
160-290 cm	Sand, brown

As a result, core recovery from these boreholes was poor and some cores were poorly preserved. For example, only 40 cm of core was recovered intact from borehole CB2. The remainder of the core was unbonded and unfrozen, although subsequent temperature measurements indicated that this material should have been well frozen.

Three main types of ice were recognized in the intact core:

- (1) Large ice lenses (at least 1 cm thick) were encountered in several cores. In core from borehole BH87-4, a lens 1.5 cm thick was observed 11 cm below the sea bottom and the interval from 16 to 33 cm below the sea bottom was principally composed of ice.
- (2) Thin ice veins and lenses (about 1 mm thick) were frequently encountered throughout fine-grained soils. Similar type of ice was observed in coarser material, although less frequently.
- (3) Massive ice was observed in cores from boreholes BH87-1 and CB-1.

Results and Discussion

Temperature measurements taken at the drill sites in August 1986 and repeated in August 1987 indicate that all sites described in this chapter are underlain by frozen materials (Kurfurst, 1986). The active layer depth along the offshore portion of the transect, determined from ground temperature measurements and by probing in August 1987, varied from 80 to 90 cm along the 1987 transect, and was about 120 cm at the 1986 sites.

All sites along the 1986 and 1987 transects were probed with a steel probe, which contained a thermistor in its tip. The probe could be pushed into coarse-grained sediments with temperatures significantly below 0°C (about -1°C). This indicates the effect of salinity on freezing point depression in these materials.

Volumetric ice content (V_i/V_t) was determined only on intact cores. Gravimetric water content (M_v/M_s) was then determined for these samples and for grab samples from other intervals. For most of the sandy sediments, volumetric ice content at saturation was approximately $0.43 \text{ cm}^3 \text{ cm}^{-3}$, and gravimetric water content approximately 0.3 g g^{-1} . Variations in bulk density due to the presence of pebbles and to packing caused some fluctuation in these values.

The results from laboratory analysis of core samples are presented in Figures 8-1 to 8-7. If an active layer depth of 1 m is assumed, then total winter seabottom heave can be estimated from column 4 of these figures. It is important to note that these estimates are conservative on two counts:

- (1) A complete active layer core profile was not obtained at all sites (i.e. sites BH87-3 and BH87-4);
- (2) Ice lenses were observed in core samples which did not release excess water on thawing (site CB-1);

These ice lenses may have caused soil strain as a result of moisture redistribution within the sampling distance of 10 cm.

The estimates of seasonal seabottom heave for each site are: 5.5 cm (BH87-1); 3.5 cm (BH87-3); 19.3 cm (BH84-4); and 2.5 cm (BH86-4).

Variations in the electrical conductivity of pore waters are also given in Figures 8-1 to 8-7. Sea ice conductivities were on the order of 1 mmhos cm^{-1} , less than those of sediment pore water. A value of $8.9 \text{ mmhos cm}^{-1}$ was determined at the sea ice - sediment interface at site BH86-4. The conductivity of a sea water sample taken from the seabottom at Station 0+300 m on the 1987 transect was $1.4 \text{ mmhos cm}^{-1}$. These data indicate salt expulsion from sea ice and enrichment in the pore water of seabottom sediments. Ice masses found within the seabottom sediments are also associated with low conductivities, thus indicating salt expulsion during ice segregation.

The data suggest that in spite of the salinity of seabottom pore water, considerable amounts of ice segregation may occur over the winter period in the near-shore submarine environment.

Acknowledgments

The field program was entirely financed by the Office of Energy, Research and Development (OERD). Midnight Sun Drilling Co. Ltd. provided the drilling operation, camp and the logistics support, ConeTec Investigations Ltd. carried out the cone penetration tests and their evaluation, and Northern Seismic Analysis Ltd. carried out seismic refraction and installation of additional thermistor cables.

Field support by the staff of the Polar Continental Shelf Project in Tuktoyaktuk greatly contributed to success of the program.

REFERENCES

A-Cubed Inc.

- 1983: General state-of-the-art review of ground probing radar; Earth Physics Branch Open File 83-14.

ConeTec Investigations Ltd.

- 1987: Presentation and interpretation of cone penetration test data; Report to GSC/TS Division.

Harrison, W.D. and Morack, J.L.

- 1985: Thermal properties from borehole heating: Experience in the Canadian Beaufort Sea 1984; Workshop on permafrost geophysics, CRREL Special Report 85-5.

Kurfurst, P.J.

- 1984: Geotechnical investigations in the southern Beaufort Sea - spring 1984; GSC Open File 1078.

Kurfurst, P.J.

- 1986: Geotechnical investigations of the near-shore zone, North Head, Richards Island, N.W.T.; GSC Open File 1376.

Northern Seismic Analysis Ltd.

- 1987: Seismic and temperature measurements, Richards Island, N.W.T.; Report to GSC/TS Division.

Rampton, V.N.

- In Press: Quaternary geology of the Tuktoyaktuk Coastlands, Northwest Territories; GSC Memoir 423.

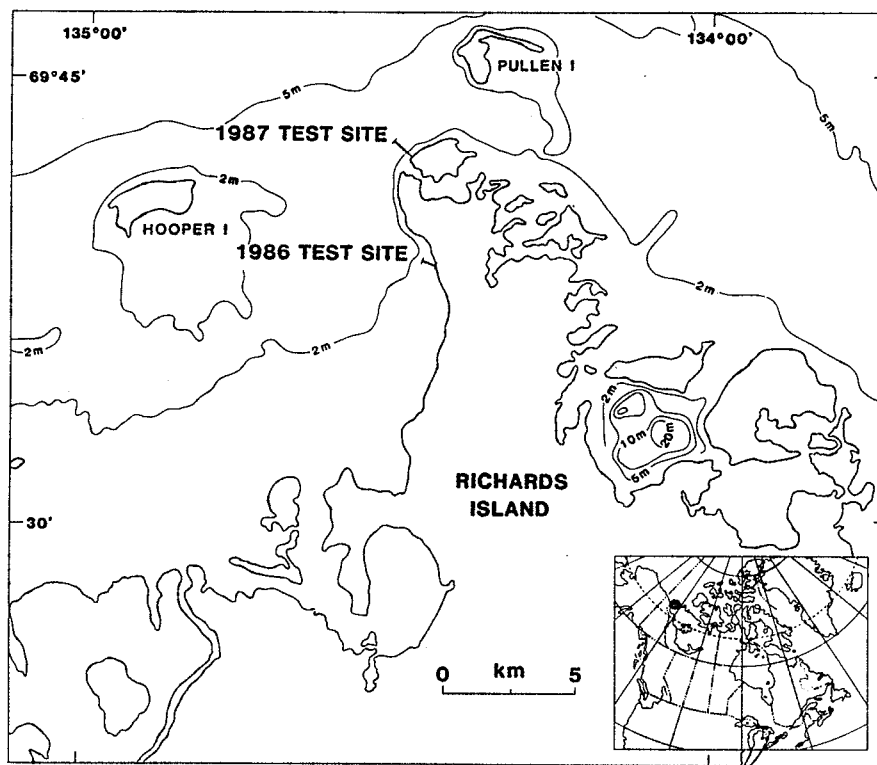


Fig. 1-1 General location map

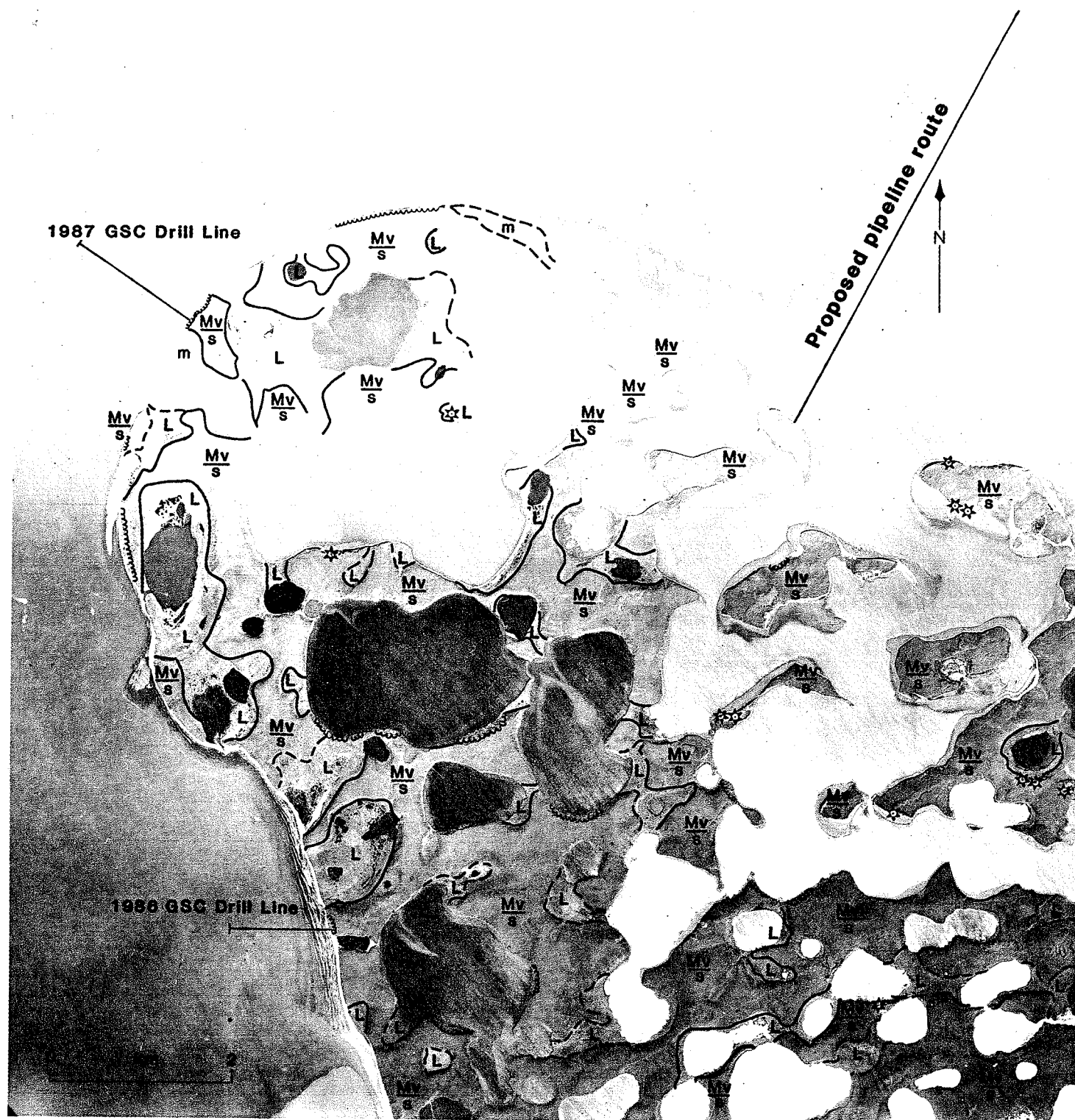


Fig. 2-1 Generalized geology map

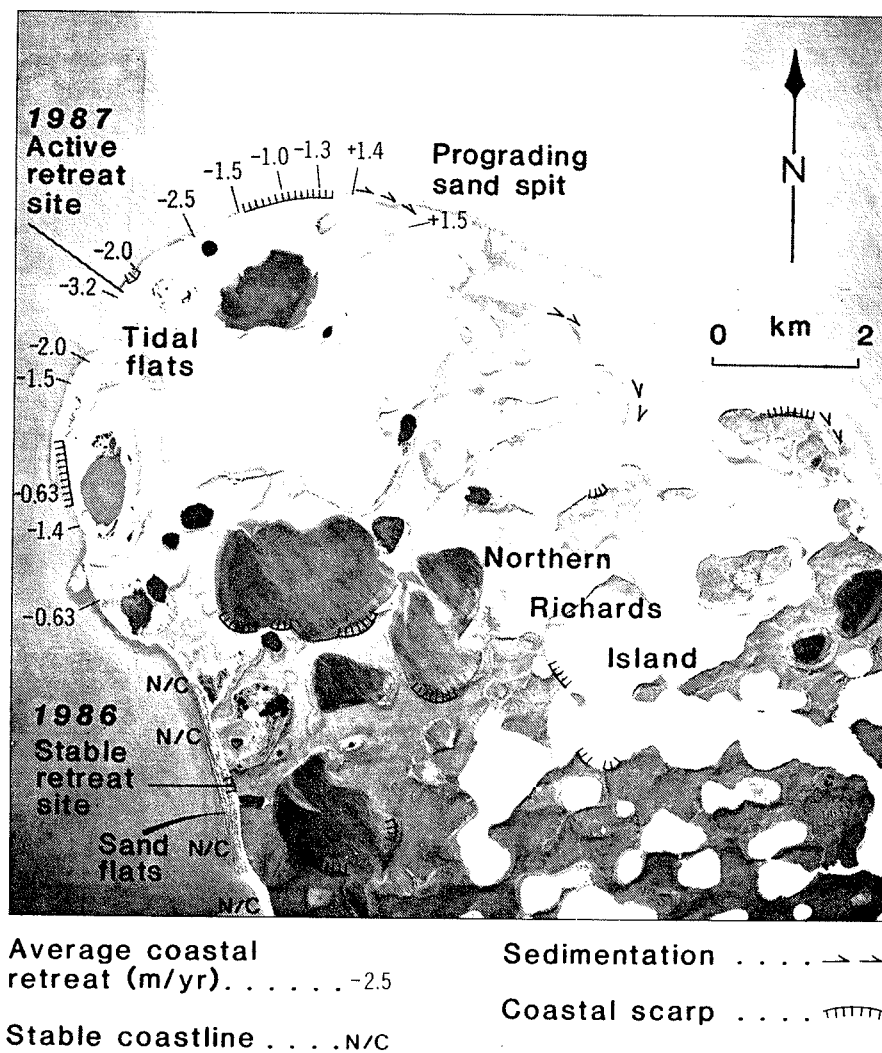


Fig. 2-2 Coastal retreat map

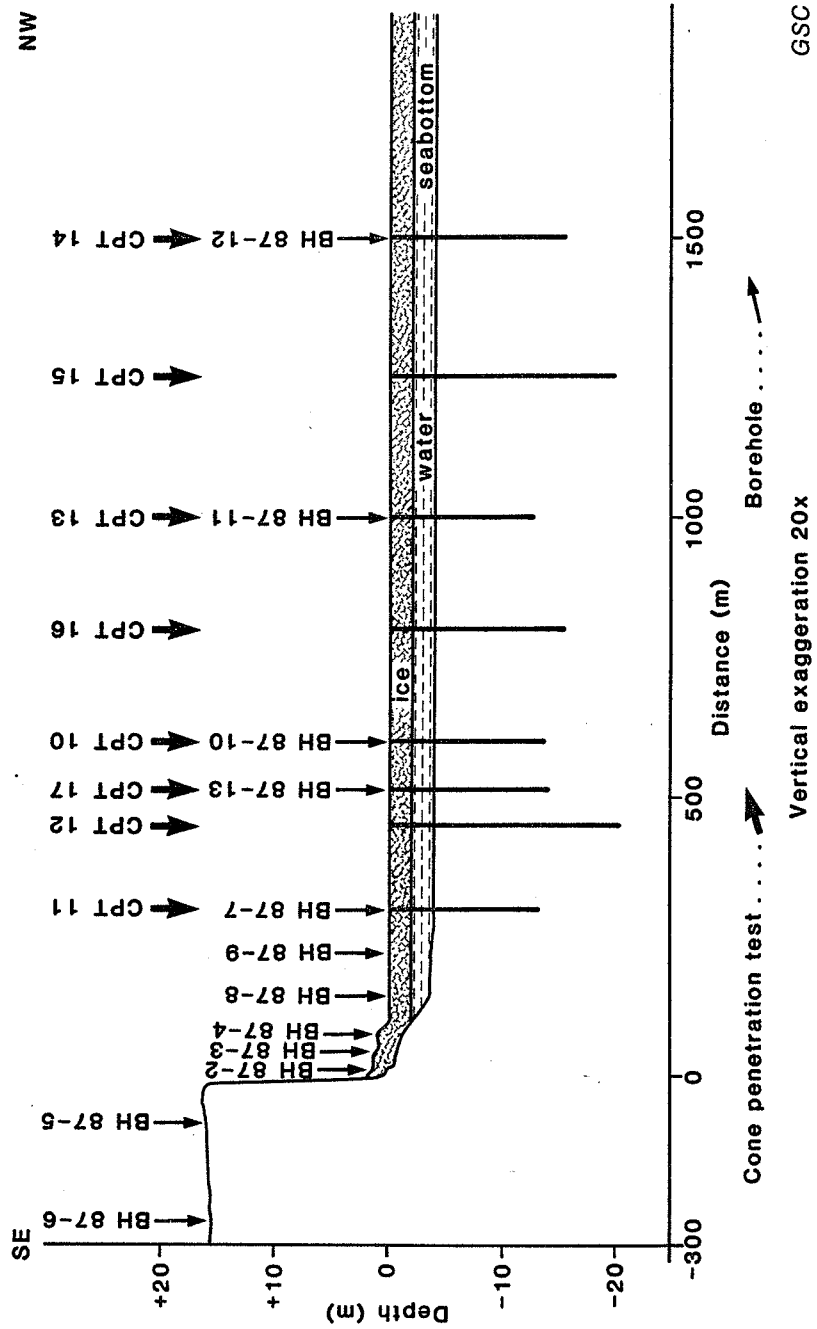


Fig. 3-1 Location of boreholes and CPTs

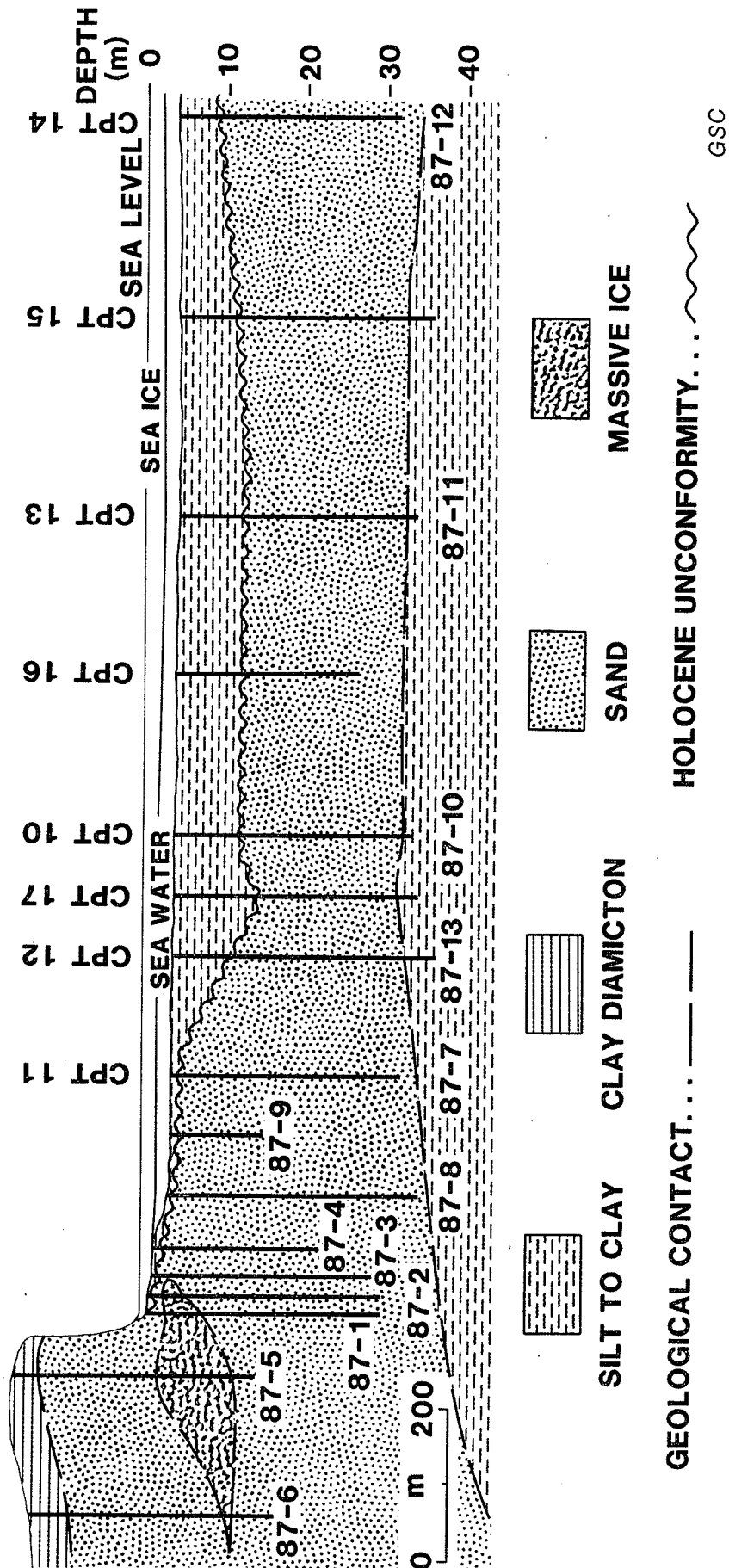
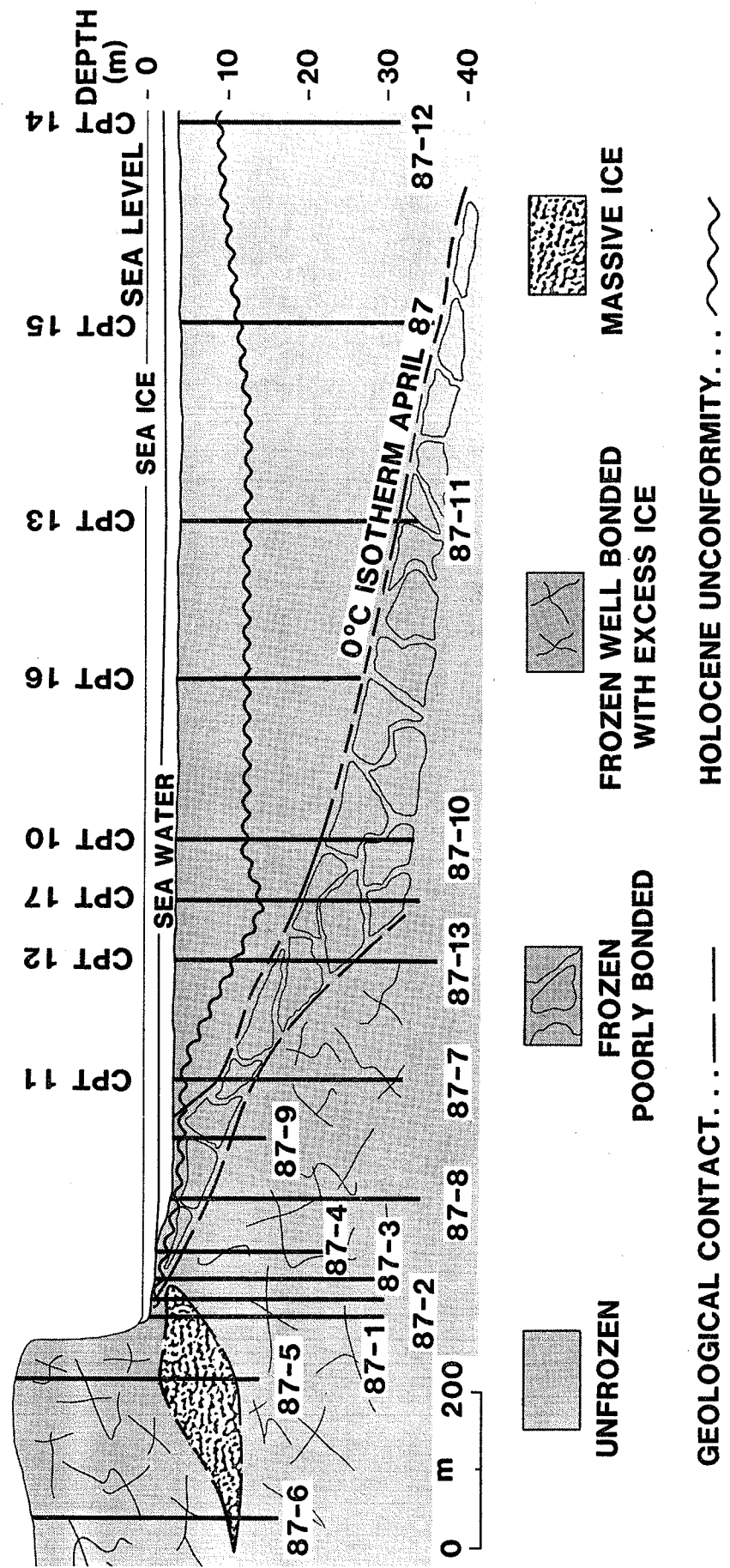


Fig. 3-2 Cross-section of geological conditions



GSC

Fig. 3-3 Cross-section of ground ice conditions

BOREHOLE DRILL LOG LEGEND



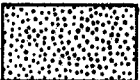

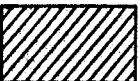
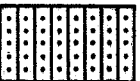

	WATER
	ICE
	SAND
	SILT
	CLAY
	DIAMICTON
	ORGANICS

Fig. 3-4 Borehole log legend

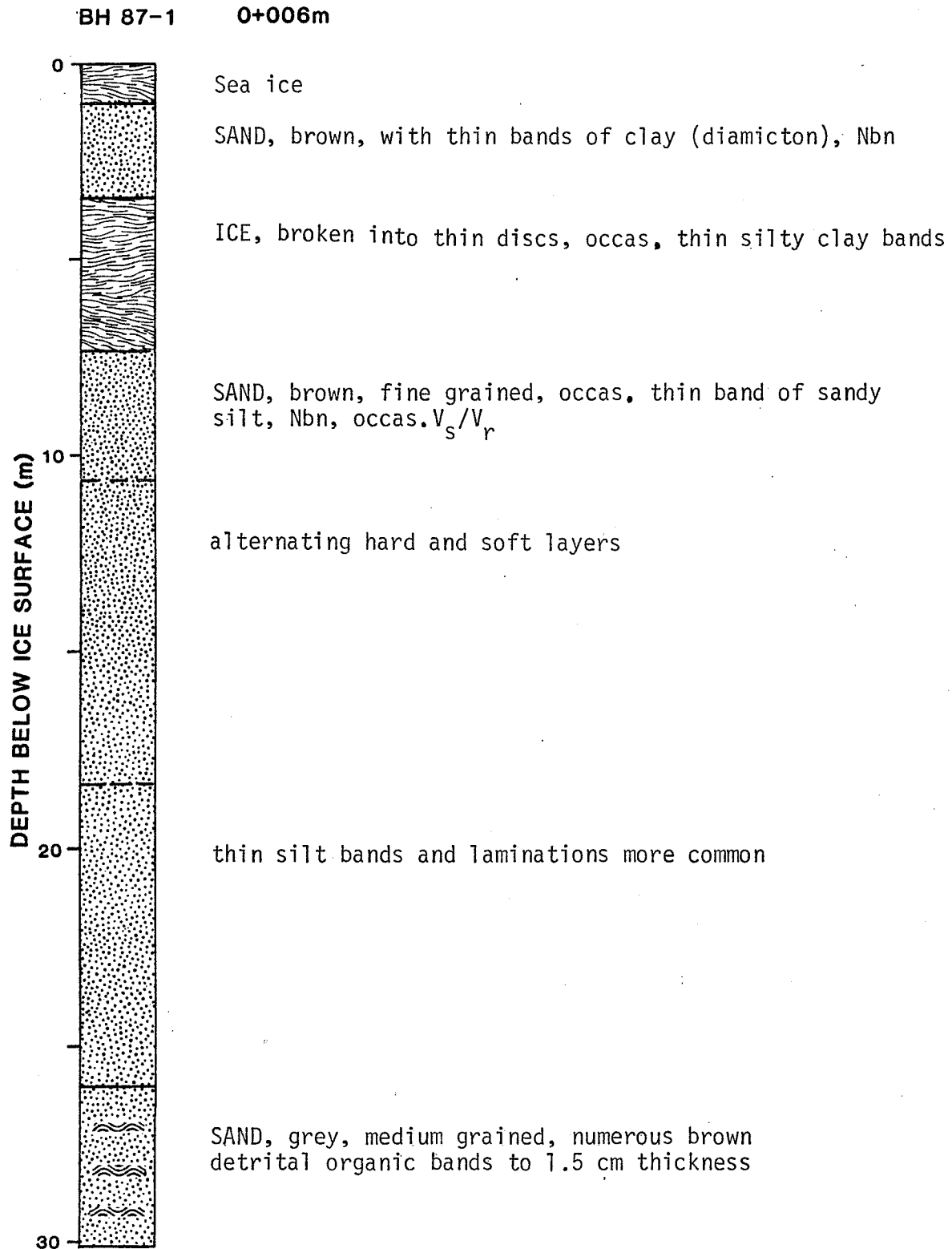


Fig. 3-5 Detailed borehole log - BH 87-1.

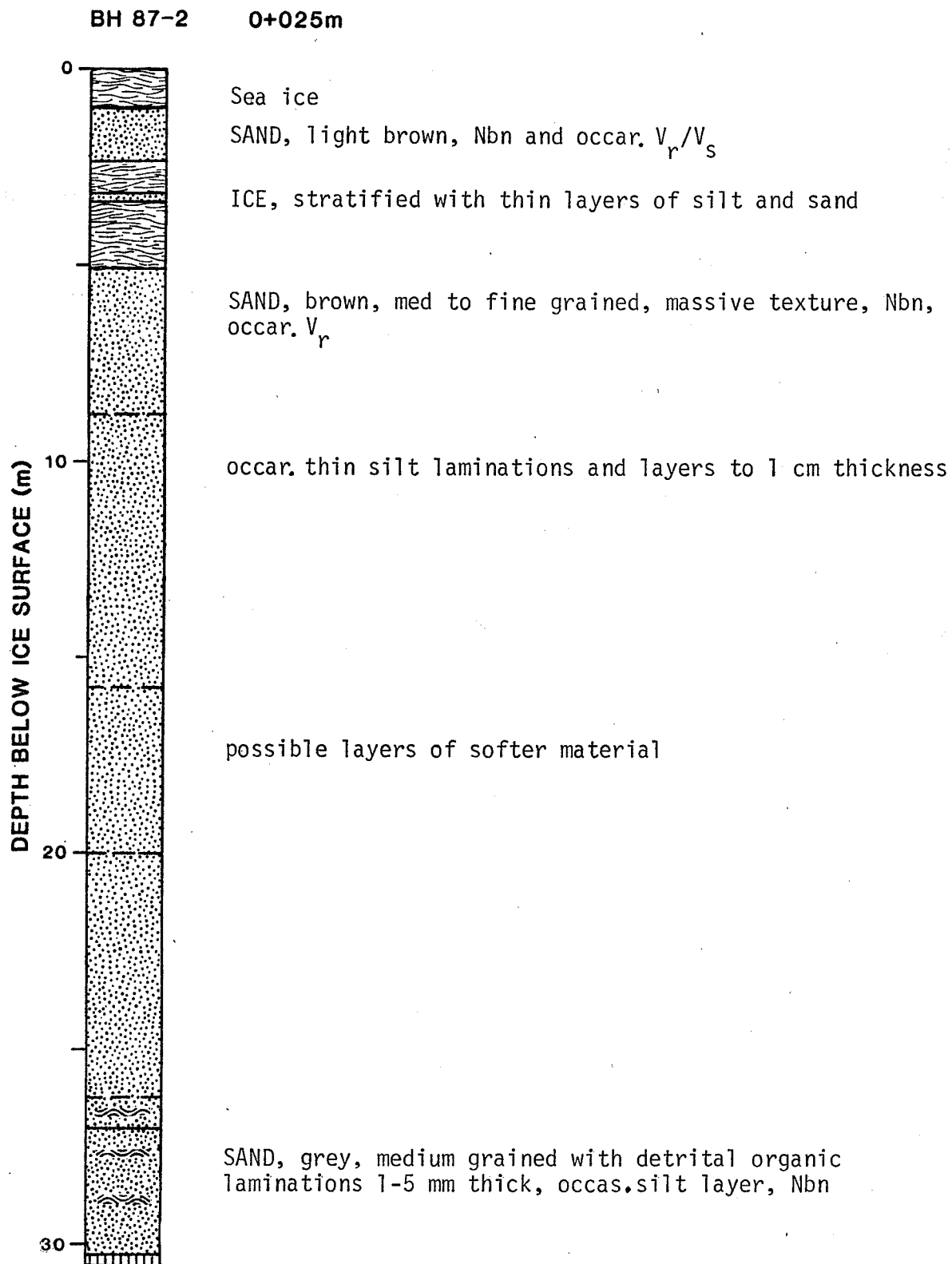


Fig. 3-6 Detailed borehole log - BH 87-2

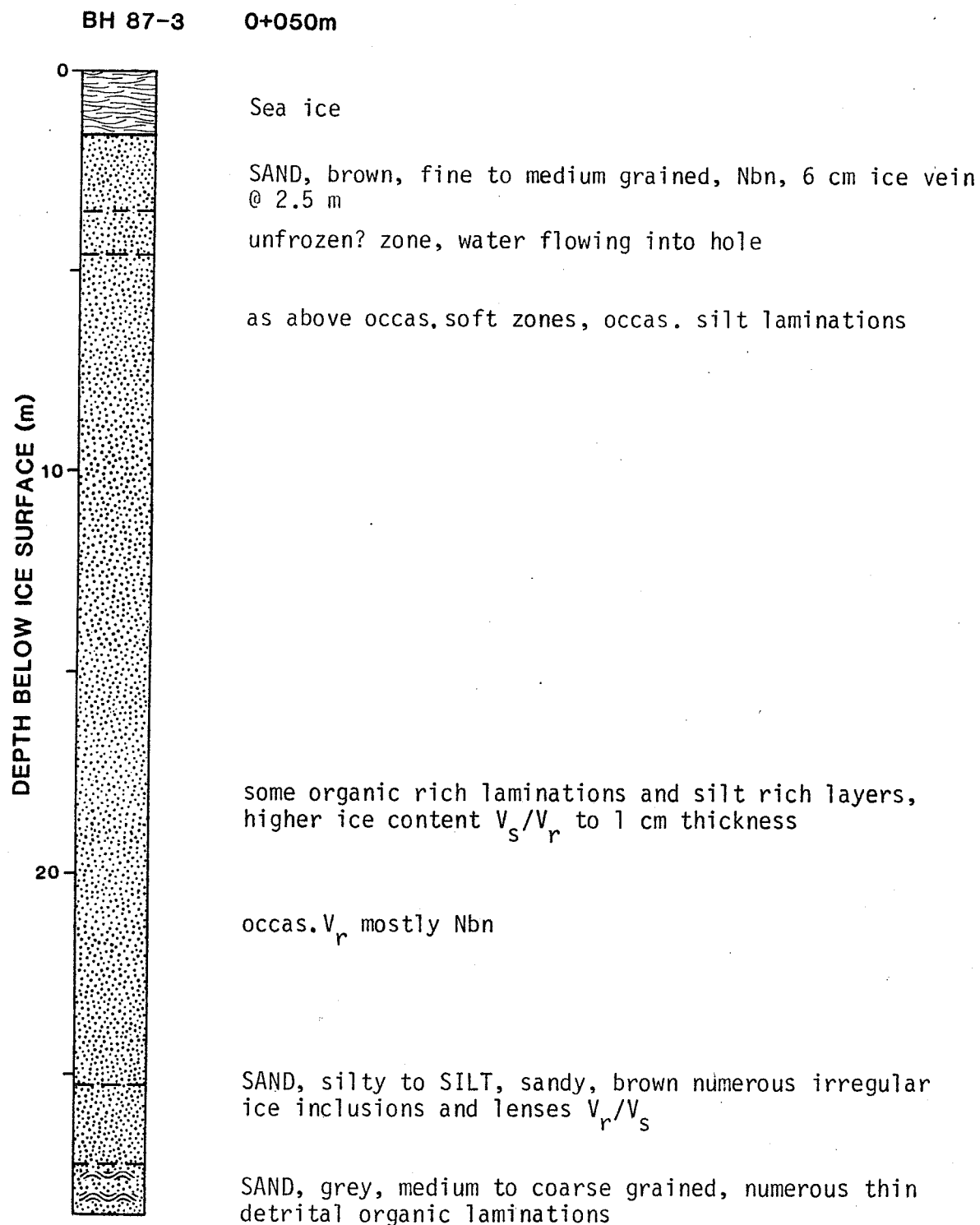


Fig. 3-7 Detailed borehole log - BH 87-3

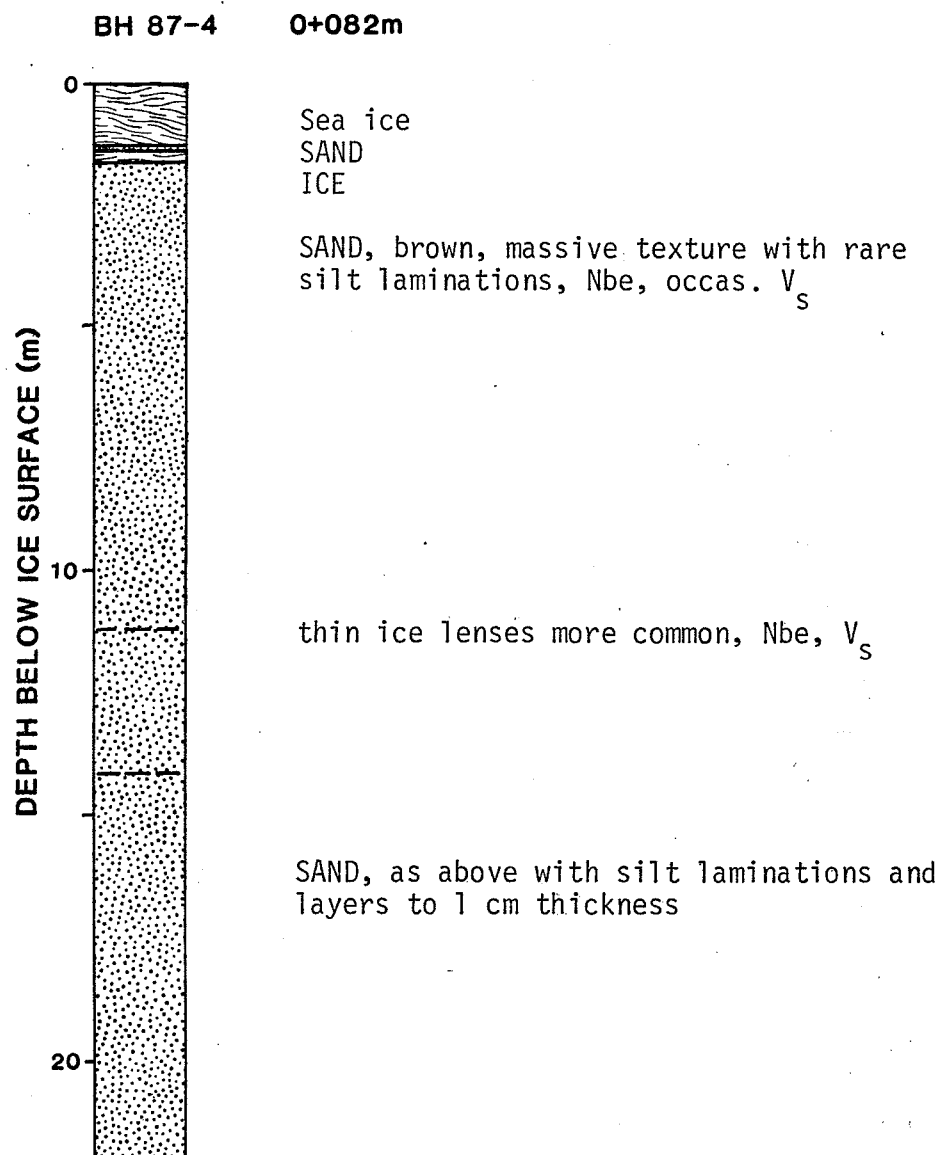


Fig. 3-8 Detailed borehole log - BH 87-4

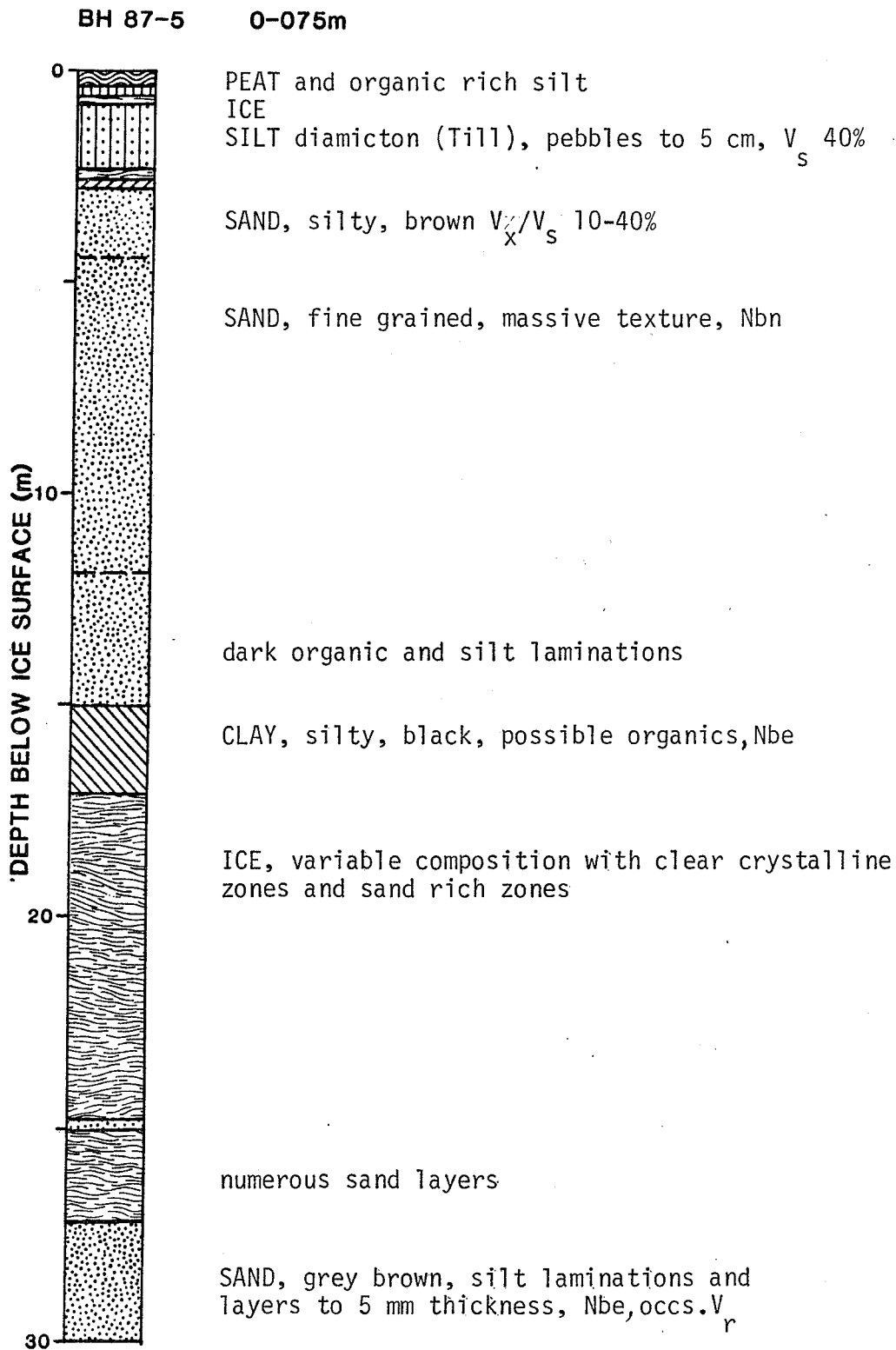


Fig. 3-9 Detailed borehole log - BH 87-5

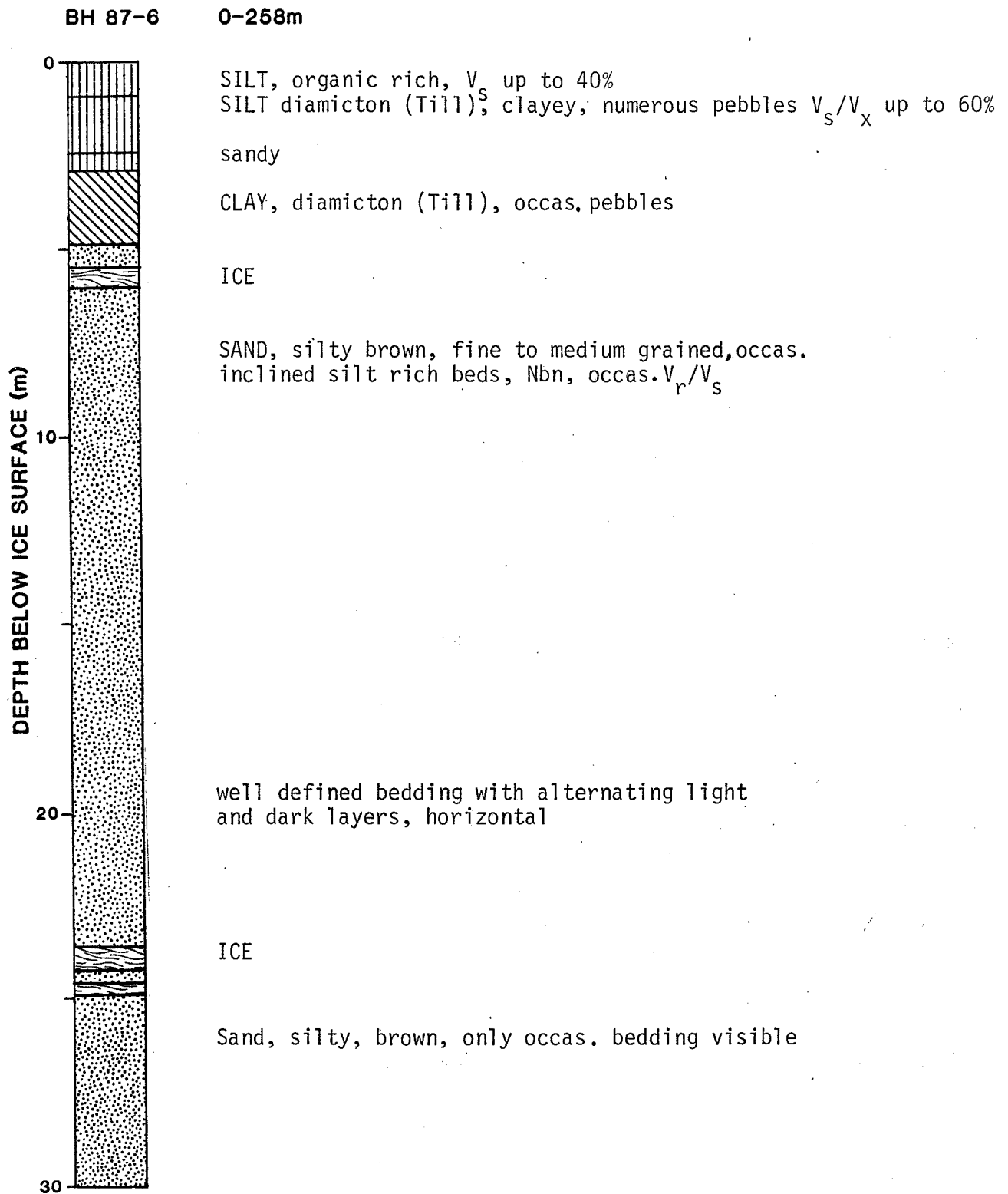


Fig. 3-10 Detailed borehole log - BH 87-6

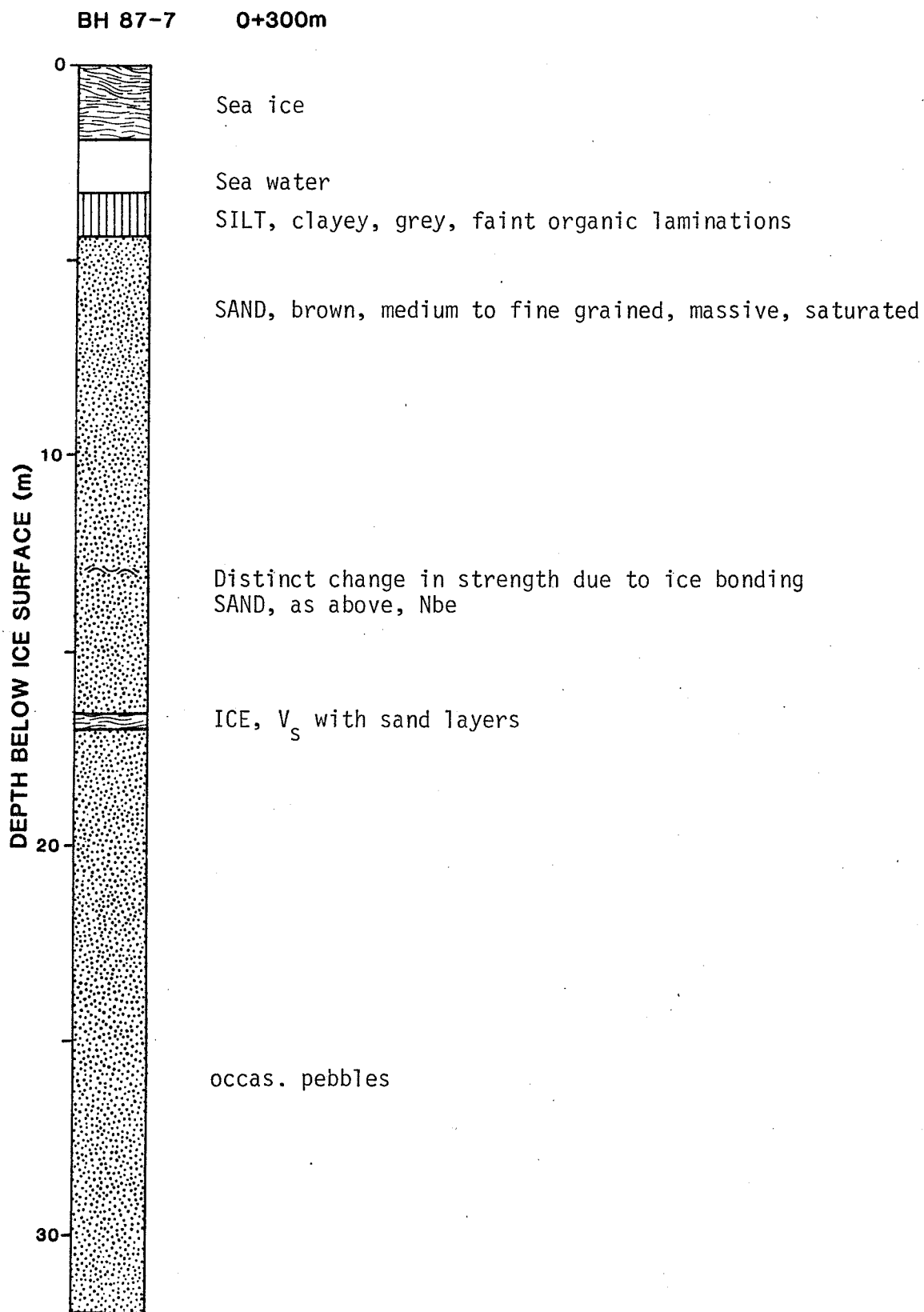


Fig. 3-11 Detailed borehole log - BH 87-7

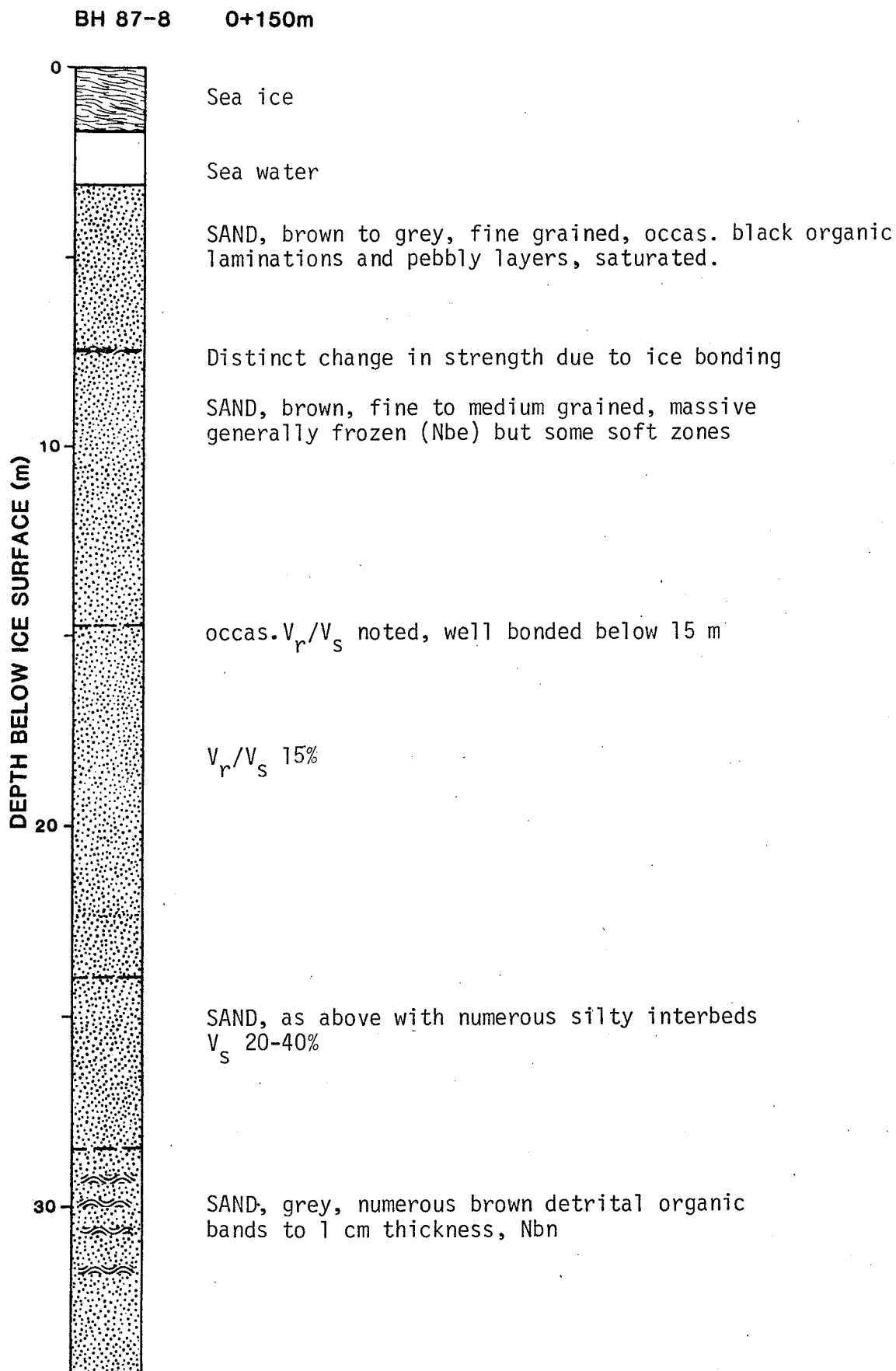


Fig. 3-12 Detailed borehole log - BH 87-8

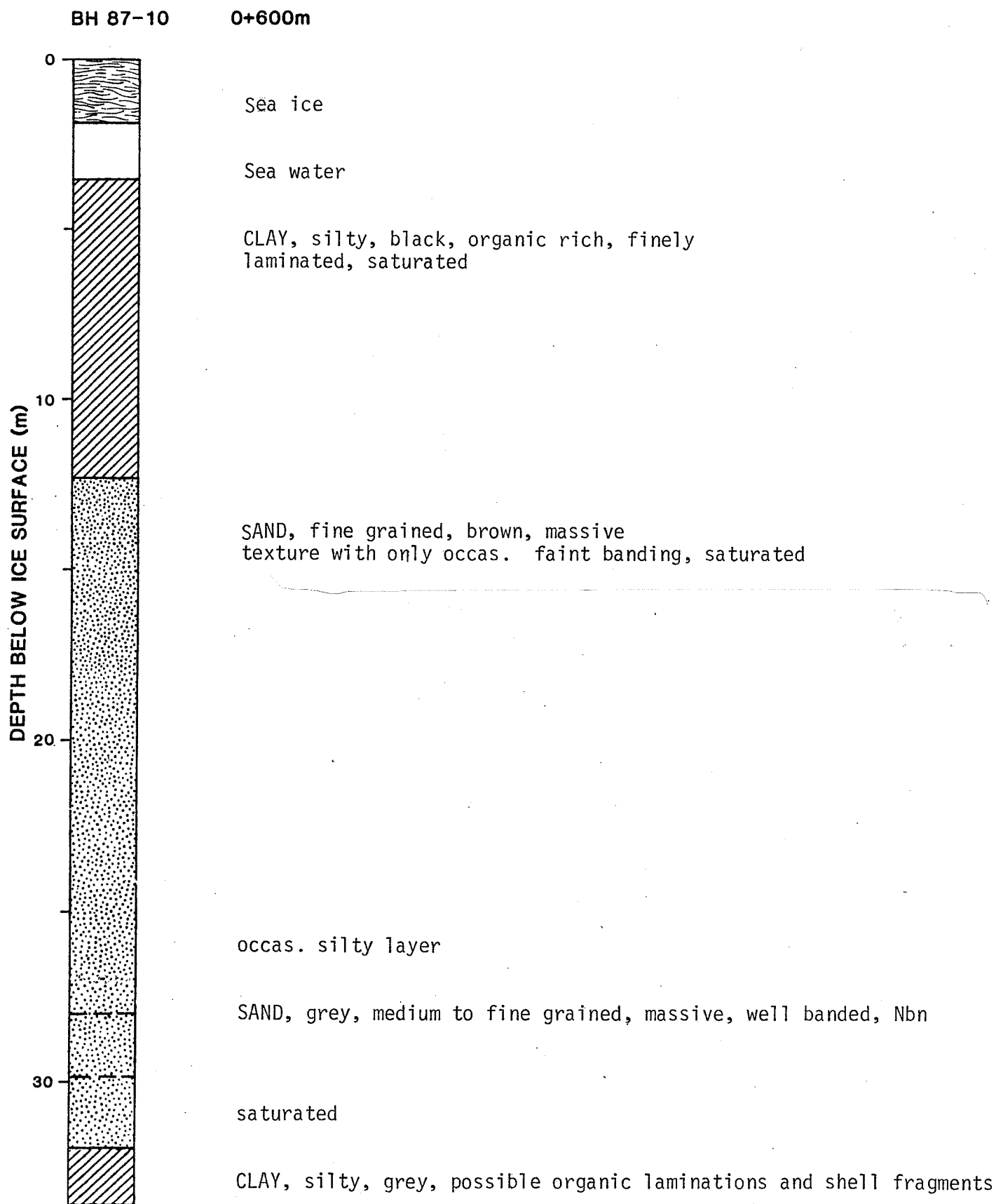


Fig. 3-13 Detailed borehole log - BH 87-10

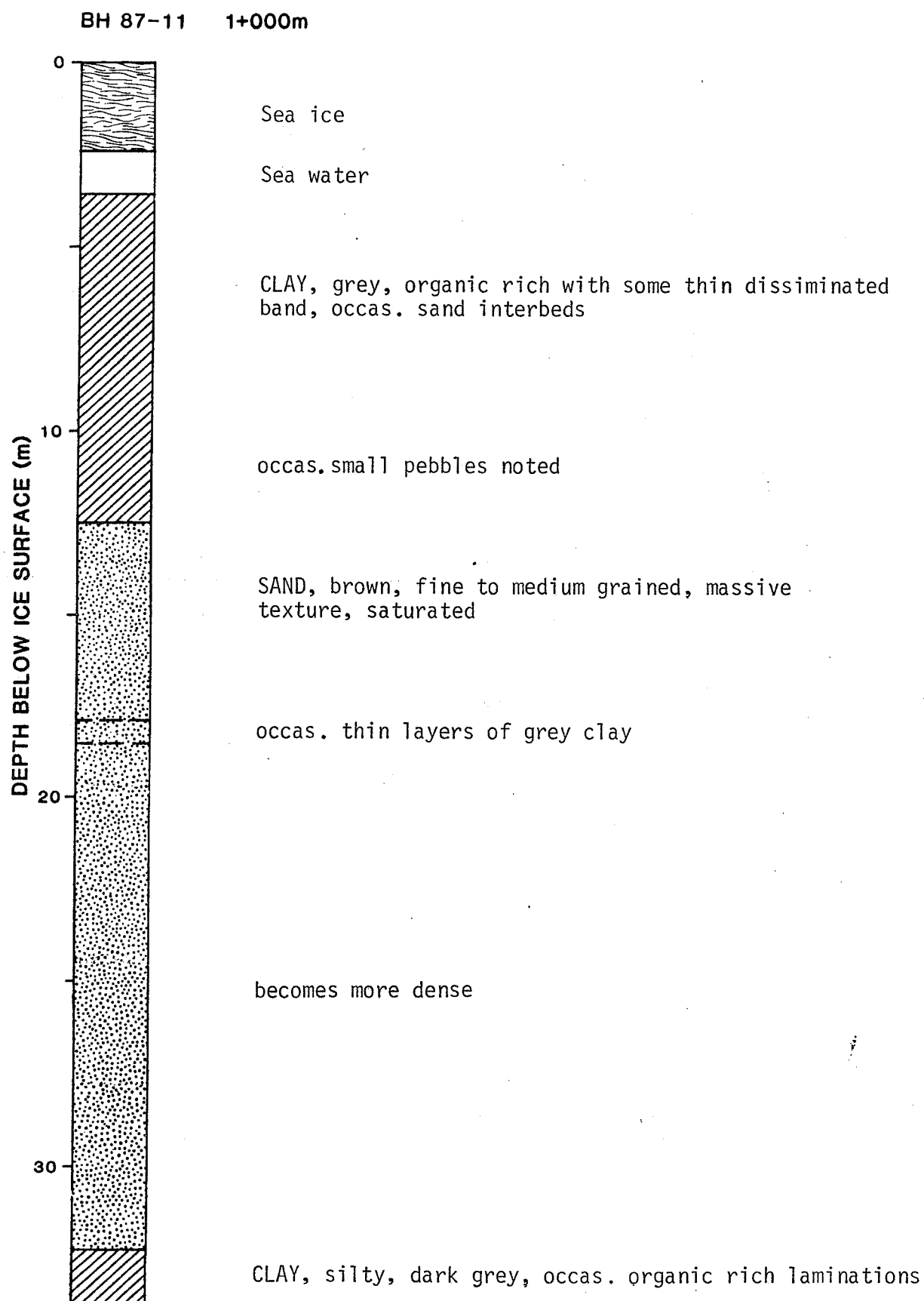


Fig. 3-14 Detailed borehole log - BH 87-11

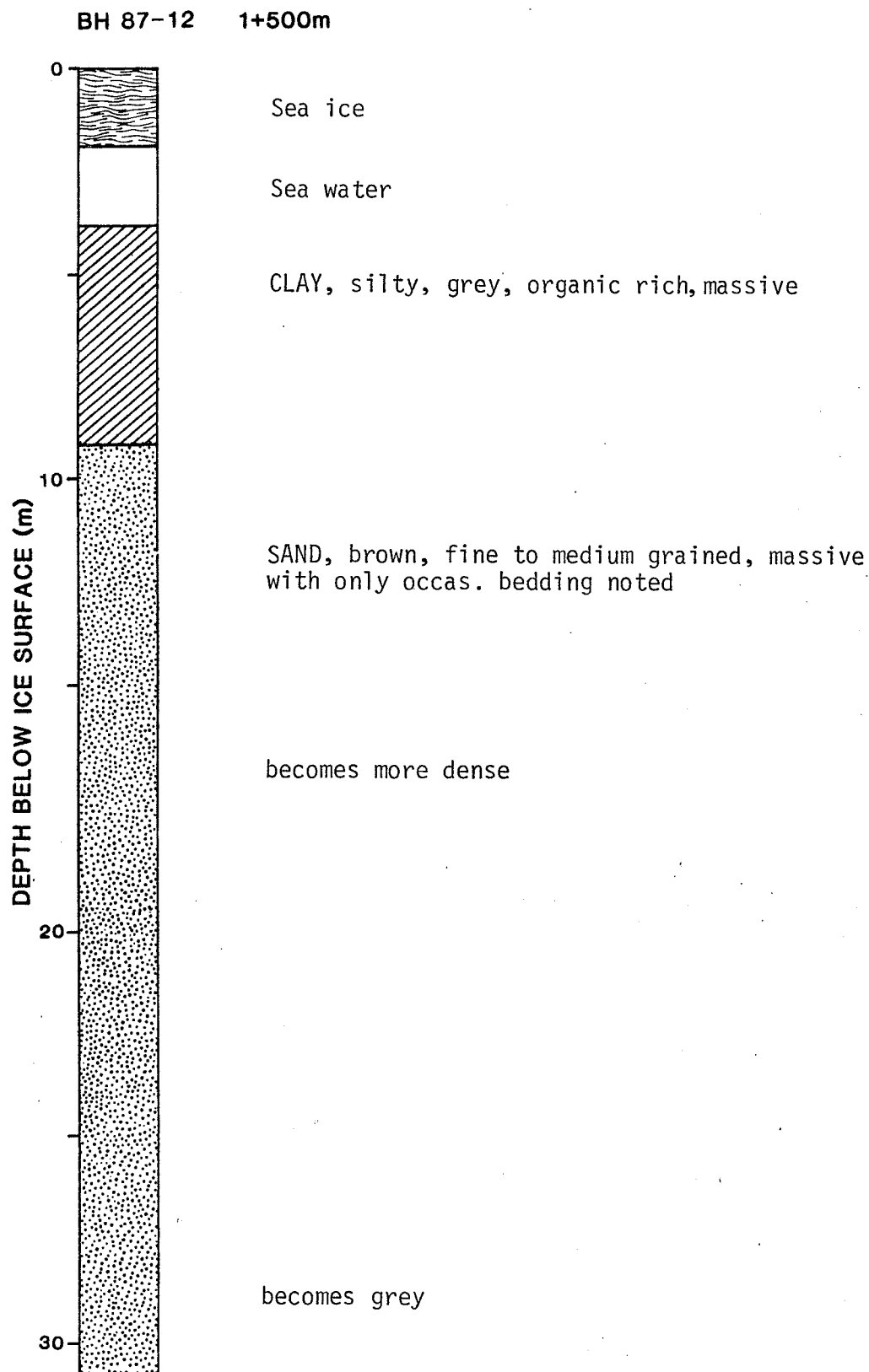


Fig. 3-15 Detailed borehole log - BH 87-12

BH 87-13 0+525m

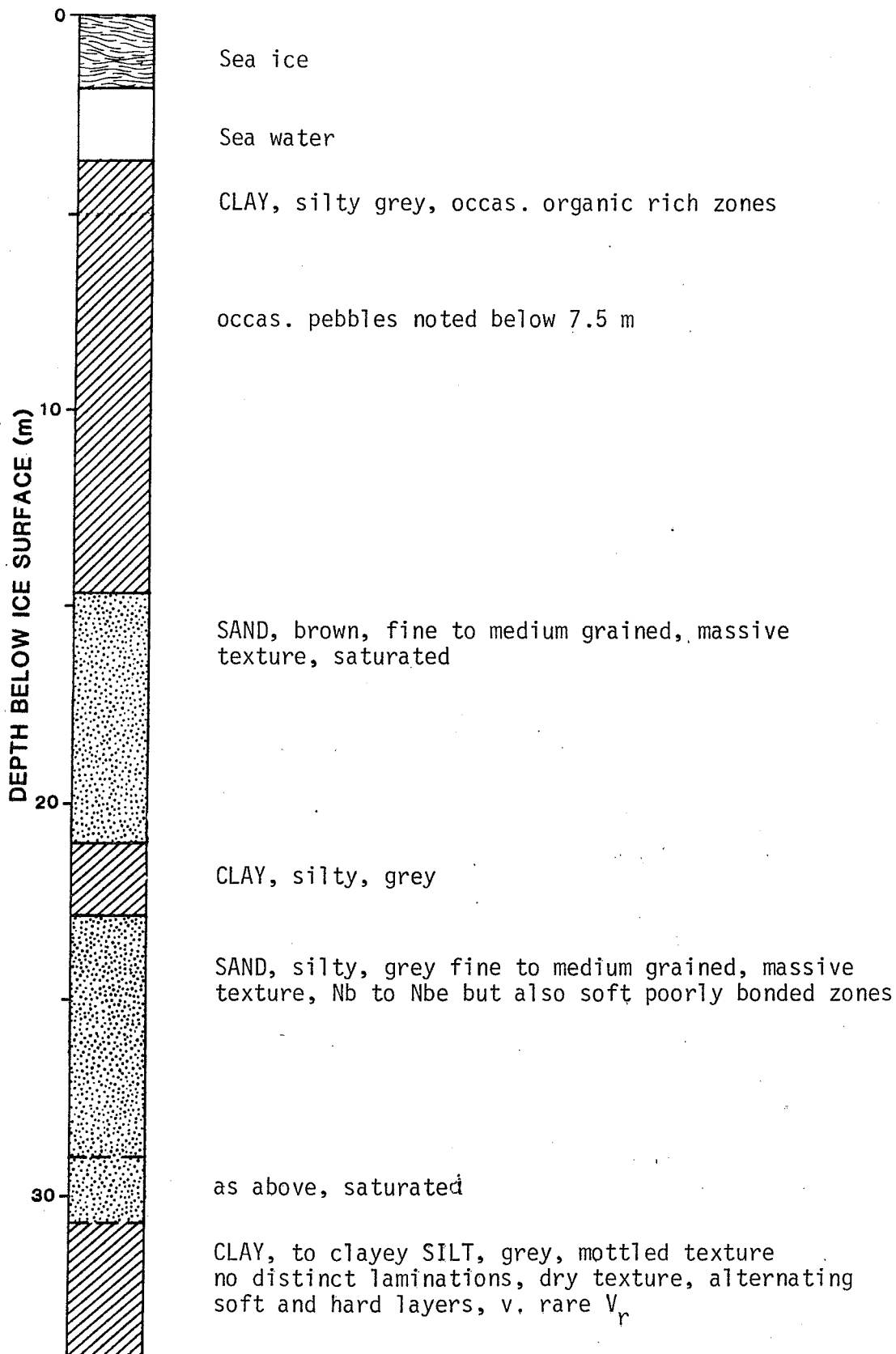


Fig. 3-16 Detailed borehole log - BH 87-13

G - S - C

CONTRACTOR: ConeTec

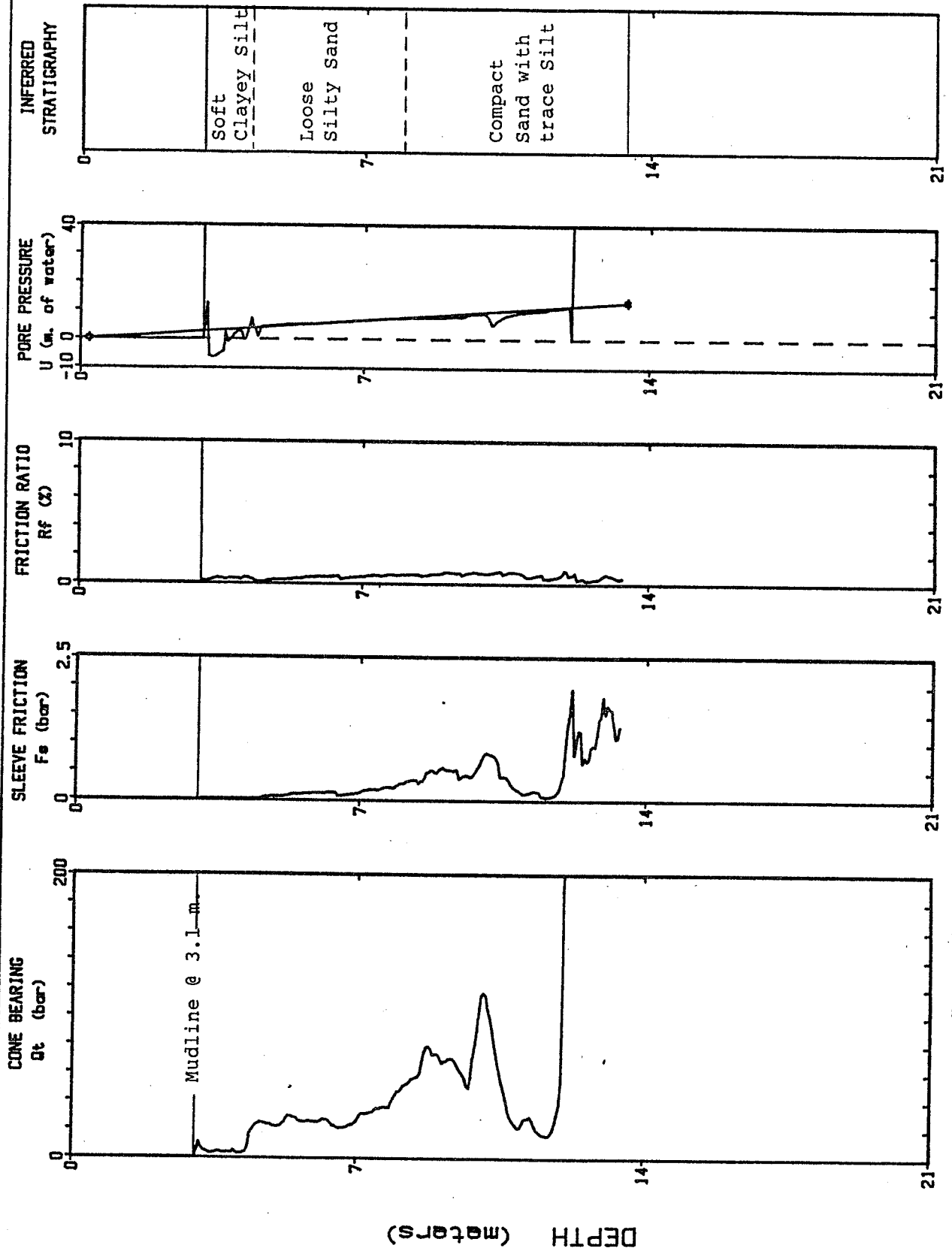
DATE: 04/06/87 15:28

Page No: 1 / 1

SITE: NORTH HEAD NWT

CONE: 10 Ton No.192

CPT LOCATION: C87-01 Sta 3+00



Max Depth: 13.45 m

Depth Increment: .05 m

Fig. 3-17 Cone penetration test data -C 87-01

CONTRACTOR: ConeTec

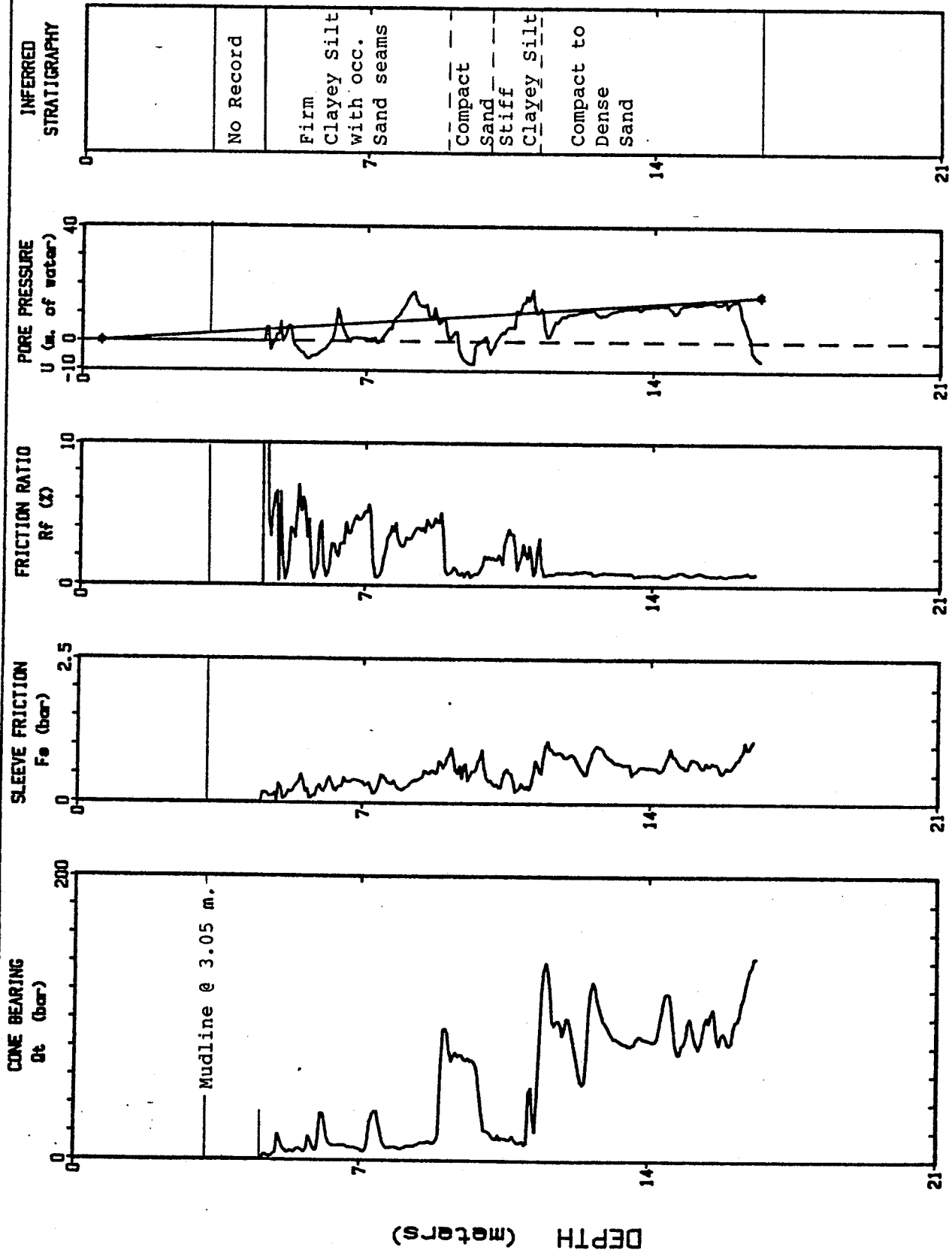
SITE: NORTH HEAD NWT

DATE: 04/06/87 18.46

CONE: 10 Ton No. 192

Page No: 1 / 1

CPT LOCATION: C87-02 Sta 4+50



Max Depth : 16.6 m

Depth Increment : .05 m

Fig. 3-18 Cone penetration test data - C 87-02

G. S. C.

CONTRACTOR: ConeTec

SITE: NORTH HEAD NWT

DATE: 04/09/87 18:57

CONE: 10 Ton No.192 .

Page No: 1 / 1

CPT LOCATION: C87-03 Sta 5+25

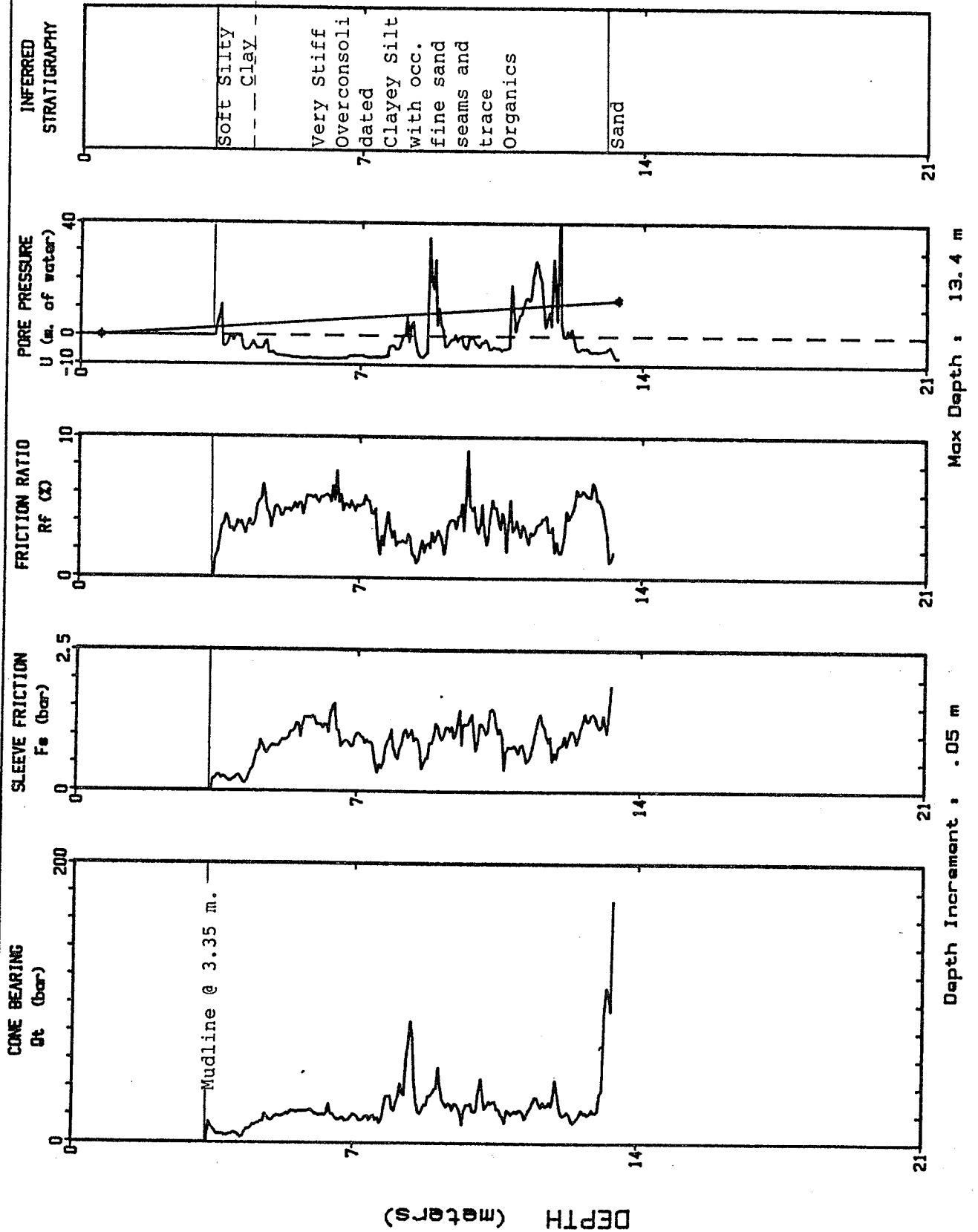


Fig. 3-19 Cone penetration test data - C 87-03

G. S. C.

CONTRACTOR: ConeTec

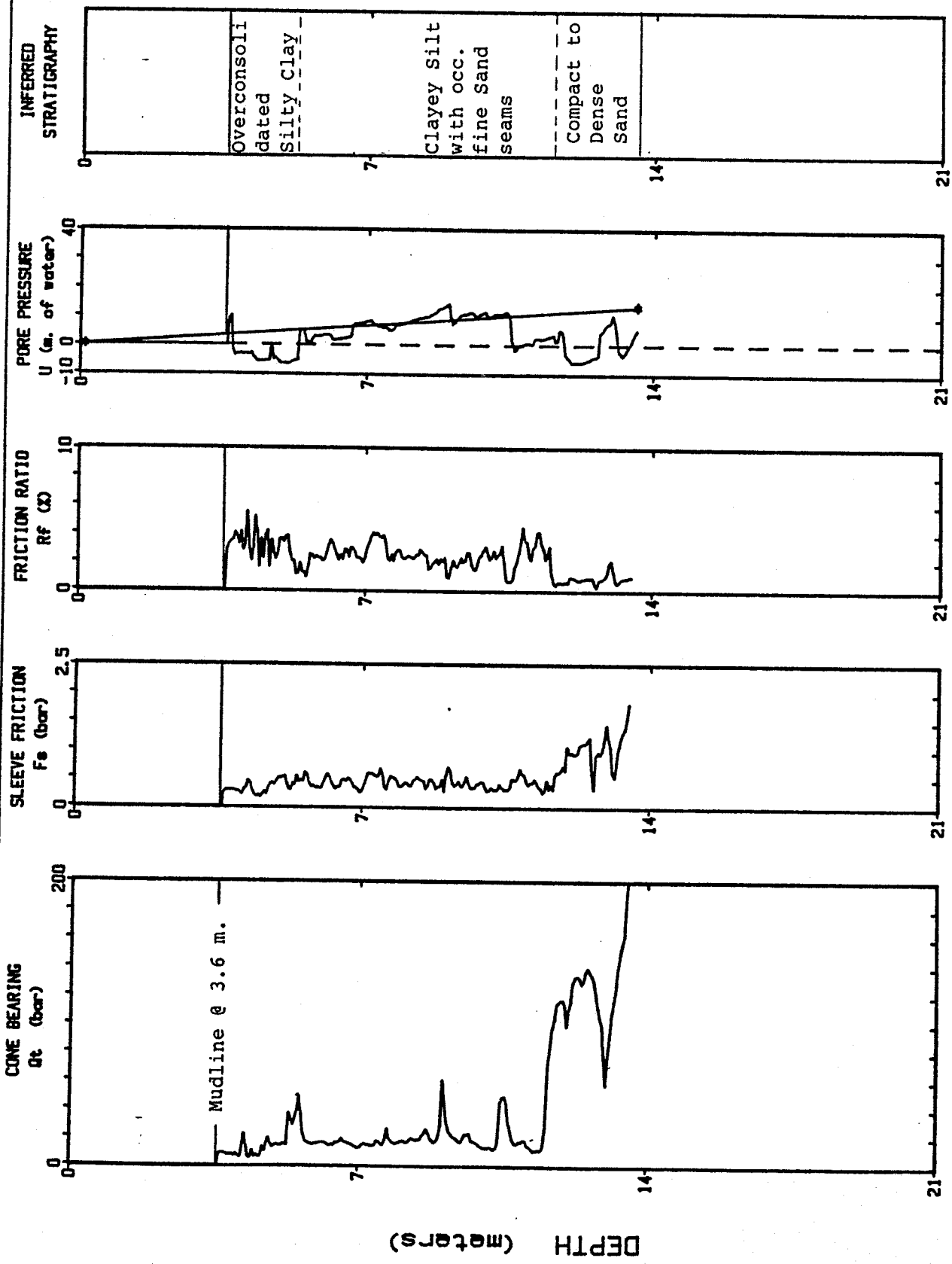
SITE: NORTH HEAD_NWT_

DATE: 04/06/87 09.47

CONE: 10 Ton No.192

Page No: 1 / 1

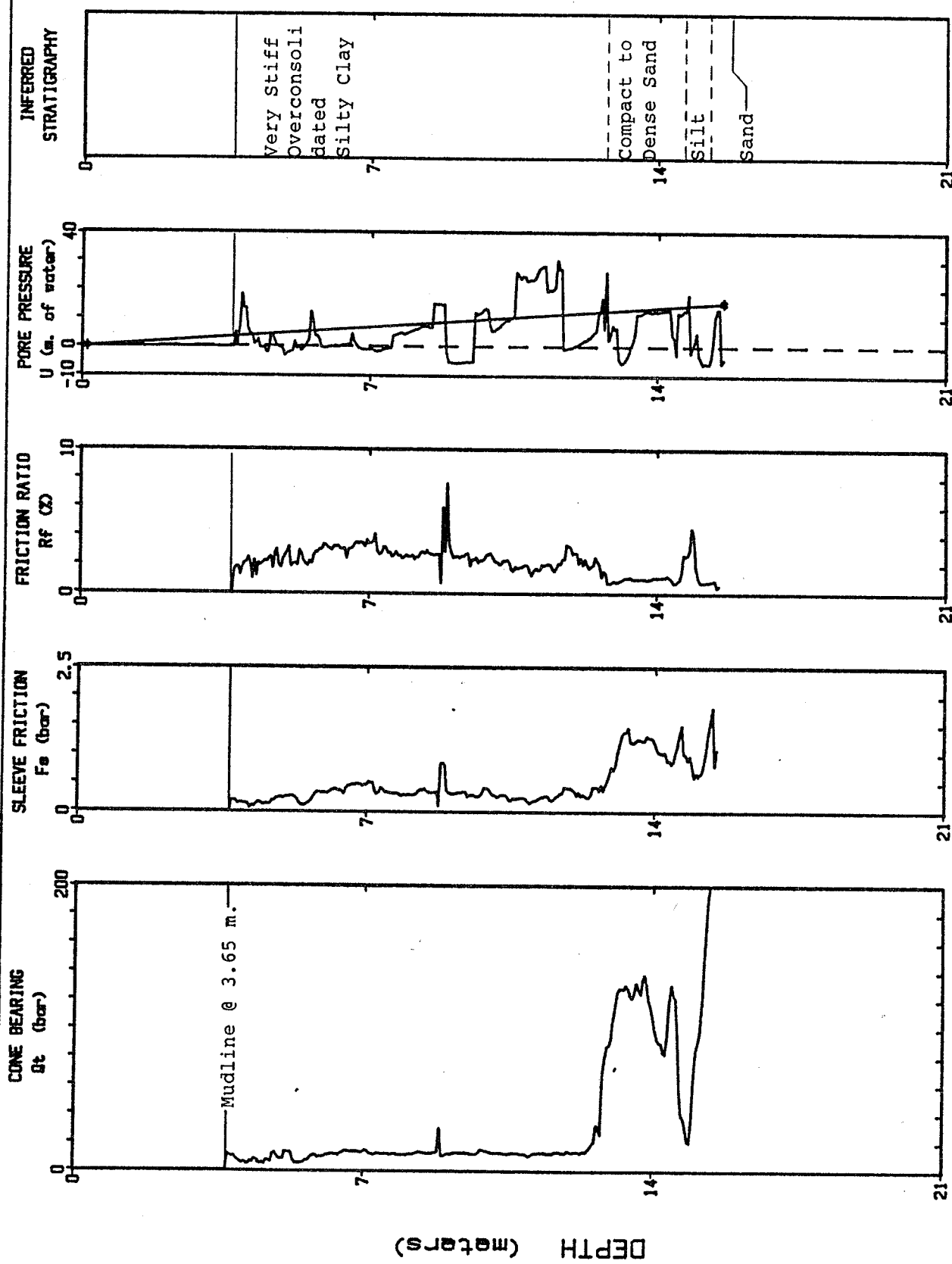
CPT LOCATION: C87-04 Sta 6+00



Max Depth : 13.6 m

Fig. 3-20 Cone penetration data - C 87-04

CONTRACTOR: ConeTec
 DATE: 04/08/87 15.59
 CPT LOCATION: C87-05 Sta 8+00
 SITE: NORTH HEAD NWT
 CONE, 10 Ton No.192
 Page No: 1 / 1



Max Depth : 15.6 m

Depth Increment : .05 m

Fig. 3-21 Cone penetration data - C 87-05

CONTRACTOR: ConeTec

DATE: 04/08/87 10:58

Page No. 1 / 1

SITE: NORTH HEAD NWT

CONE: 10 Ton No. 192

CPT LOCATION: C87-06 Sta 10+00

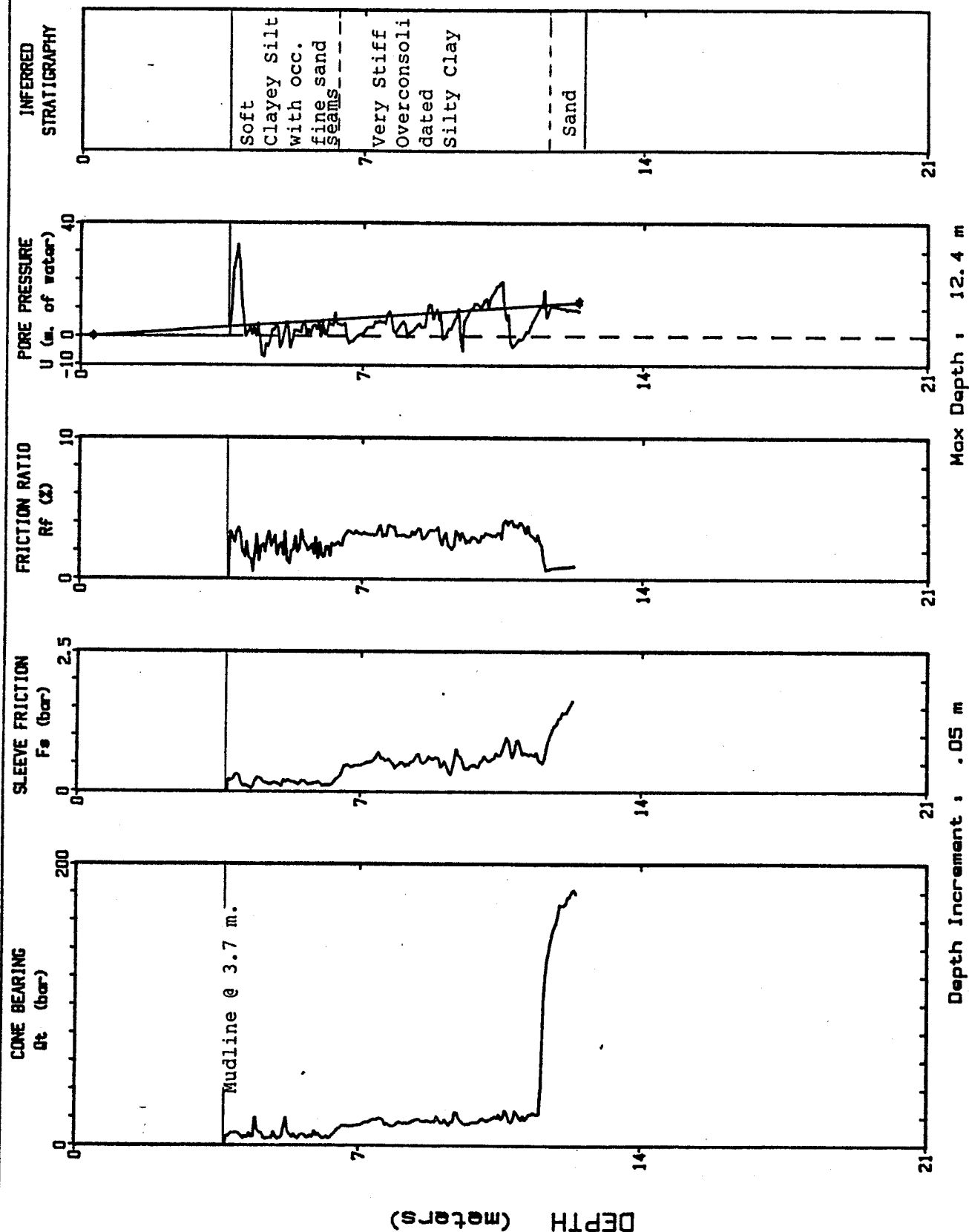
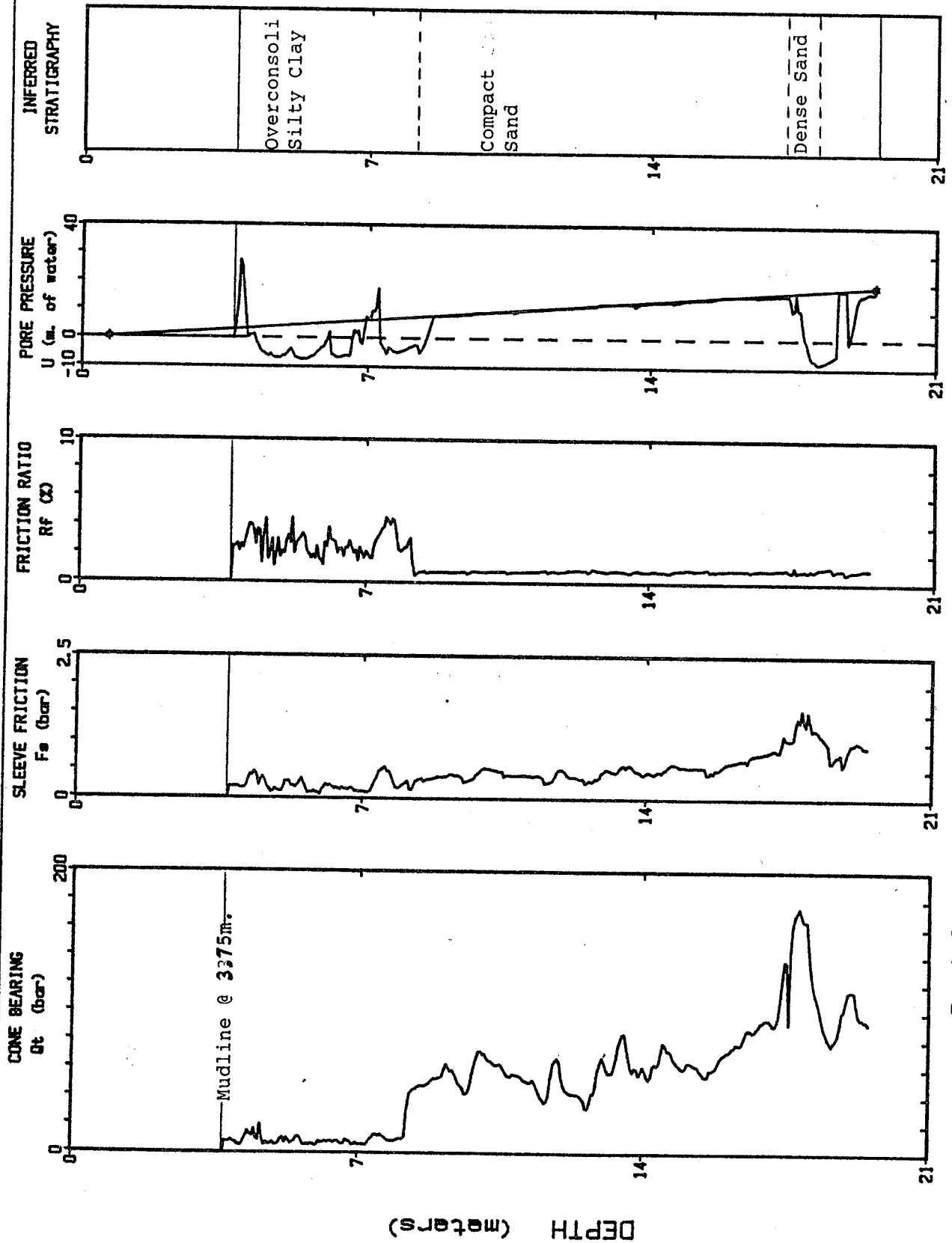


Fig. 3-22 Cone penetration data - C 87-06

CONTRACTOR: ConeTec		G. S. C.		Page No: 1 / 1	
SITE: NORTH HEAD NWT		DATE: 04/09/87 12:15		CPT LOCATION: C87-07 Sta 12+50	
		CONE: 10 TonNo. 192			



Max Depth : 18.55 m

Depth Increment : .05 m

Fig. 3-23 Cone penetration data -- C 87-07

G. S. C.

CONTRACTOR: ConeTec

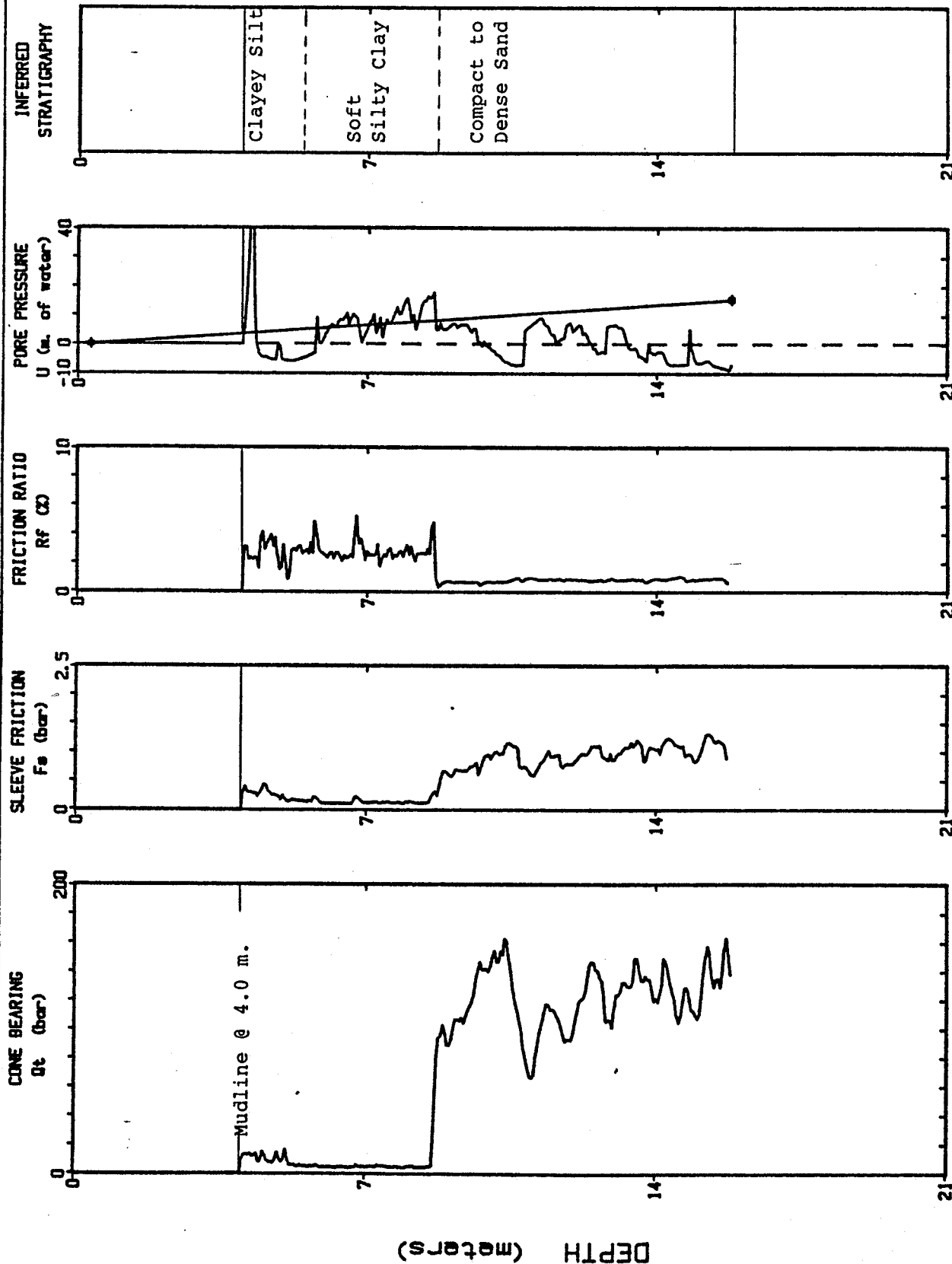
SITE: NORTH HEAD NWT

DATE: 04/08/87 17.05

CONE: 10 TonNo. 192.

Page No: 1 / 1

CPT LOCATION: CB7-08 Sta 15+00



Max Depth : 15.8 m

Depth Increment : .05 m

Fig. 3-24 Cone penetration data - C 87-08

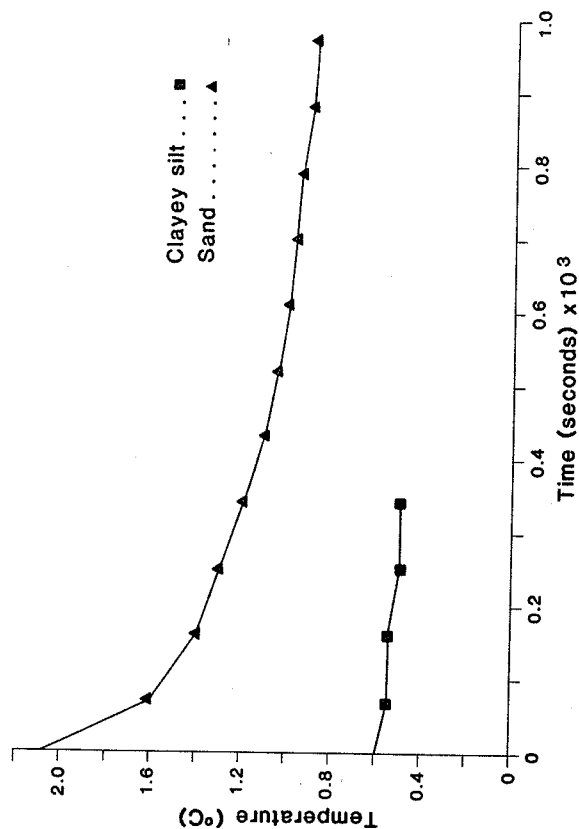
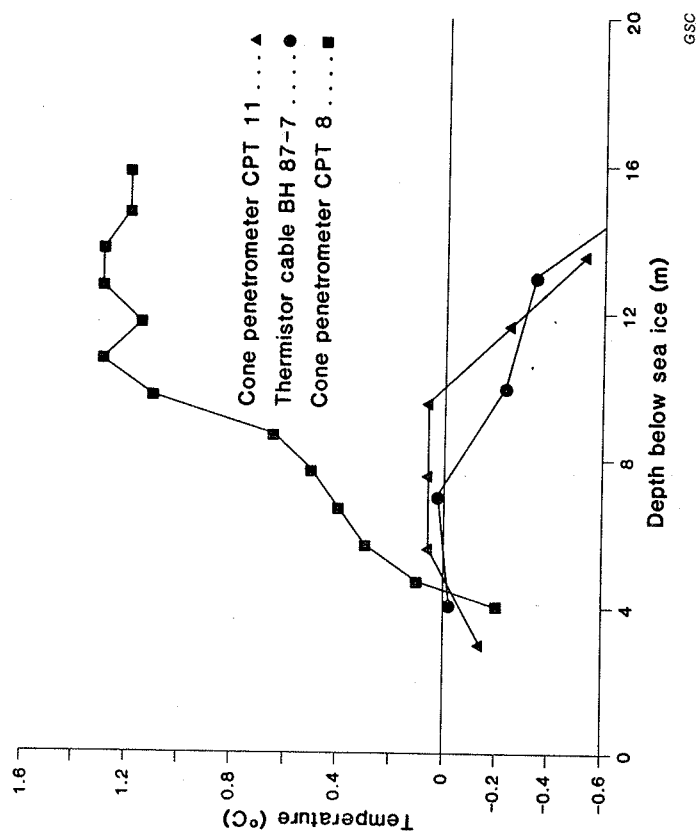


Fig. 3-25a CPT temperature dissipation vs time plot

Fig. 3-25b Comparison of CPT and thermistor cable temperature data

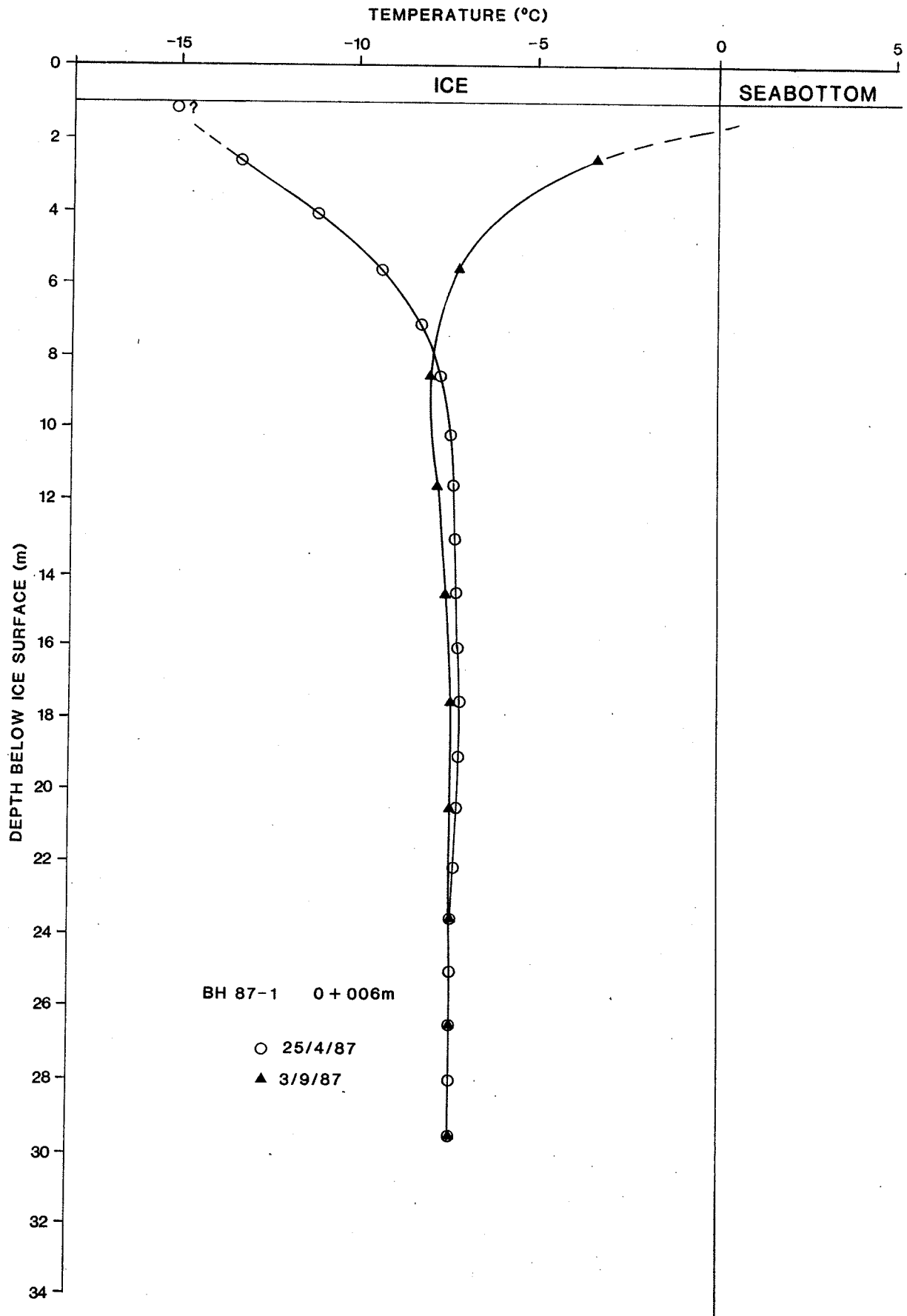


Fig. 4-1 Equilibrium temperature profile - BH 87-1

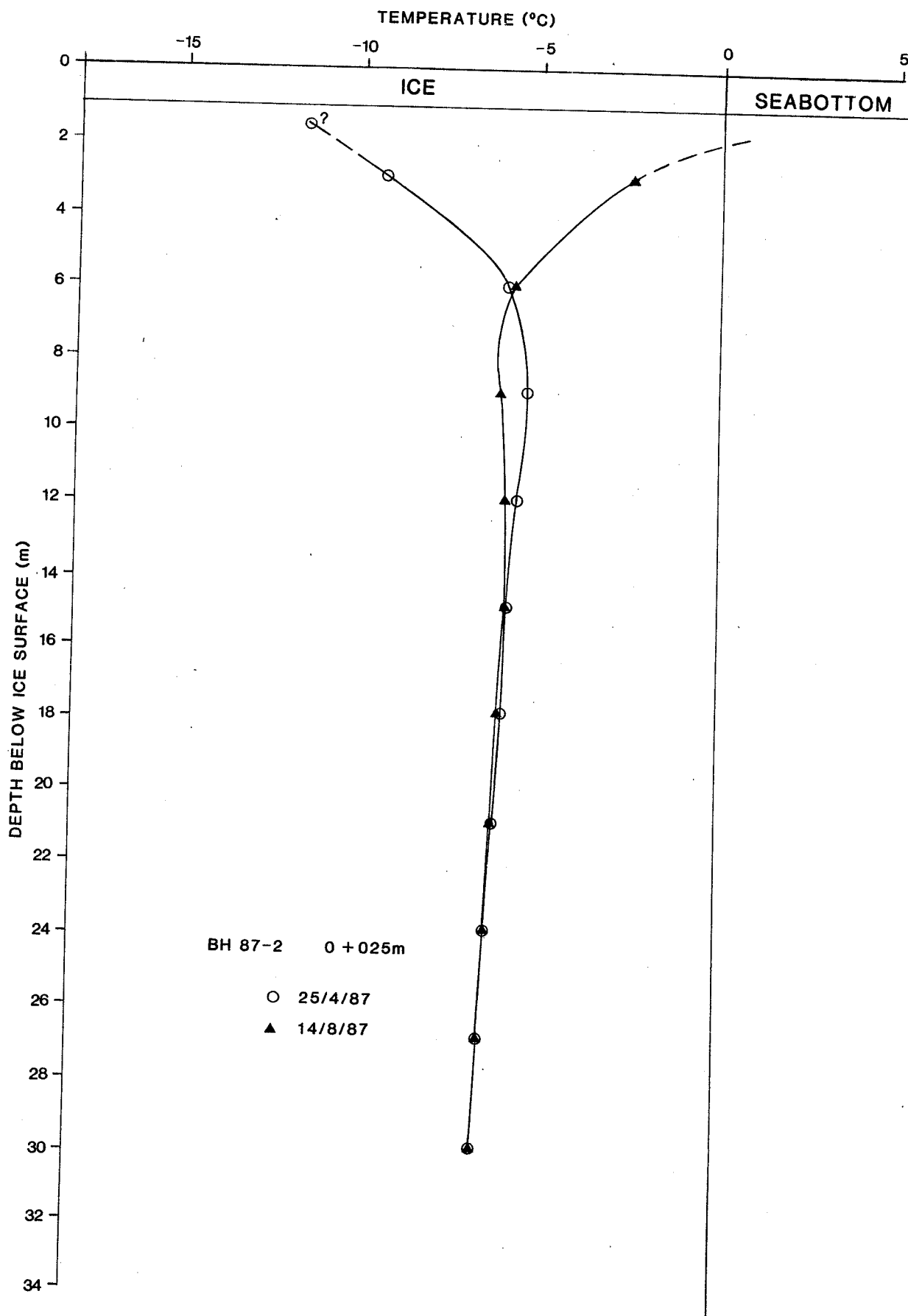


Fig. 4-2 Equilibrium temperature profile - BH 87-2

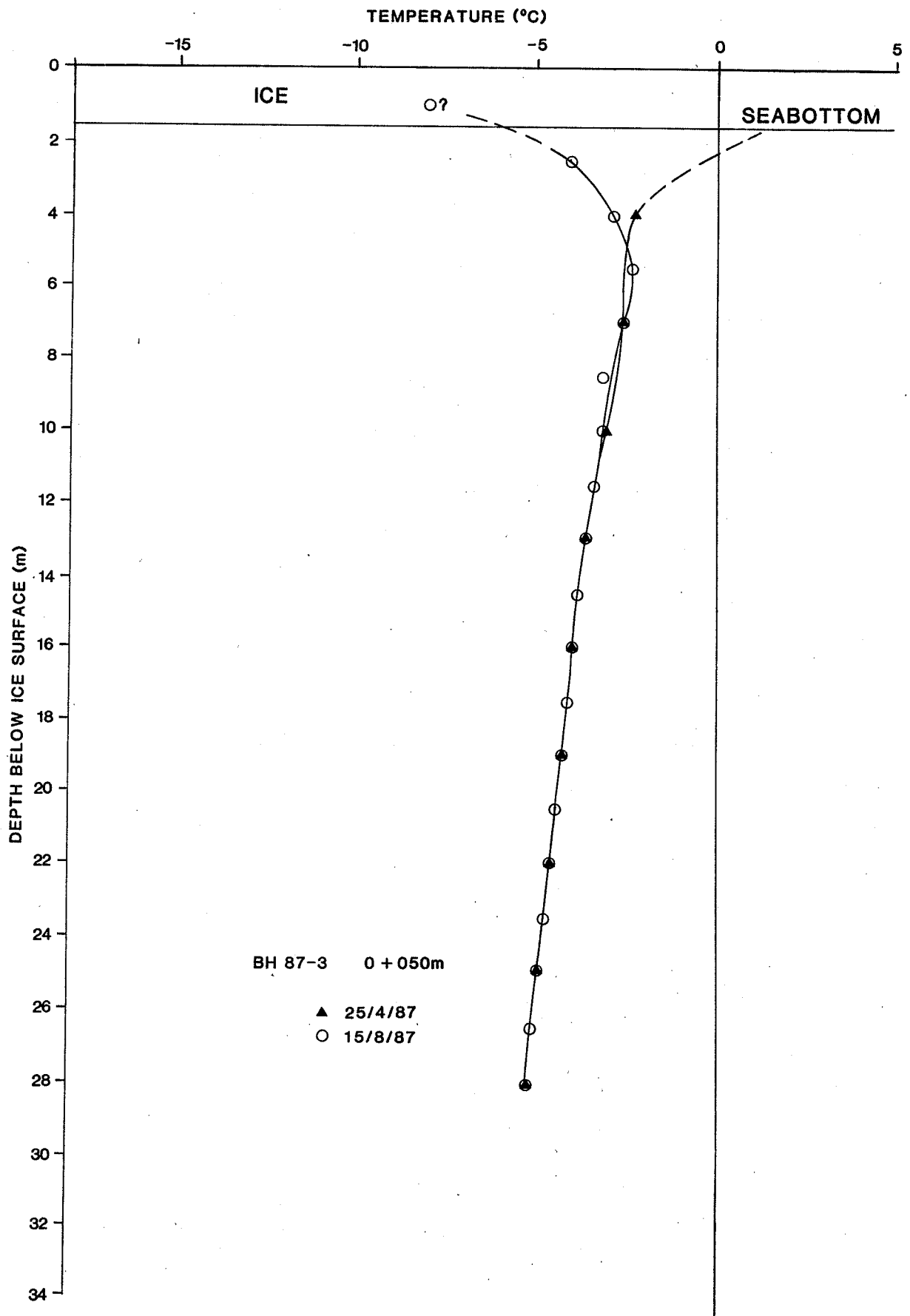


Fig. 4-3 Equilibrium temperature profile - BH 87-3

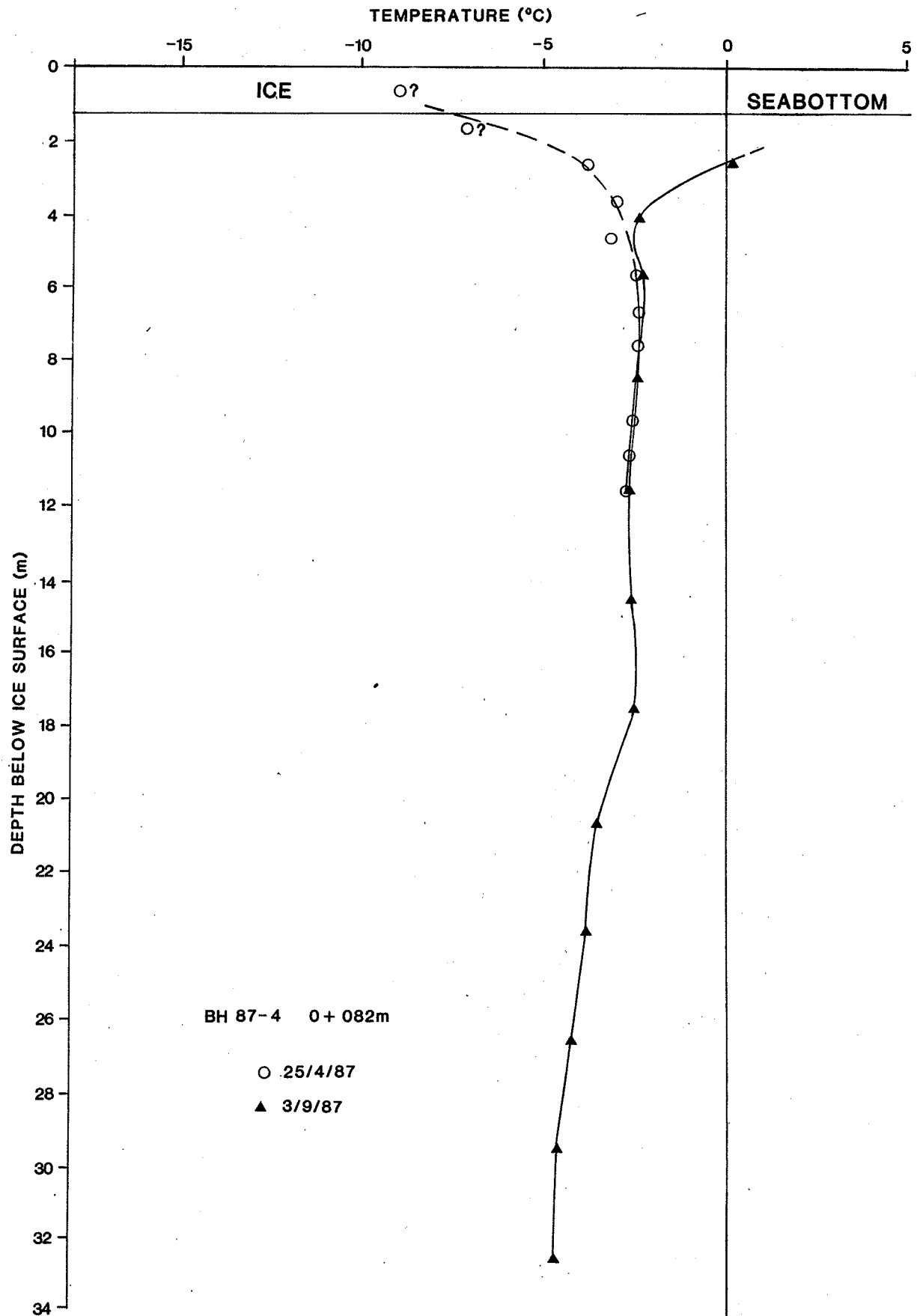


Fig. 4-4 Equilibrium temperature profile - BH 87-4

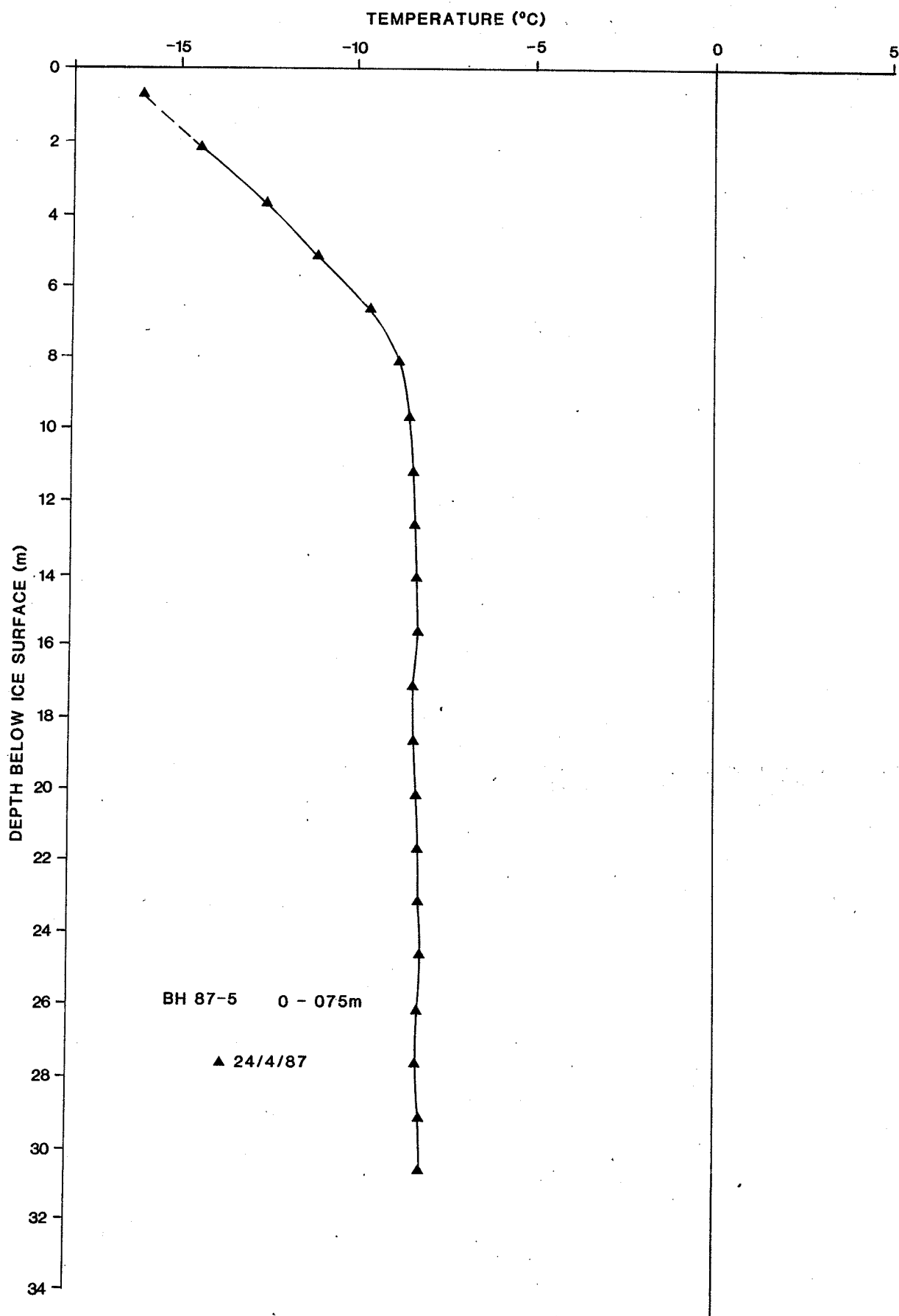


Fig. 4-5 Equilibrium temperature profile - BH 87-5

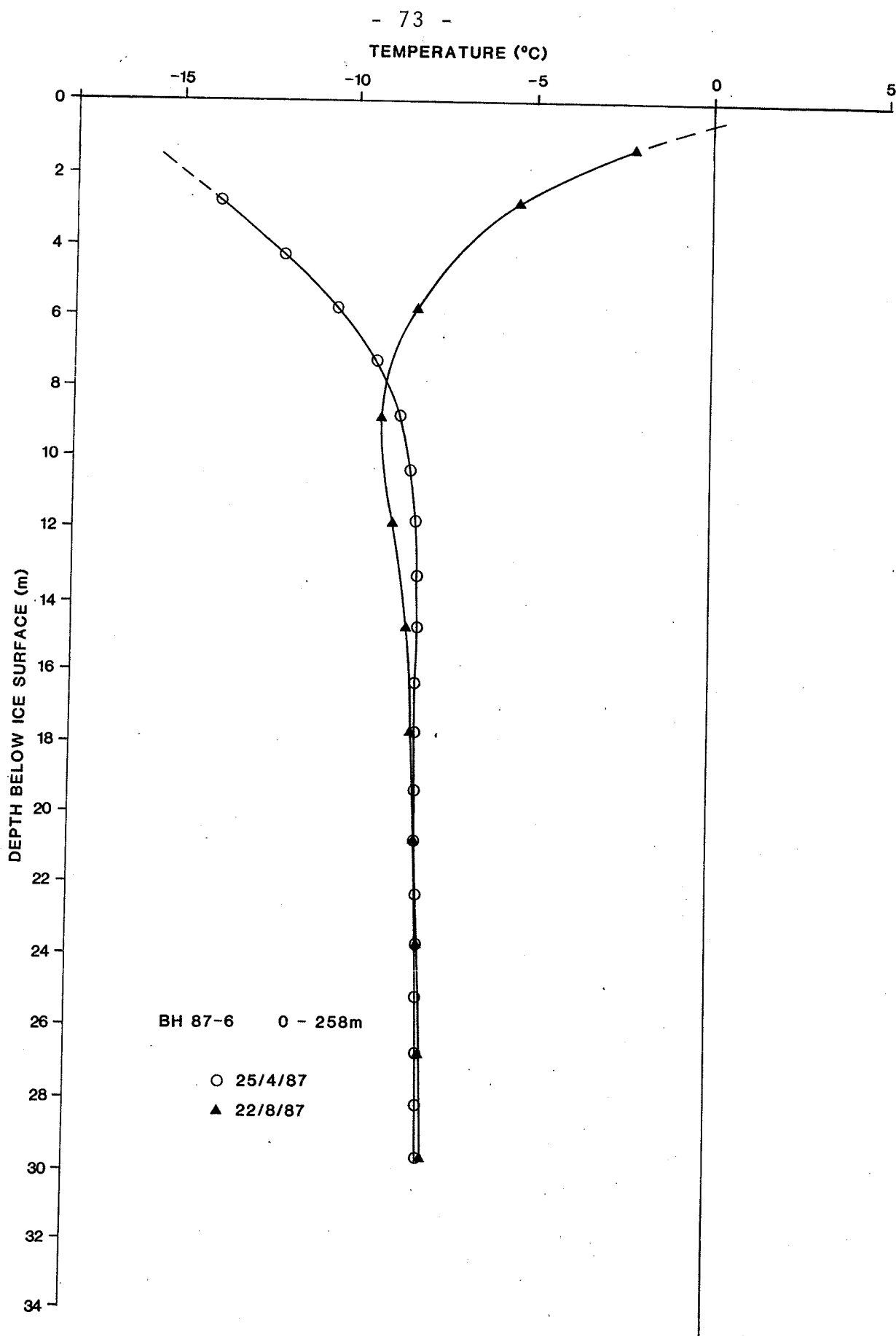


Fig. 4-6 Equilibrium temperature profile - BH 87-6

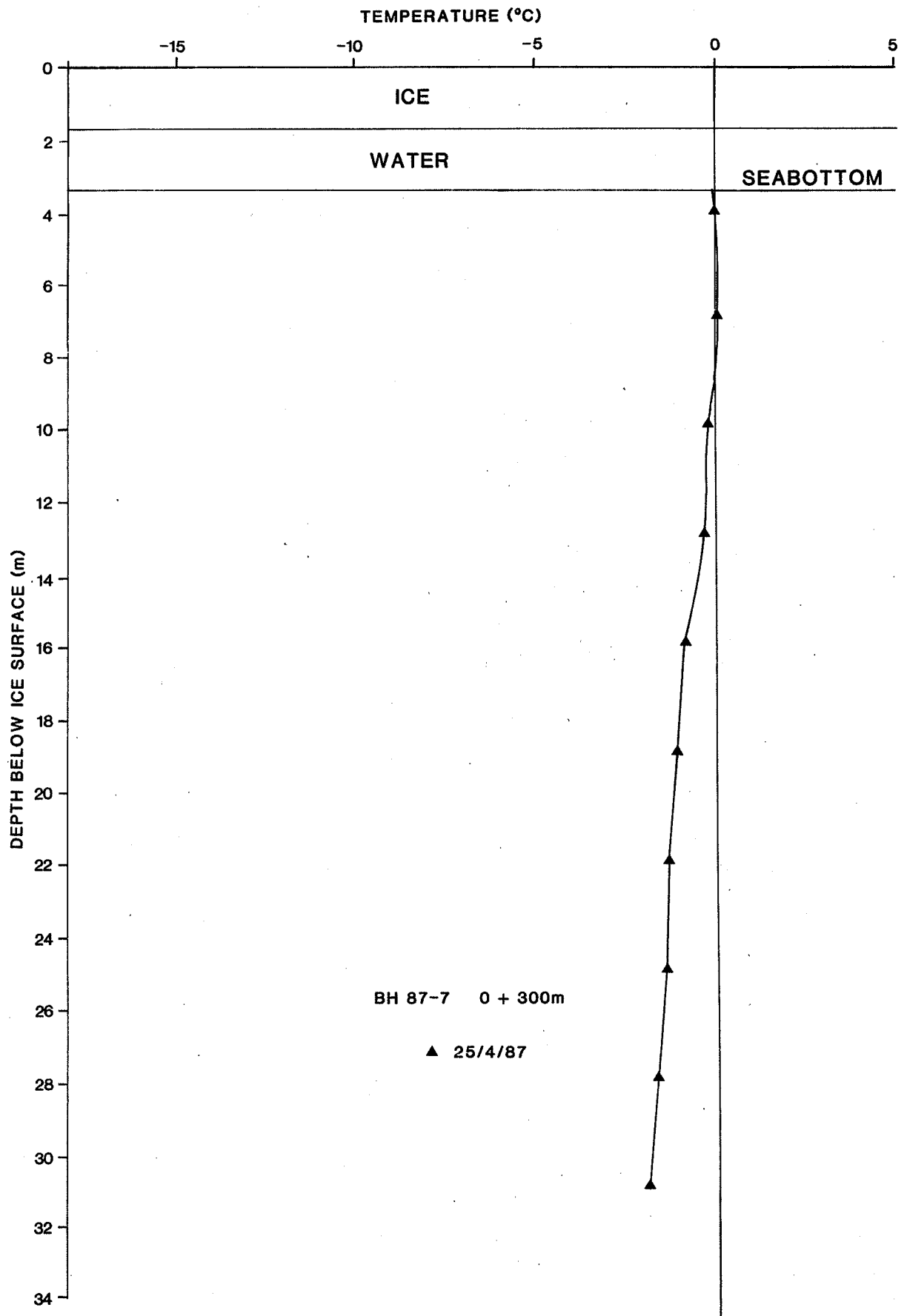


Fig. 4-7 Equilibrium temperature profile - BH 87-7

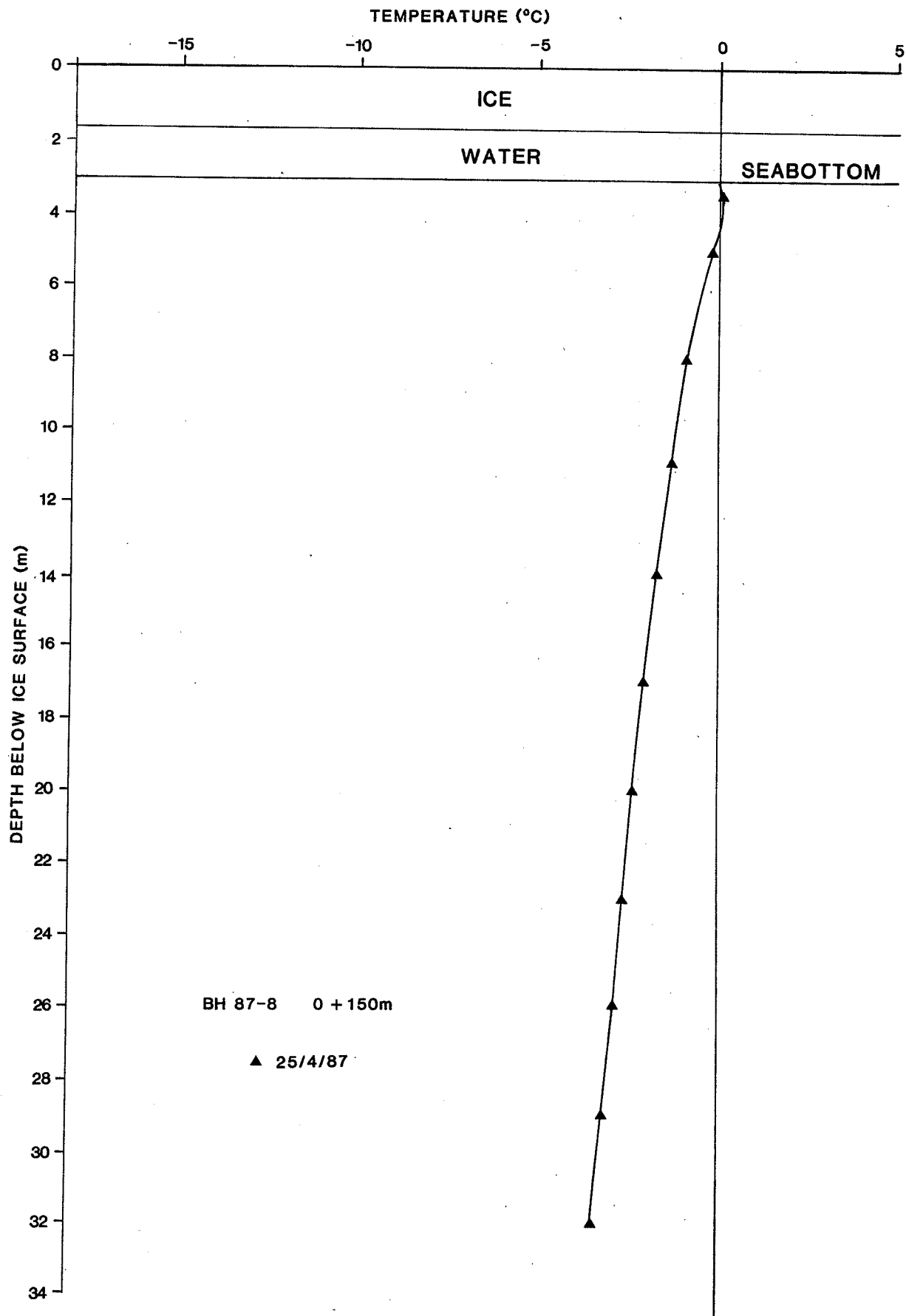


Fig. 4-8 Equilibrium temperature profile - BH 87-8

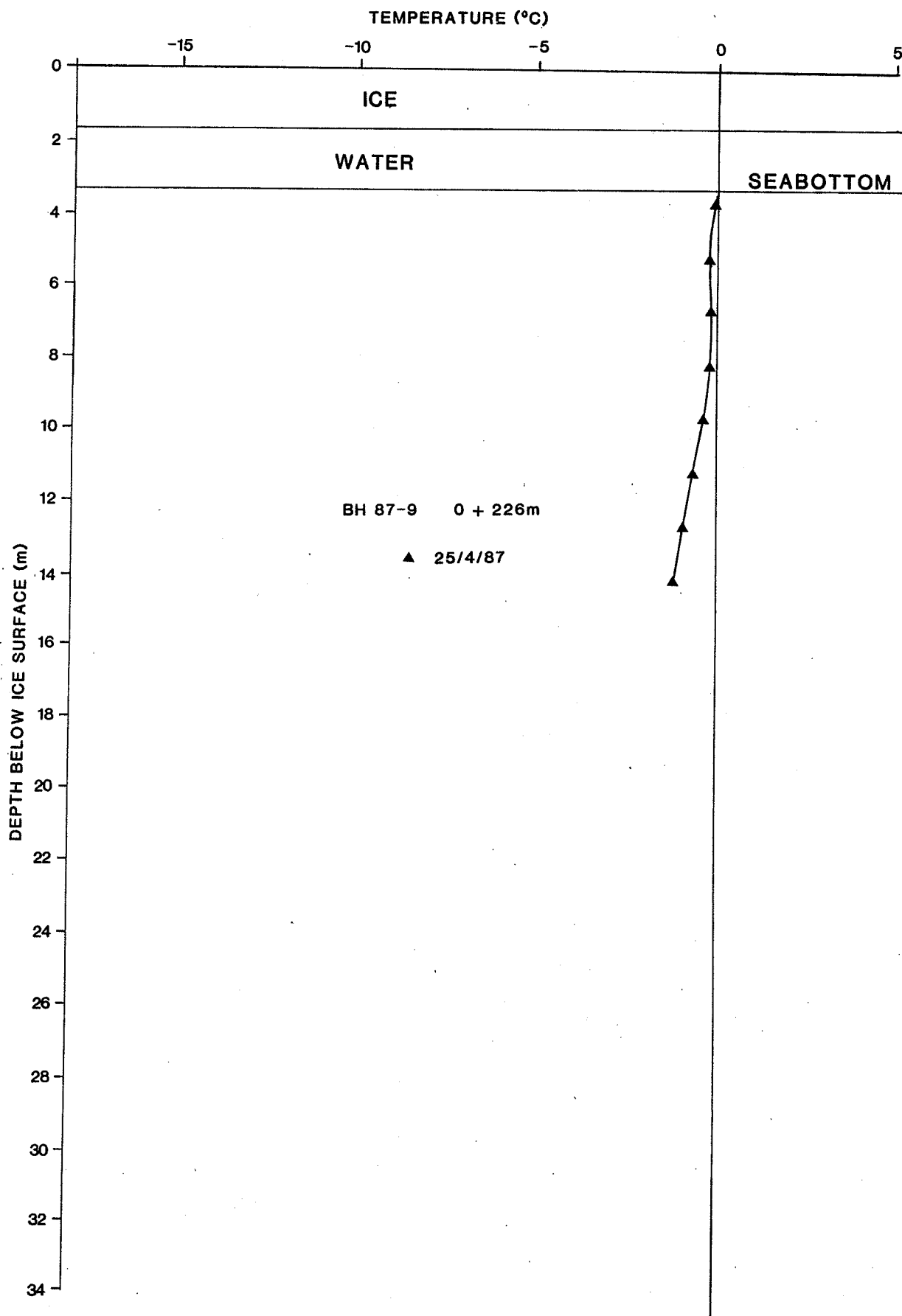


Fig. 4-9 Equilibrium temperature profile - BH 87-9

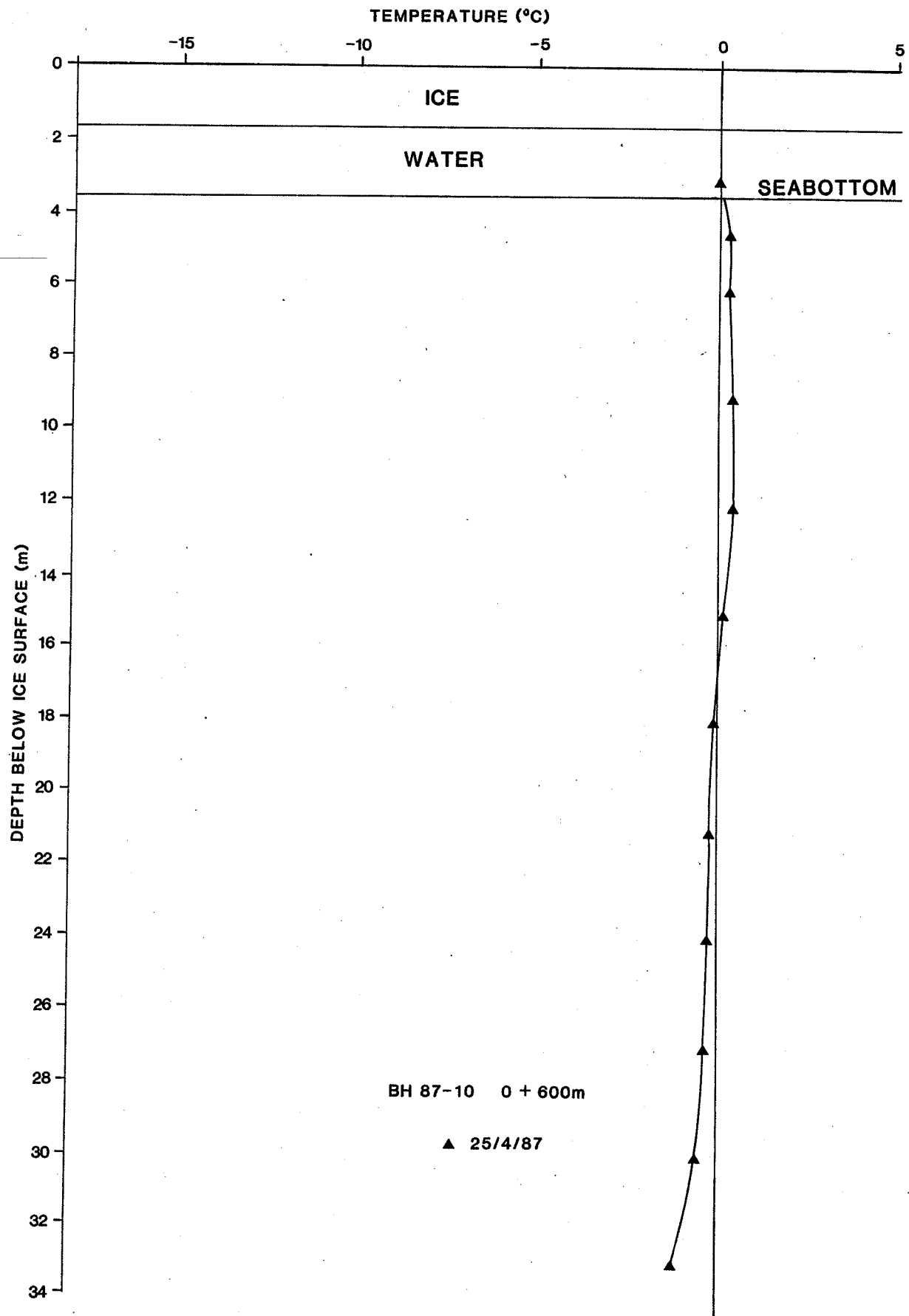


Fig. 4-10 Equilibrium temperature profile - BH 87-10

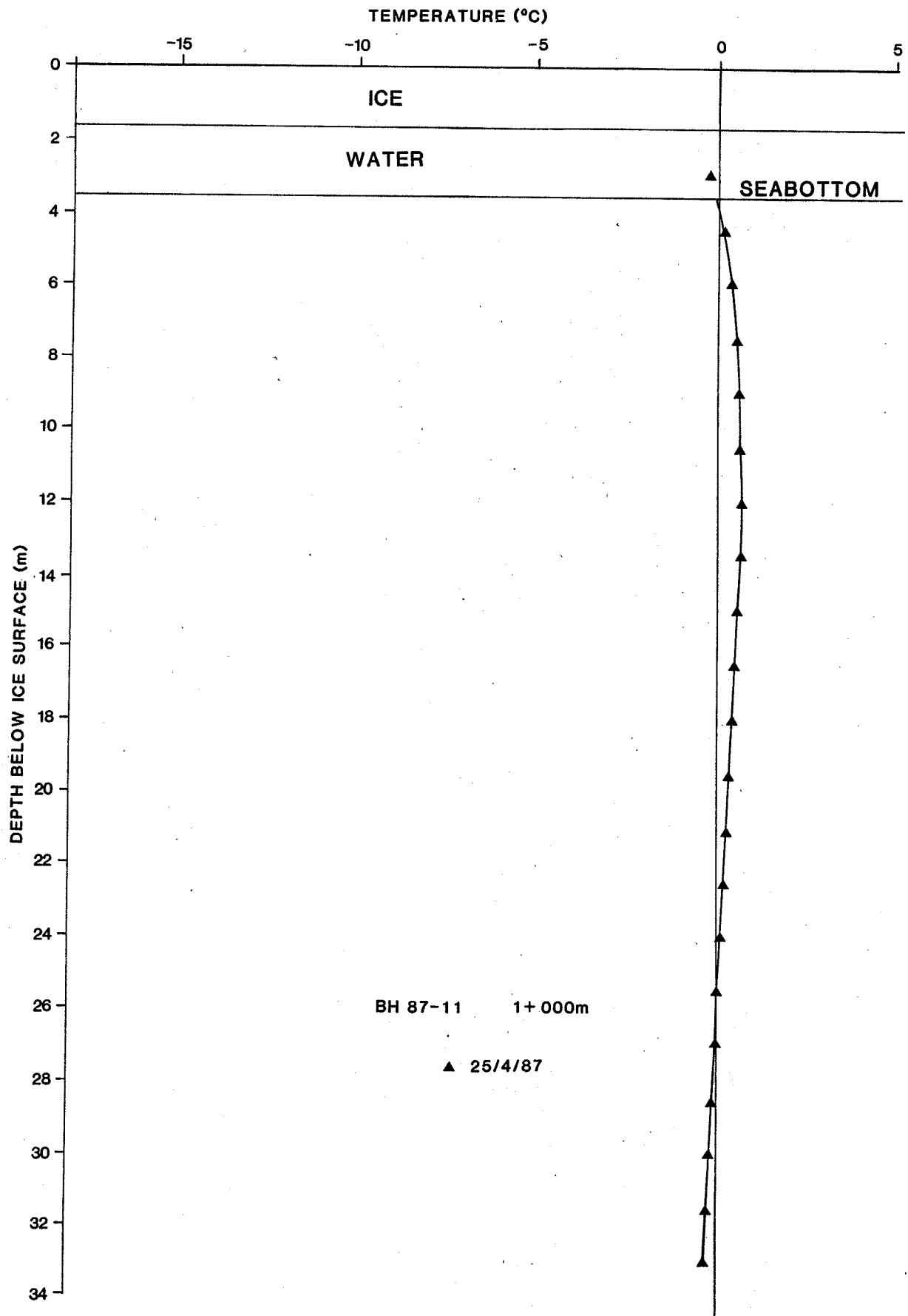


Fig. 4-11 Equilibrium temperature profile - BH 87-11

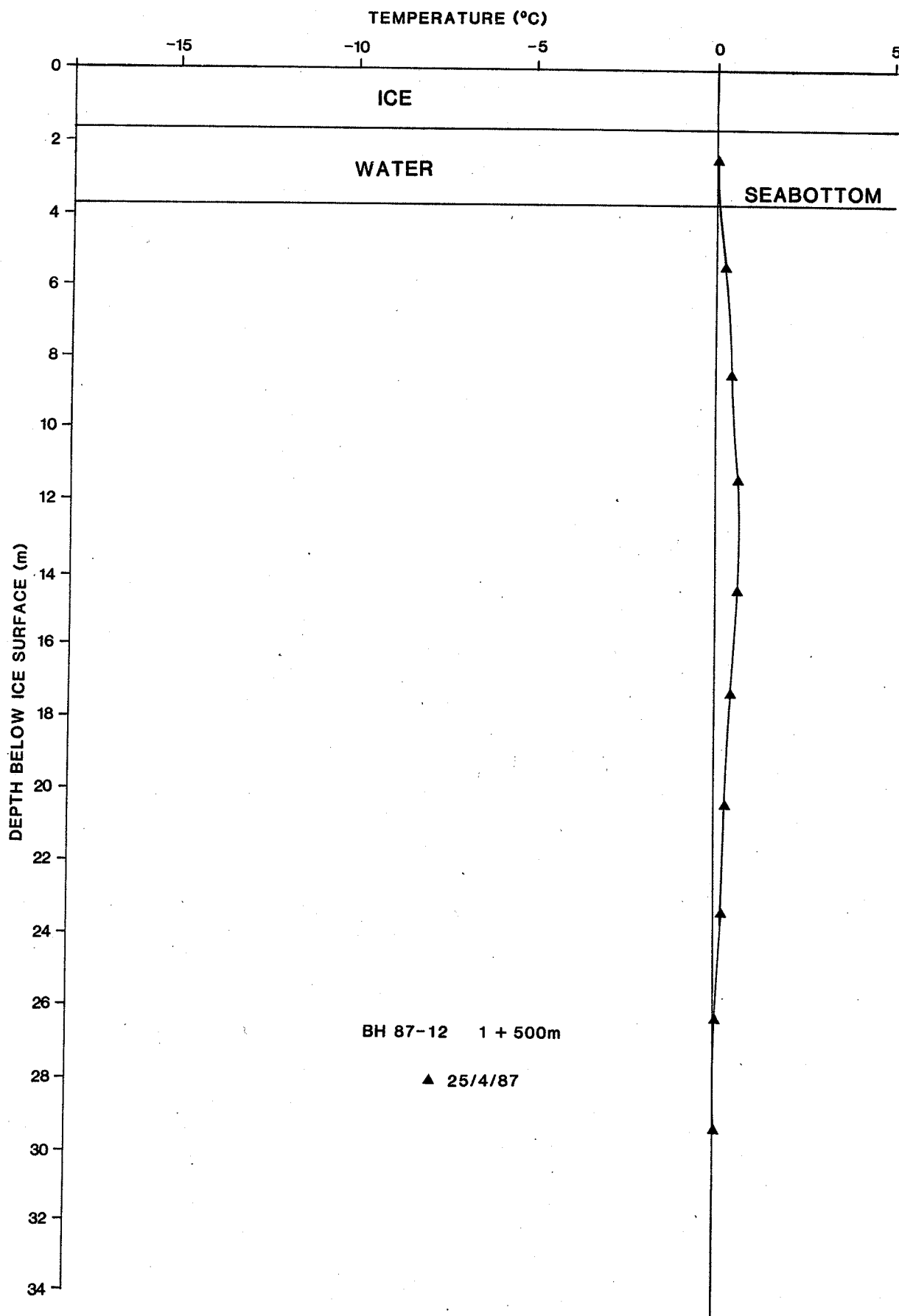


Fig. 4-12 Equilibrium temperature profile - BH 87-12.

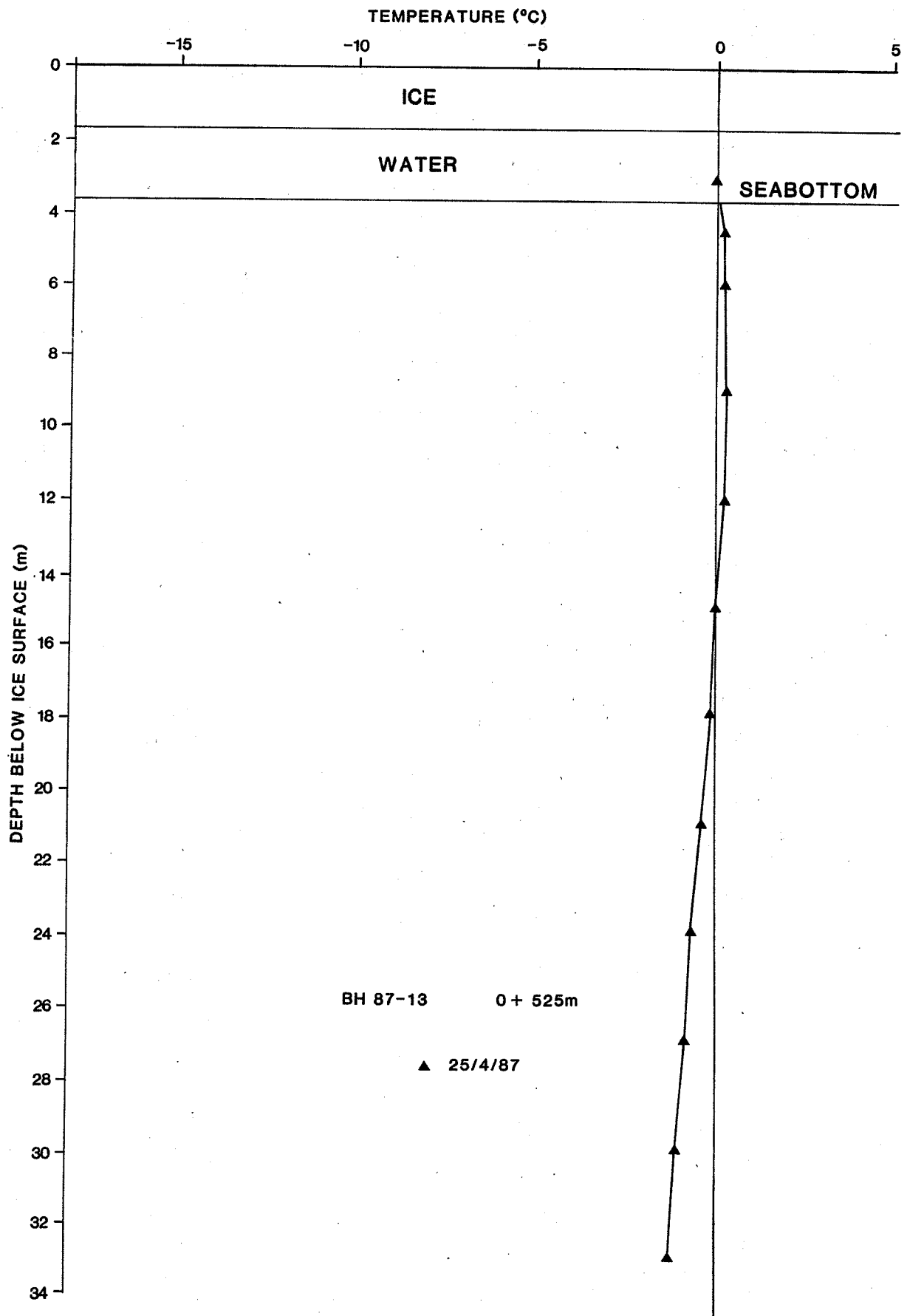


Fig. 4-13 Equilibrium temperature profile - BH 87-13.

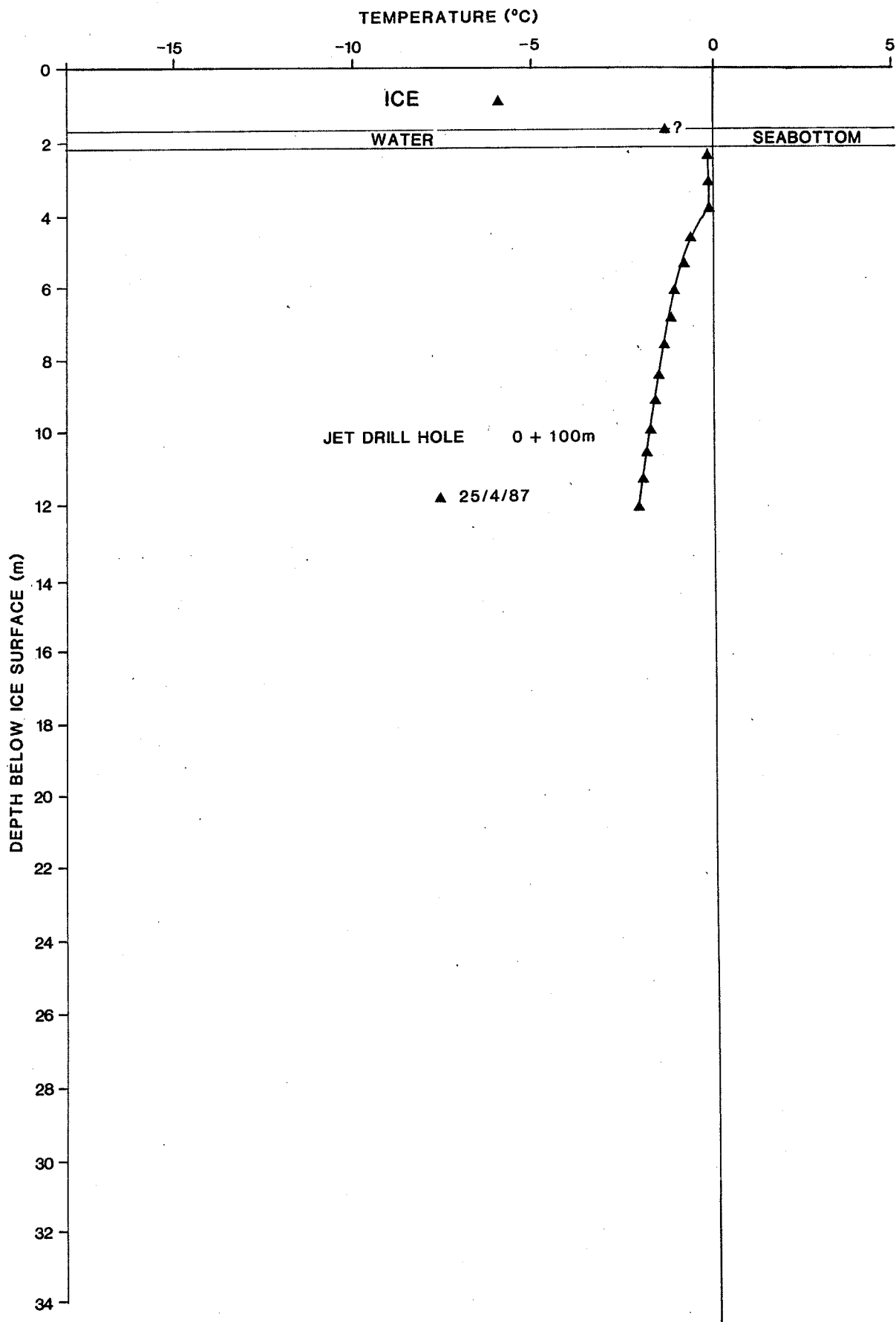


Fig. 4-14 Equilibrium temperature profile - JD-1

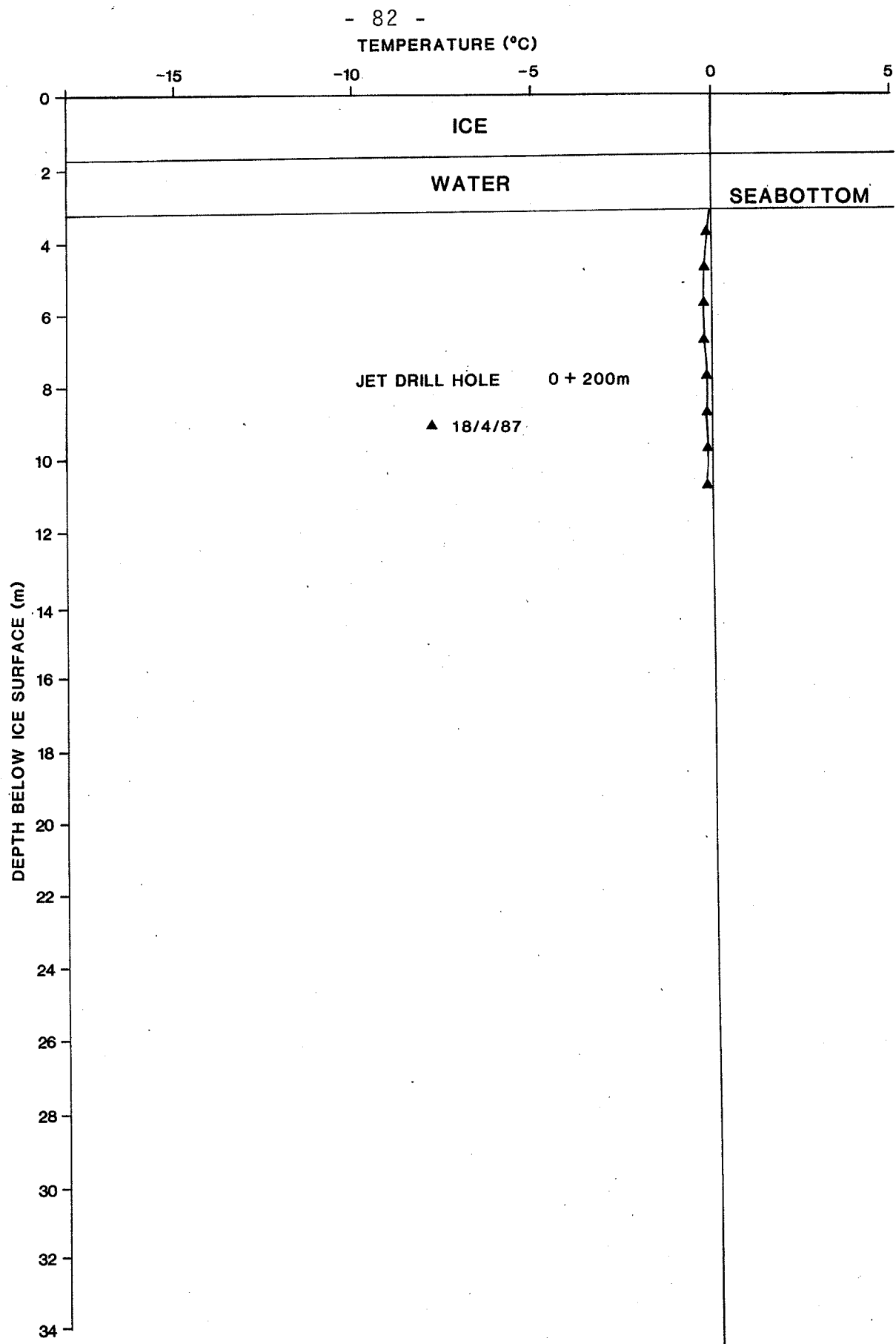


Fig. 4-15 Equilibrium temperature profile - JD-2

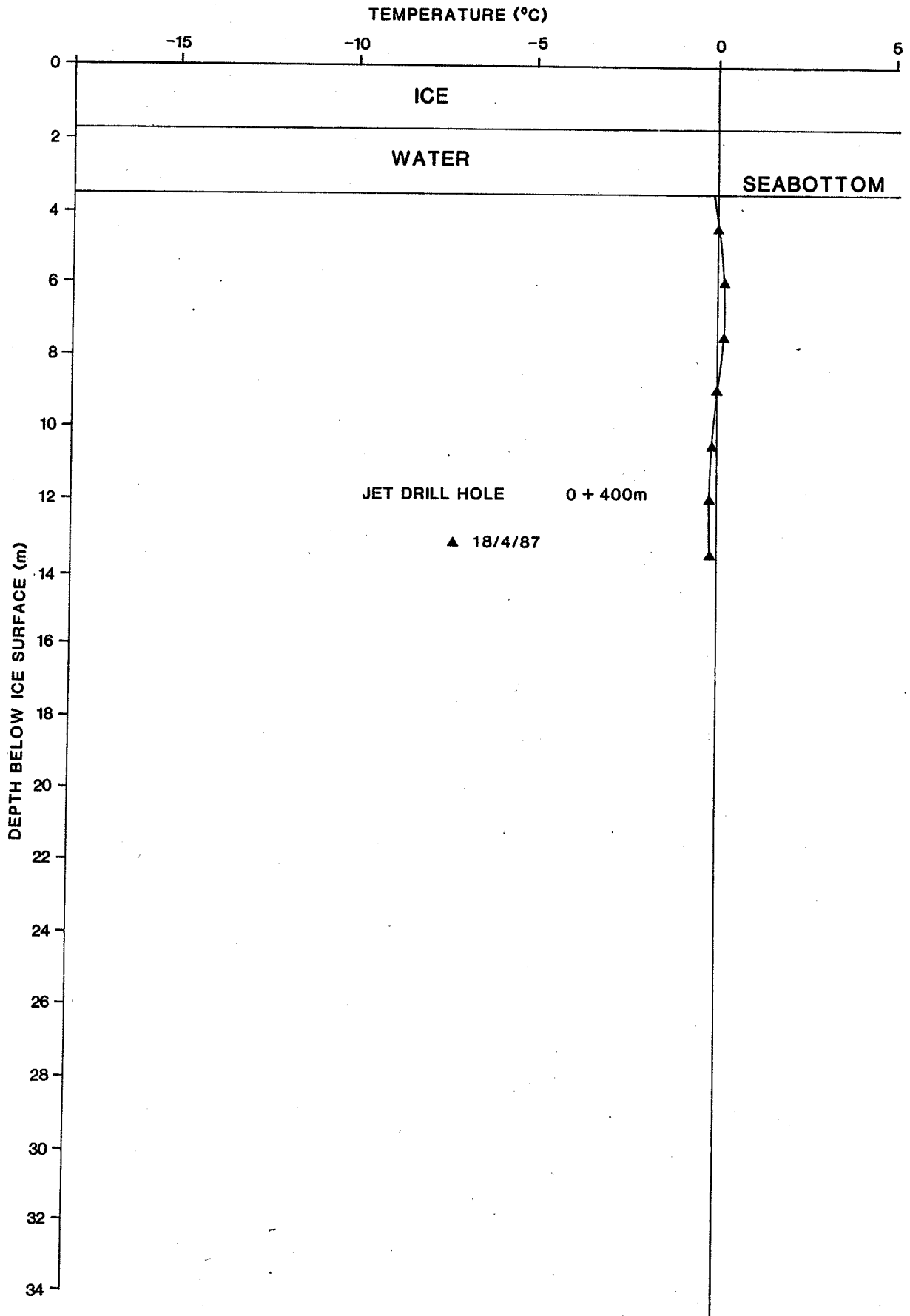


Fig. 4-16 Equilibrium temperature profile - JD-3

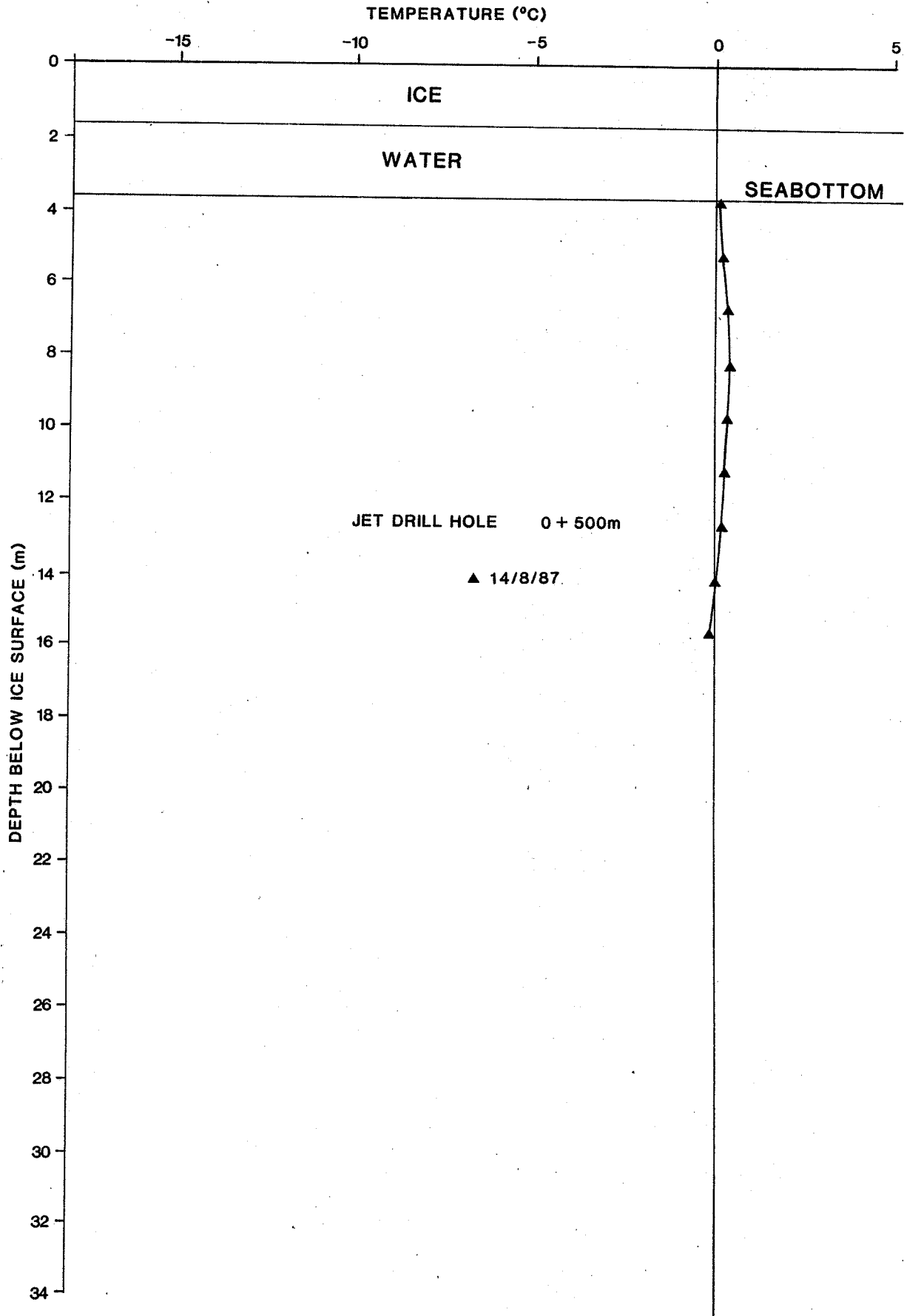


Fig. 4-17 Equilibrium temperature profile - JD-4

TEMPERATURE SECTION - NORTH HEAD (April 87)

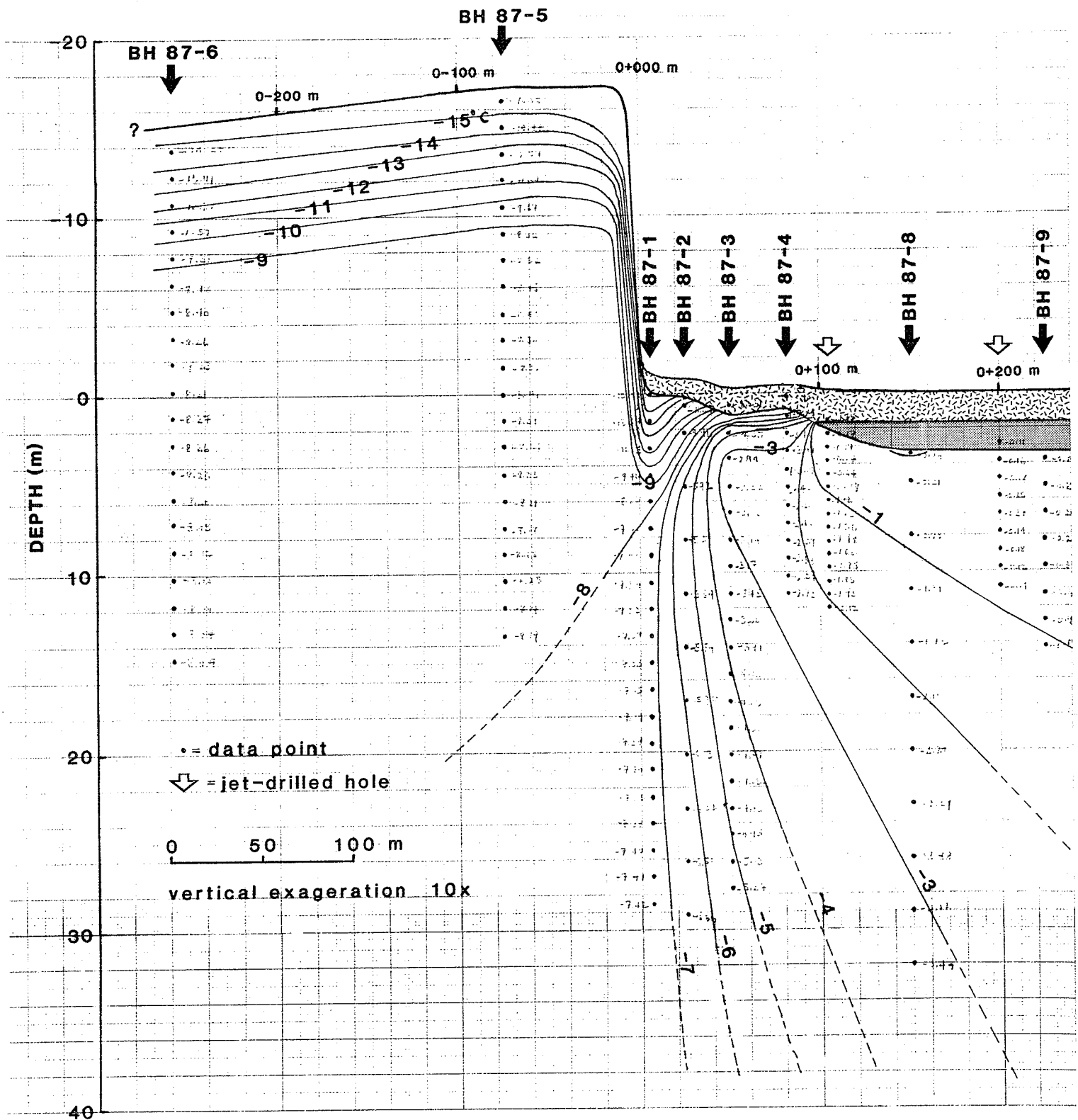
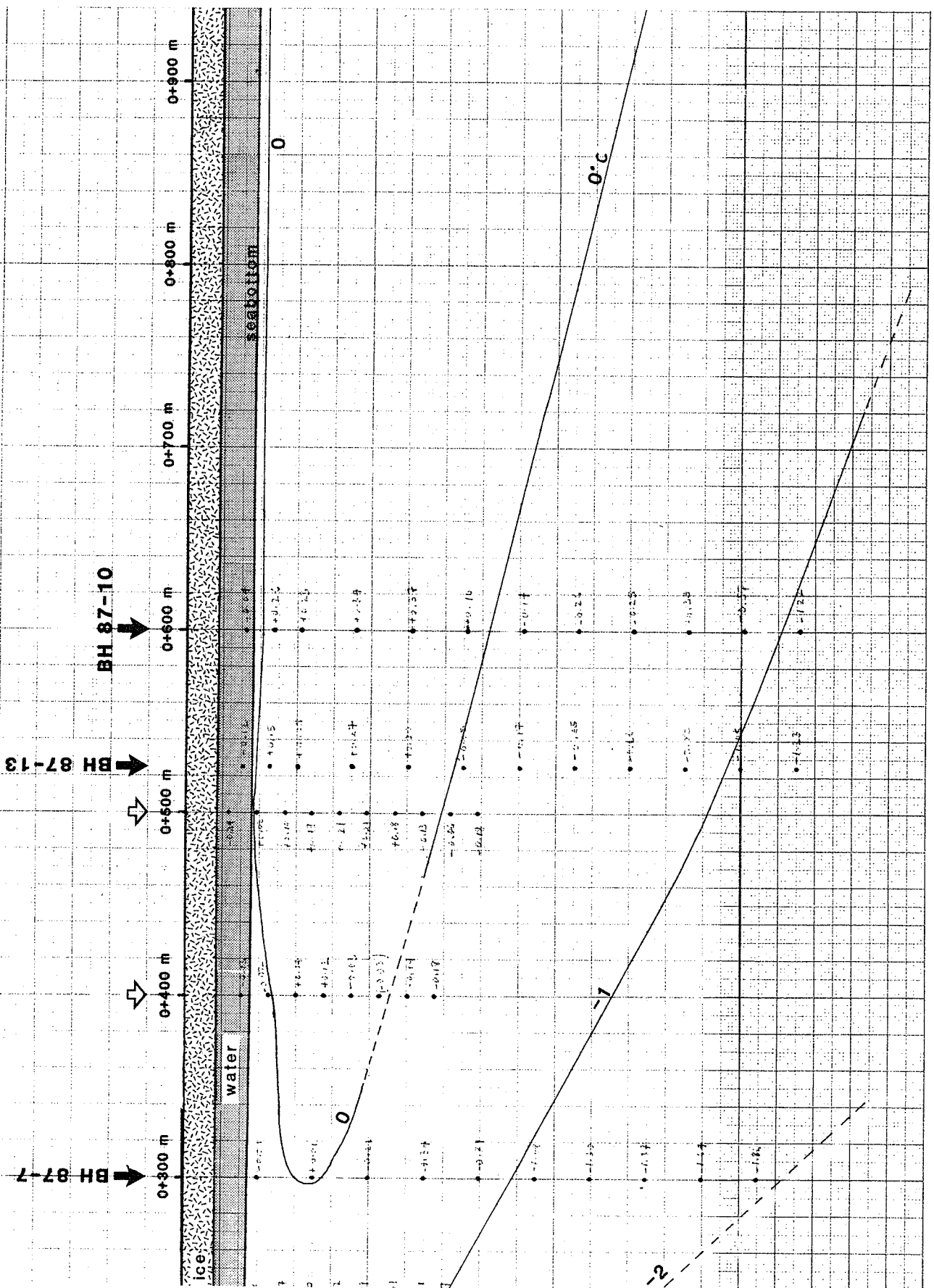
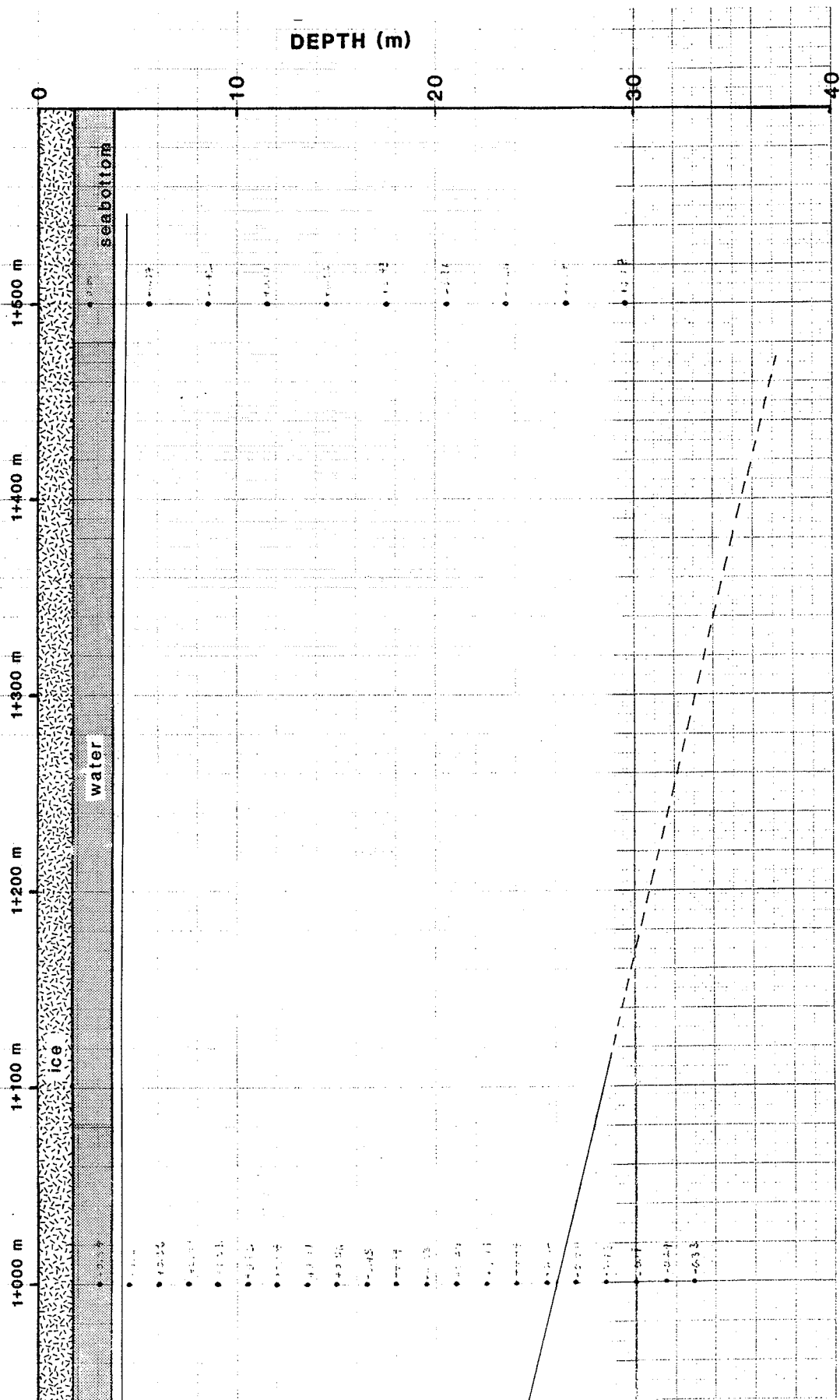


Fig. 4-18 Temperature profile along drill transect - winter 1987



BH 87-11

BH 87-12



TEMPERATURE SECTION AT SHORELINE - NORTH HEAD (April 87)

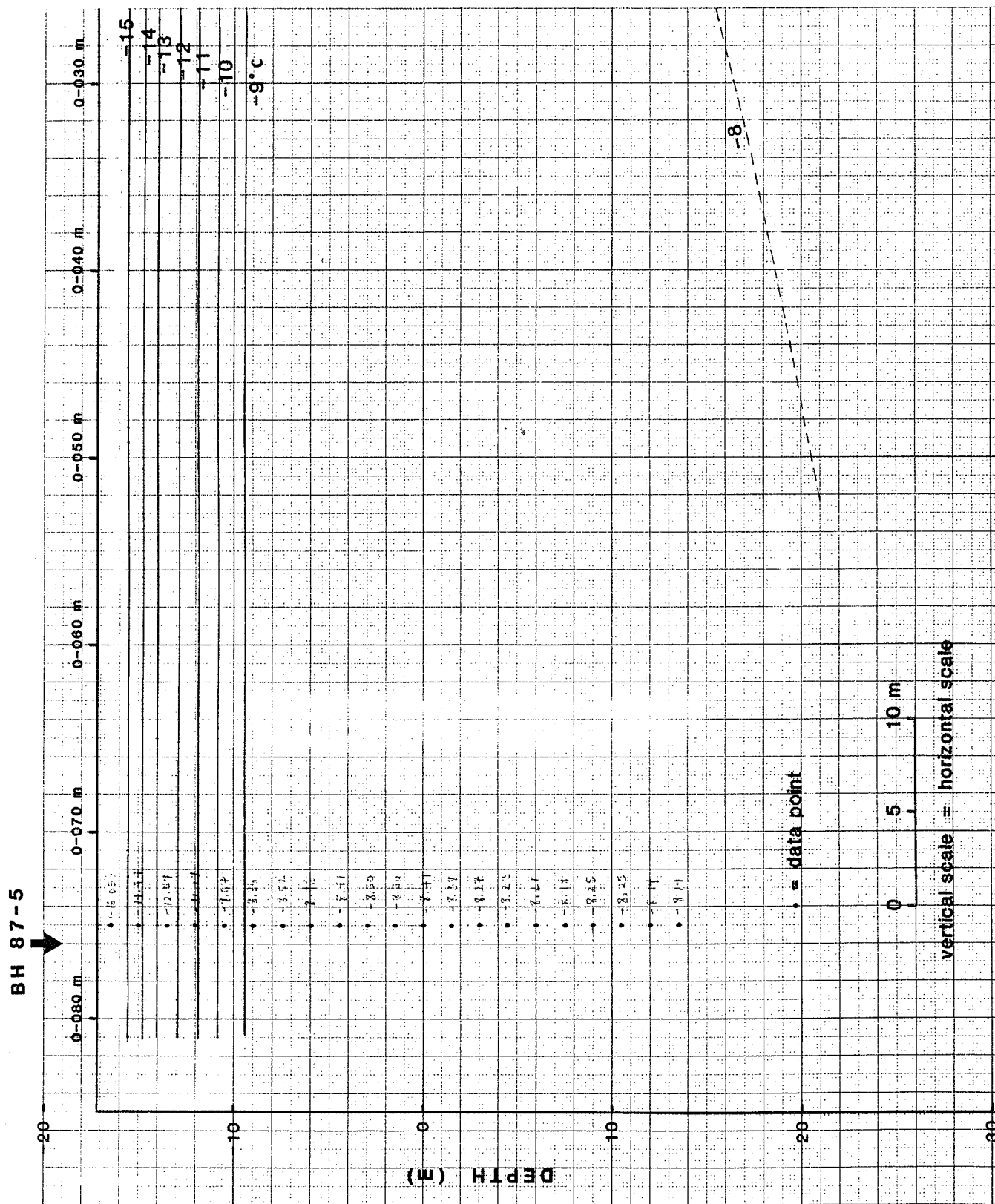
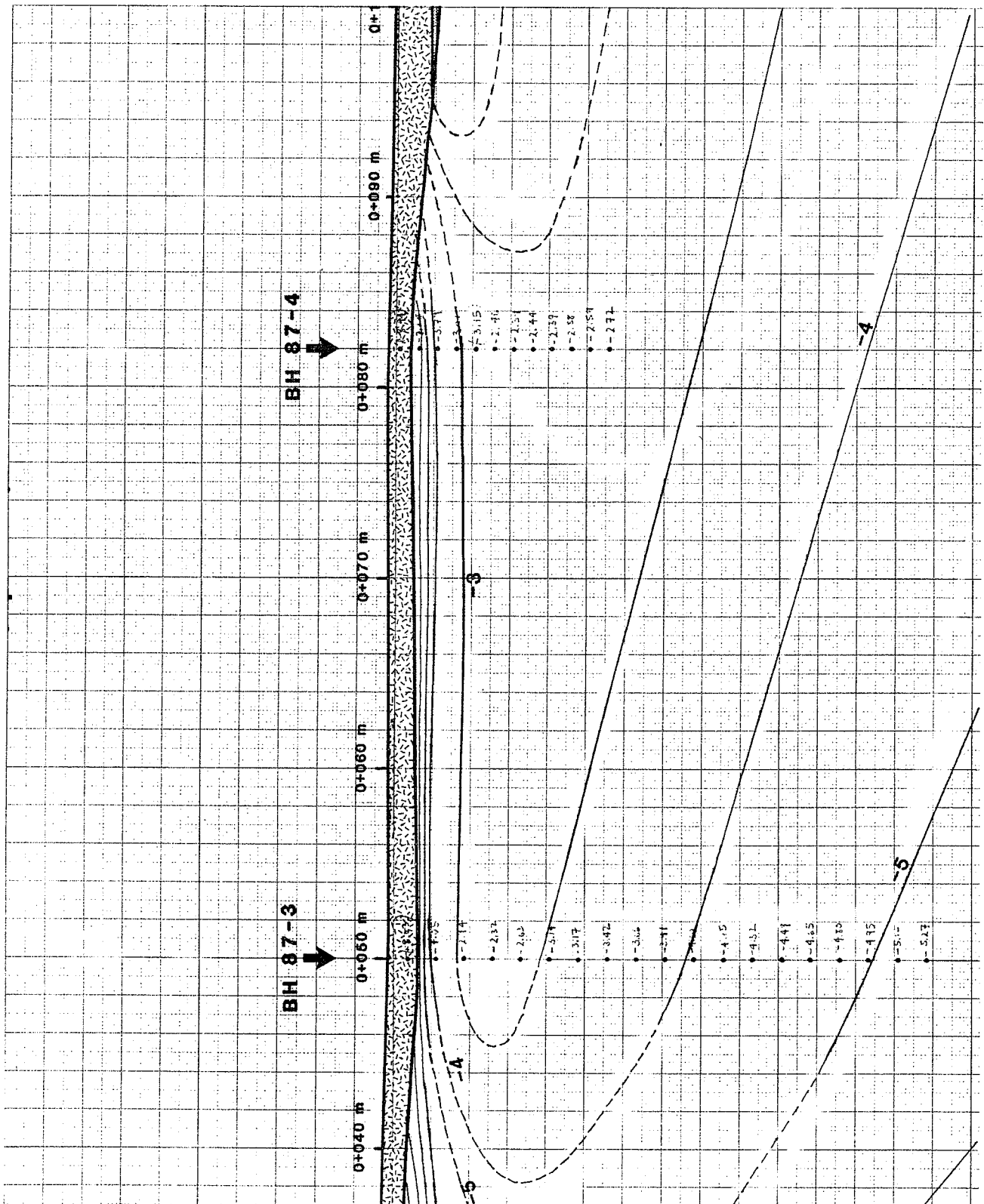
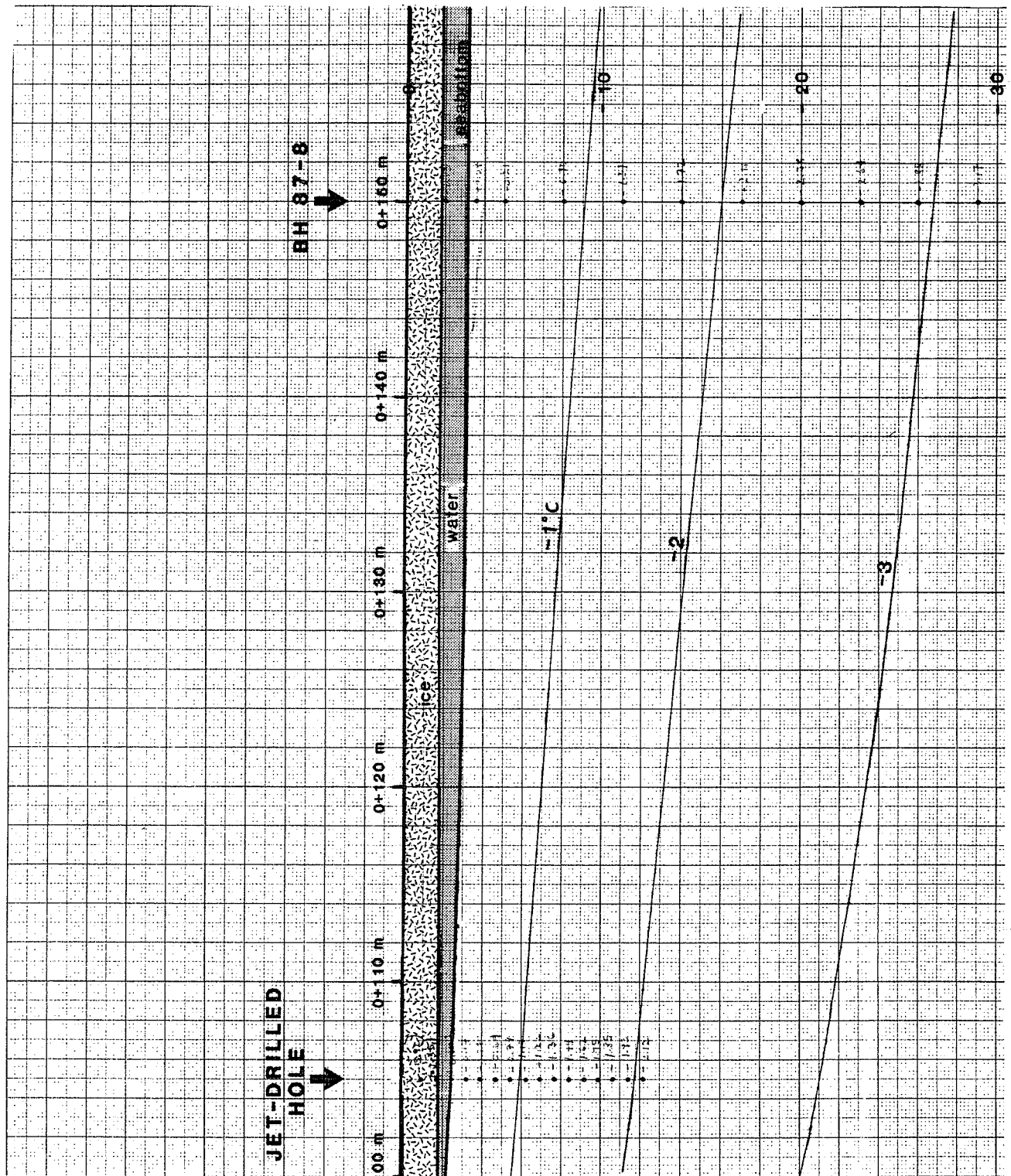


Fig. 4-19 Temperature profile along drill transect (-80 to 150 m) - winter 1987





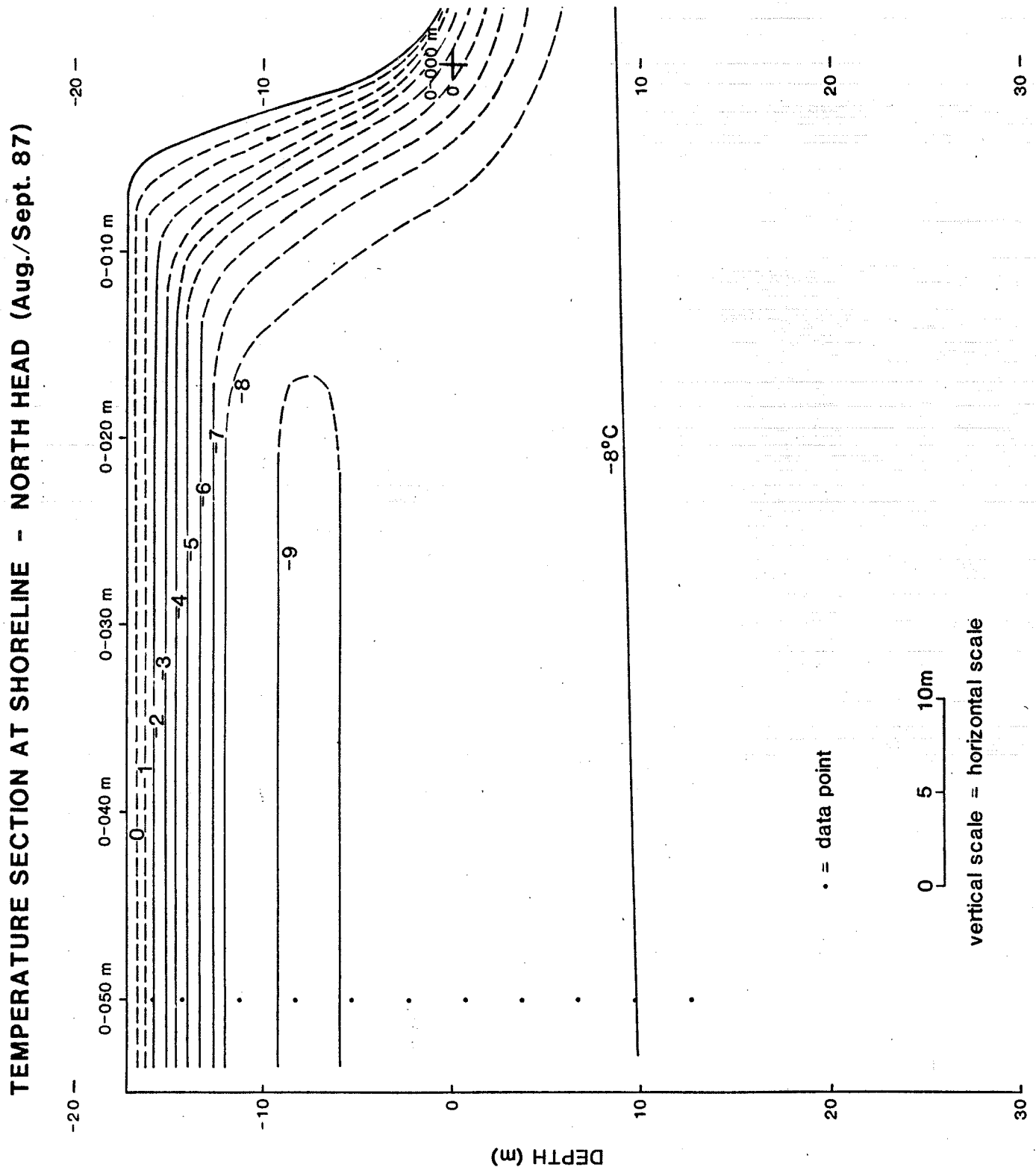
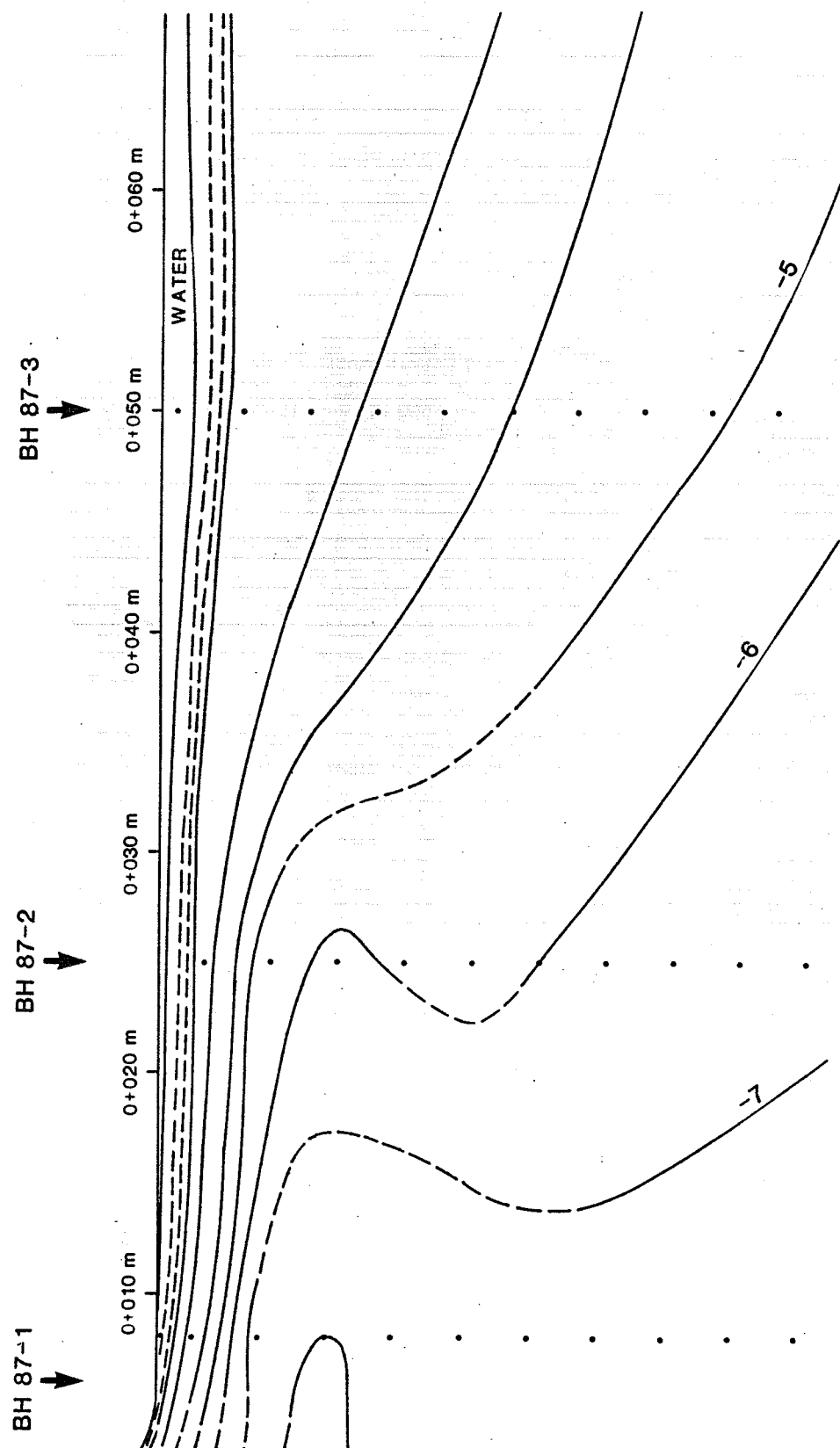
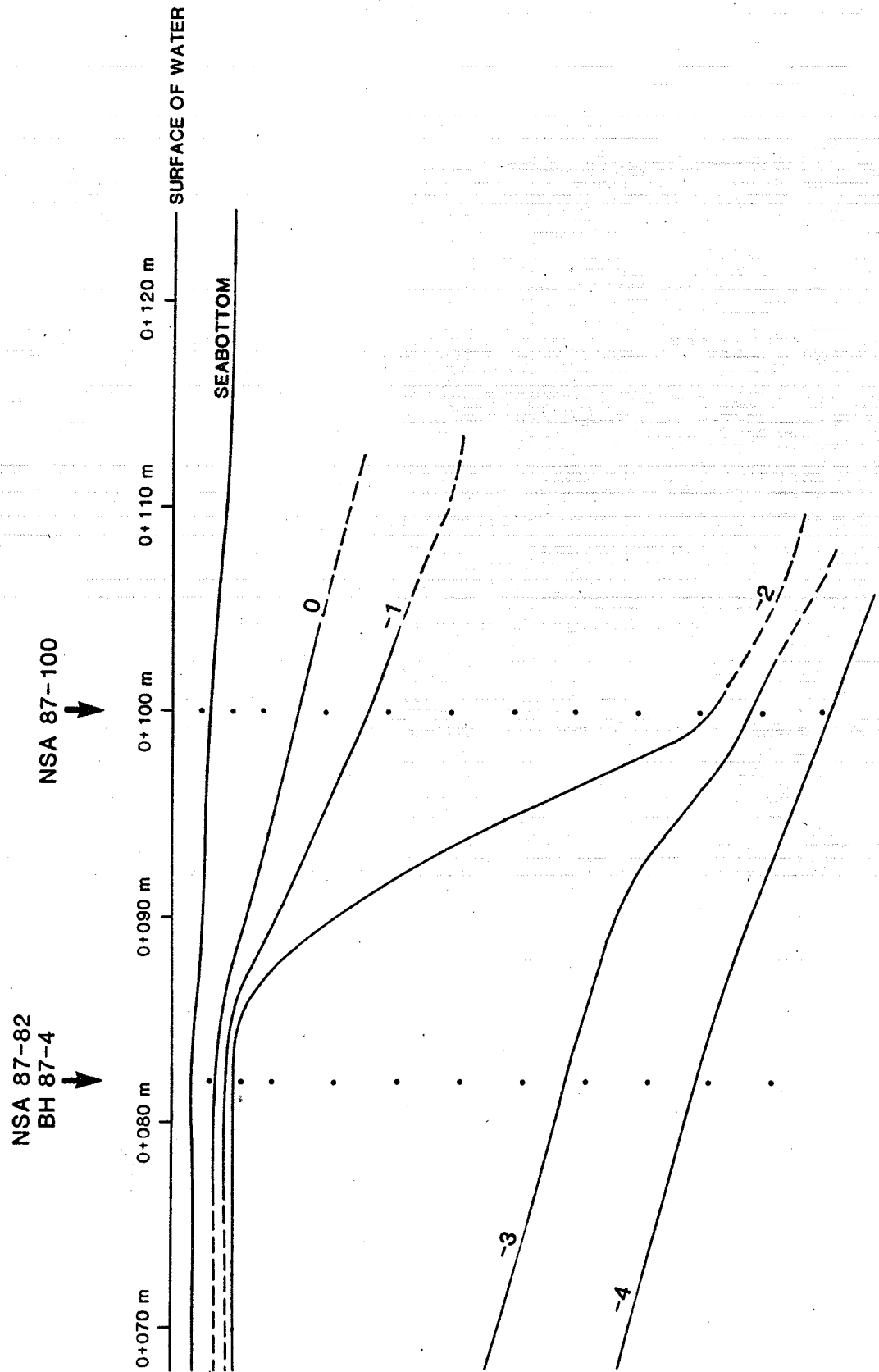


Fig. 4-20 Temperature profile along drill transect - summer 1987





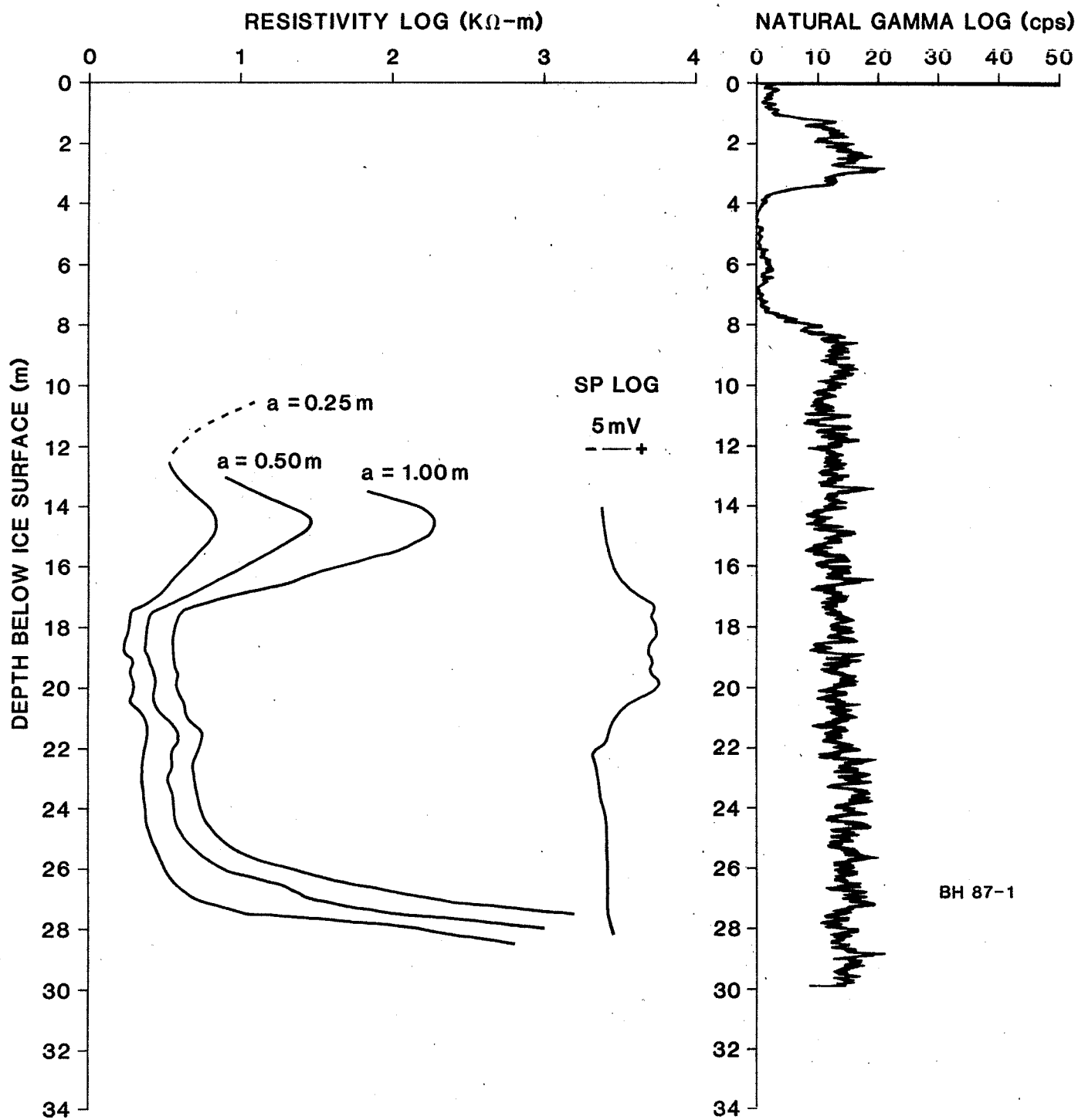


Fig. 4-21 Geophysical borehole logs - BH 87-1

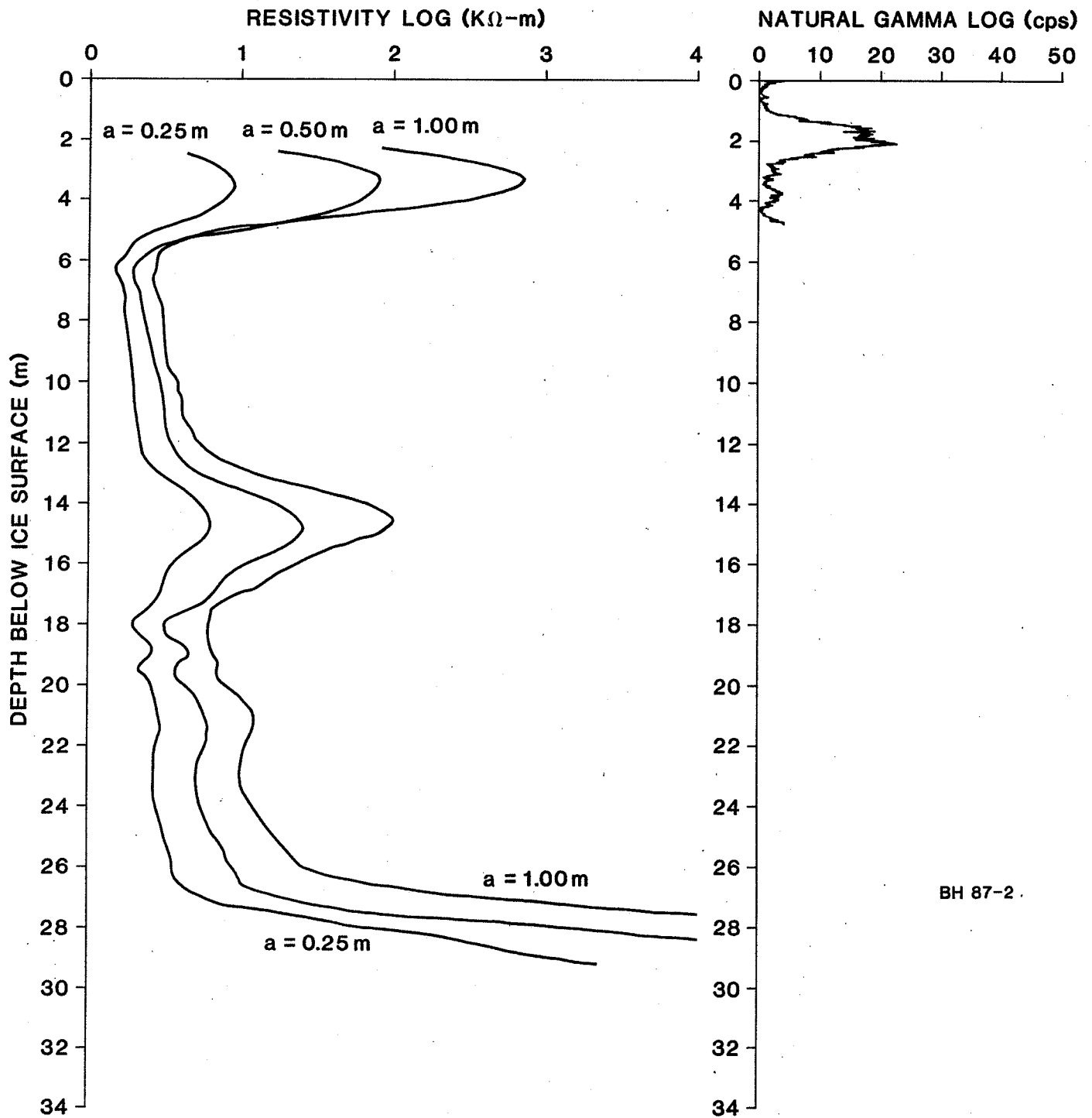


Fig. 4-22 Geophysical borehole logs - BH 87-2

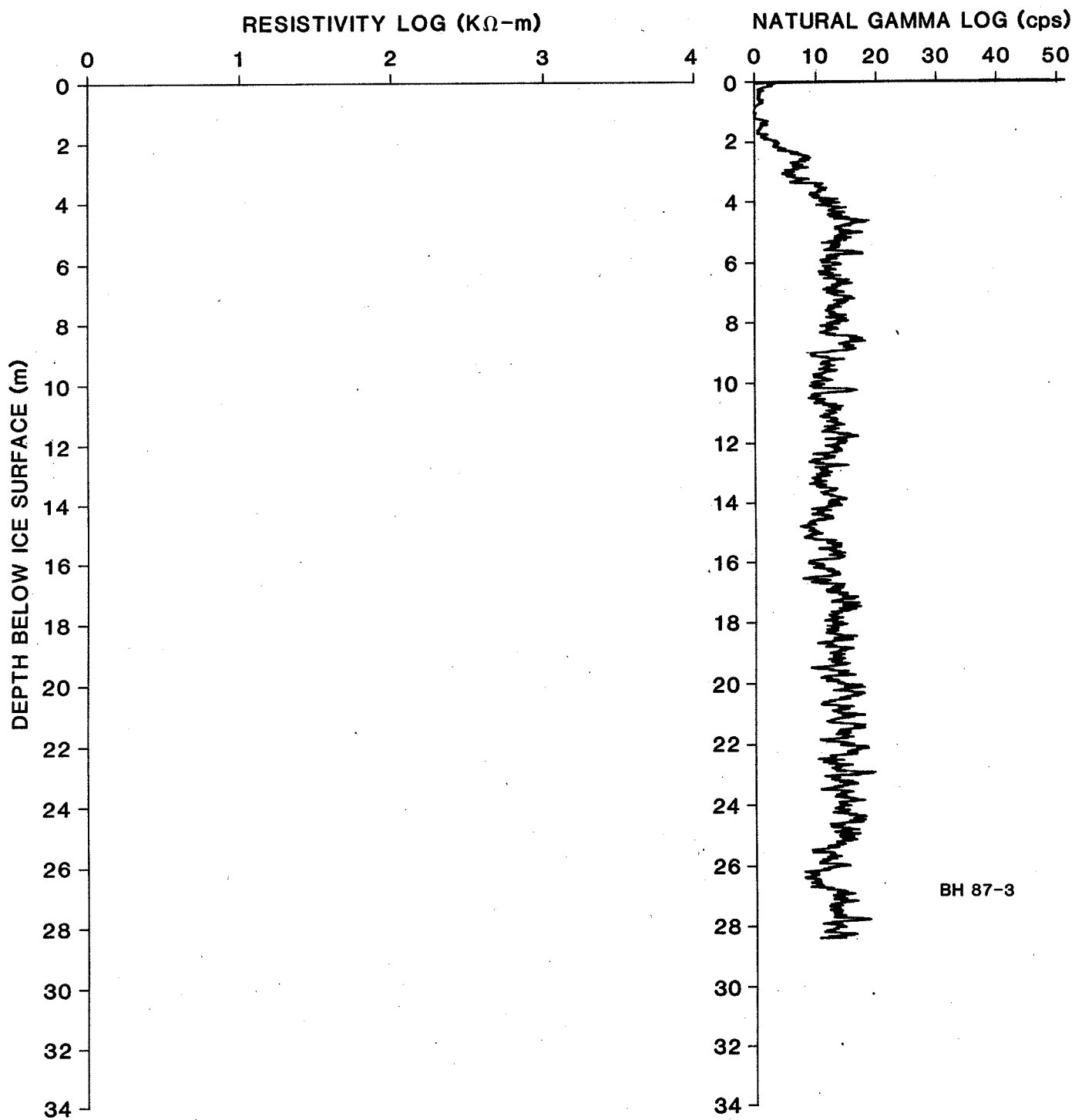
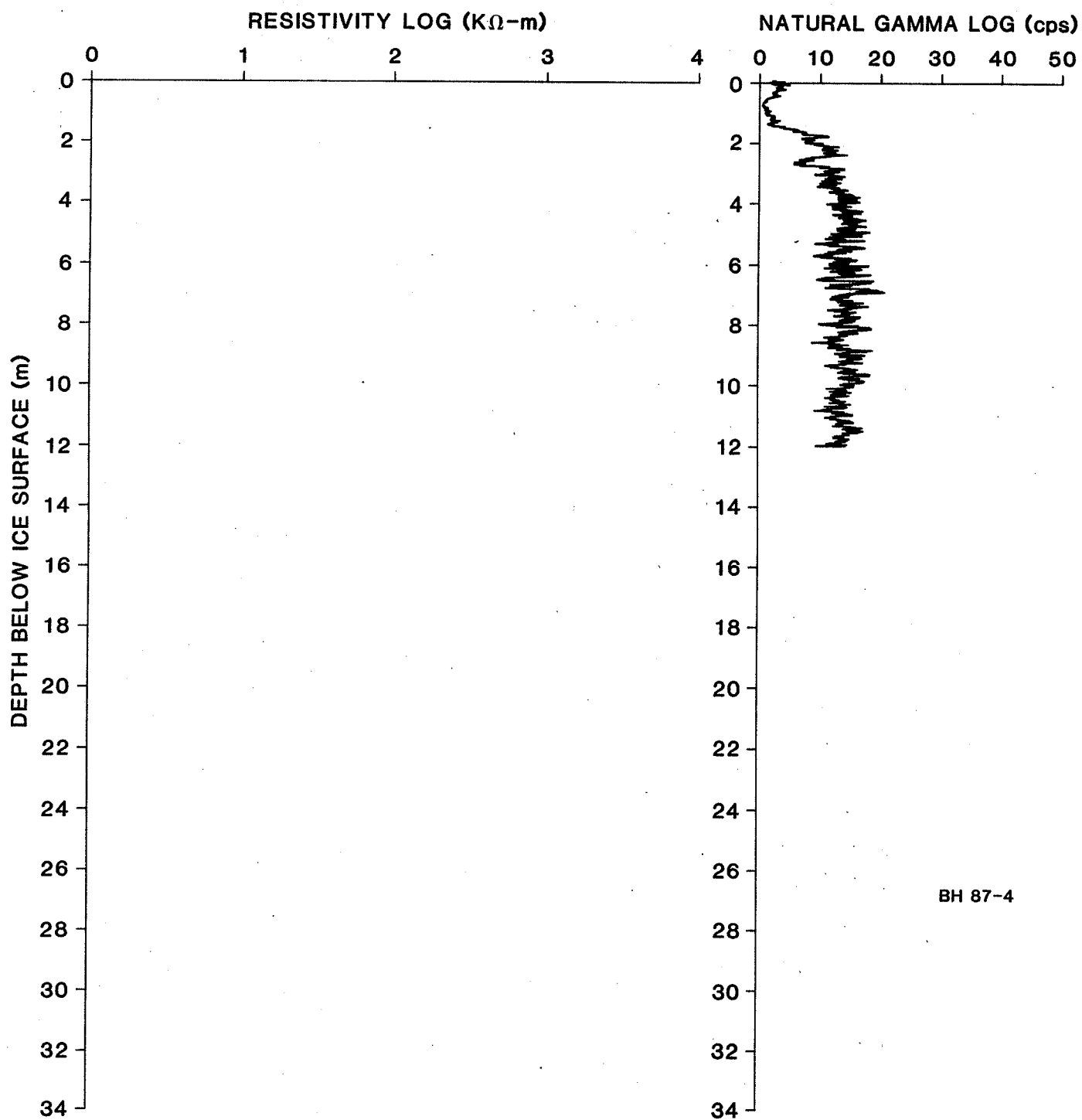


Fig. 4-23 Geophysical borehole logs - BH 87-3



BH 87-4

Fig. 4-24 Geophysical borehole logs - BH 87-4

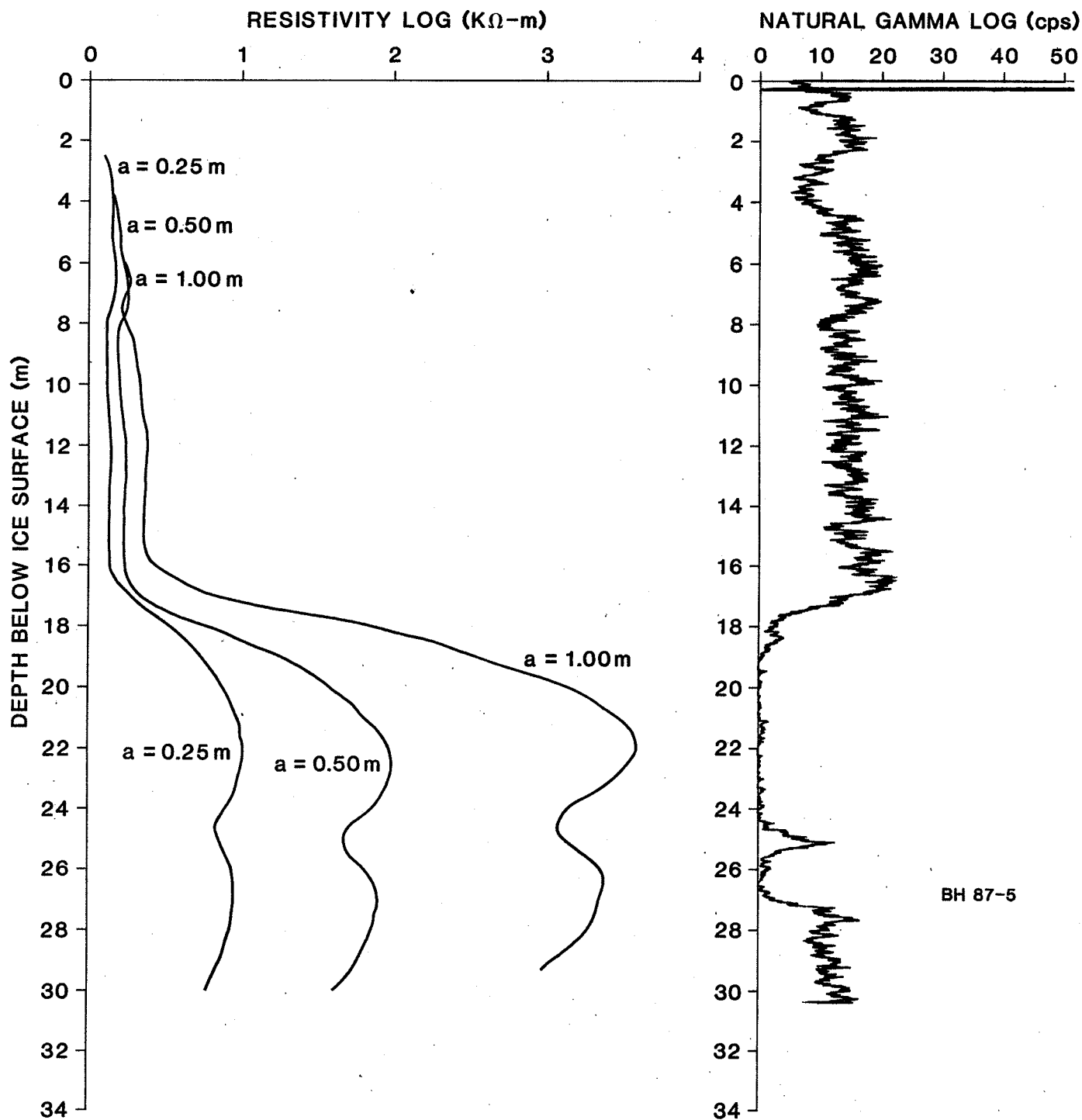


Fig. 4-25 Geophysical borehole logs - BH 87-5

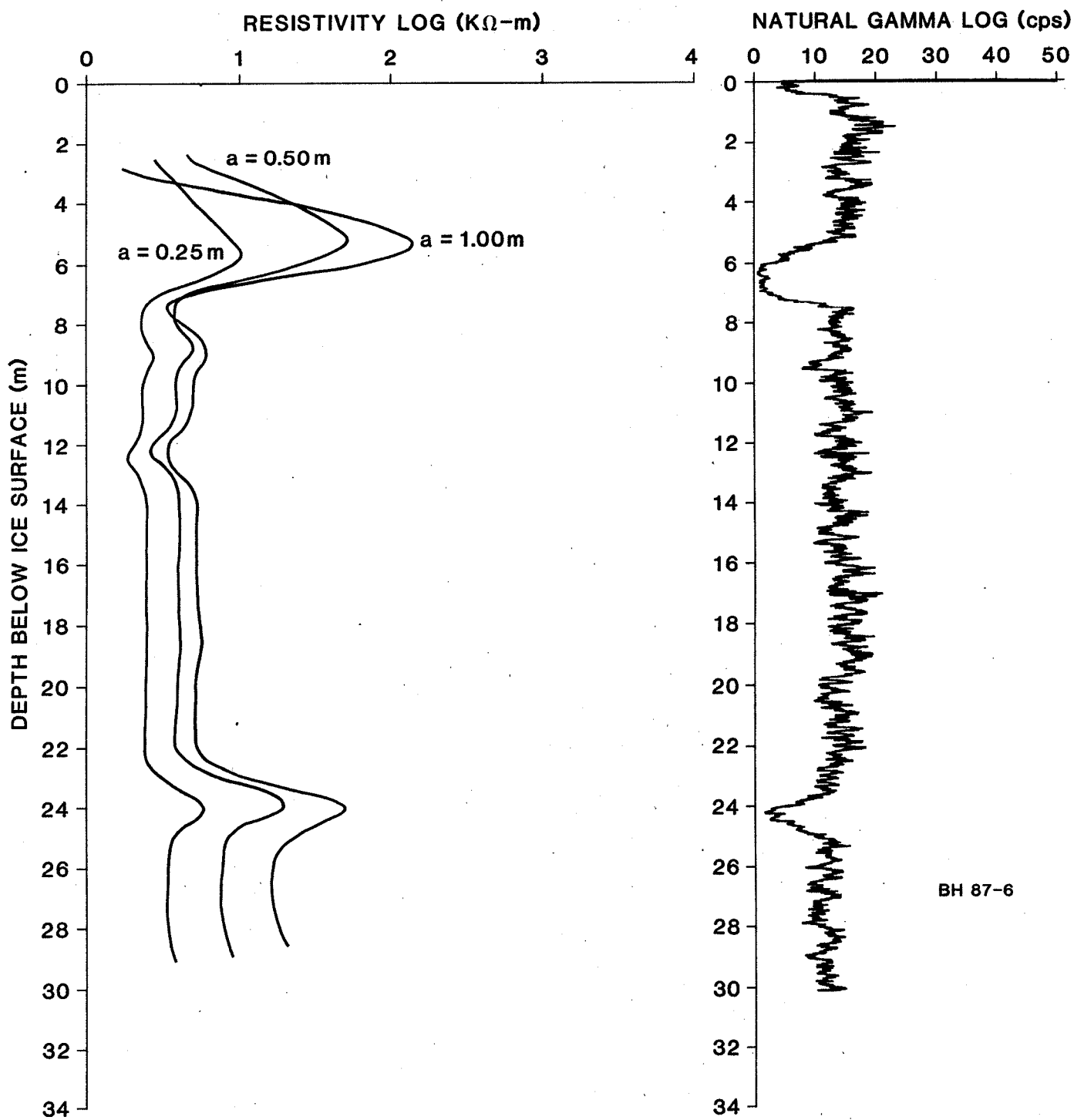


Fig. 4-26 Geophysical borehole logs - BH 87-6

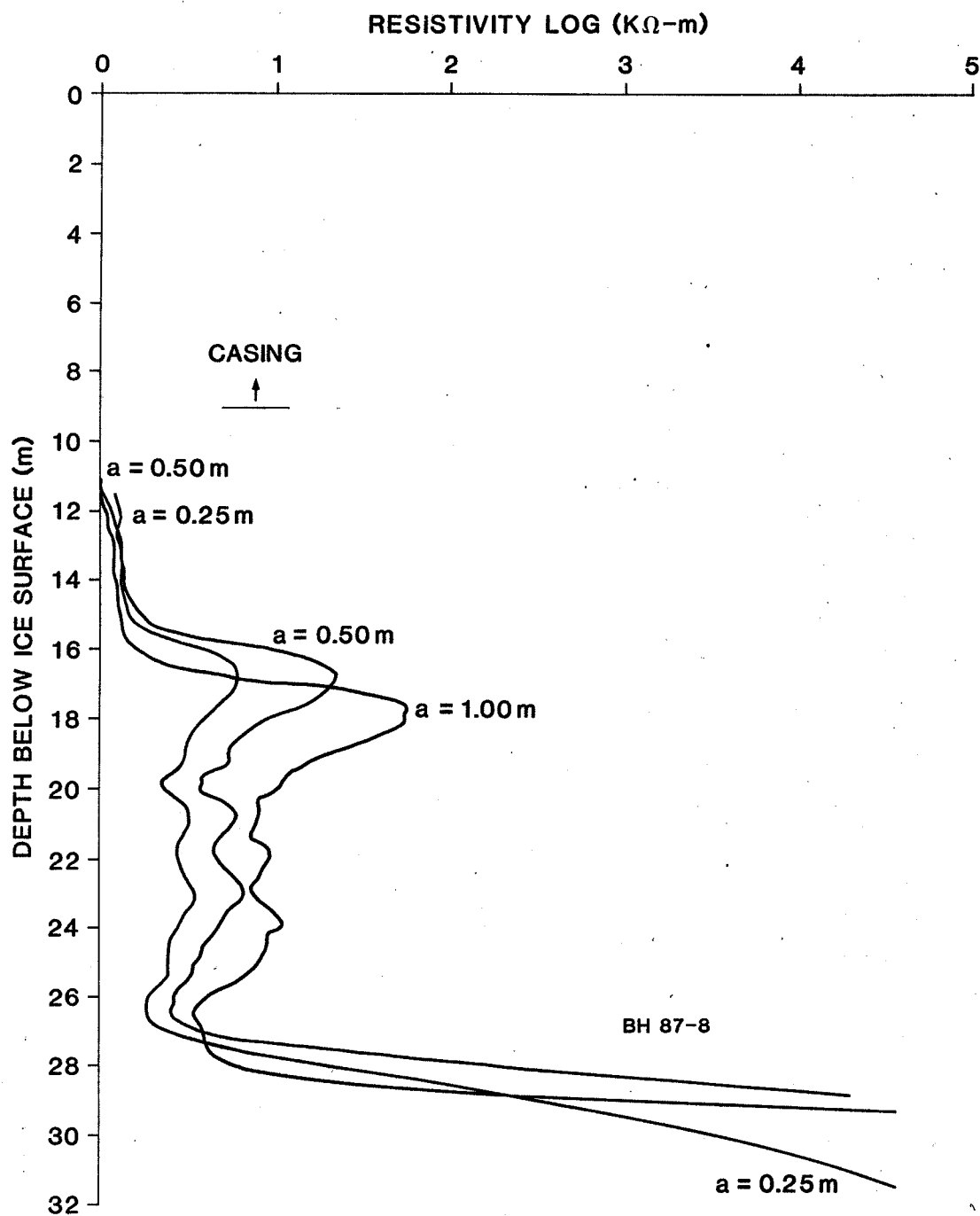


Fig. 4-27 Geophysical borehole logs - BH 87-8

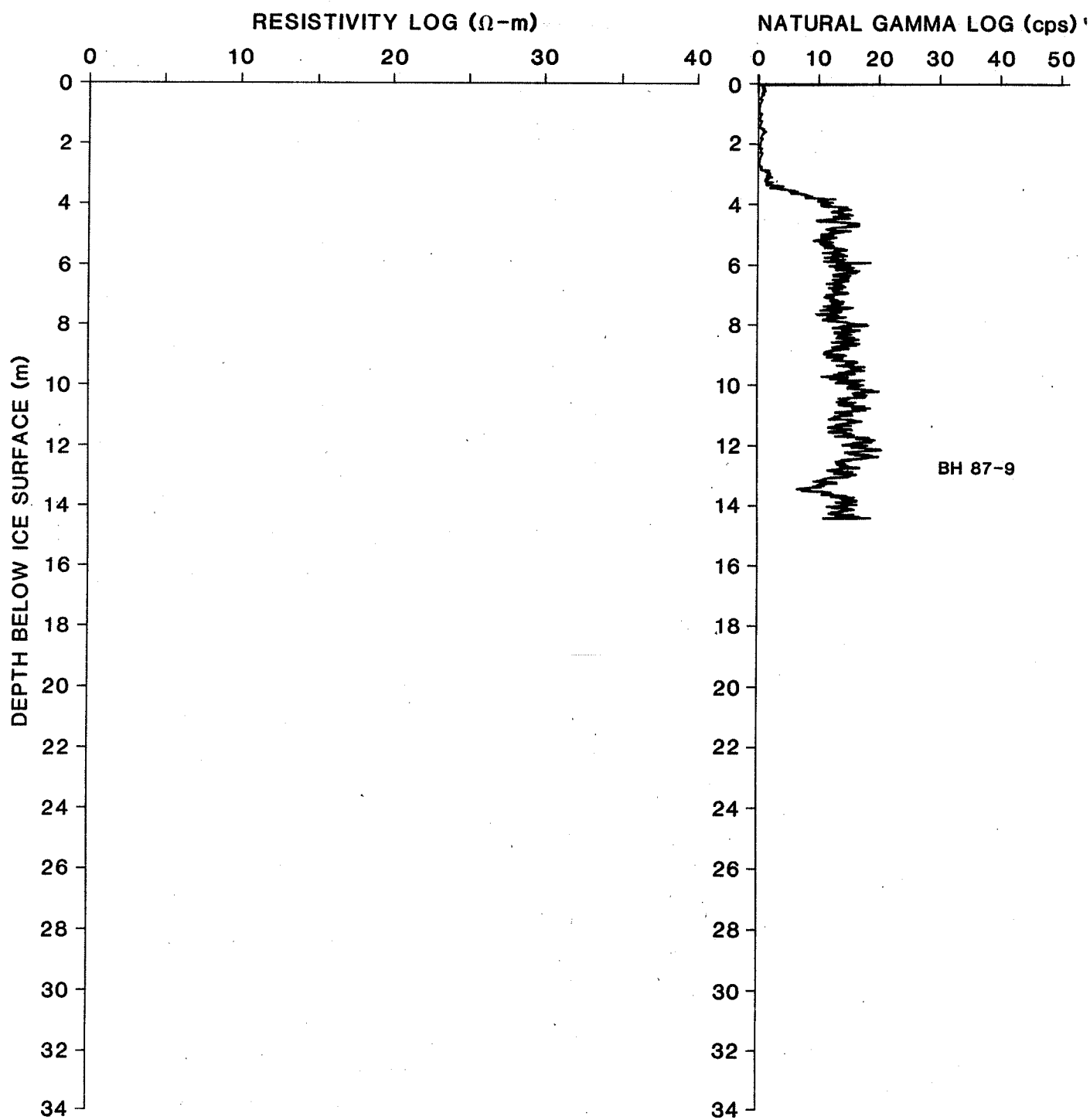
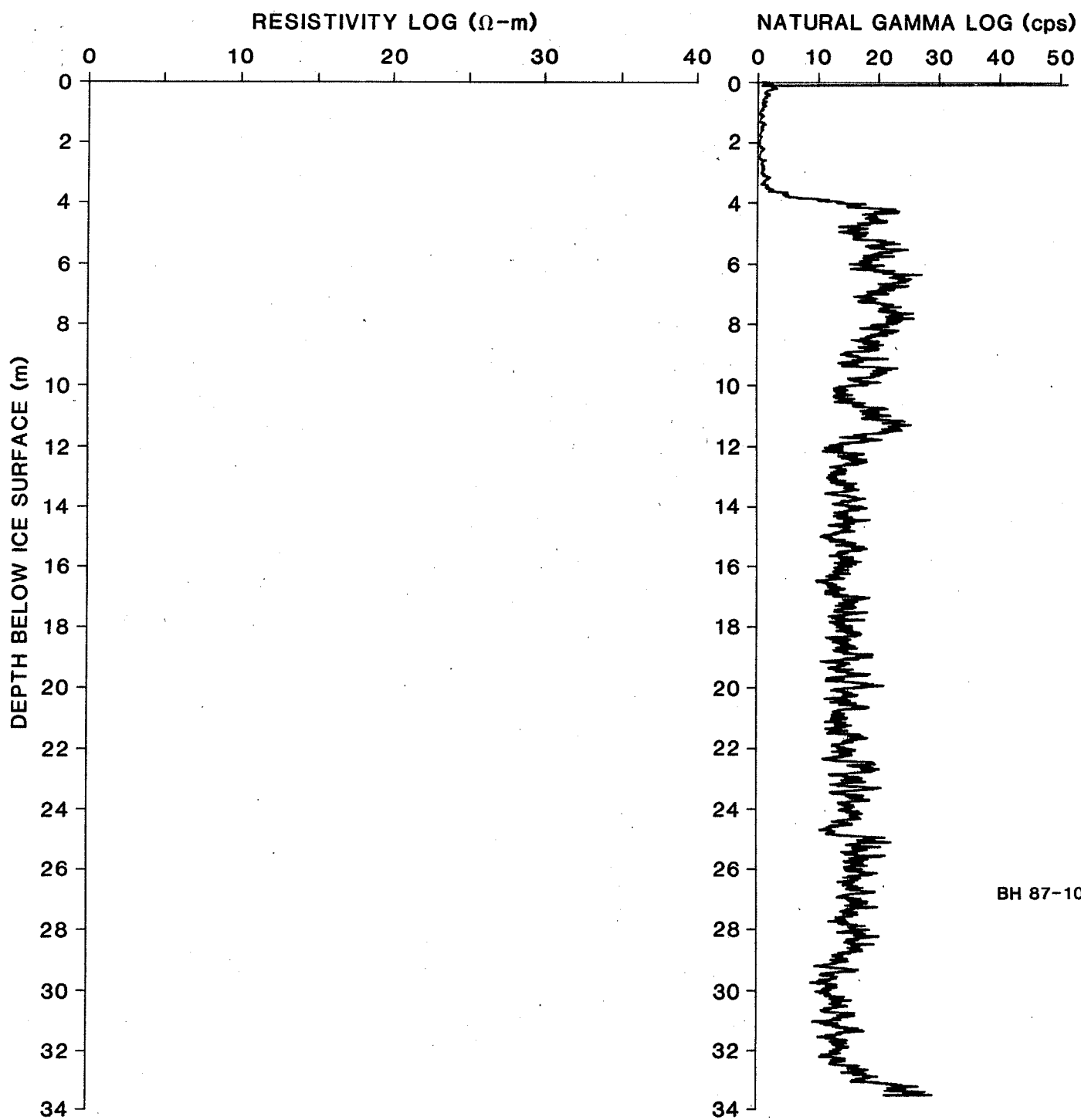


Fig. 4-28 Geophysical borehole logs - BH 87-9



BH 87-10

Fig. 4-29 Geophysical borehole logs - BH 87-10

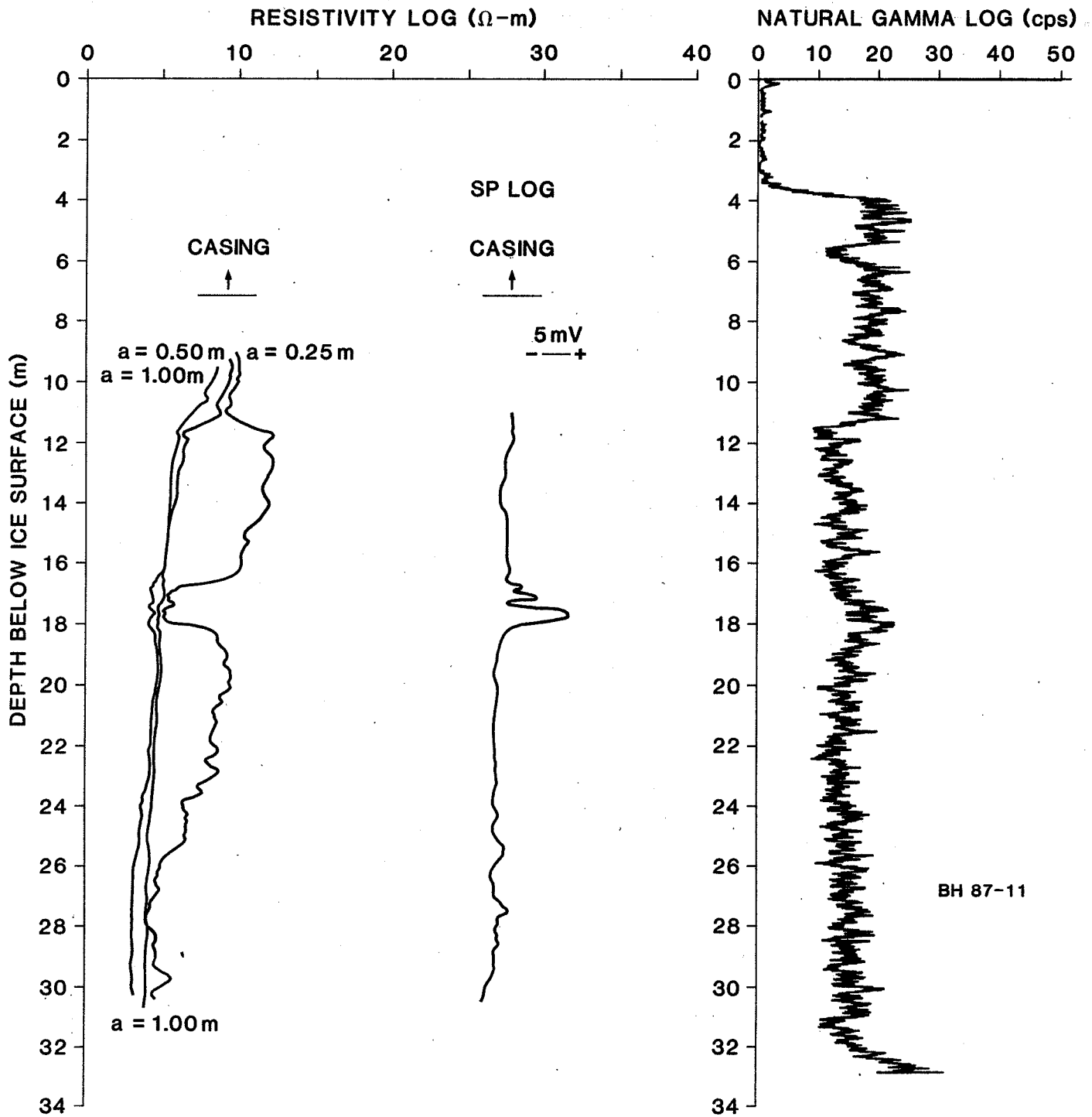


Fig. 4-30 Geophysical borehole logs - BH 87-11

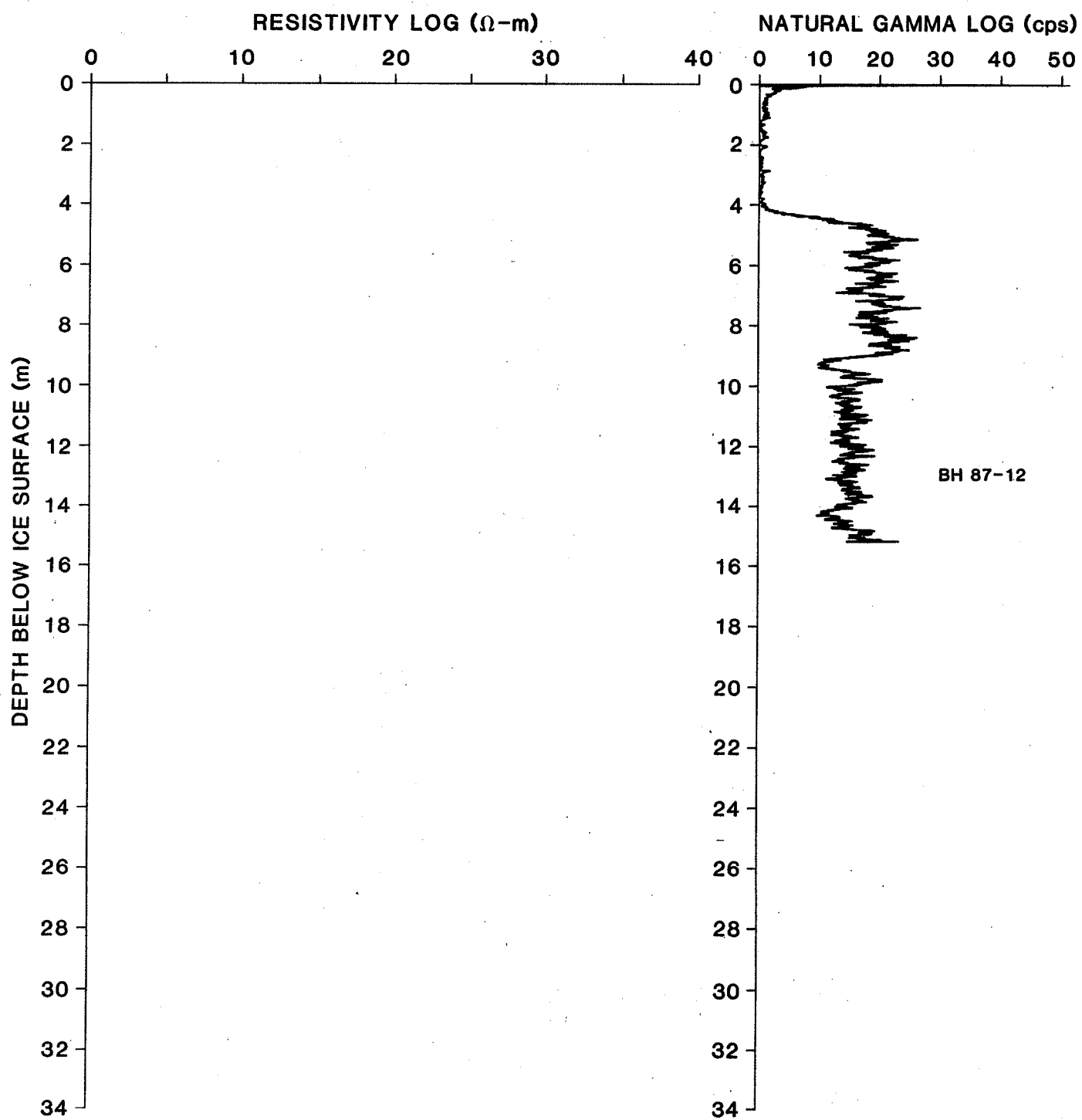


Fig. 4-31 Geophysical borehole logs - BH 87-12

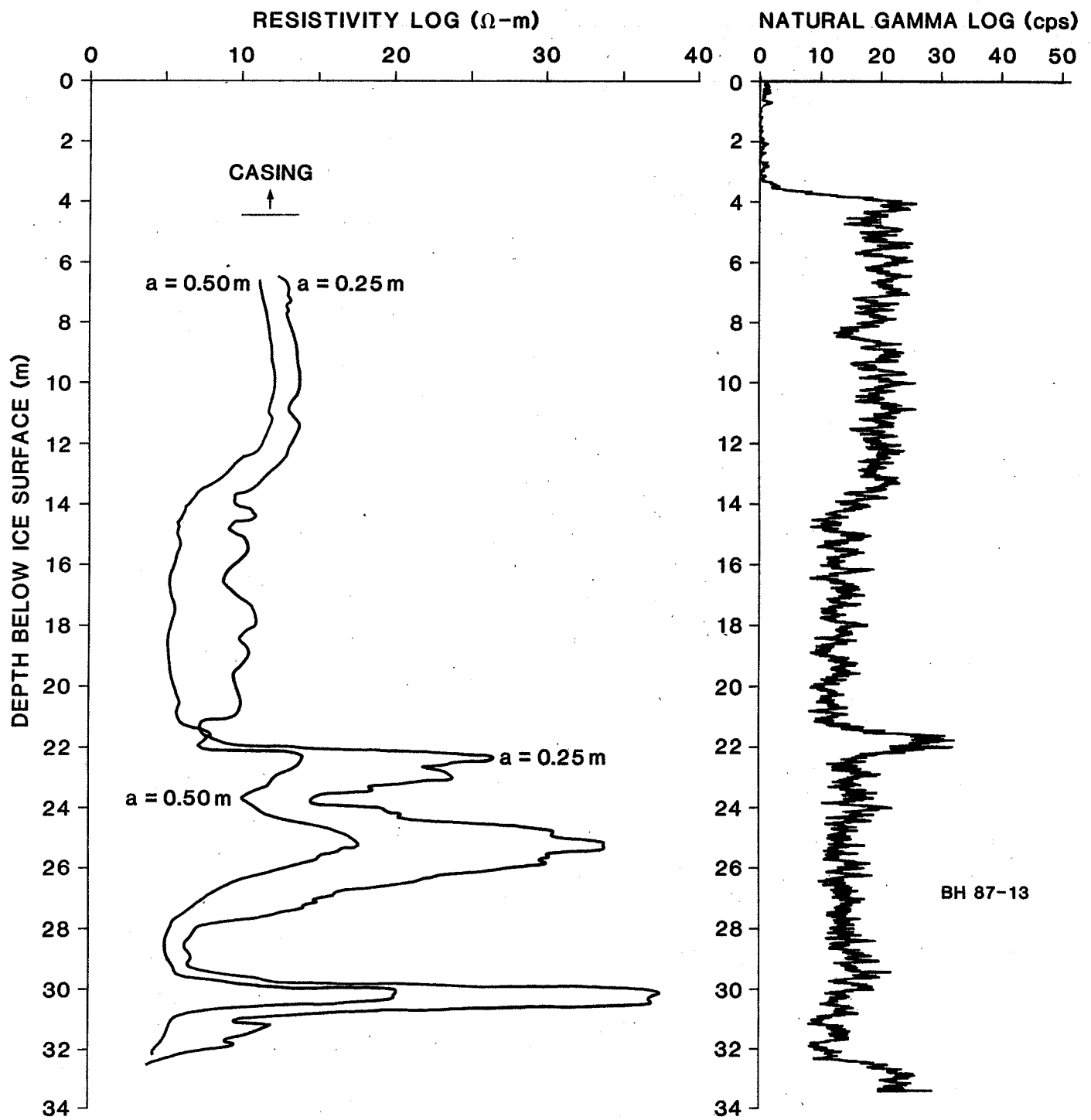


Fig. 4-32 Geophysical borehole logs - BH 87-13

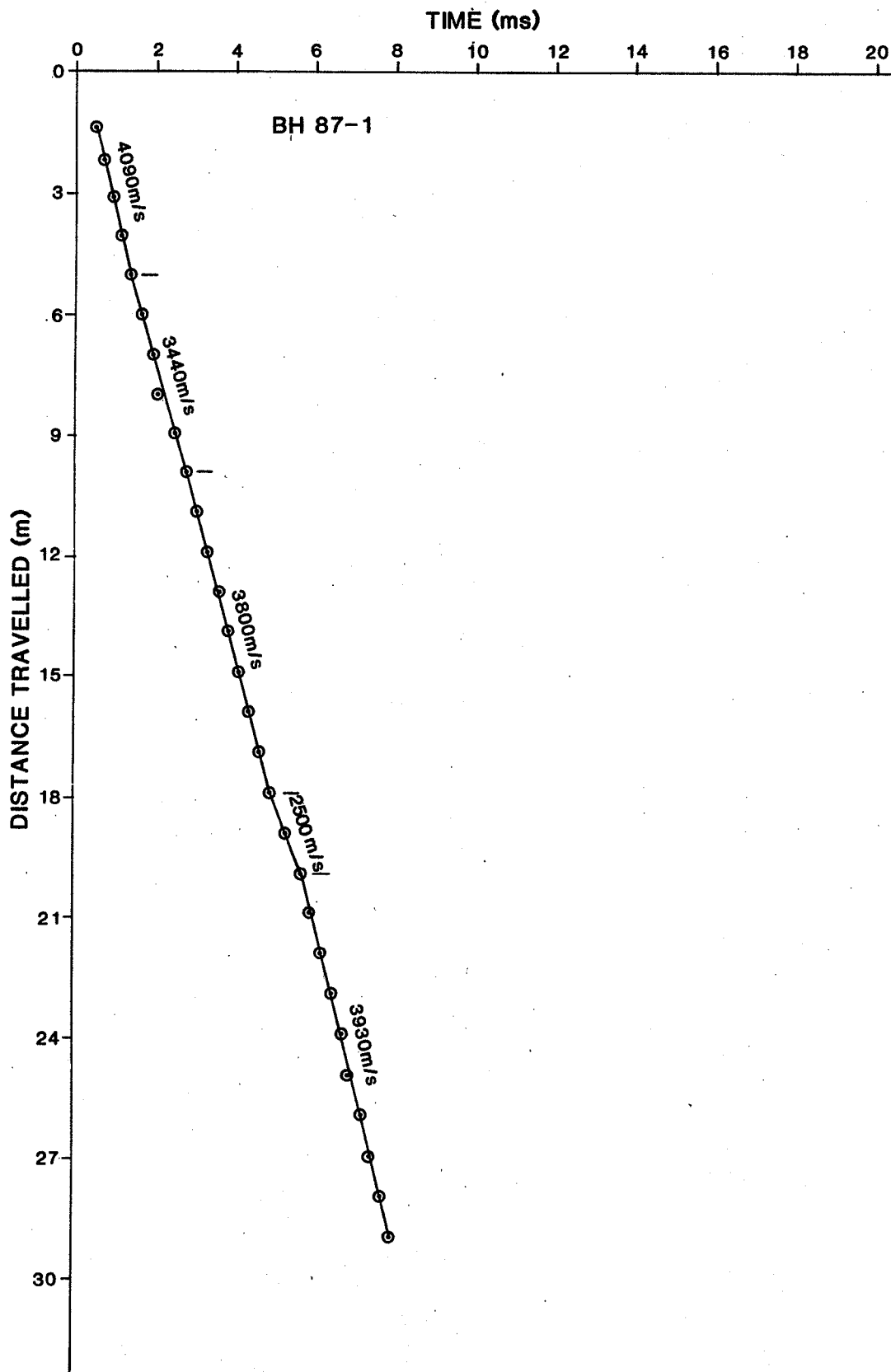


Fig. 4-33a Travel time vs. distance - BH 87-1

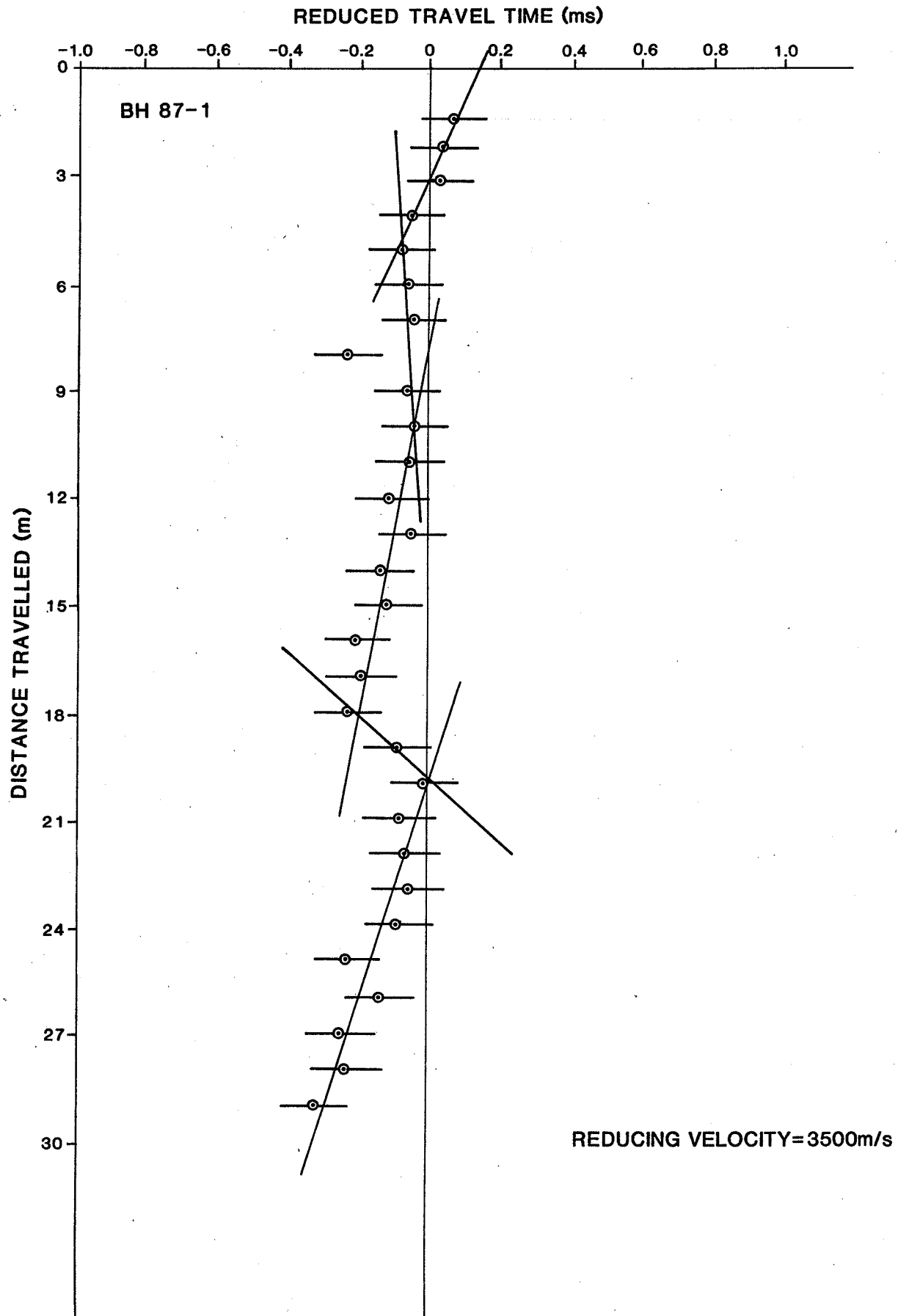


Fig. 4-33b Reduced travel time vs. distance - BH 87-1

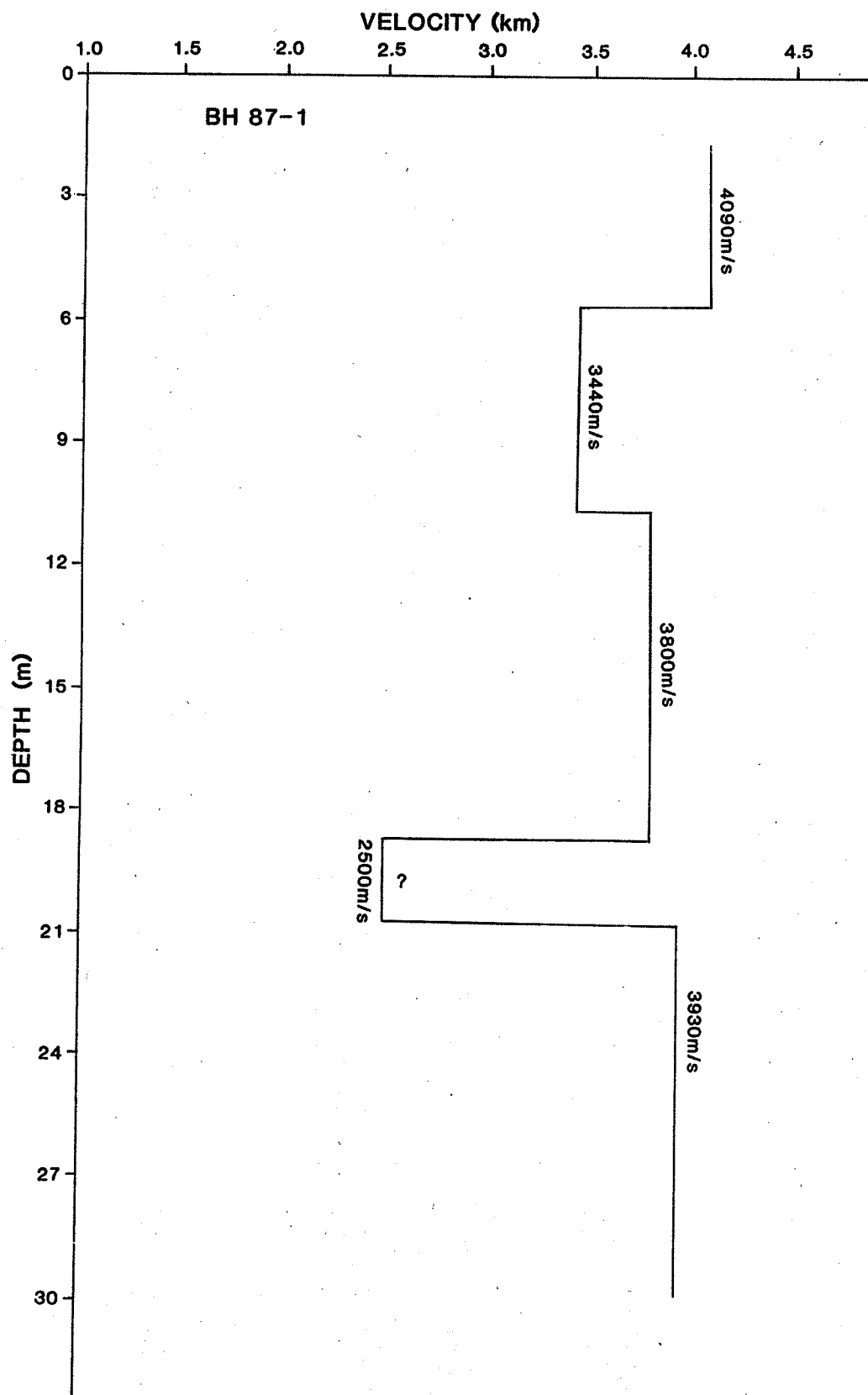


Fig. 4-33c Interval velocity vs. depth - BH 87-1

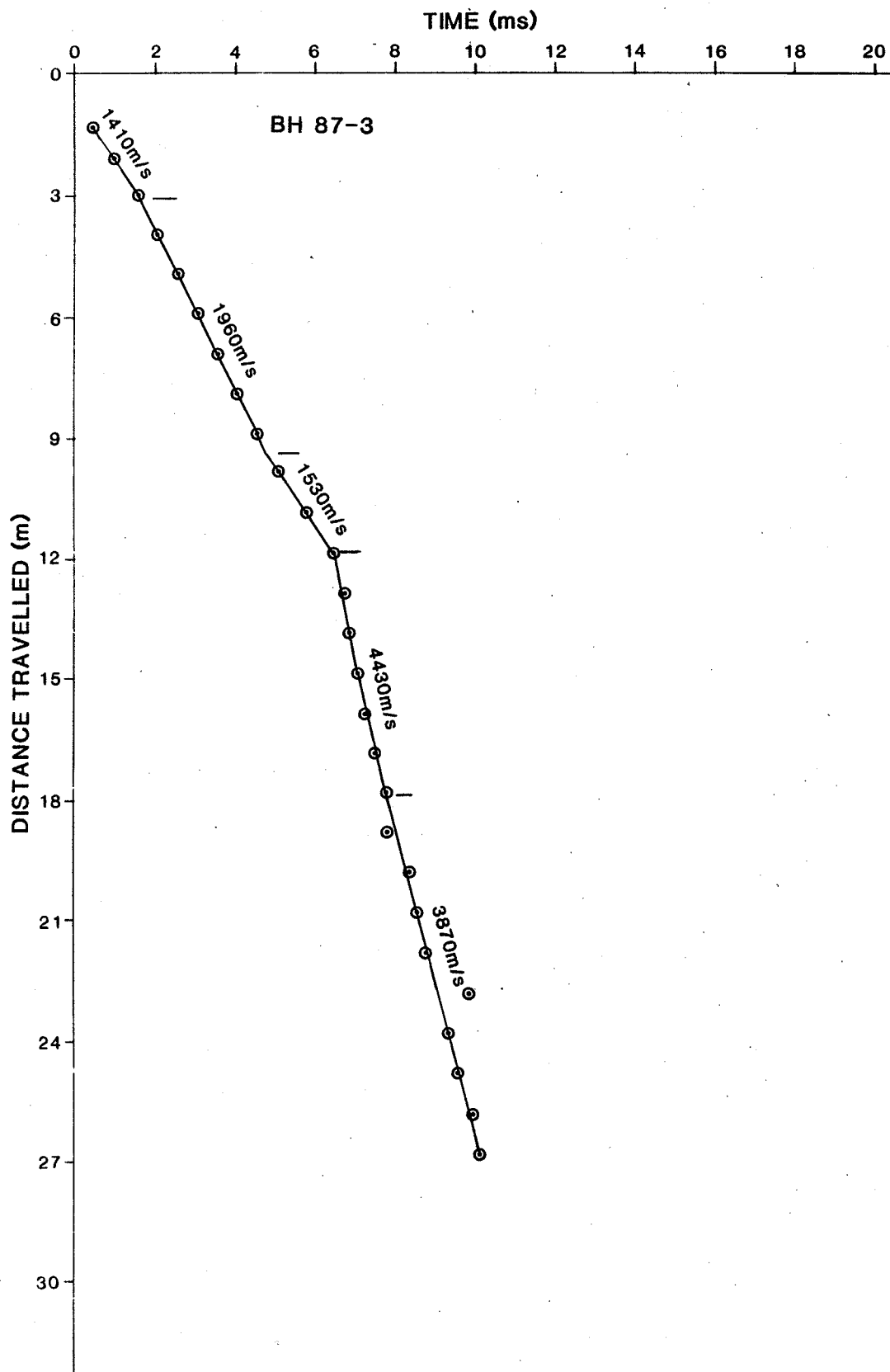


Fig. 4-34a Travel time vs. distance - BH 87-3

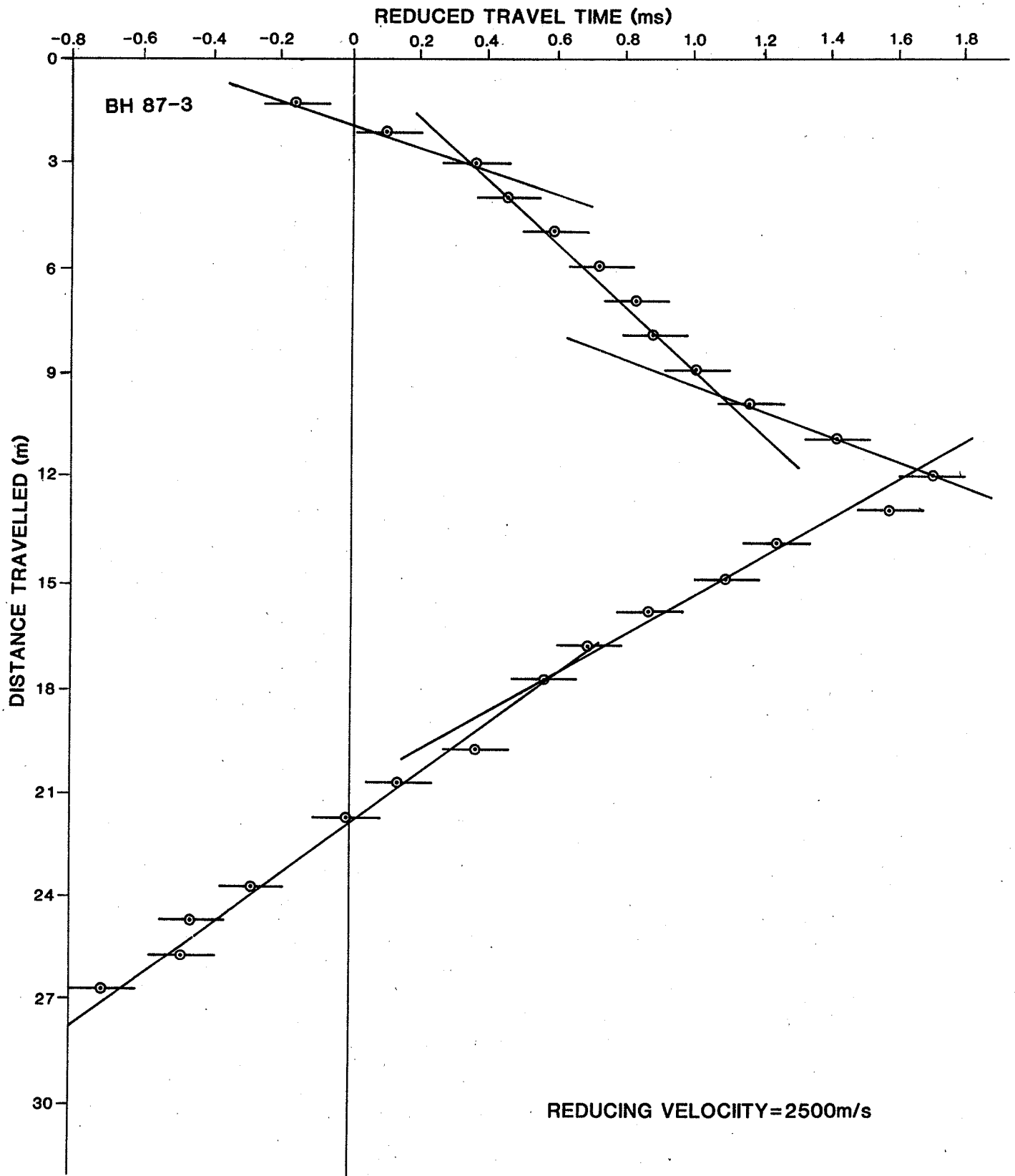


Fig. 4-34b Reduced travel time vs. distance - BH 87-3

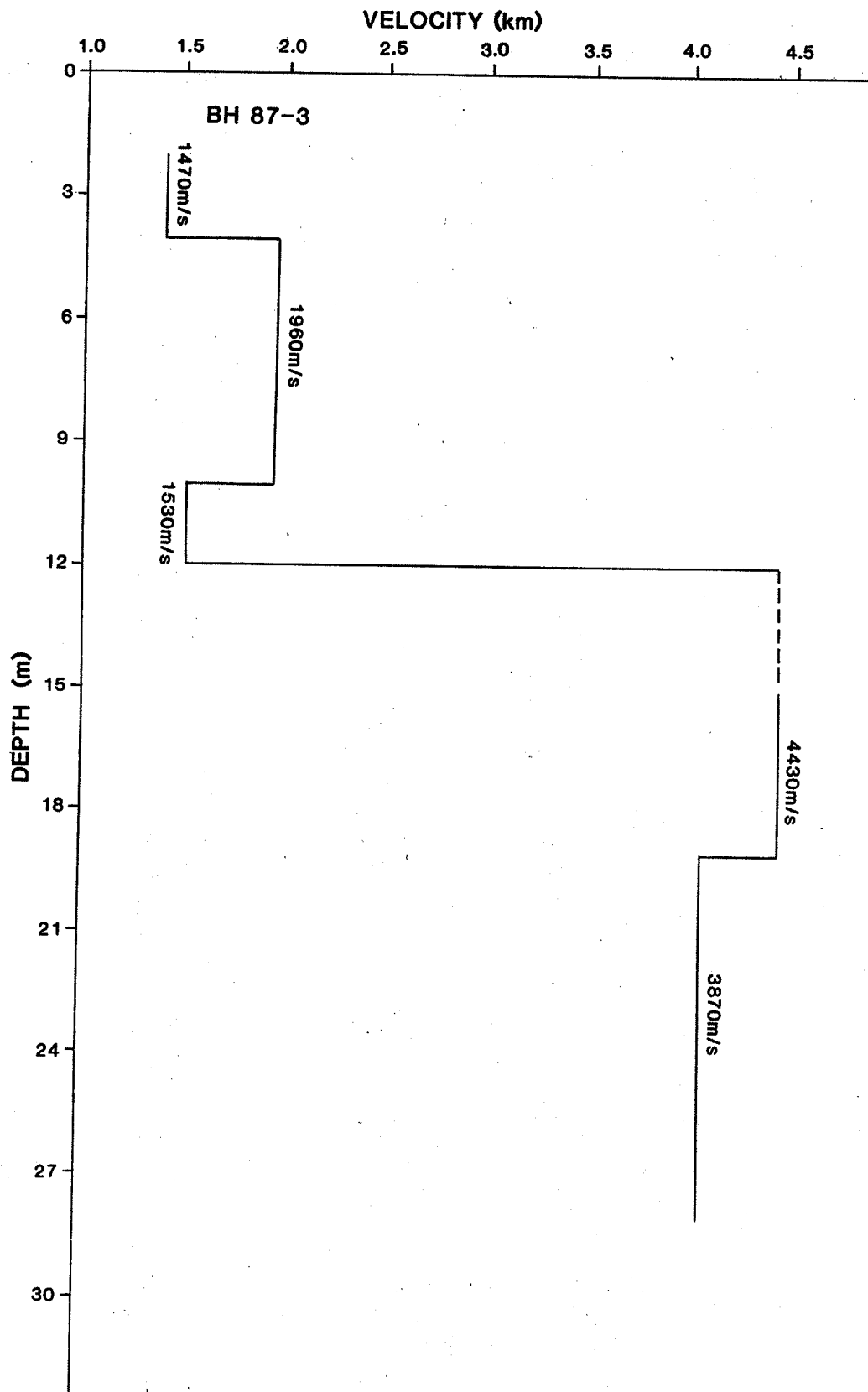


Fig. 4-34c Interval velocity vs. depth - BH 87-3

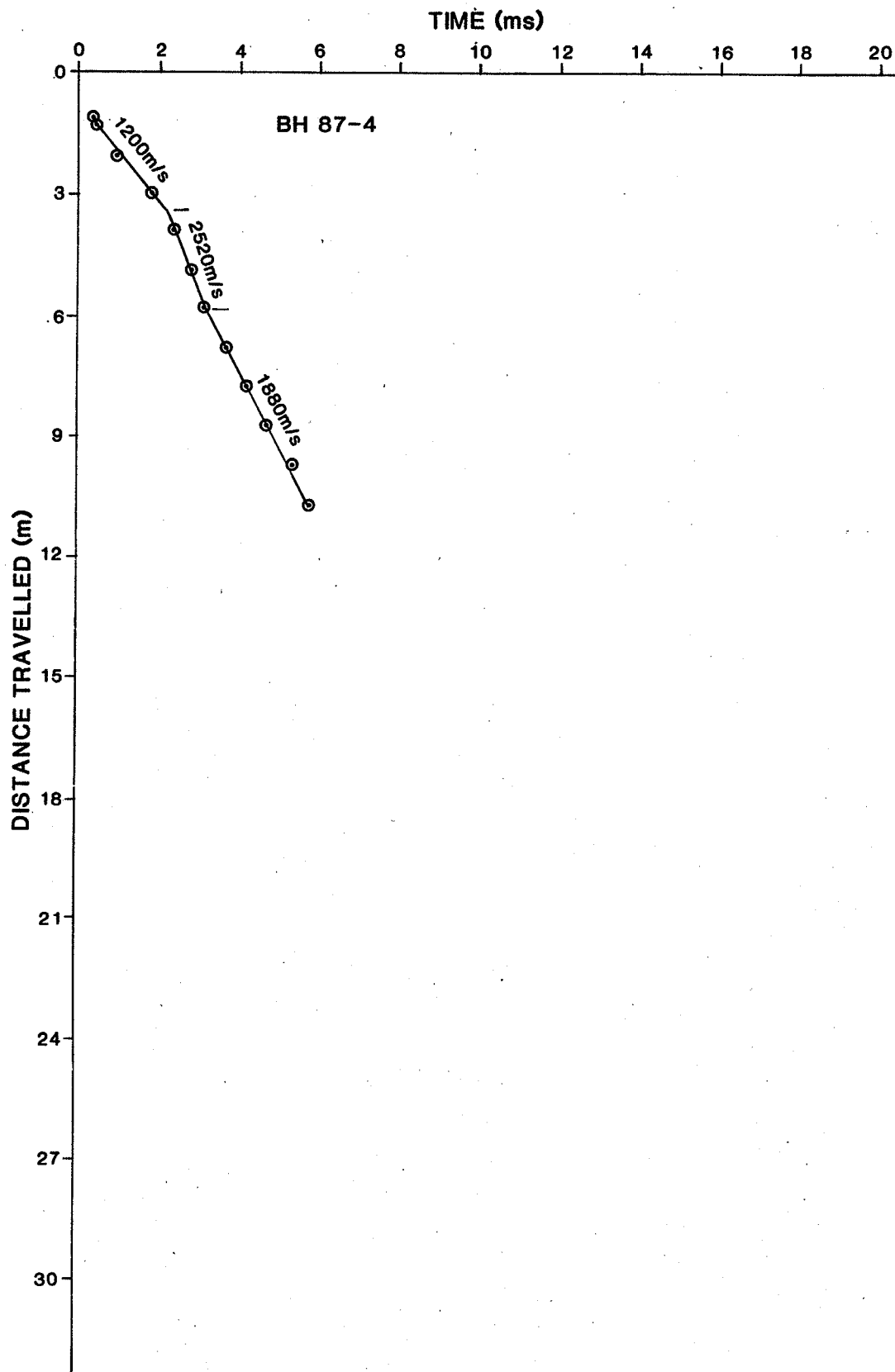


Fig. 4-35a Travel time vs. distance - BH 87-4

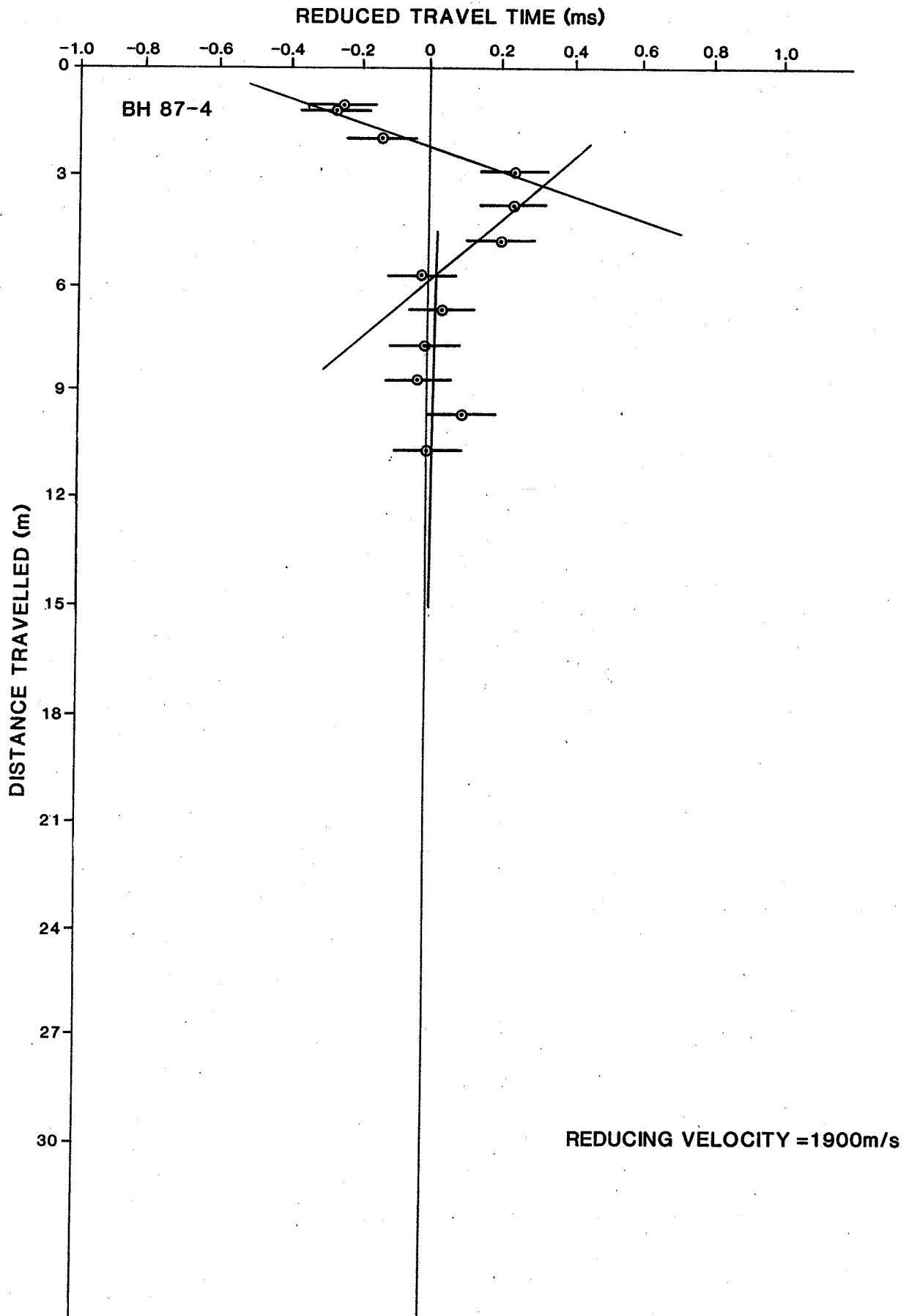


Fig. 4-35b Reduced travel time vs. distance - BH 87-4

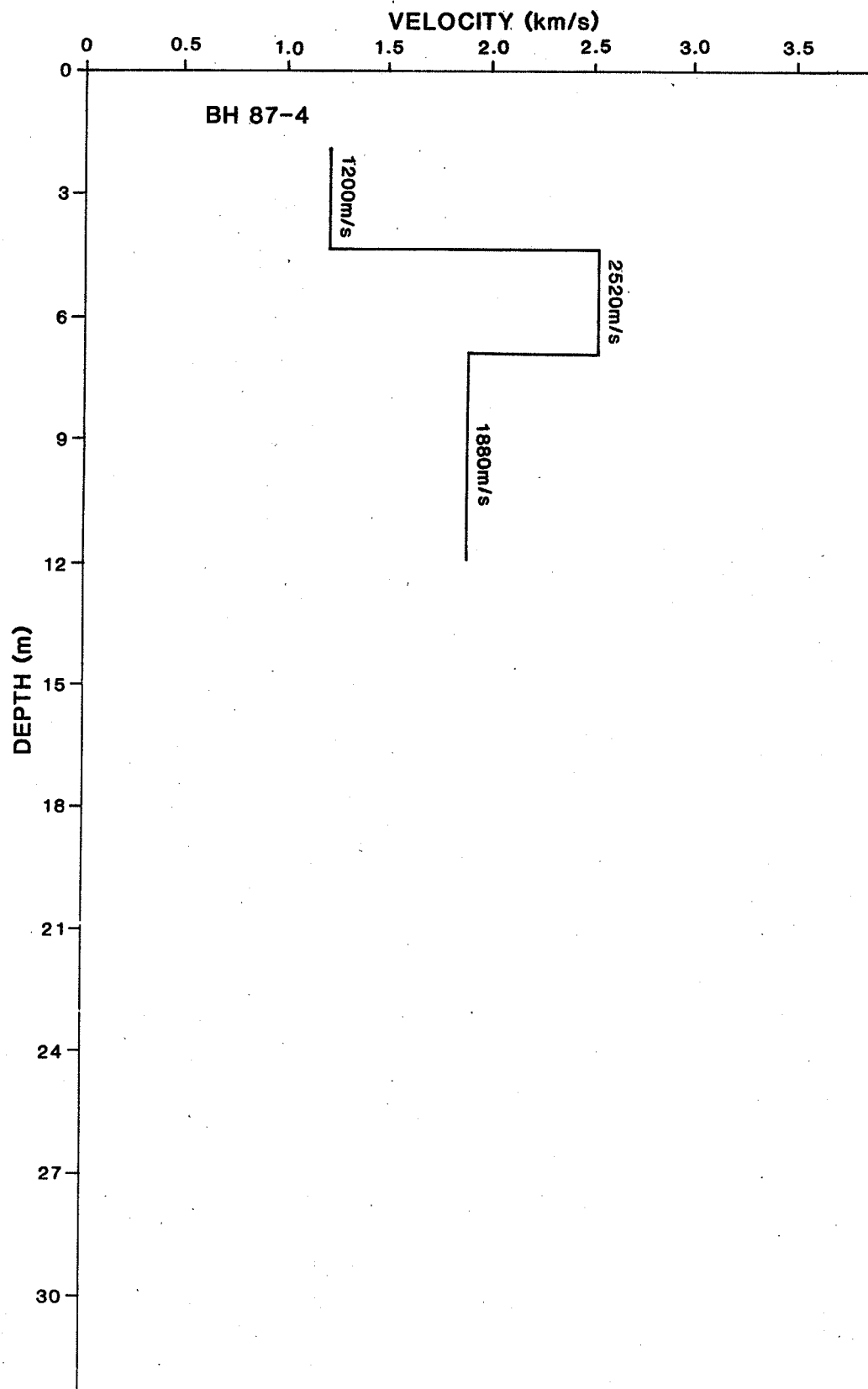


Fig. 4-35c Interval velocity vs. depth - BH 87-4

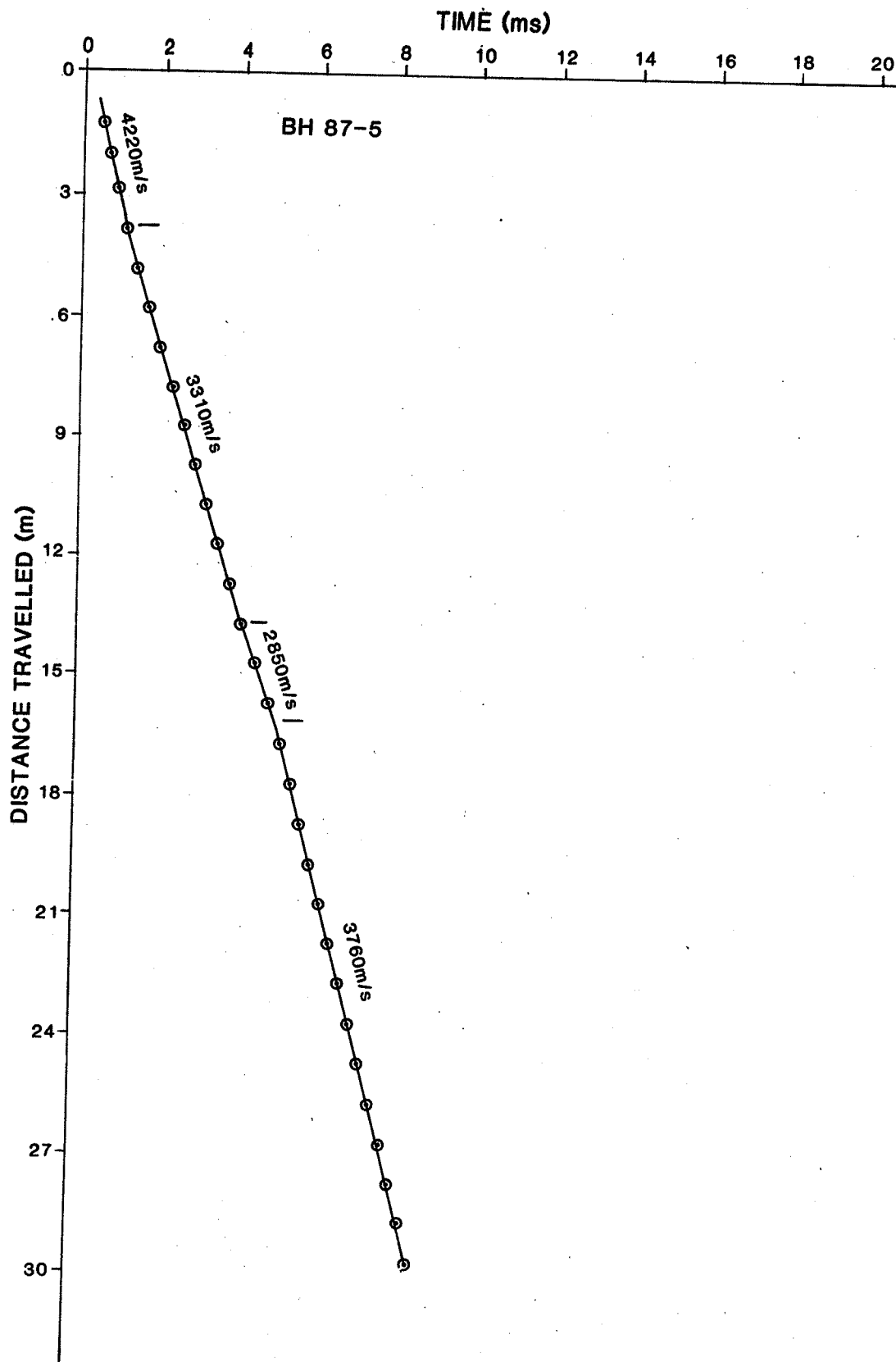


Fig. 4-36a Travel time vs. distance - BH 87-5

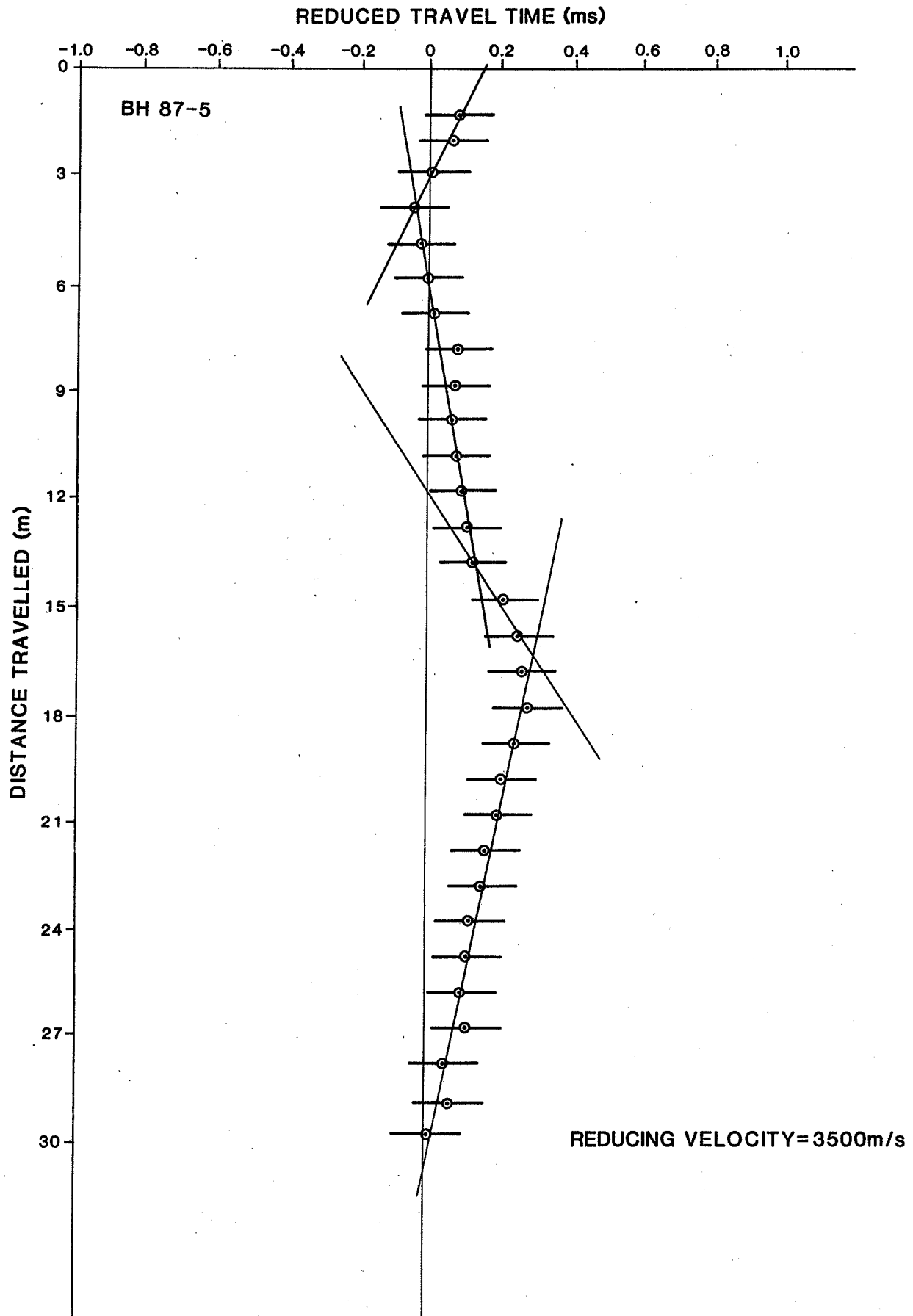


Fig. 4-36b Reduced travel time vs. distance - BH 87-5

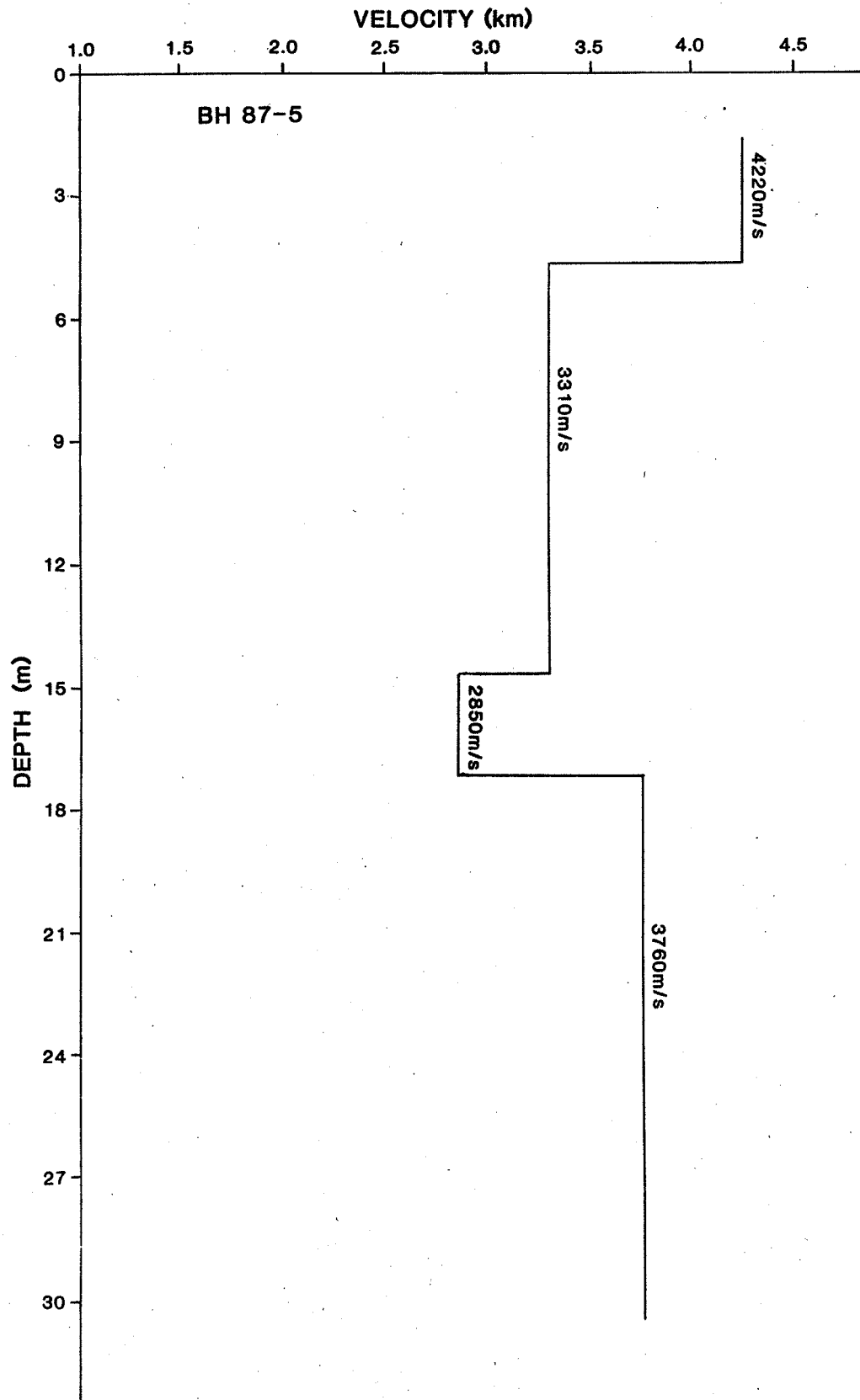


Fig. 4-36c Interval velocity vs. depth - BH 87-5

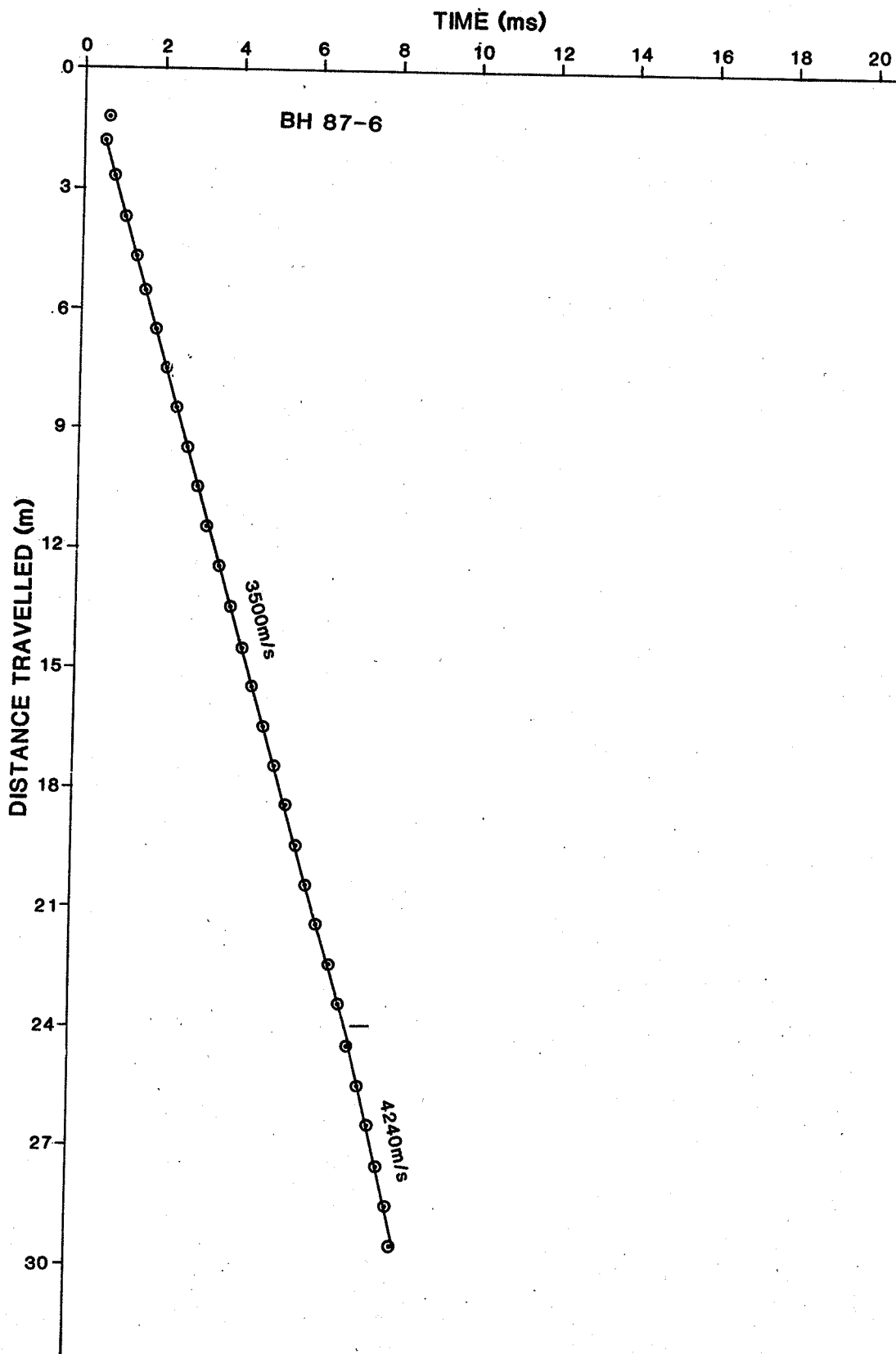


Fig. 4-37a Travel time vs. distance - BH 87-6

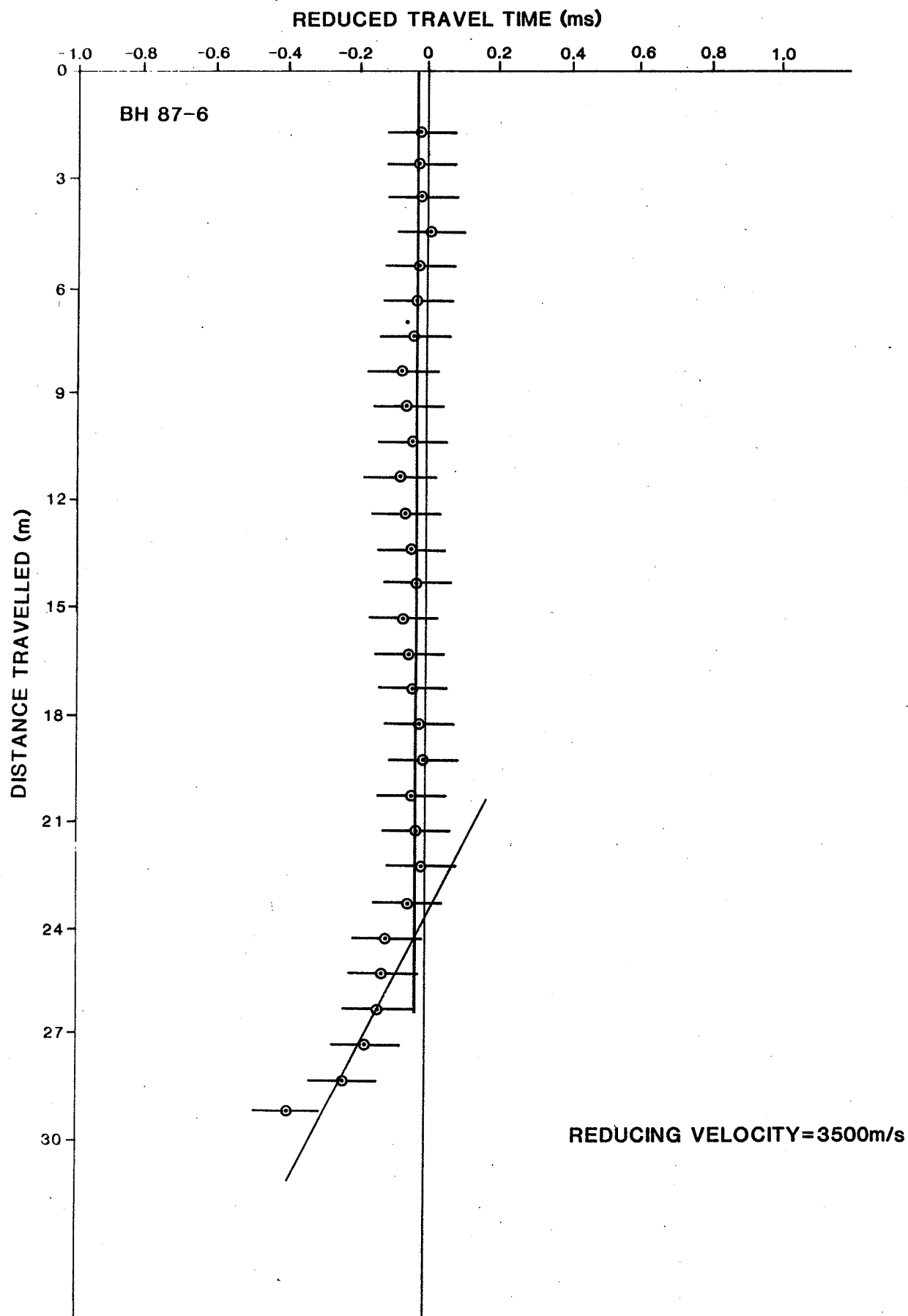


Fig. 4-37b Reduced travel time vs. distance - BH 87-6

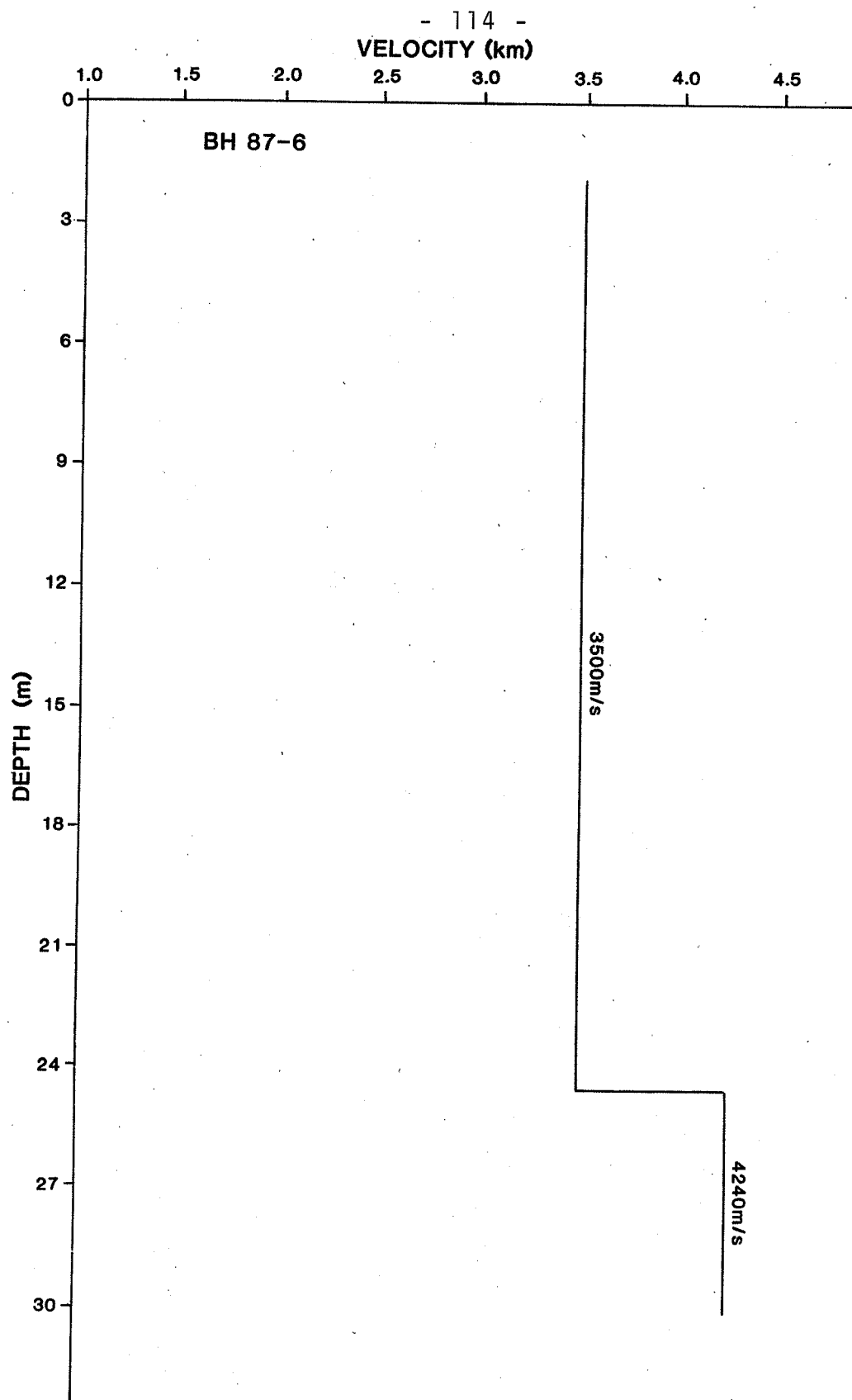


Fig. 4-37c Interval velocity vs. depth - BH 87-6

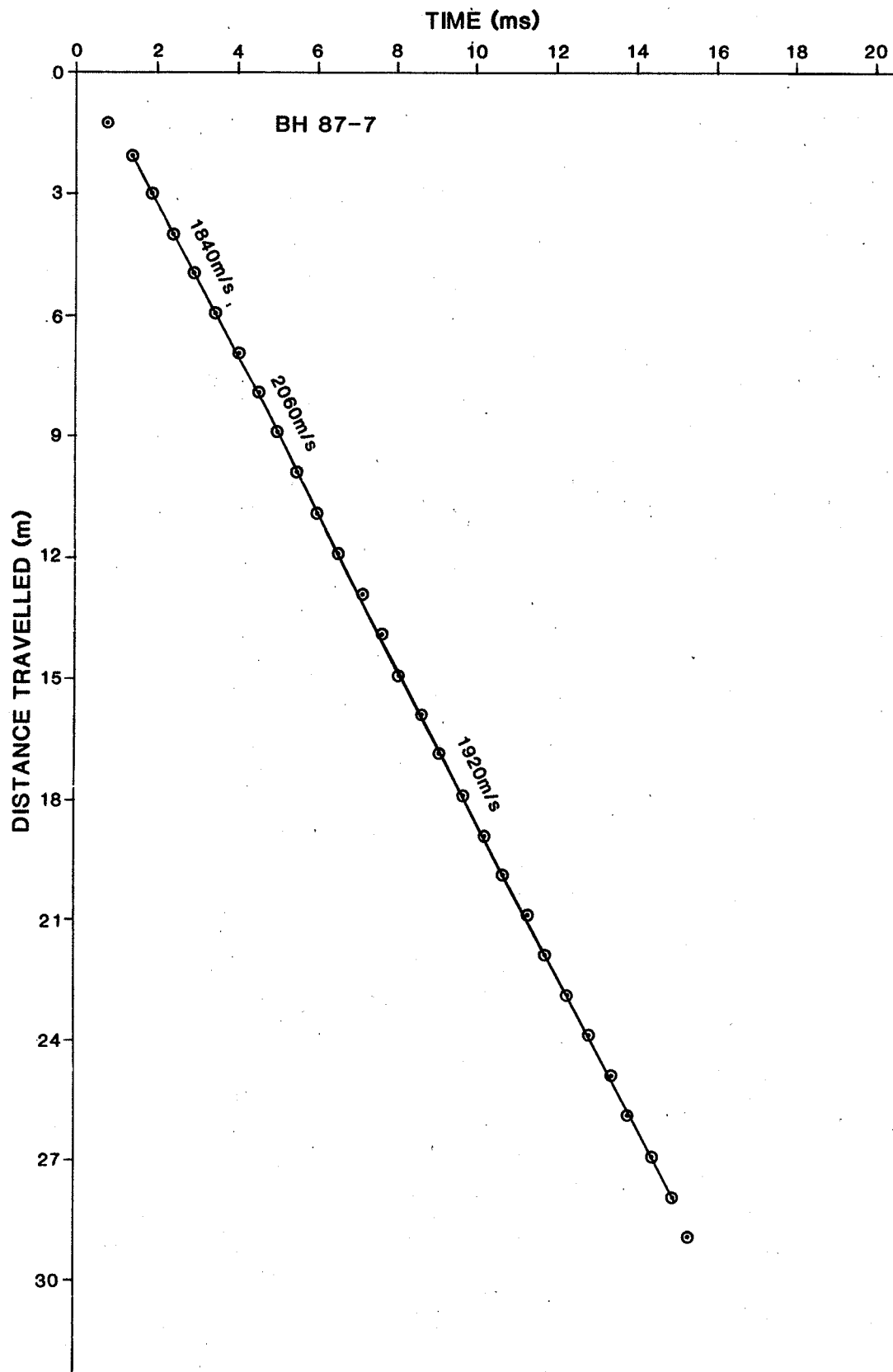


Fig. 4-38a Travel time vs. distance - BH 87-7

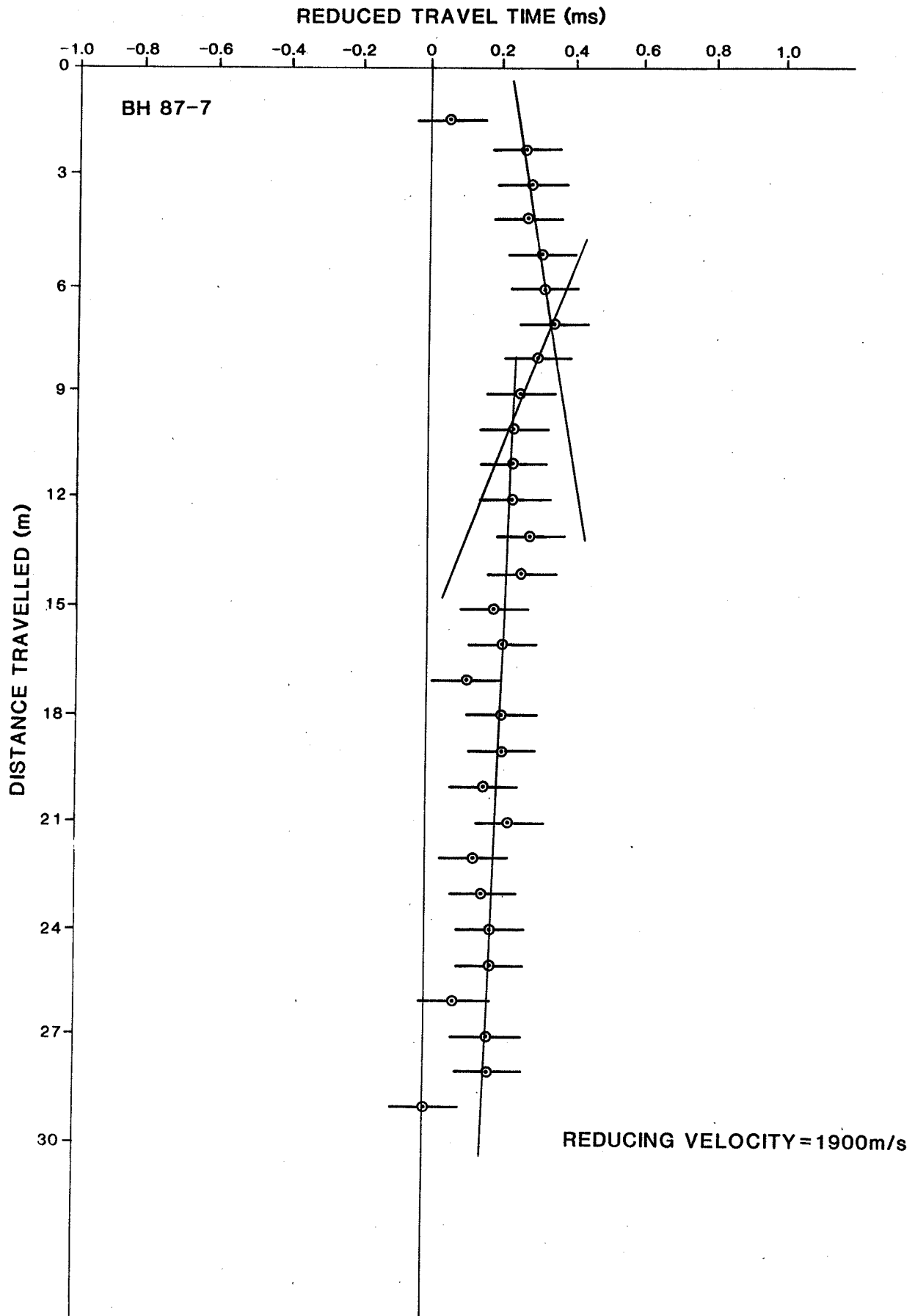


Fig. 4-38b Reduced travel time vs. distance - BH 87-7

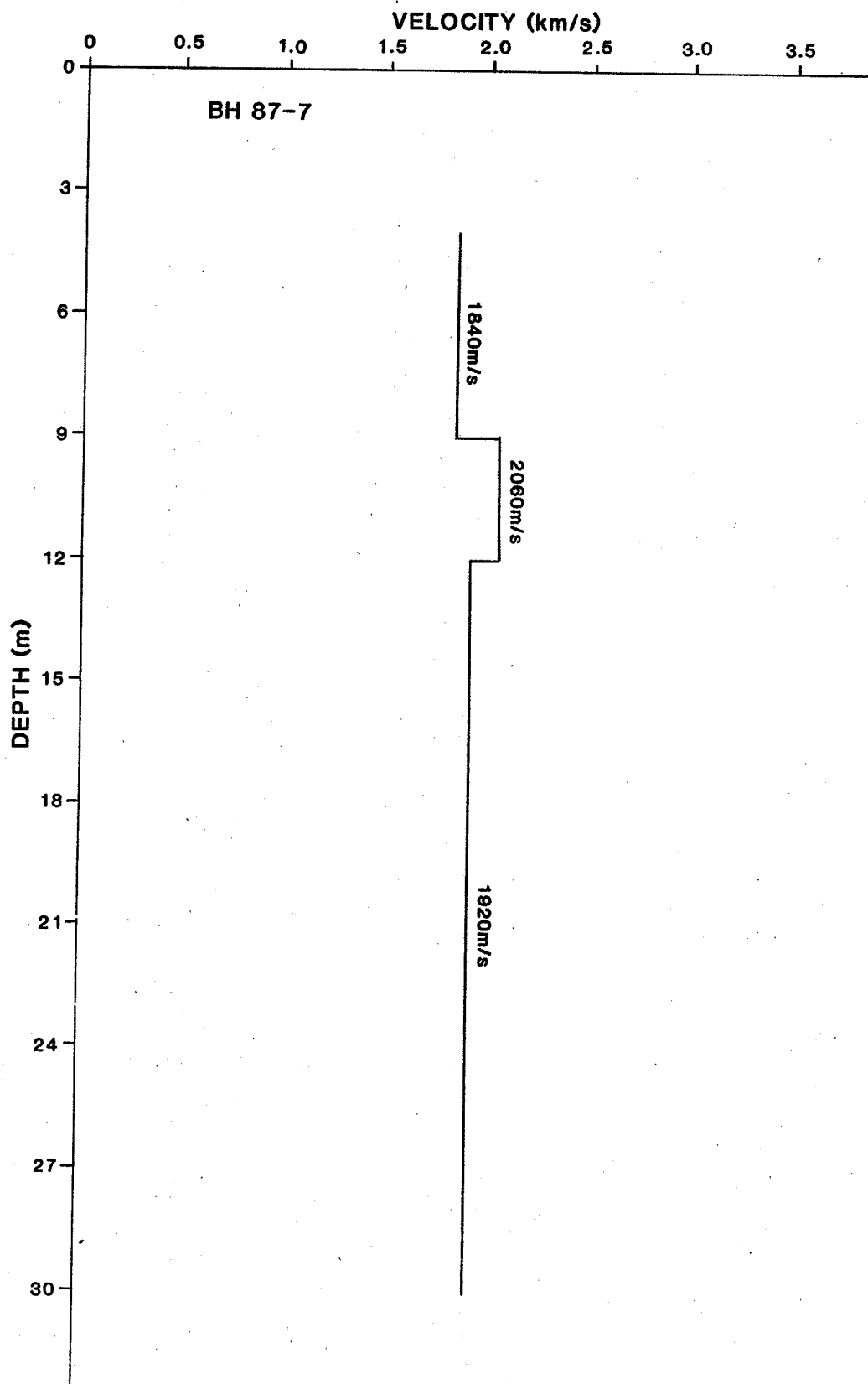


Fig. 4-38c Interval velocity vs. depth -- BH 87-7

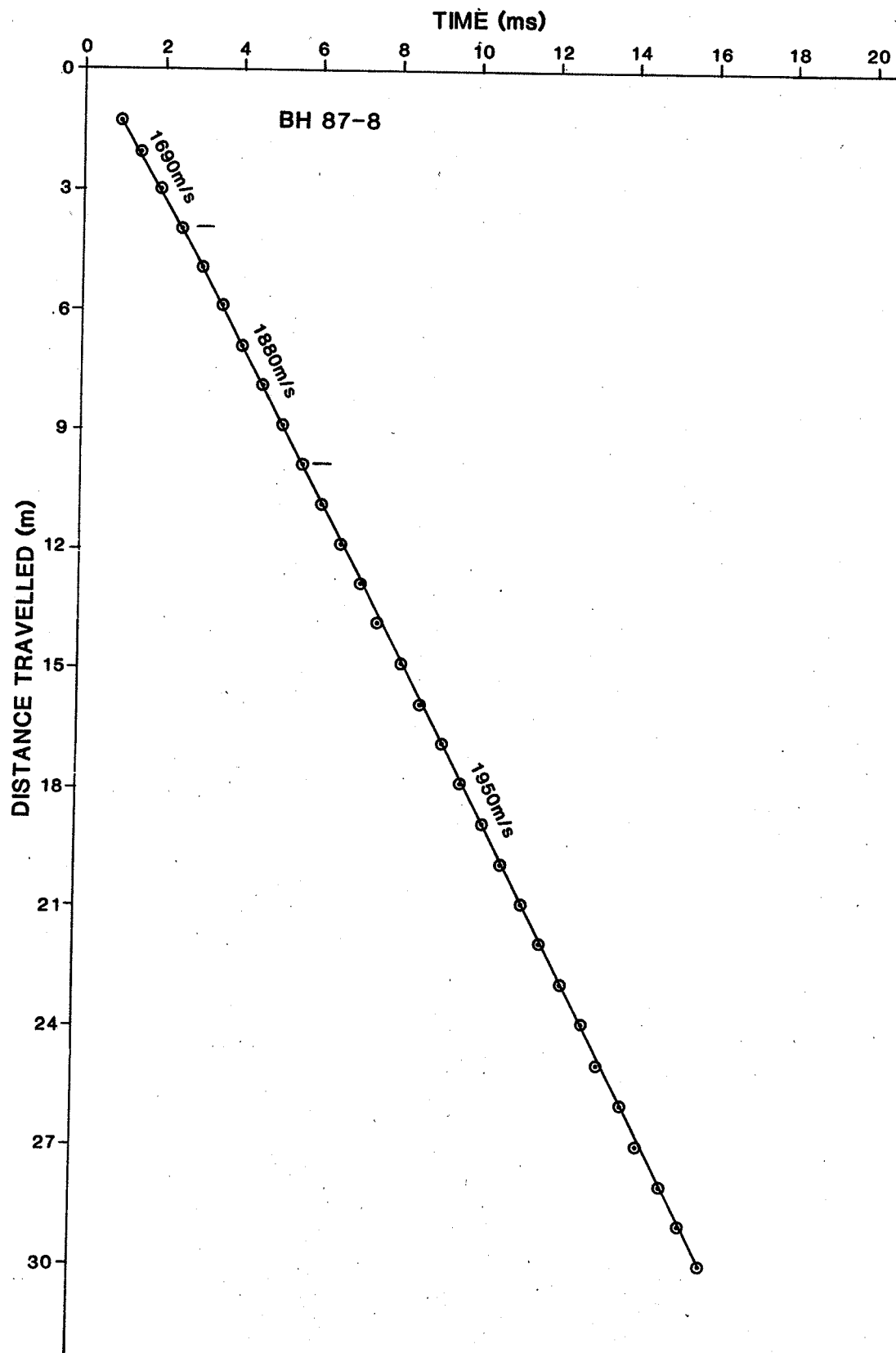


Fig. 4-39a Travel time vs. distance - BH 87-8

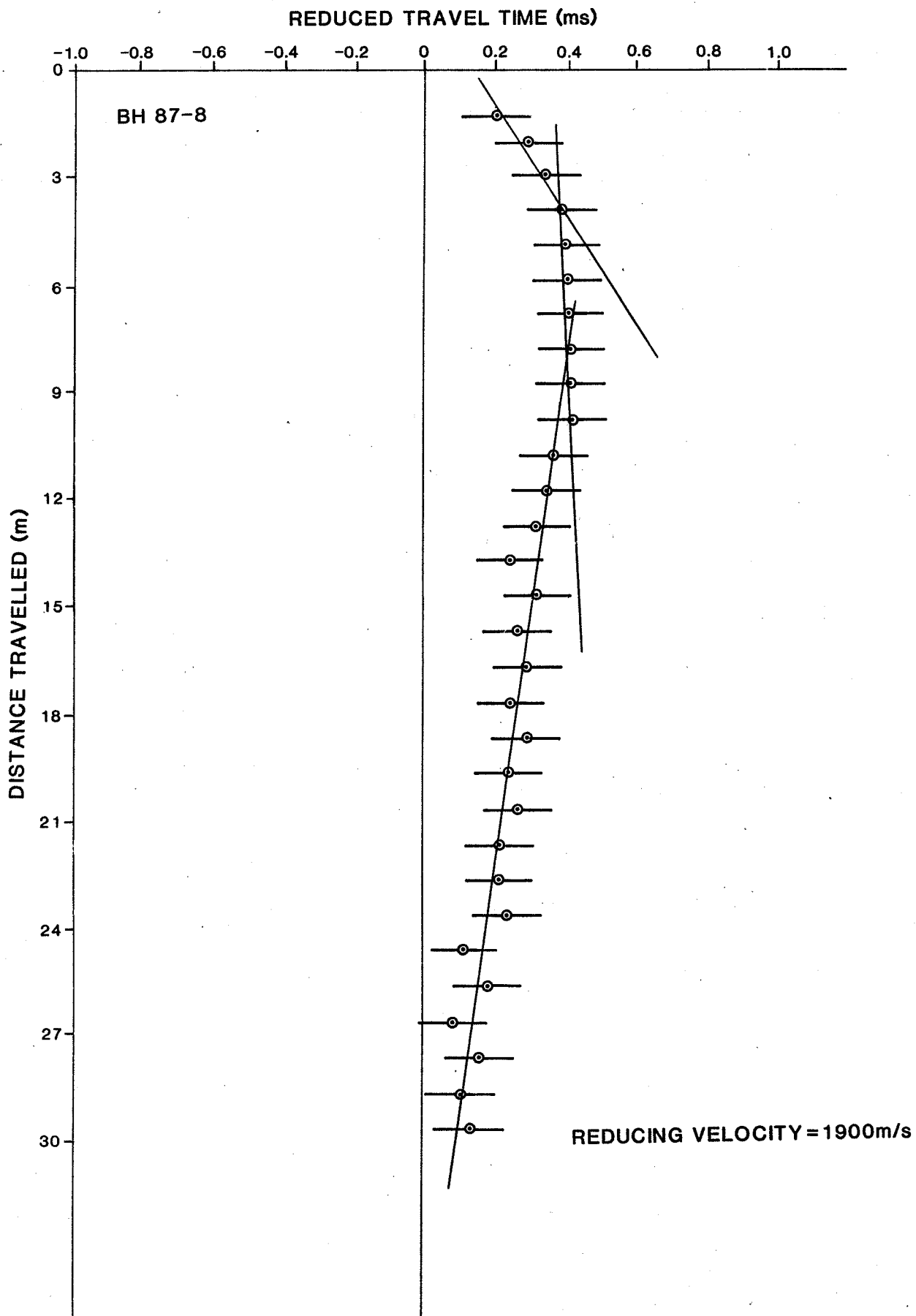


Fig. 4-39b Reduced travel time vs. distance - BH 87-8

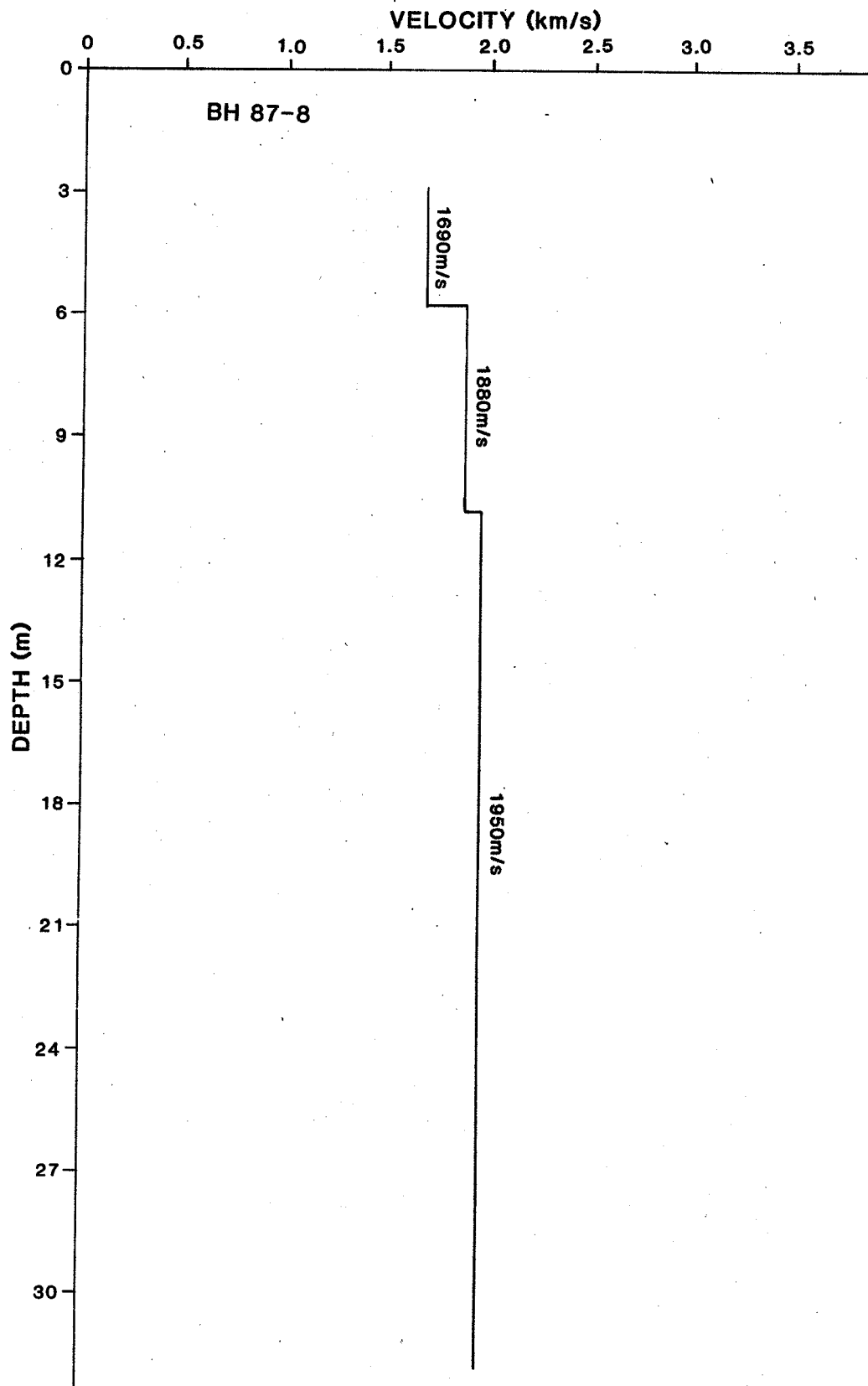


Fig. 4-39c Interval velocity vs. depth - BH 87-8

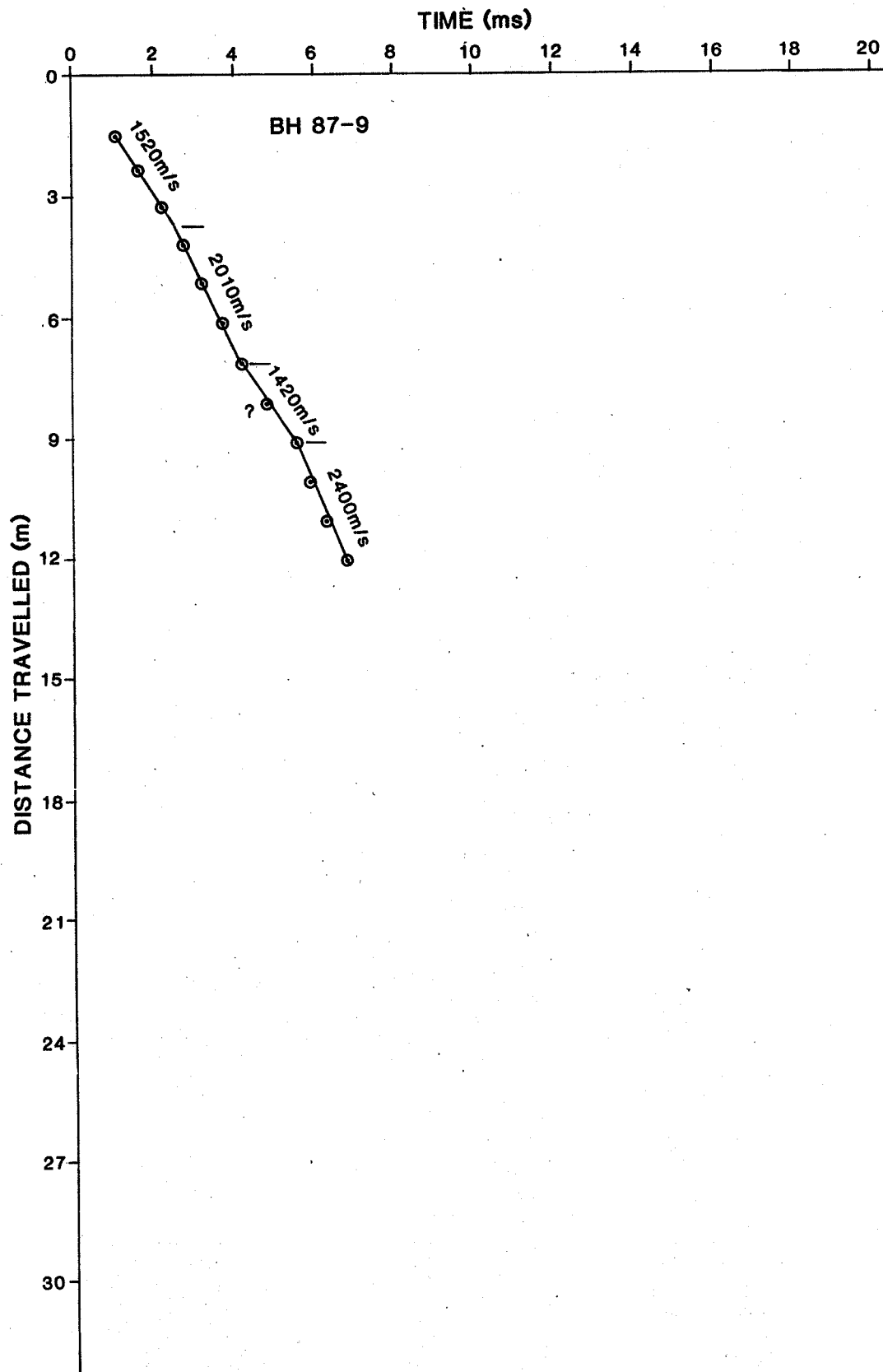


Fig. 4-40a Travel time vs. distance - BH 87-9

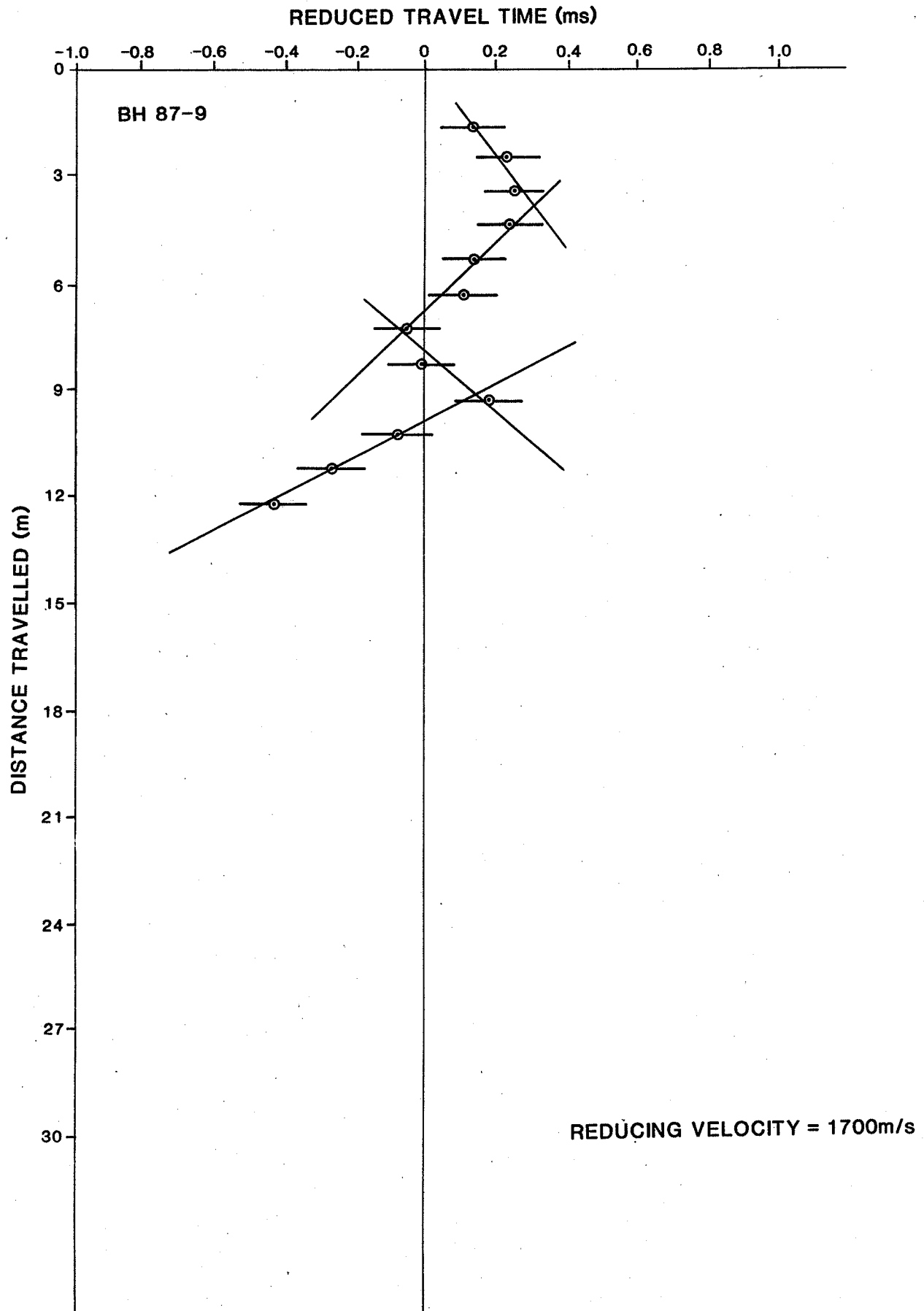


Fig. 4-40b Reduced travel time vs. distance - BH 87-9

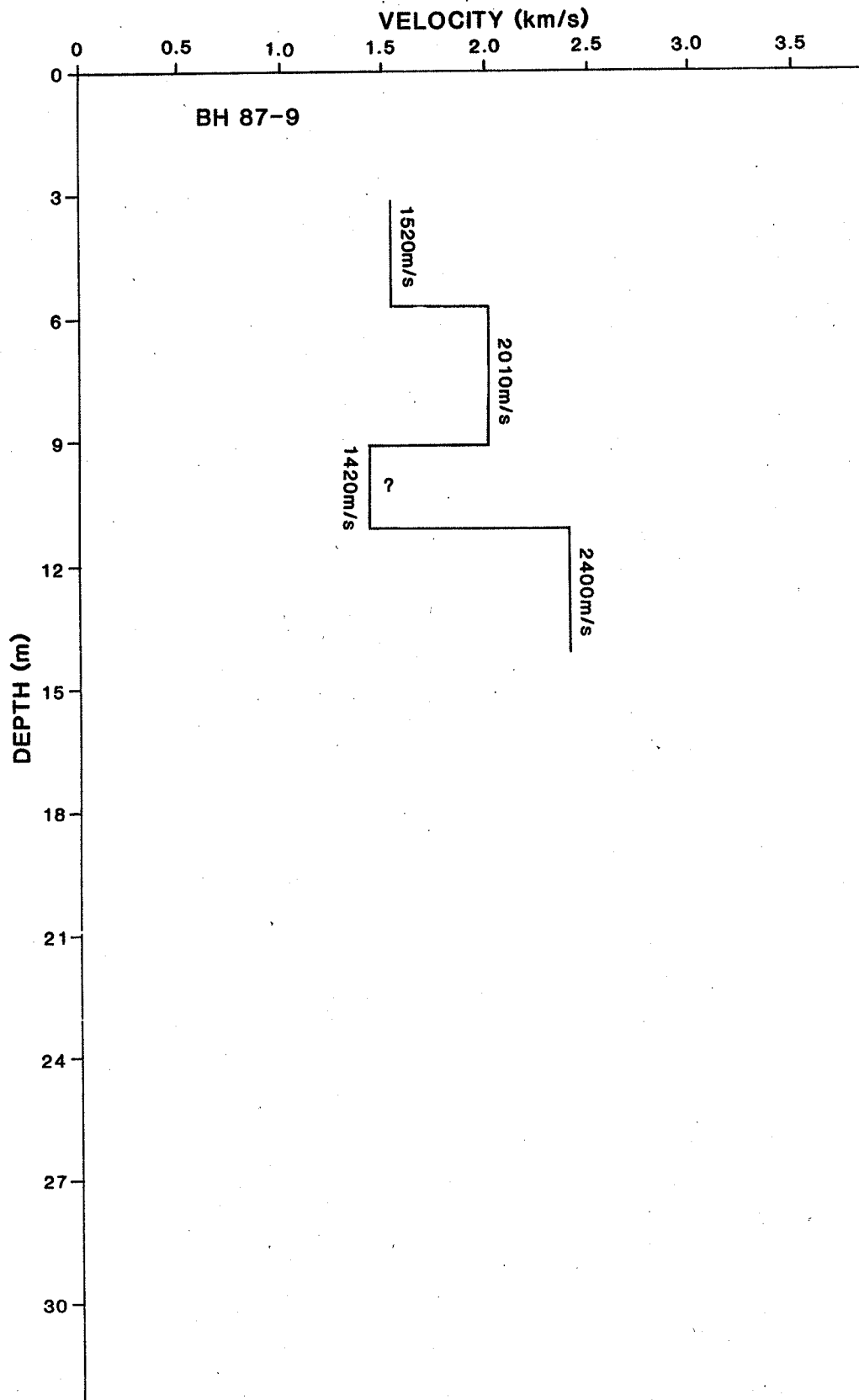


Fig. 4-40c Interval velocity vs. depth - BH 87-9

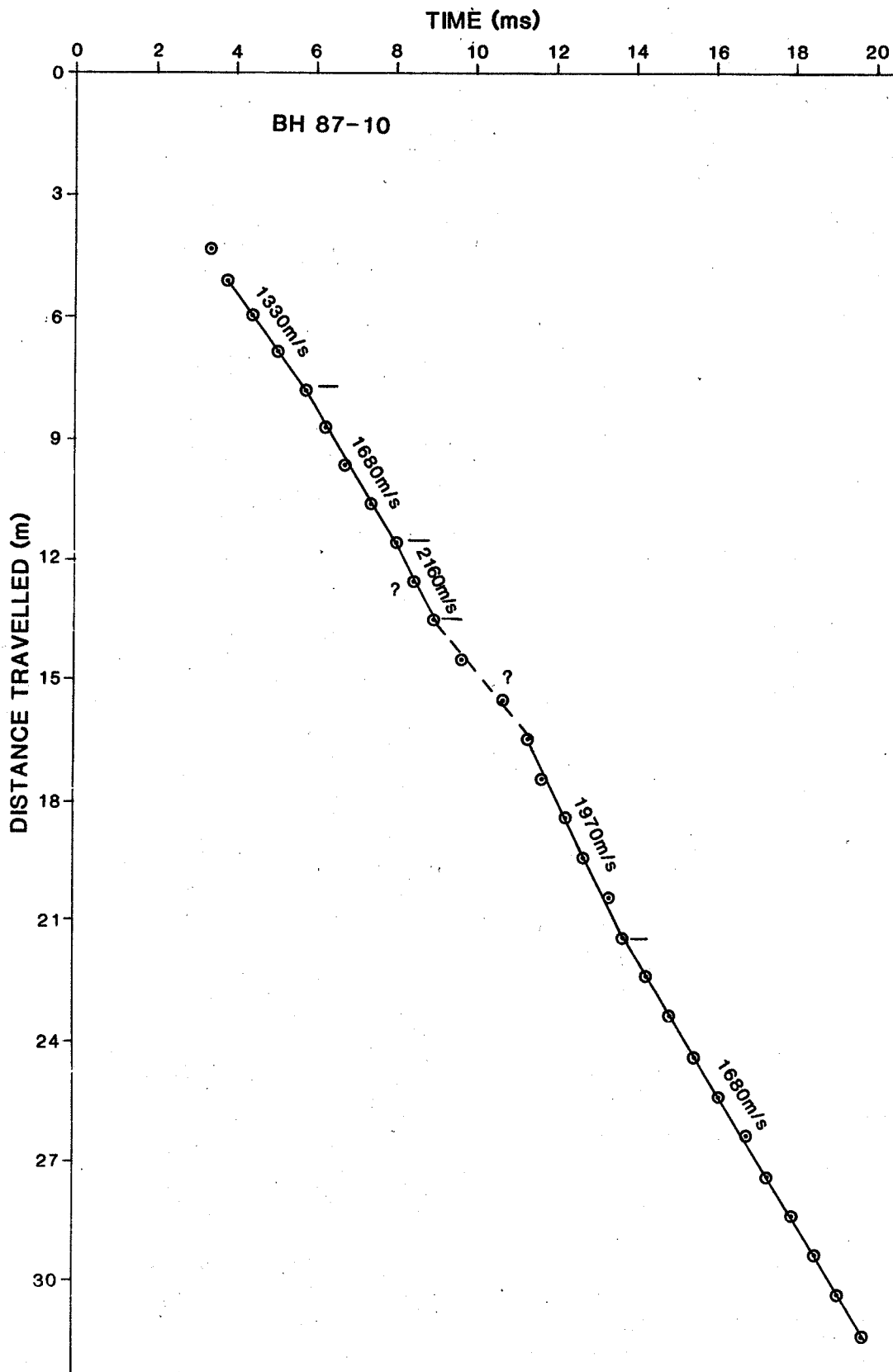


Fig. 4-41a Travel time vs. distance - BH 87-10

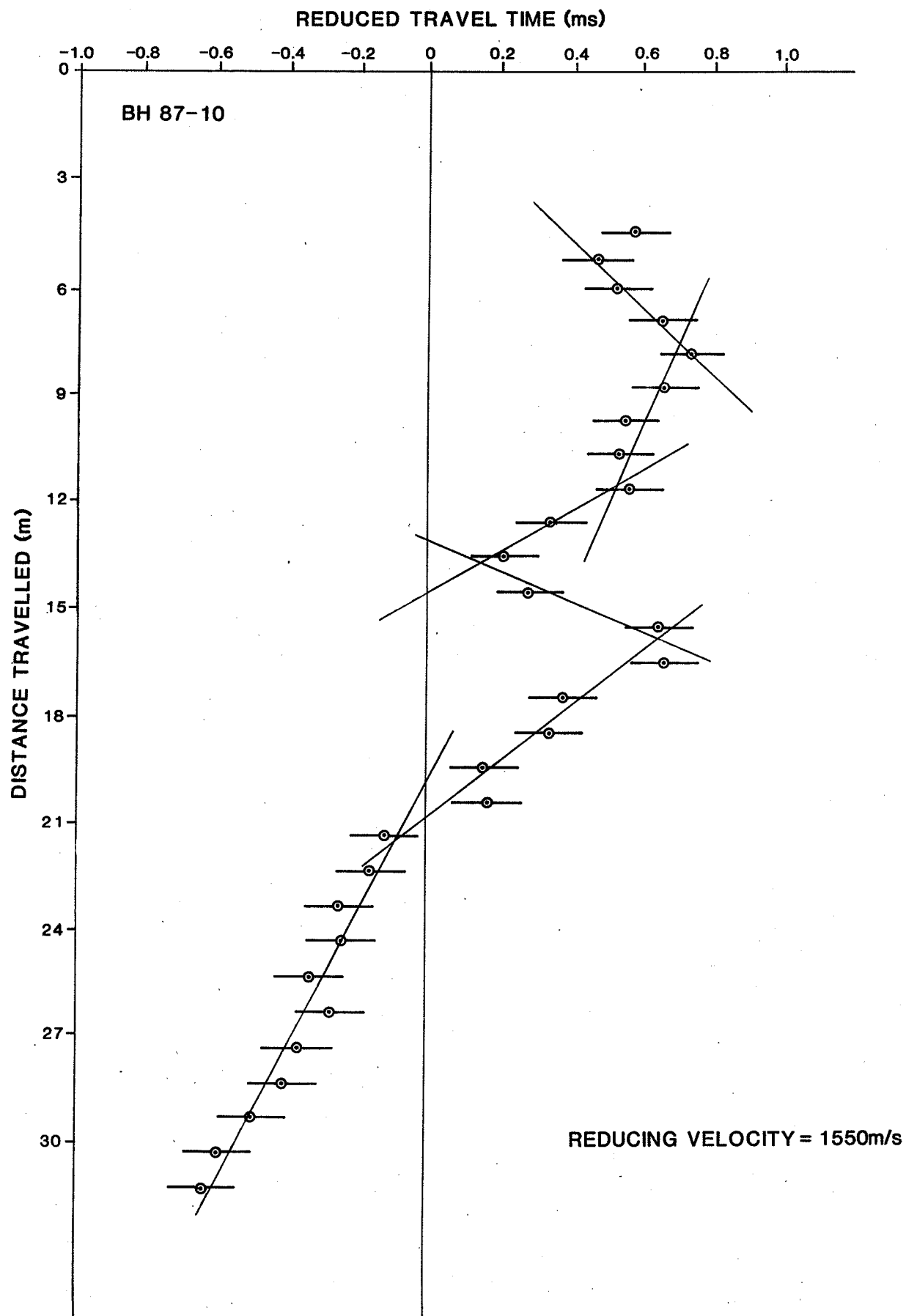


Fig. 4-41b Reduced travel time vs. distance - BH 87-10

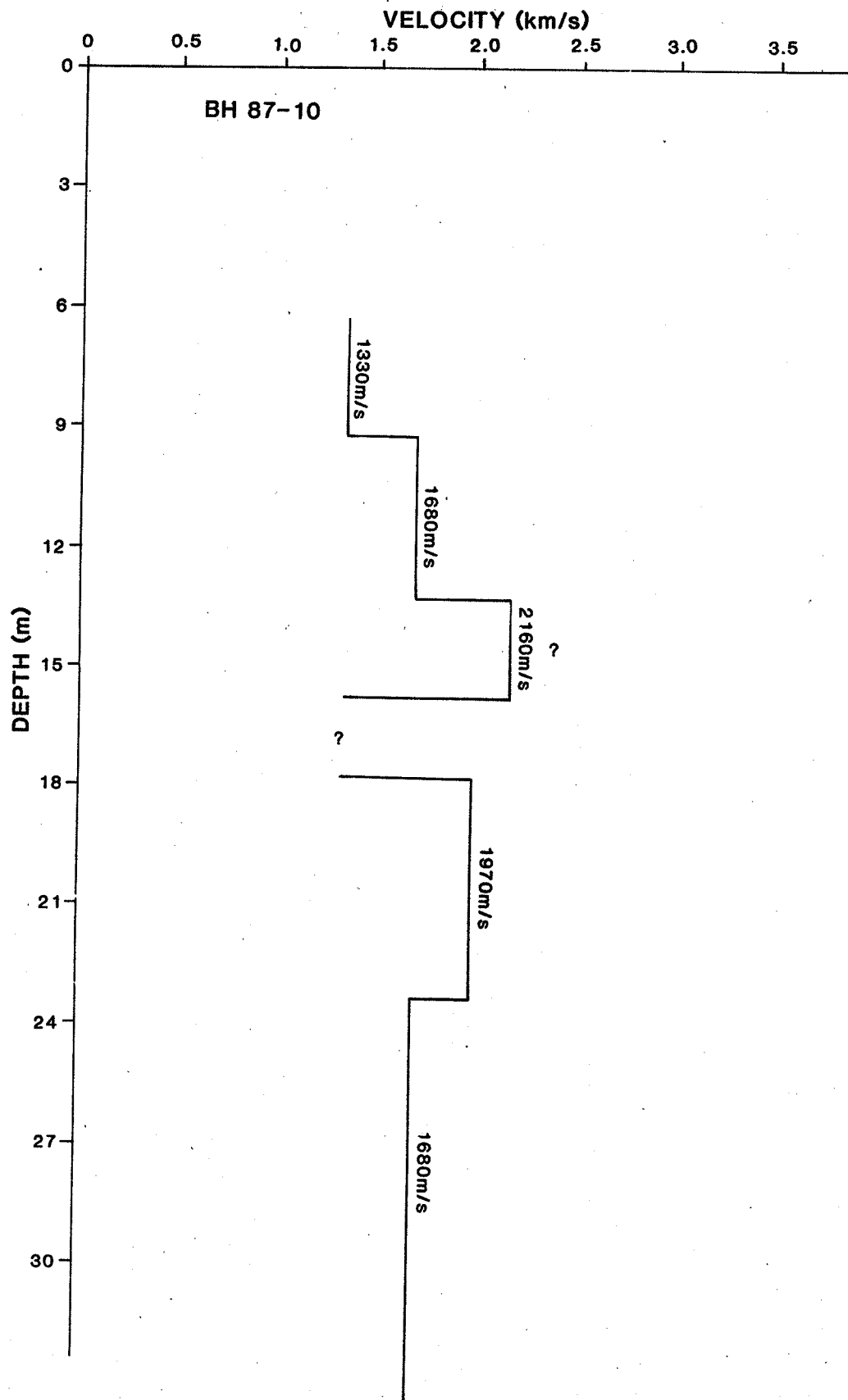


Fig. 4-41c Interval velocity vs. depth - BH 87-10

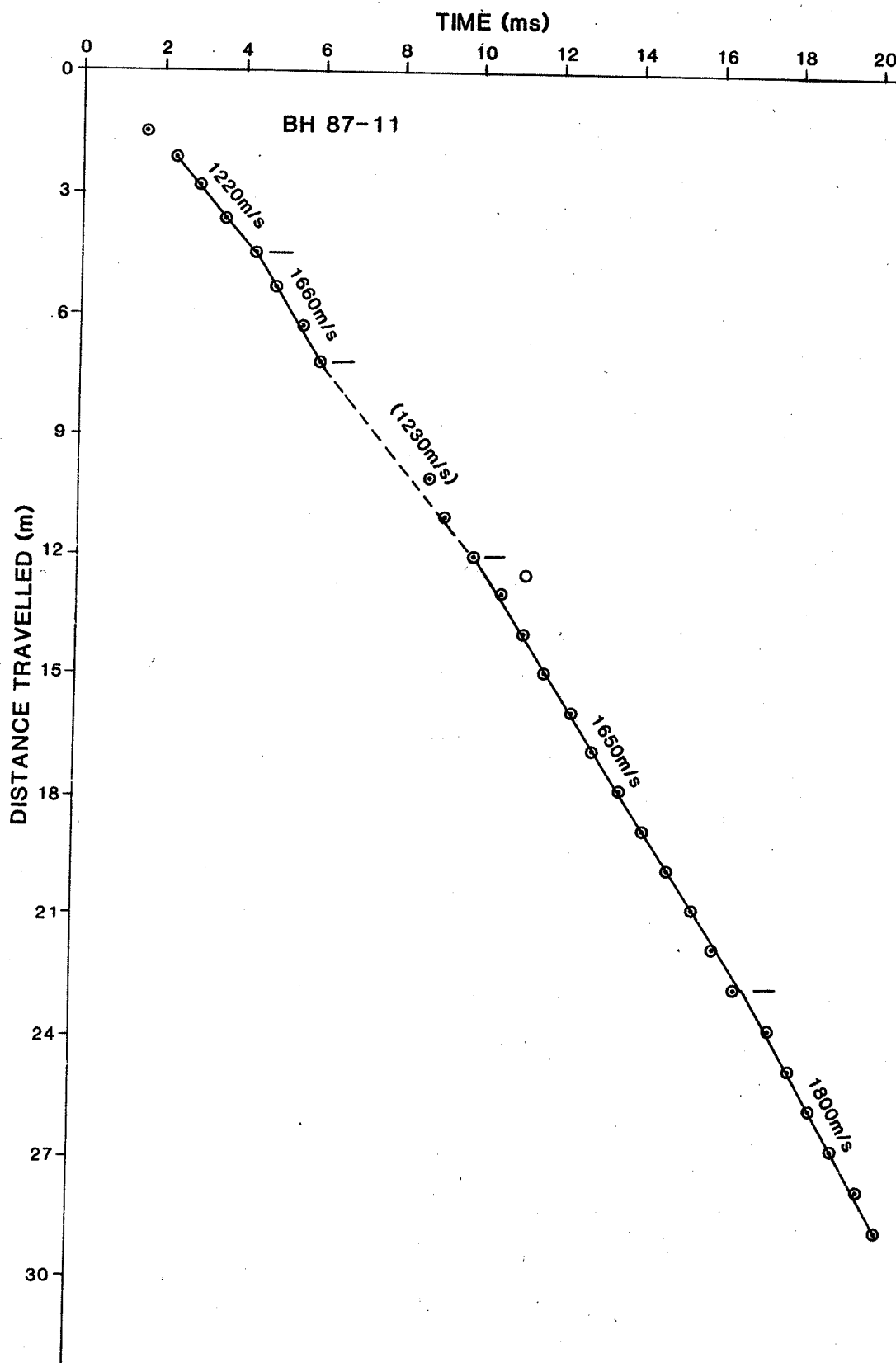


Fig. 4-42a Travel time vs. distance - BH 87-11

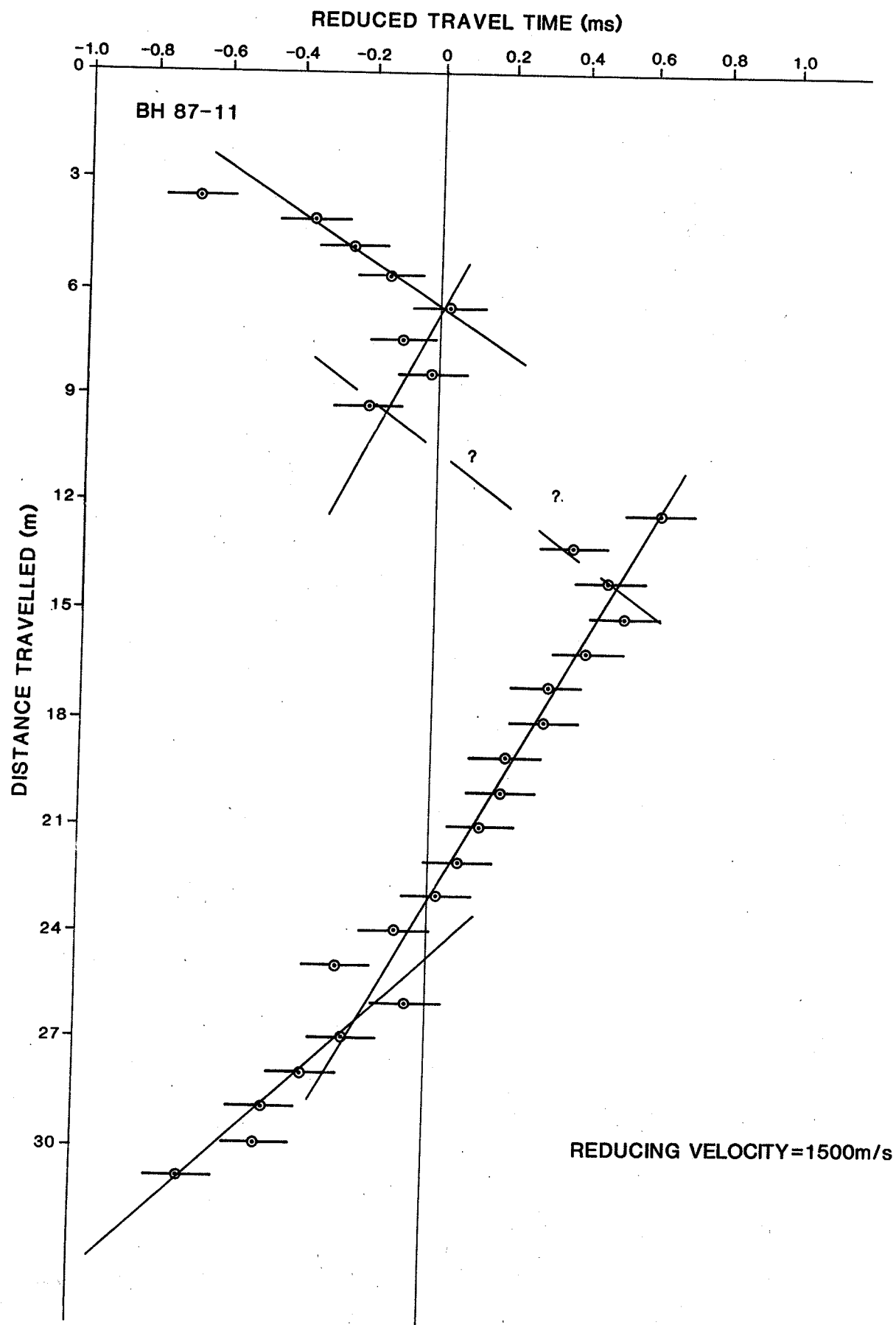


Fig. 4-42b Reduced travel time vs. distance - BH 87-11

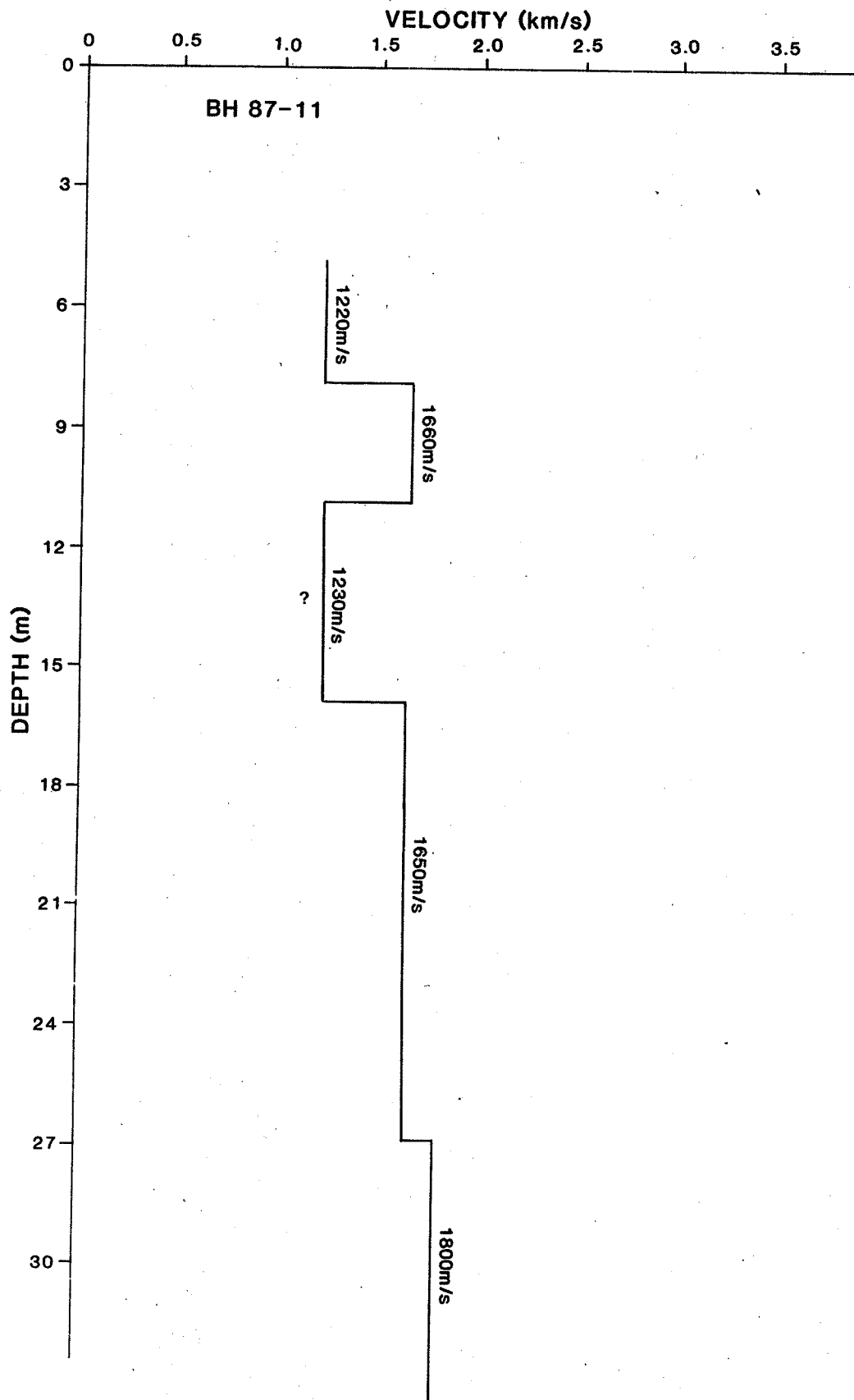


Fig. 4-42c Interval velocity vs. depth - BH 87-11

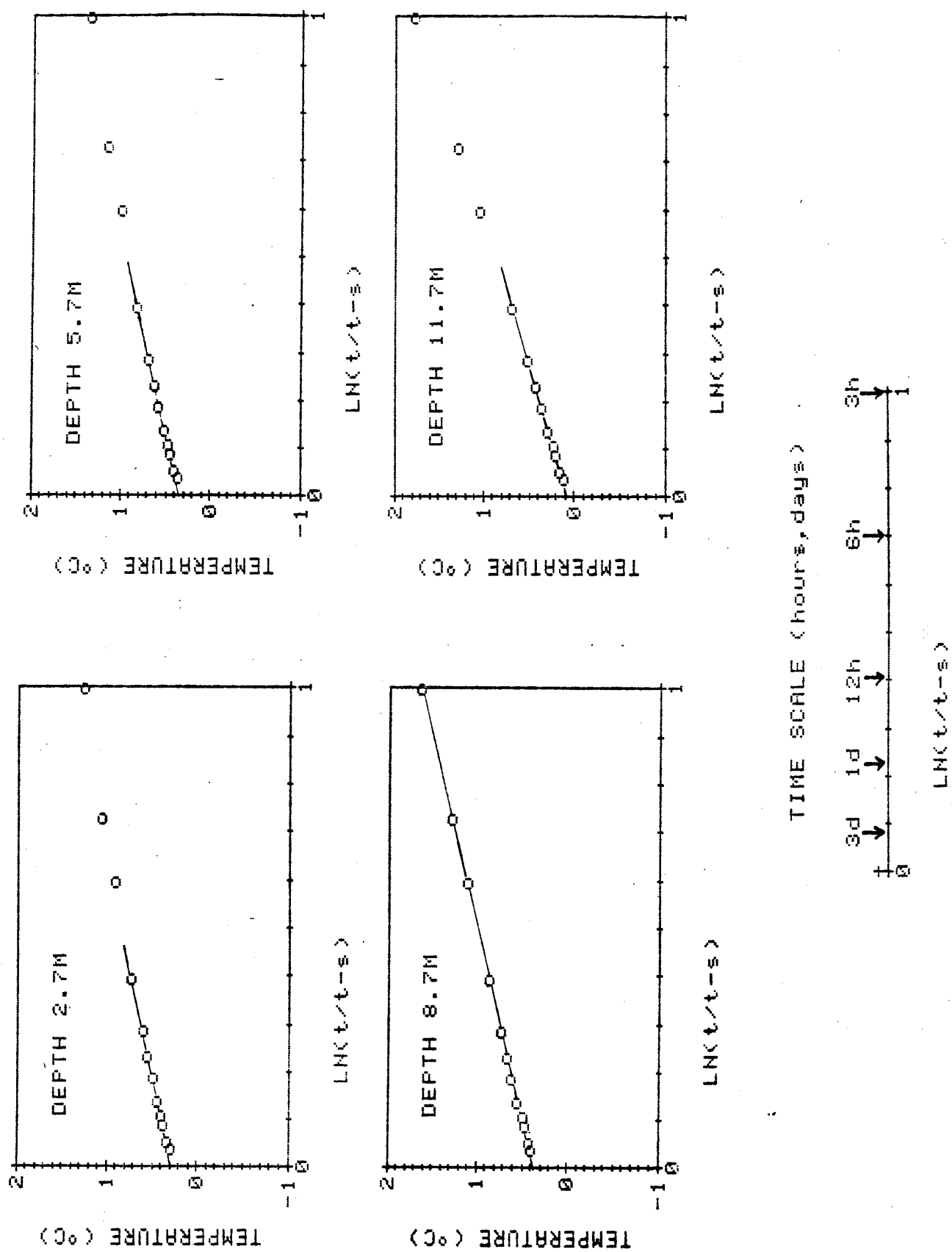


Fig. 5-1a Time vs. temperature data - BH 87-10.

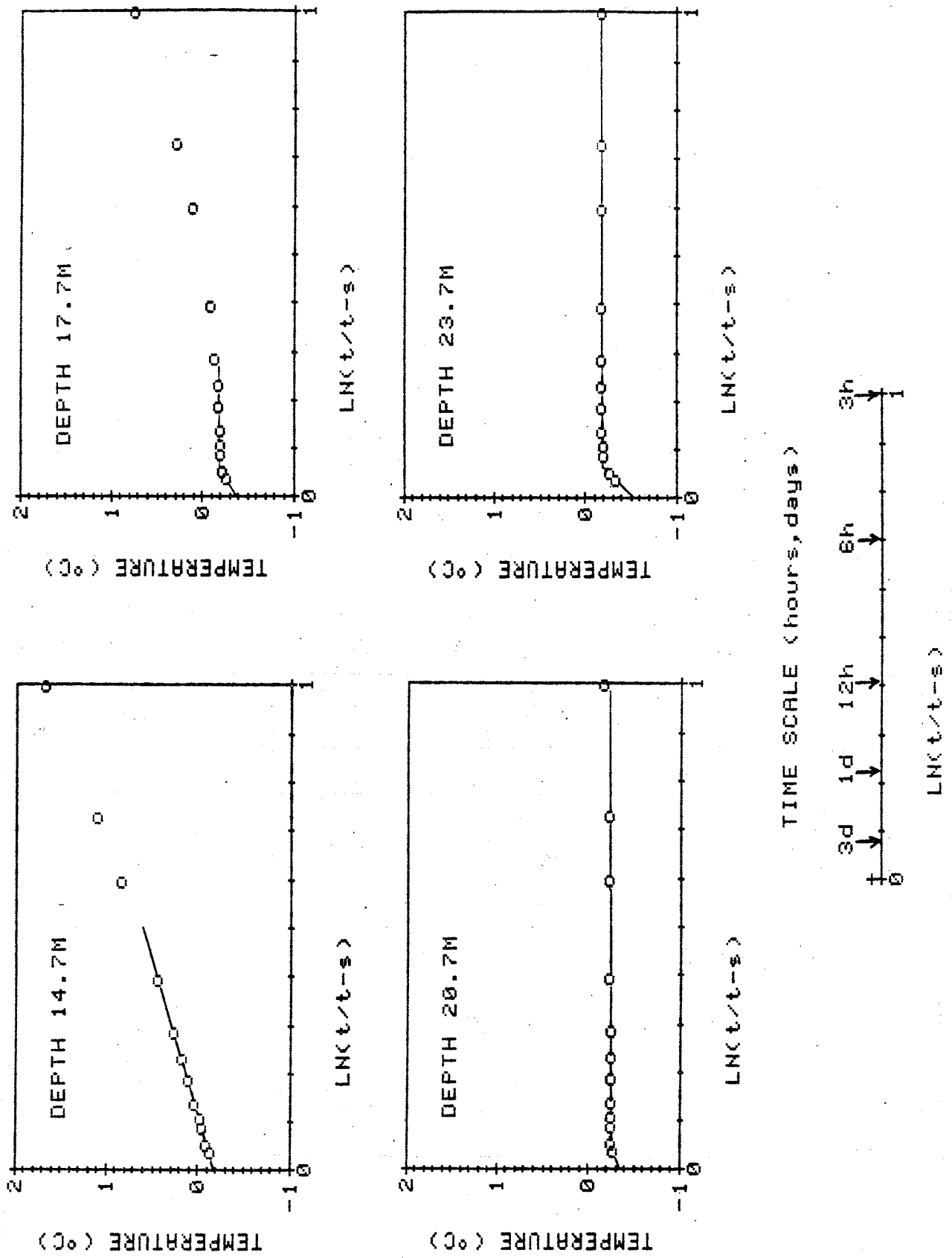


Fig. 5-1b Time vs. temperature data - BH 87-10

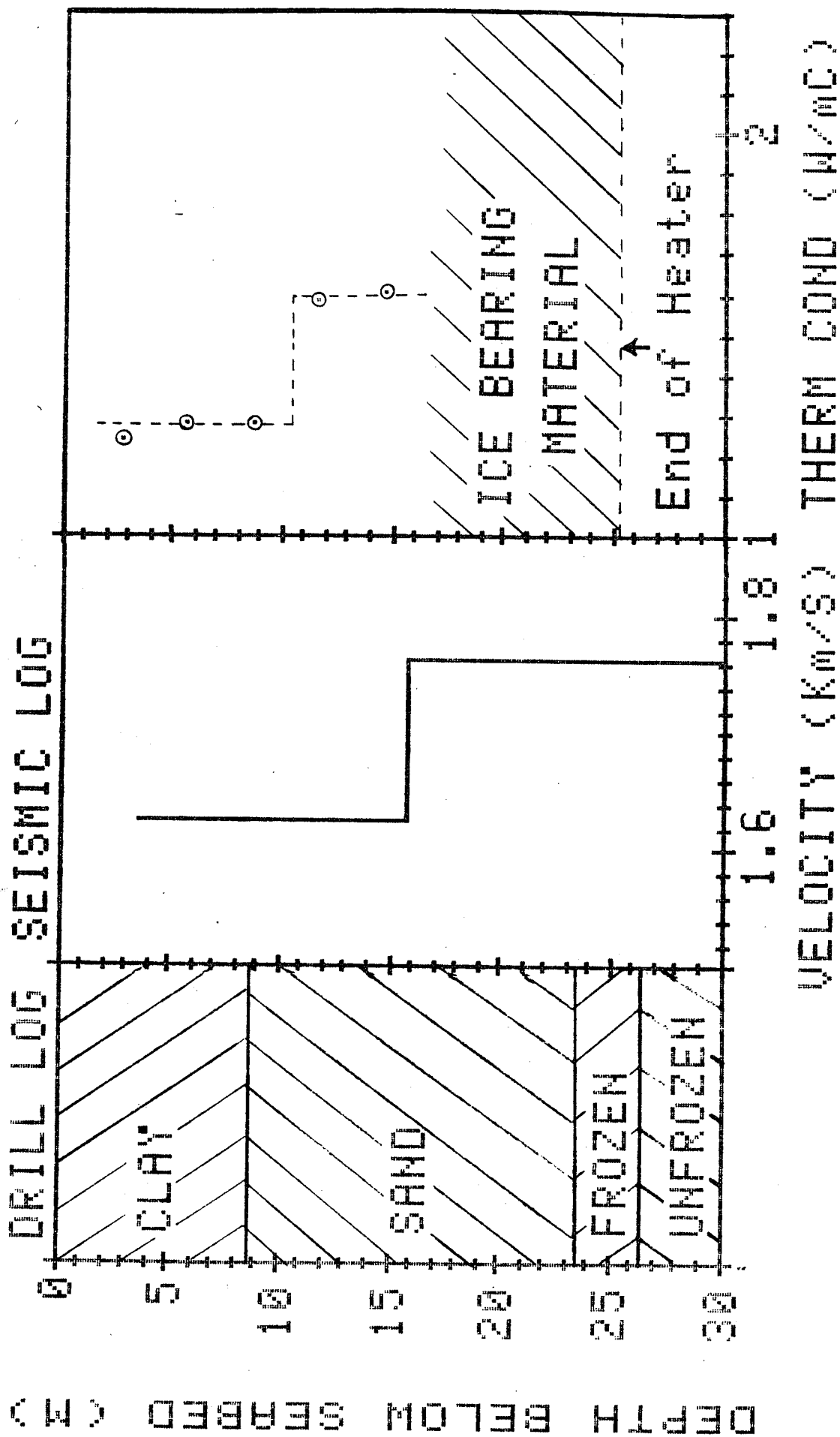


Fig. 5-2 Summary of geophysical data - BH 87-10

GROUND RADAR PROFILES - (OFFSHORE) NORTH HEAD, RICHARDS ISLAND N.W.T.
 PROFILS GÉORADAR - (EXTRA-COTIERS) NORTH HEAD, ÎLE RICHARDS T.N.-O.

APRIL 1987 / AVRIL 1987

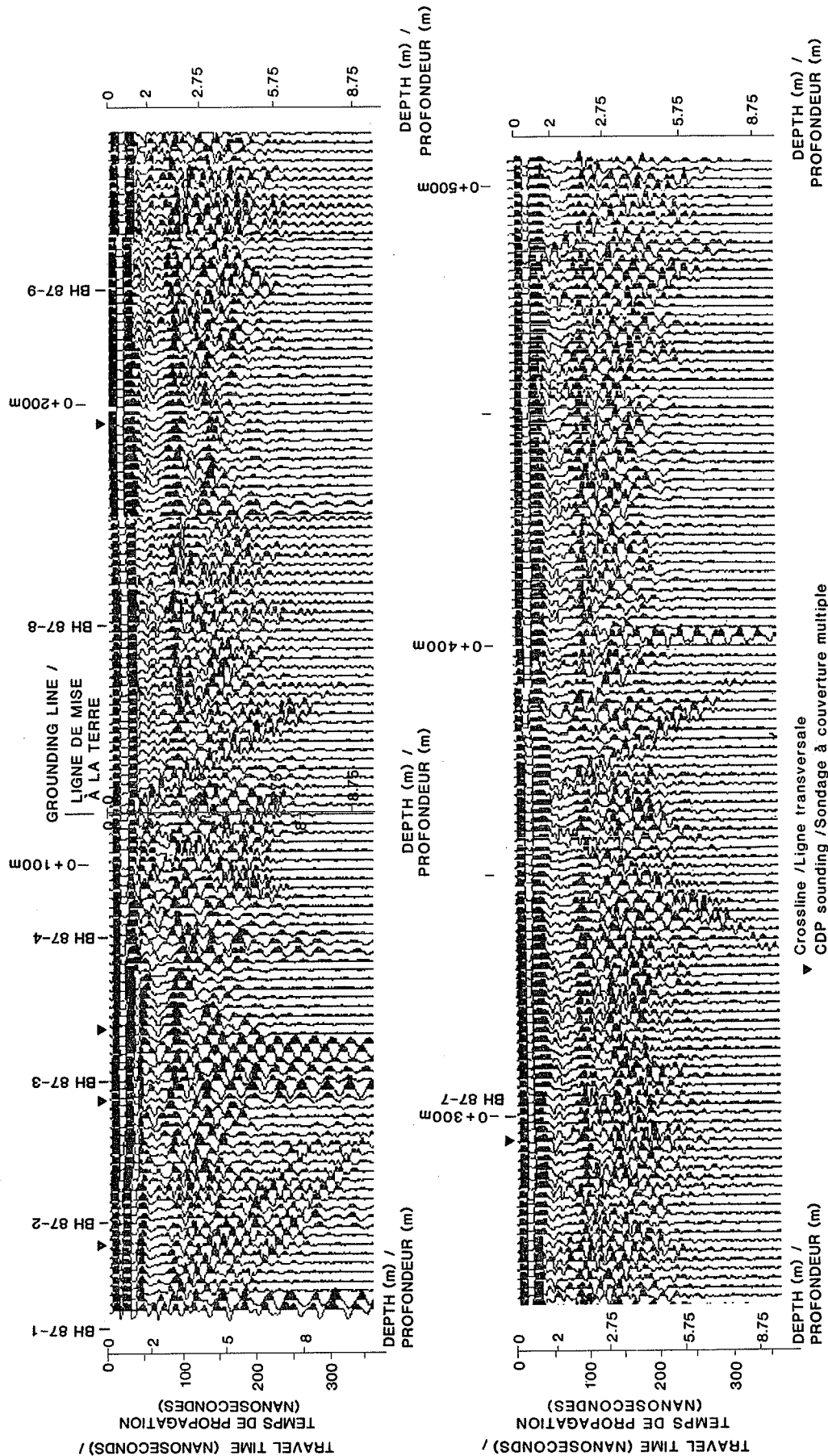


Fig. 6-1a Radar profile (offshore section) - April 1987, raw data

GROUND RADAR PROFILES - (OFFSHORE) NORTH HEAD, RICHARDS ISLAND N.W.T.
 PROFILS GÉORADAR - (EXTRA-COTIERS) NORTH HEAD, ÎLE RICHARDS T.N.-O.

APRIL 1987 / AVRIL 1987

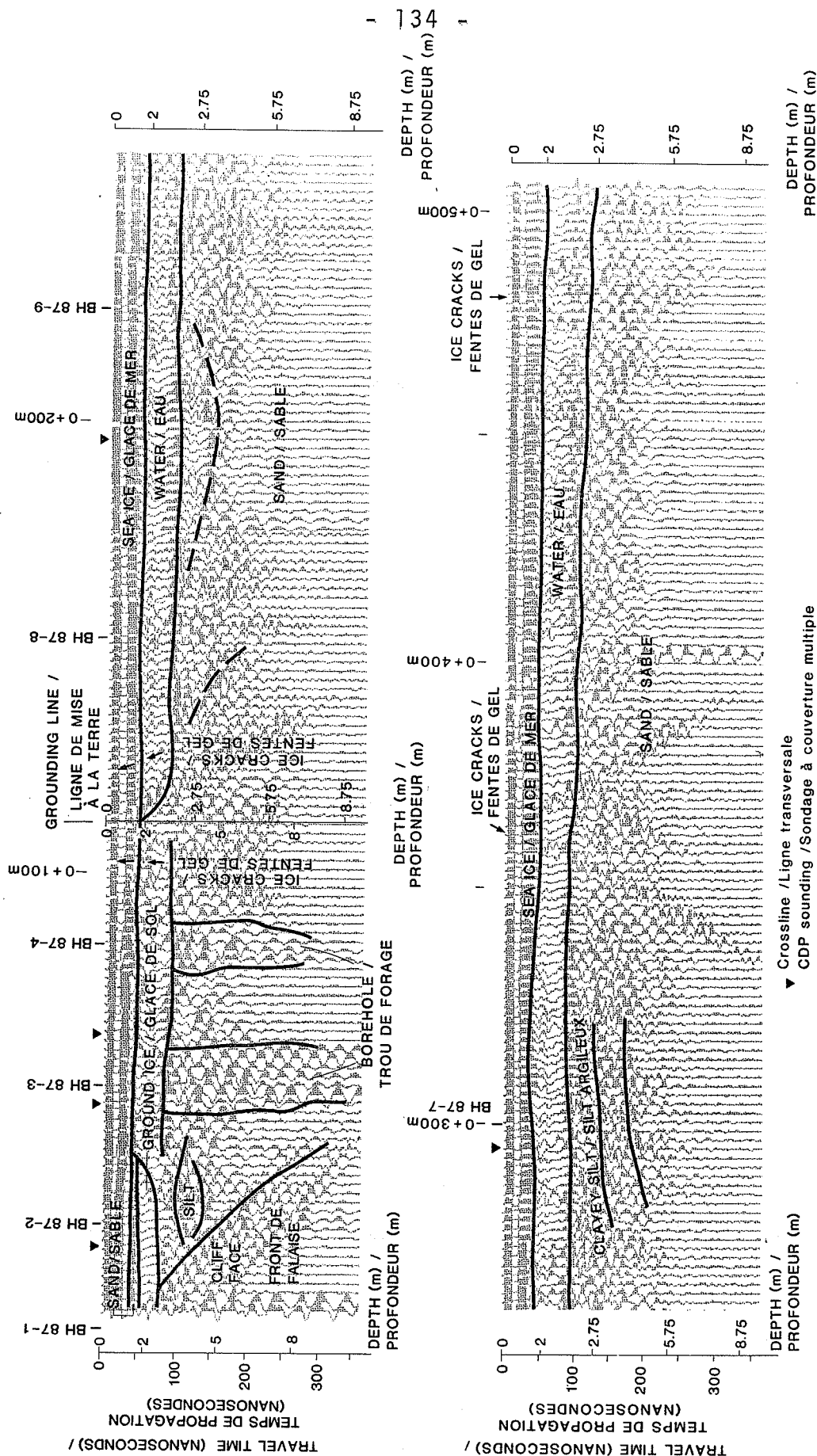
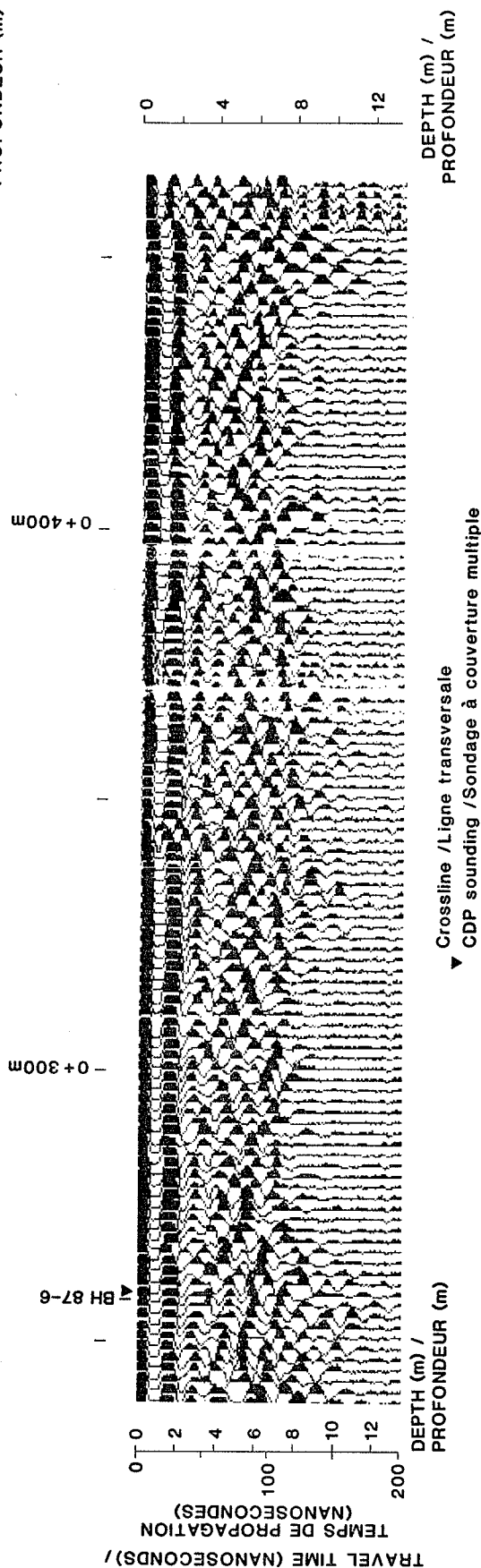
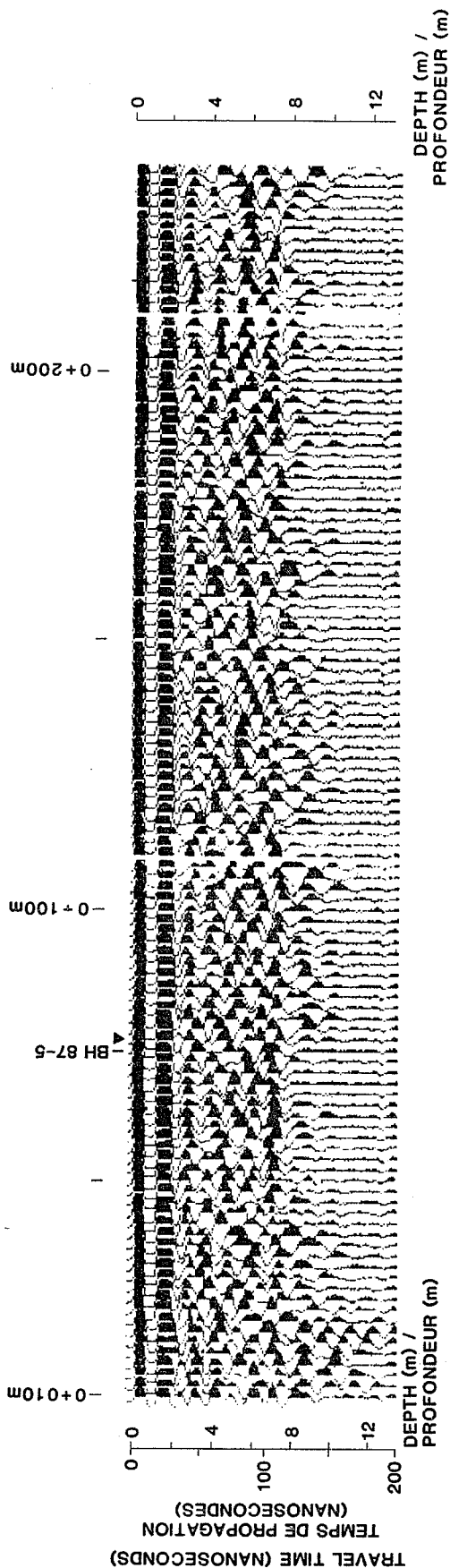


Fig. 6-1b Radar profile (offshore section) - April 1987, interpretation

GROUND RADAR PROFILES - (ONSHORE) NORTH HEAD, RICHARDS ISLAND N.W.T.
 PROFILS GÉORADAR - (CONTINENTAUX) NORTH HEAD, ÎLE RICHARDS T.N.-O.

APRIL 1987 / AVRIL 1987



▼ Crossline / Ligne transversale
 ▼ CDP sounding / Sondage à couverture multiple

Fig. 6-2a Radar profile (onshore section) - April 1987, raw data

GROUND RADAR PROFILES - (ONSHORE) NORTH HEAD, RICHARDS ISLAND N.W.T.
 PROFILS GÉORADAR - (CONTINENTAUX) NORTH HEAD, ÎLE RICHARDS T.N.-O.

APRIL 1987 / AVRIL 1987

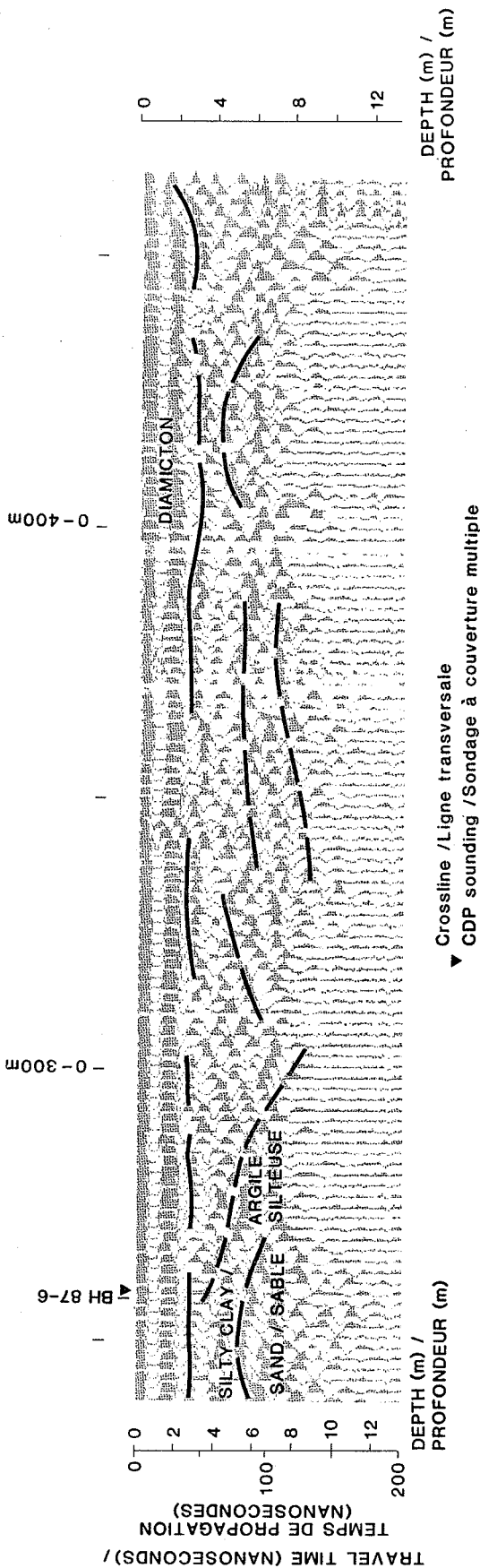
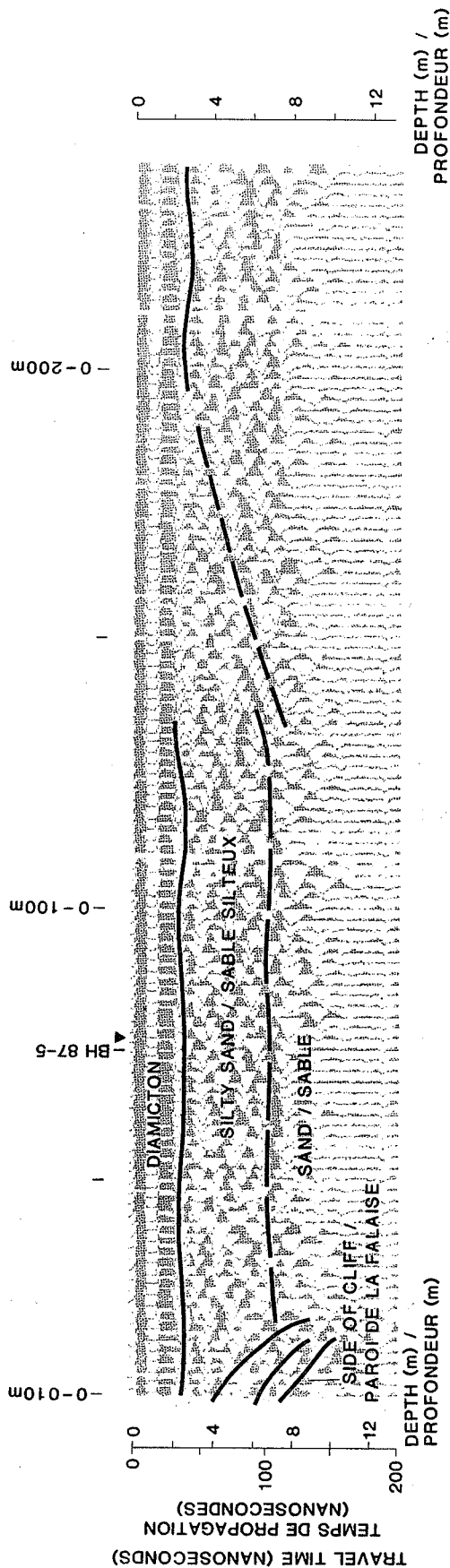


Fig. 6-2b Radar profile (onshore section) - April 1987, interpretation

GROUND RADAR PROFILES - (ONSHORE) NORTH HEAD, RICHARDS ISLAND N.W.T.
 PROFILS GEORADAR - (CONTINENTAUX) NORTH HEAD, ÎLE RICHARDS T.N.-O.

SEPTEMBER 1987 / SEPTEMBRE 1987

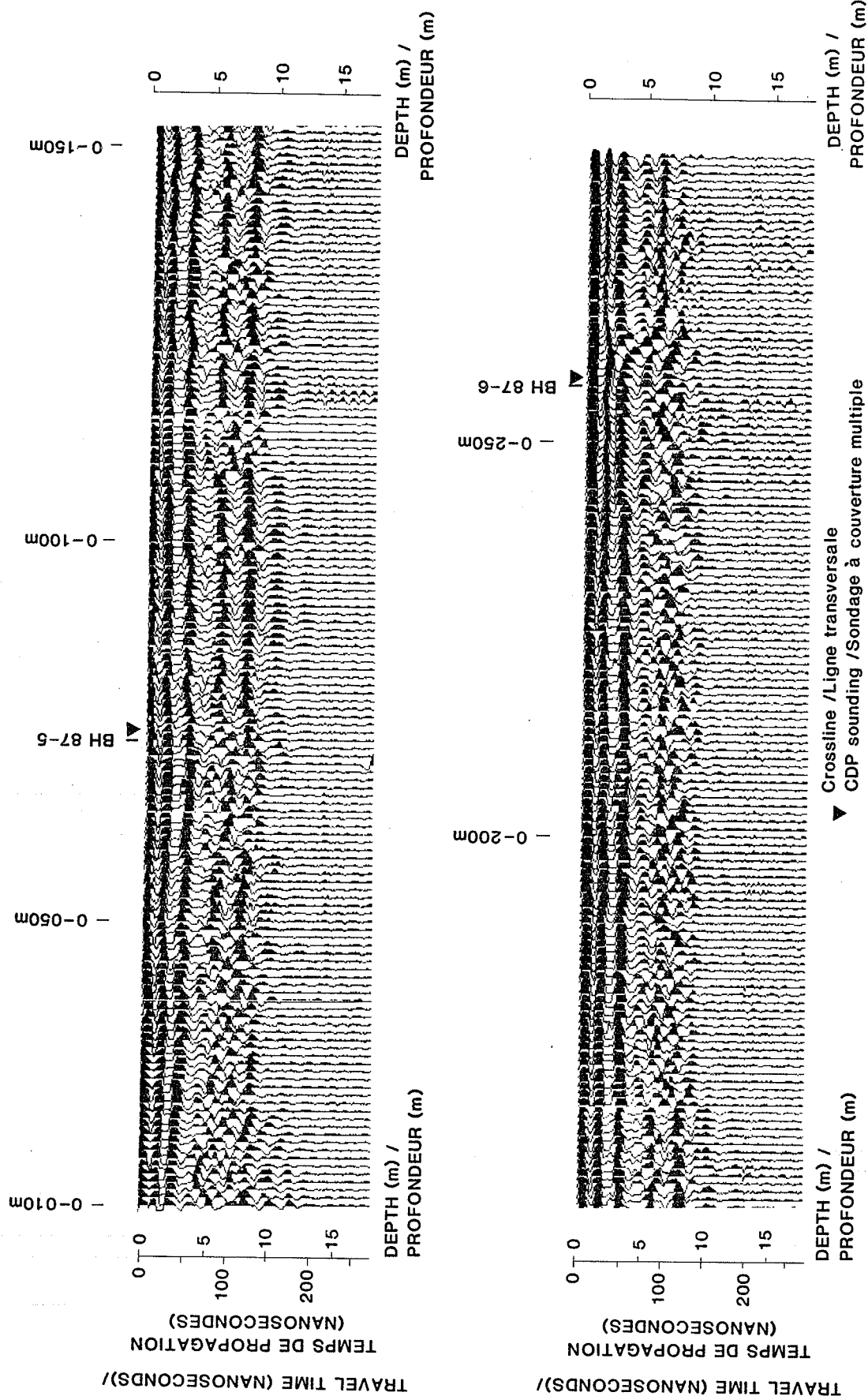


Fig. 6-3a Radar profile (onshore section) - September 1987, raw data

GROUND RADAR PROFILES - (ONSHORE) NORTH HEAD, RICHARDS ISLAND N.W.T.
 PROFILS GEORADAR - (CONTINENTAUX) NORTH HEAD, ÎLE RICHARDS T.N.-O.

SEPTEMBER 1987 / SEPTEMBRE 1987

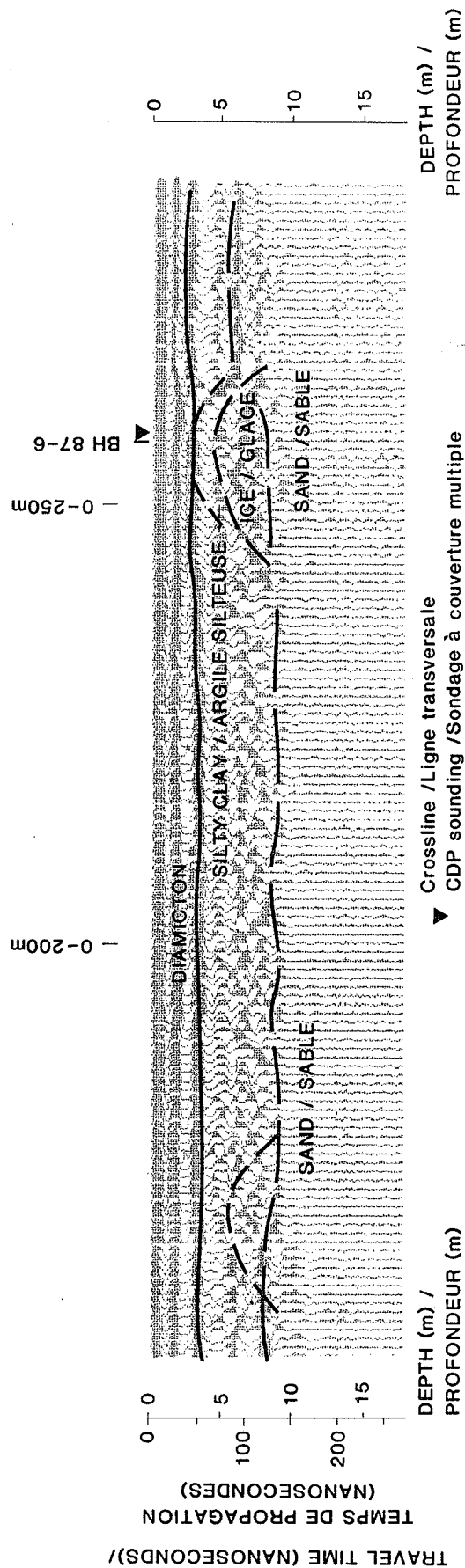
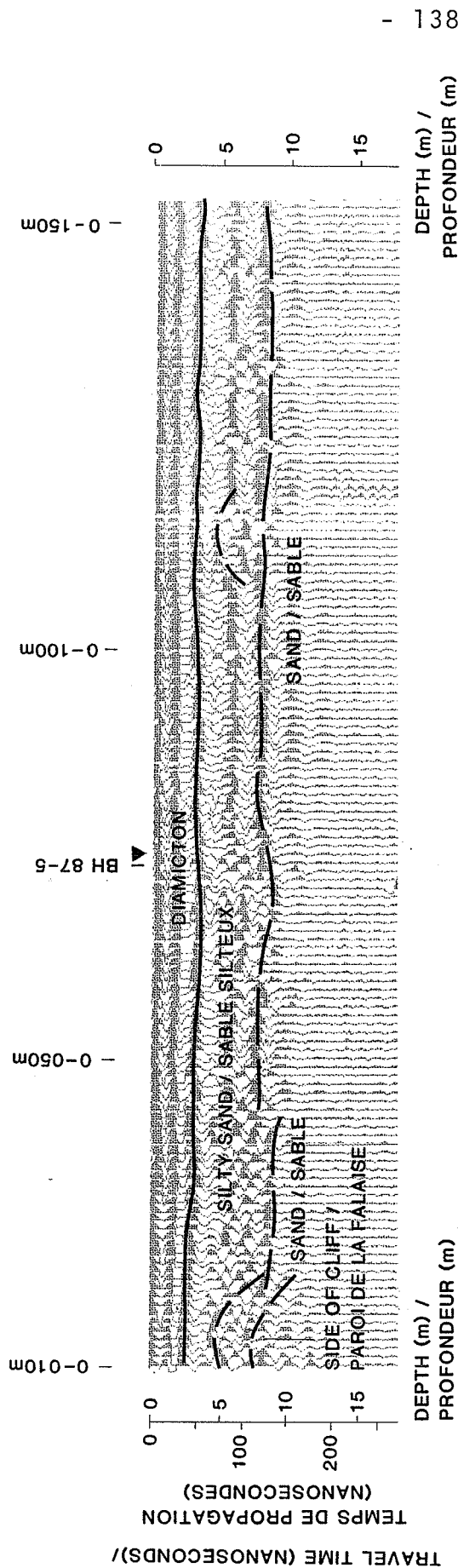


Fig. 6-3b Radar profile (onshore section) - September 1987, interpretation

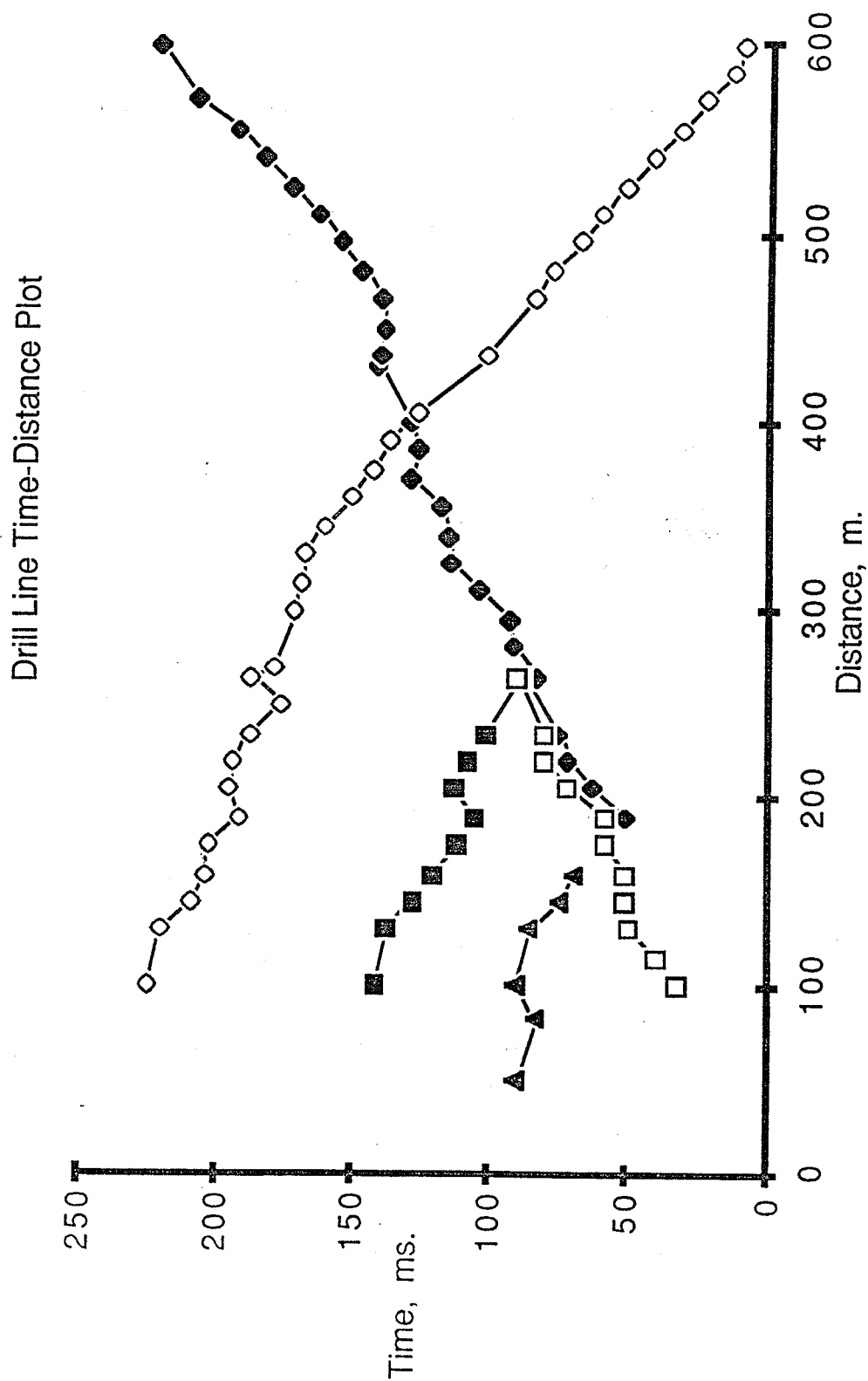


Figure 7 - 1 Drill line seismic time-distance plot.

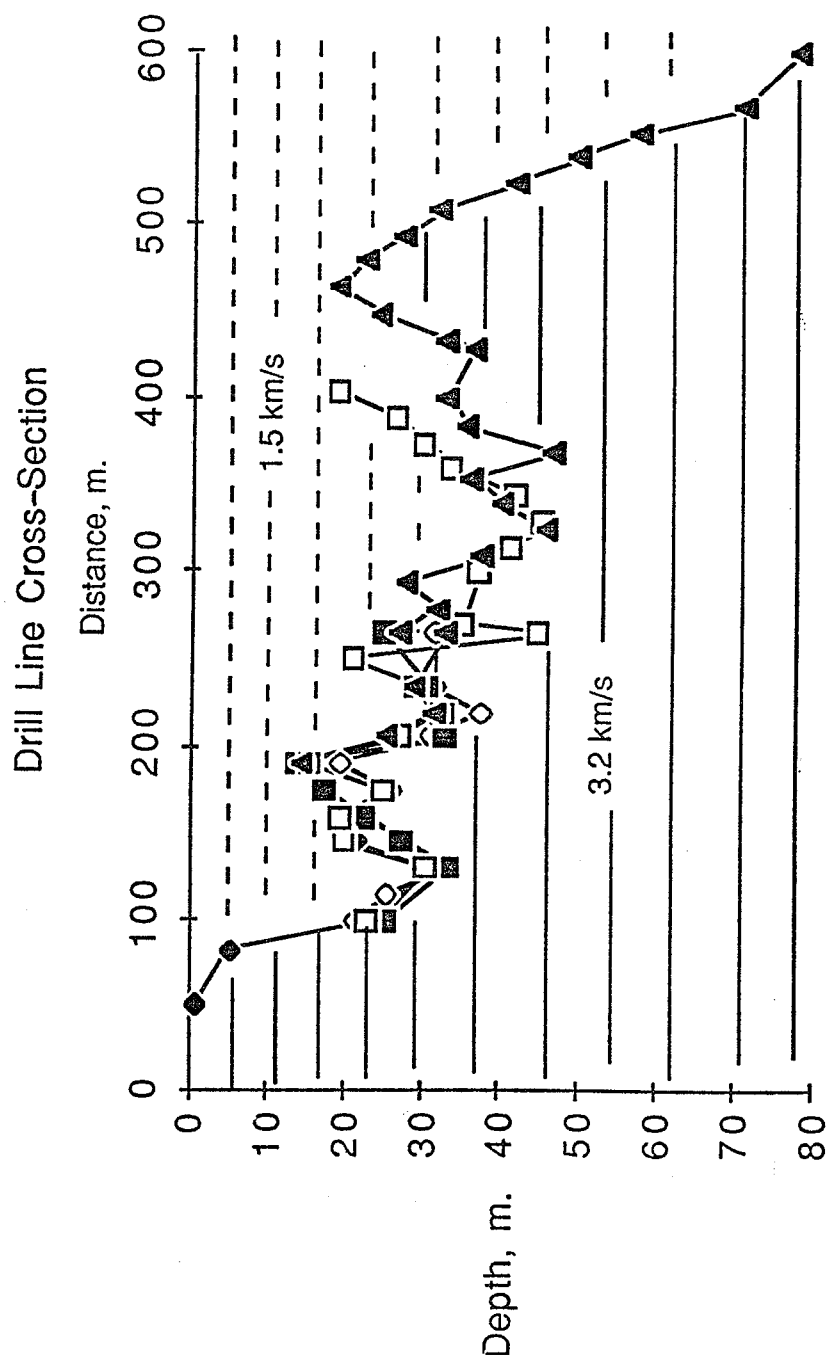


Figure 7-2 Drill line seismic cross-section.

BH 87-1 0 + 006 m

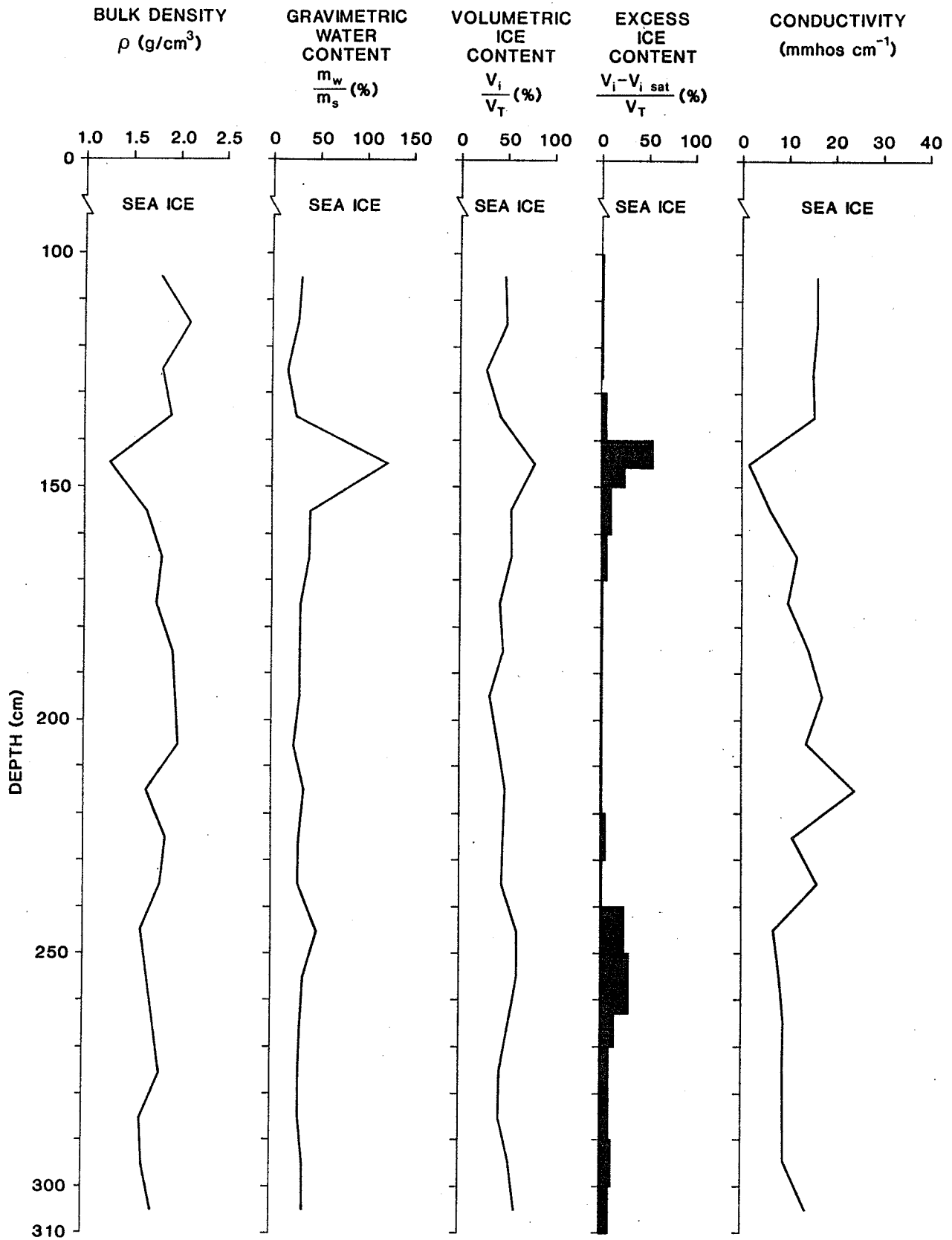


Fig. 8-1 Laboratory results - BH 87-1

CB1 0 + 035m

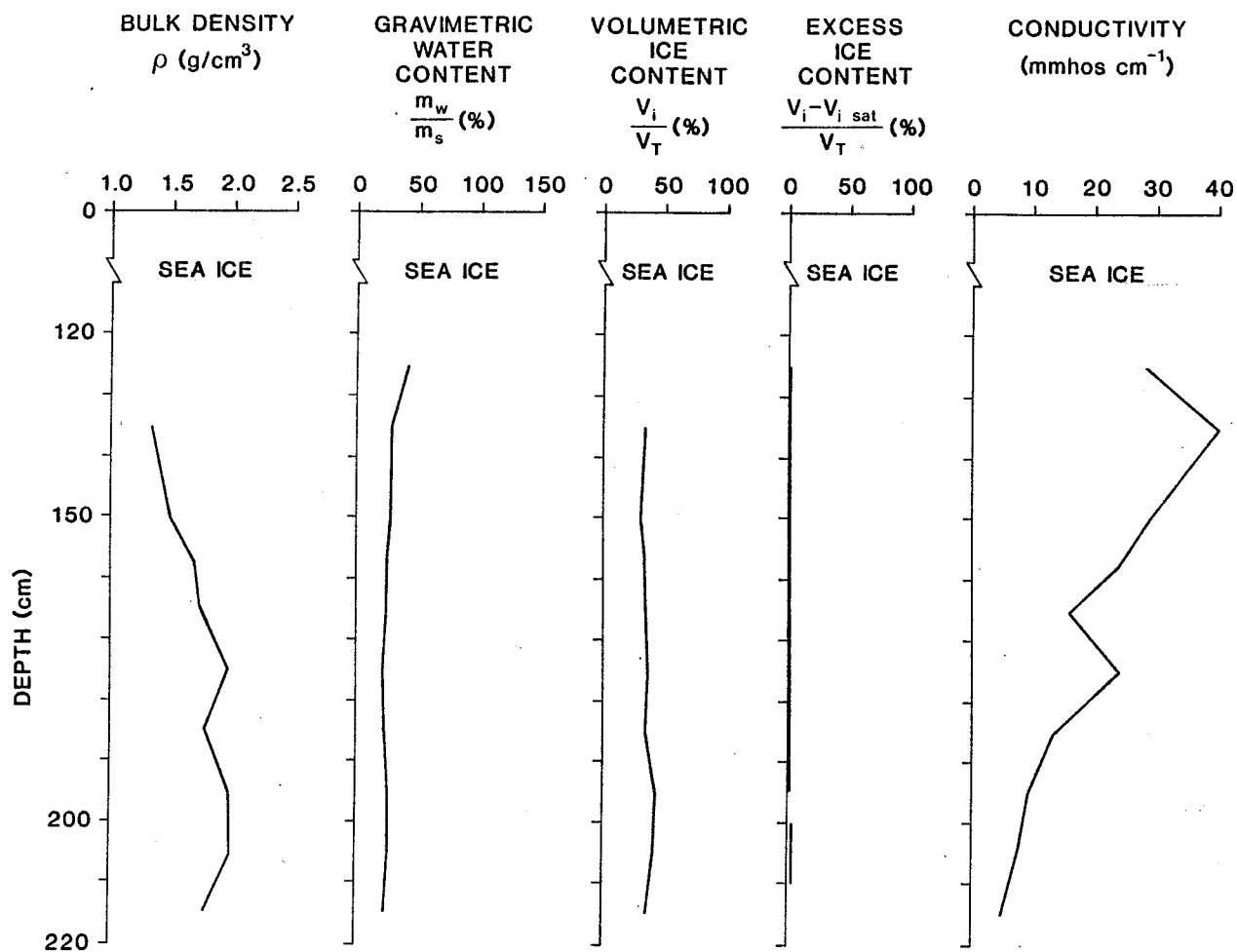


Fig. 8-2 Laboratory results - CB 1

BH 87-3 0 + 050m

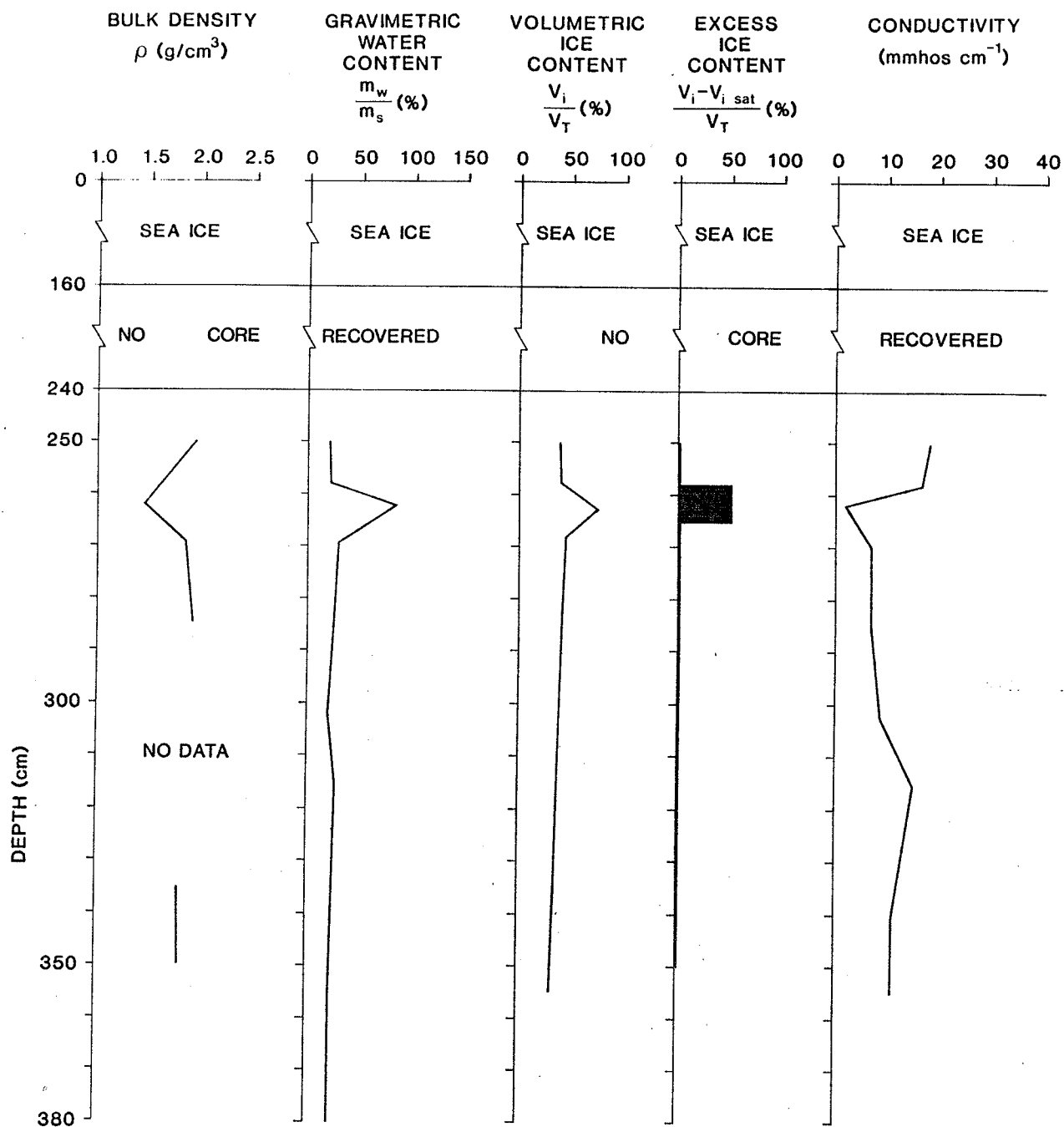


Fig. 8-3 Laboratory results - BH 87-3

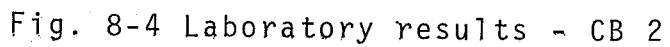


Fig. 8-4 Laboratory results - CB 2

BH 87-4 0 + 082m

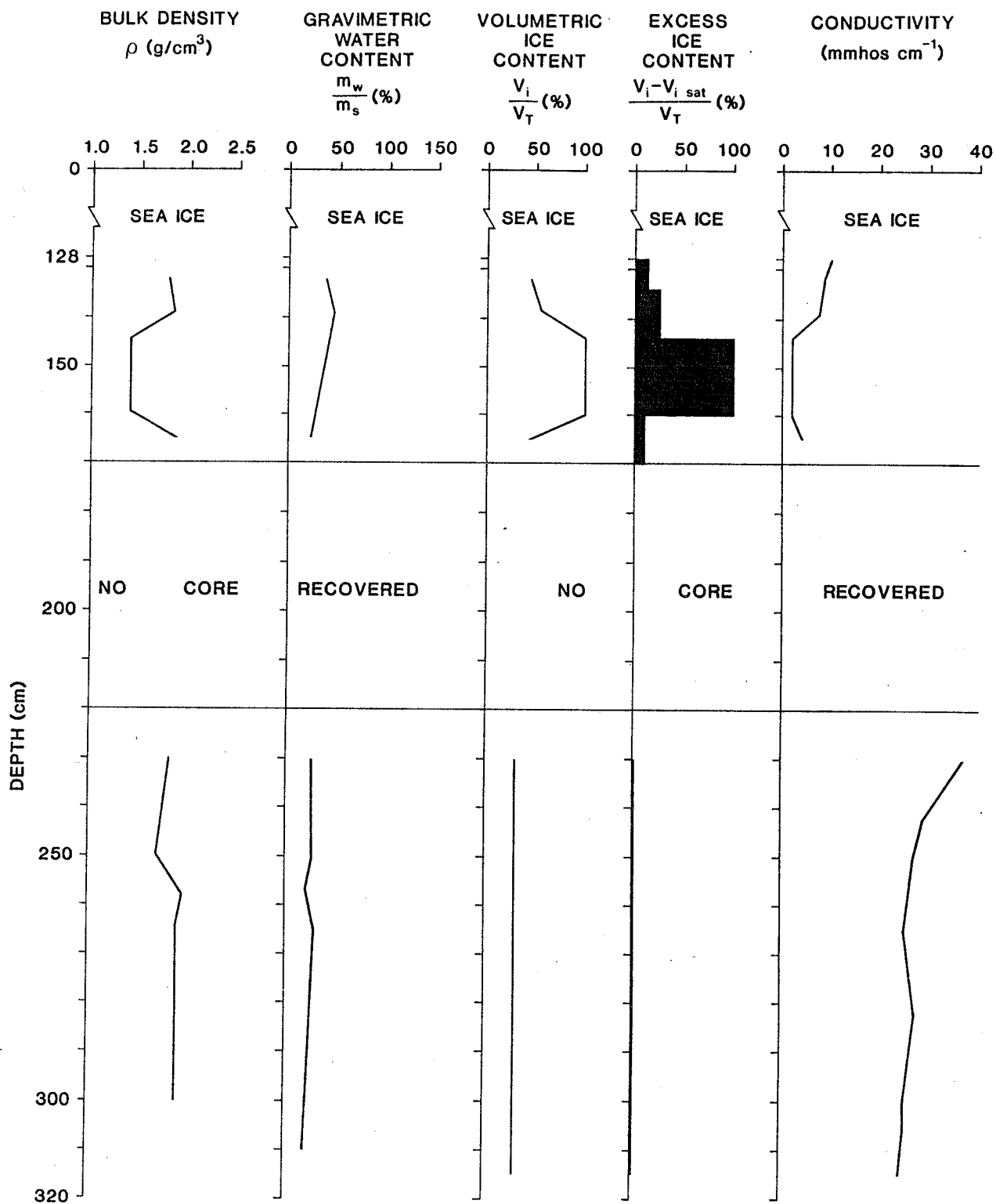


Fig. 8-5 Laboratory results - BH 87-4

BH 86-4 0 + 100m

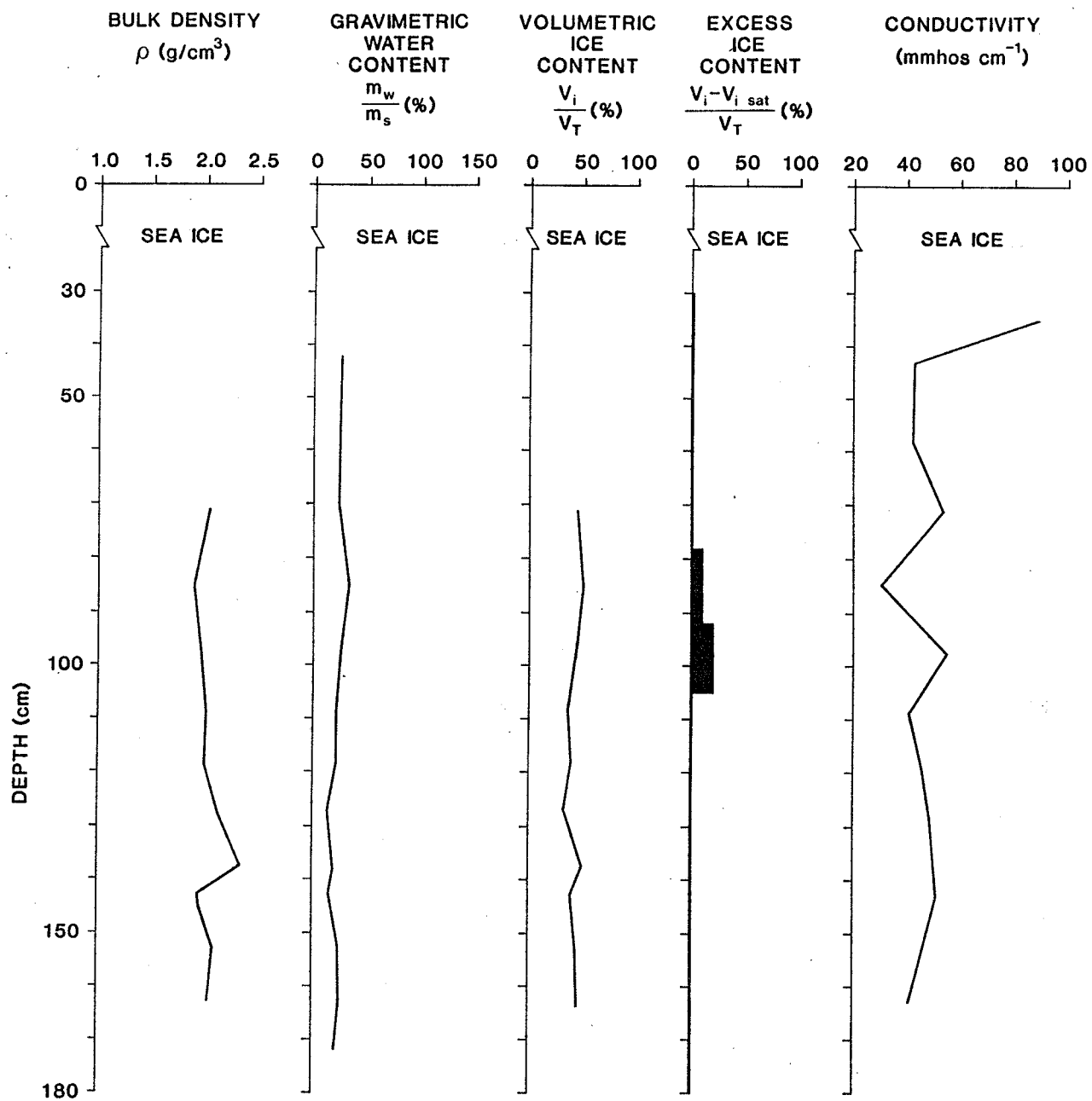


Fig. 8-6 Laboratory results - BH 86-4

BH 86-6 0 + 300m

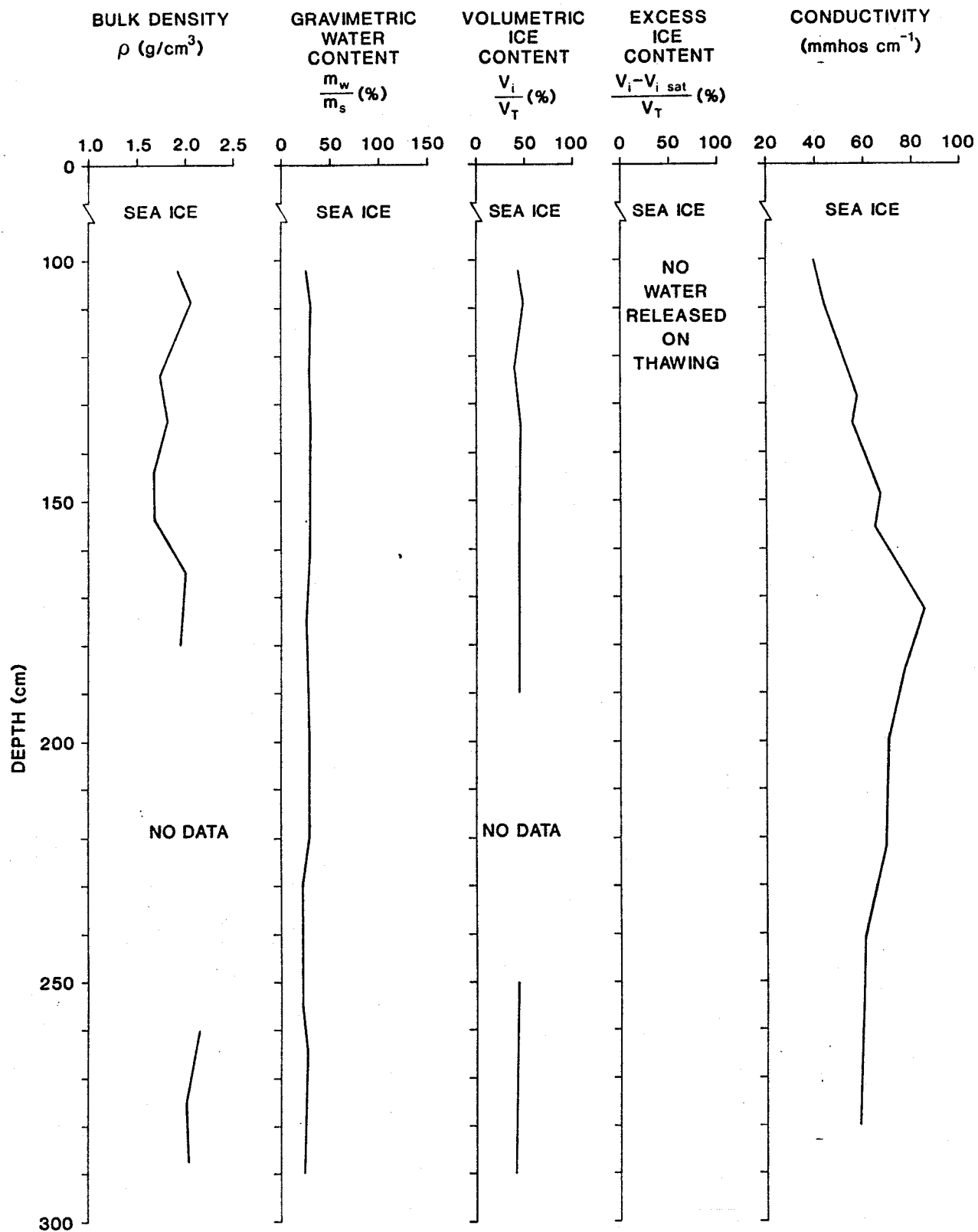


Fig. 8-7 Laboratory results - BH 86-6

BH 86-6 0 + 300m

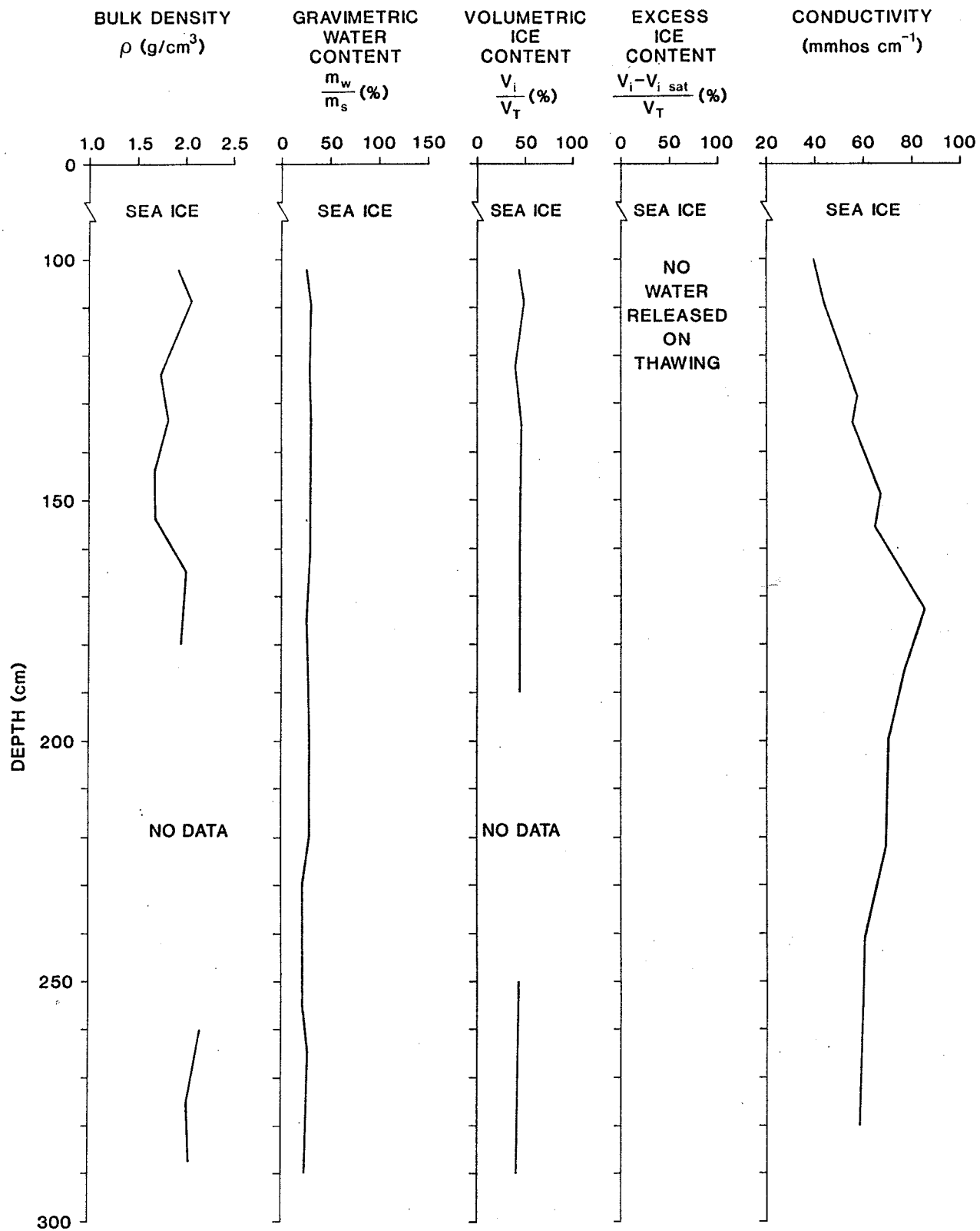


Fig. 8-7 Laboratory results - BH 86-6

GEOLOGICAL SURVEY OF CANADA

OPEN FILE 1707

**GEOTECHNICAL INVESTIGATIONS OFF
NORTHERN RICHARDS ISLAND, N.W.T. - 1987**

Compiled and edited by

P.J. Kurfurst¹

Contributors:

**J.G. Bisson¹, R.A. Burns¹, S.R. Dallimore¹, R.M. Gagné¹,
R.L. Good¹, J.A. Hunter¹, A.S. Judge¹, P. Lafleche¹,
S.E. Pullan¹, C.R. Burn², W.D. Harrison³, J.L. Morack³,
K.G. Neave⁴ and H.A. MacAulay⁴**

- ¹ Geological Survey of Canada, Terrain Sciences Division, Ottawa
- ² University of British Columbia, Department of Geography, Vancouver, B.C.
- ³ University of Alaska, Physics Department and Geophysical Institute, Fairbanks, Alaska, U.S.A.
- ⁴ Northern Seismic Analysis Ltd., Echo Bay, Ontario

GEOLOGICAL SURVEY OF CANADA

OPEN FILE 1707

**GEOTECHNICAL INVESTIGATIONS OFF
NORTHERN RICHARDS ISLAND, N.W.T. - 1987**

Compiled and edited by

P.J. Kurfurst¹

Contributors:

**J.G. Bisson¹, R.A. Burns¹, S.R. Dallimore¹, R.M. Gagné¹,
R.L. Good¹, J.A. Hunter¹, A.S. Judge¹, P. Lafleche¹,
S.E. Pullan¹, C.R. Burn², W.D. Harrison³, J.L. Morack³,
K.G. Neave⁴ and H.A. MacAulay⁴**

- ¹ Geological Survey of Canada, Terrain Sciences Division, Ottawa
- ² University of British Columbia, Department of Geography, Vancouver, B.C.
- ³ University of Alaska, Physics Department and Geophysical Institute, Fairbanks, Alaska, U.S.A.
- ⁴ Northern Seismic Analysis Ltd., Echo Bay, Ontario



1988

G. S. C.

CONTRACTOR: ConeTec

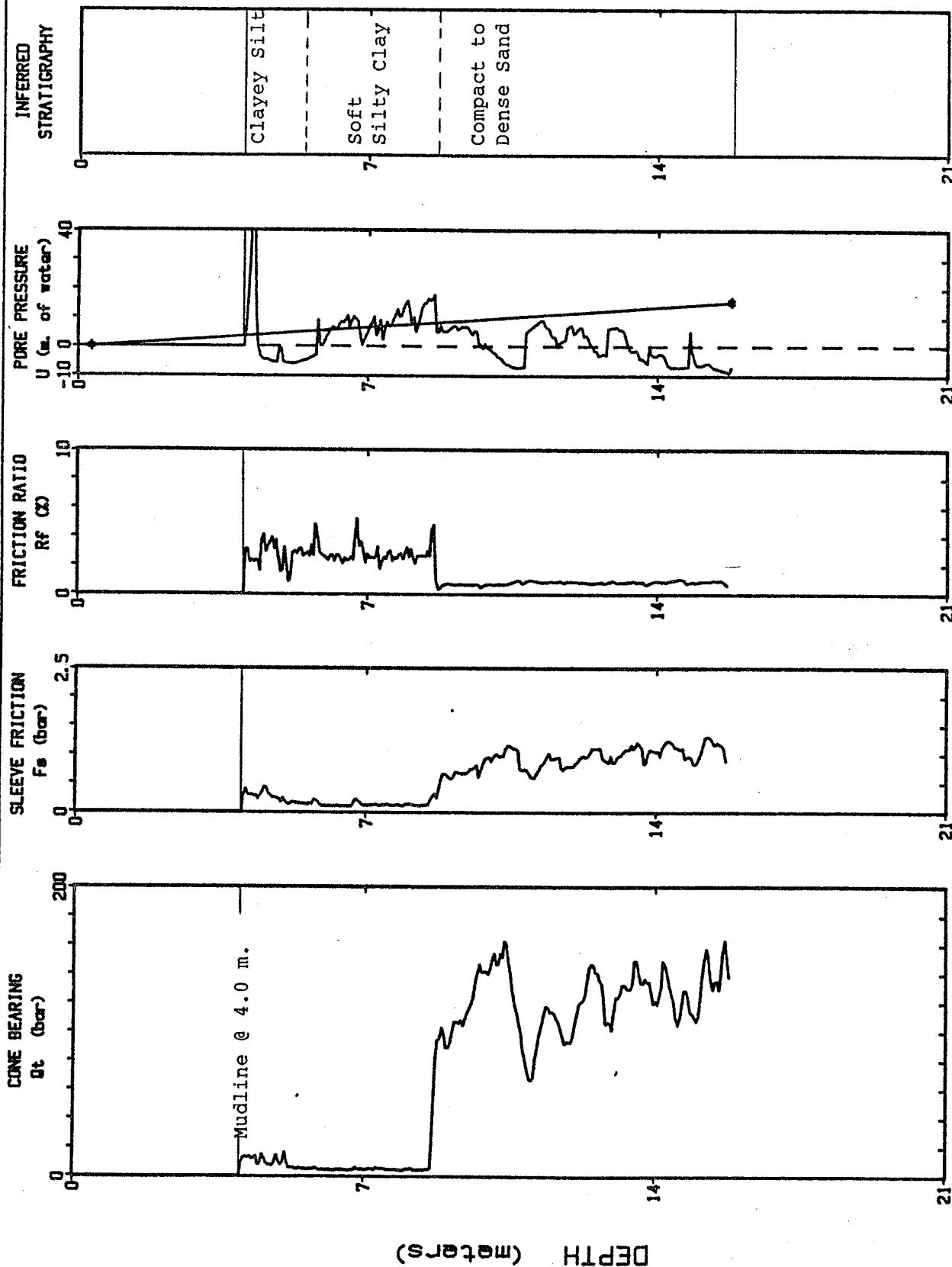
SITE: NORTH HEAD NWT

DATE: 04/08/87 17:05

CONE: 10 TonNo. 192.

Page No: 1 / 1

CPT LOCATION: C87-08 Sta 15+00



Max Depth : 15.8 m

Depth Increment : .05 m

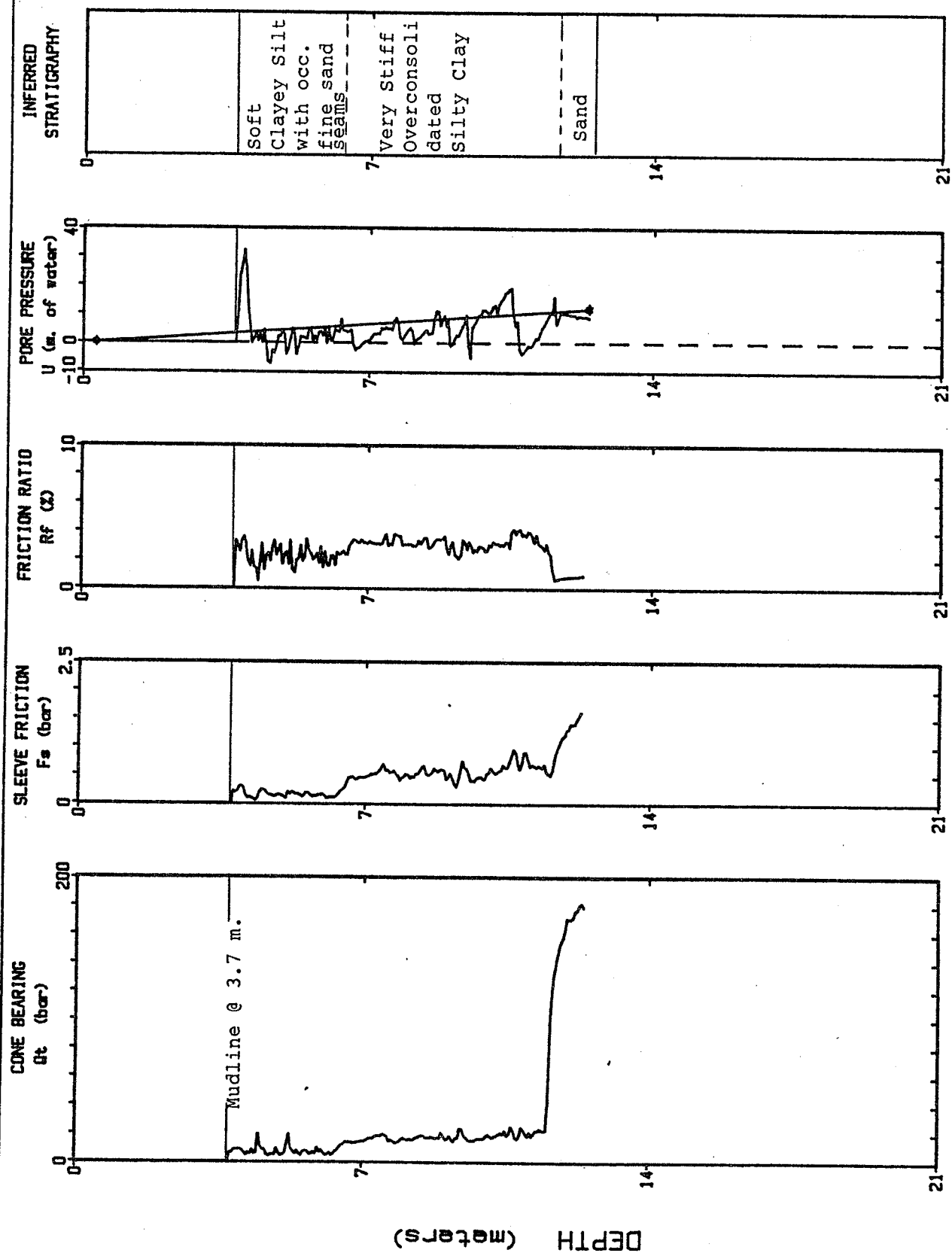
Fig. 3-24 Cone penetration data

G. S. C.

CONTRACTOR: ConeTec
SITE: NORTH HEAD NWT

DATE: 04/08/87 10:58
CONE: 10 Ton No.192 .

Page No: 1 / 1
CPT LOCATION: C87-06 Sta 10+00



Max Depth : 12.4 m

Depth Increment : .05 m

Fig. 3-22 Cone penetration data - C 87-06

G. S. C.

CONTRACTOR: ConeTec

DATE: 04/06/87 09:47

Page No: 1 / 1

SITE: NORTH HEAD_NWT_

CONE: 10 Ton No.192 .

CPT LOCATION: C87-04 Sta 6+00

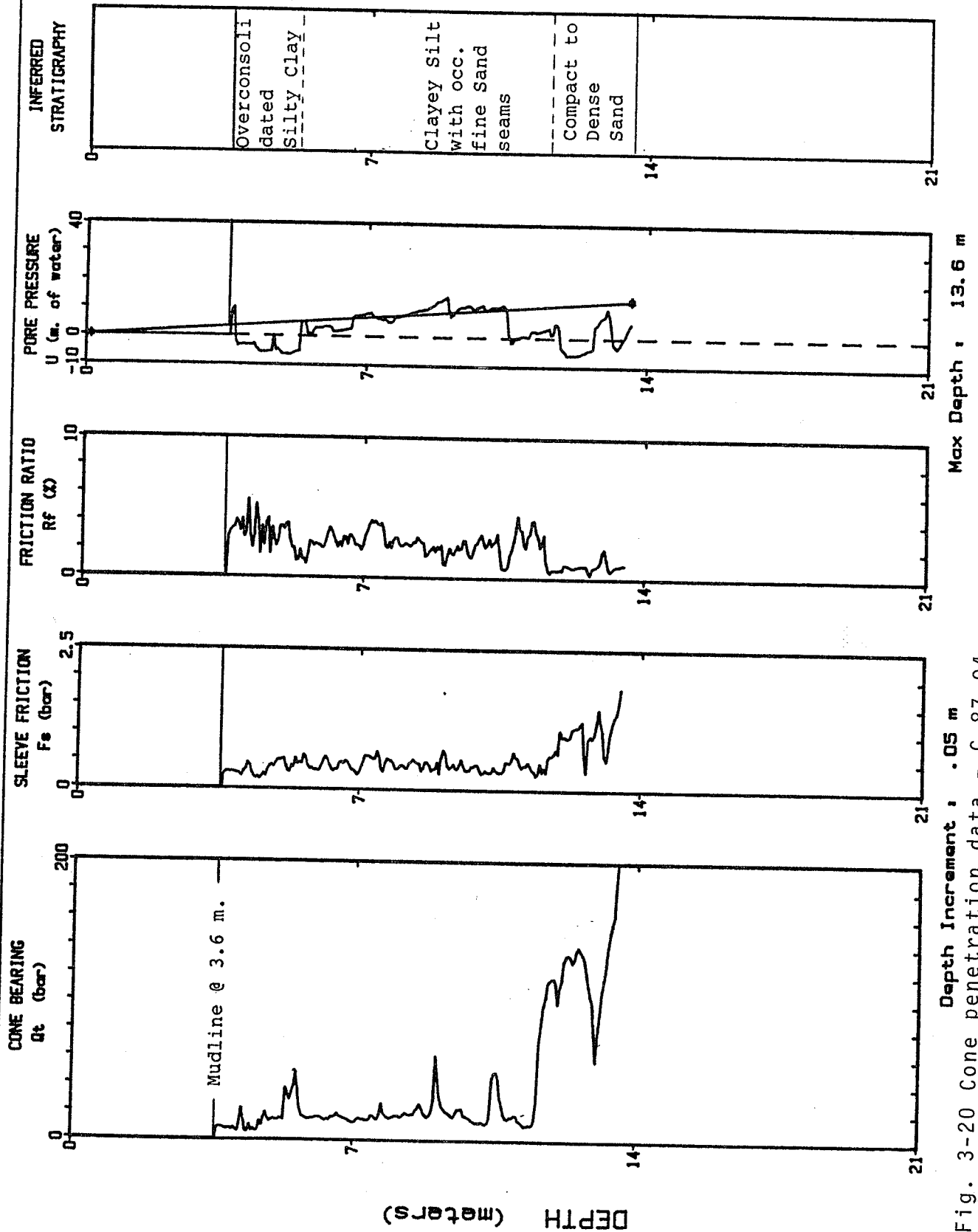


Fig. 3-20 Cone penetration data - C 87-04

Depth Increment : .05 m

CONTRACTOR: ConeTec
SITE: NORTH HEAD NWT

G. S. C.

Page No: 1 / 1
DATE: 04/06/87 18:46
CONE: 10 Ton No. 192 . CPT LOCATION: C87-02 Sta 4+50

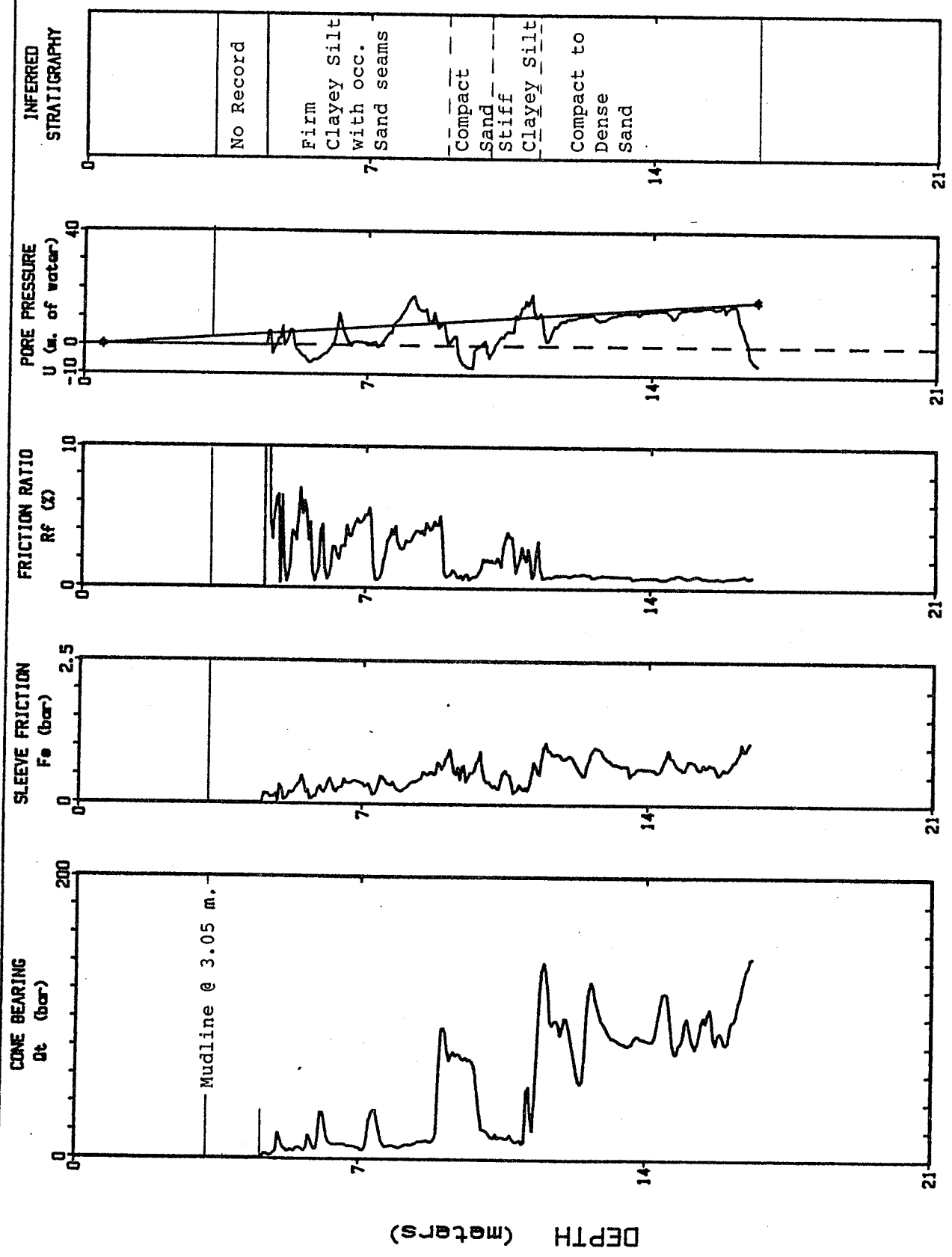


Fig. 3-18 Cone penetration test data - C 87-02

Depth Increment : .05 m

Max Depth : 16.6 m